Development of Mix Design Guidelines for High Performance RAP-Predominant Asphalt Mixtures

by

Reza IMANINASAB

MANUSCRIPT-BASED THESIS PRESENTED TO ÉCOLE DE TECHNOLOGIE SUPÉRIEURE IN PARTIAL FULFILLMENT FOR THE DEGREE OF DOCTOR OF PHILOSOPHY
Ph.D.

MONTREAL, APRIL 03, 2023

ÉCOLE DE TECHNOLOGIE SUPÉRIEURE
UNIVERSITÉ DU QUÉBEC

BOARD OF EXAMINERS

THIS THESIS HAS BEEN EVALUATED

BY THE FOLLOWING BOARD OF EXAMINERS

Mr. Alan Carter, Thesis Supervisor
Department of construction engineering at École de technologie supérieure

Mr. Luis G. Loria-Salazar, Thesis Co-supervisor
Civil Engineering School at Isaac Newton University

Mr. Éric David, President of the Board of Examiners
Department of mechanical engineering at École de technologie supérieure

Mr. Michel Vaillancourt, Member of the jury
Department of construction engineering at École de technologie supérieure

Mr. Lucas Babadopulos, External Evaluator
Departamento de Engenharia Estrutural e Construção Civil (DEECC) at Universidade Federal do Ceará

THIS THESIS WAS PRENSENTED AND DEFENDED

IN THE PRESENCE OF A BOARD OF EXAMINERS AND PUBLIC

ON MARCH 22, 2023

AT ÉCOLE DE TECHNOLOGIE SUPÉRIEURE

ACKNOWLEDGMENT

Doing PhD is a tough job. I am grateful to have some great hands to accomplish it. First, I would like to thank my advisor, Mr. Alan Carter, to have borne with me during my study. Within my PhD, I did what I liked to do. So, I sincerely appreciate Mr. Alan Carter for the trust and freedom that he gave me. I also thank my co-advisor, Mr. Luis Loria-Salazar, for accompanying me in my thesis. I appreciate his support. I would like to mention I liked my advisors' positive attitude and I am thankful for that. Alongside, I benefitted from the best technicians of the world, Mr. Sylvain Bibeau, Mr. Francis Bilodeau and Mr. Mauricio Rios. They did a great job and well-instructed me to stand on my own in Lab. I appreciate Mr. Eric David, president of the jury, Mr. Michel Vaillancourt, internal jury member, and Mr. Babadopulos, the external evaluator for the time and effort they put to review my thesis. My friends have always been treasure. I cannot name them here because they are many and I am afraid I miss one. I know you guys and many thanks for being around. However, I would like to acknowledge Gabriel Orozco, Mohsen Shamsaei, and Marc-André Bérubé for their great help on improving my presentation. Finally, I thank my family back in Iran for all their support: My father, Hossein, my mother, Nooshin, and my brother: Hessam. They are the best!

Développement de directives de conception de l'enrobé et évaluation des performances d'enrobés à prédominance de GBR

Reza IMANINASAB

RÉSUMÉ

L'incorporation de quantité élevée de granulat bitumineux recyclé (GBR) dans les enrobés a toujours été une bonne chose, car elle réduit l'utilisation de matières premières comme le bitume et les granulats. Par conséquent, non seulement les enrobés bitumineux à forte teneur en GBR sont moins chers que ceux qui contiennent une quantité plus faible de matériaux recyclés, mais ils sont également plus respectueux de l'environnement. Cette thèse traite des mélanges bitumineux dans lesquels la quantité d'enrobés recyclés (GBR) l'emporte sur les agrégats vierges. Jusqu'à présent, l'utilisation de jusqu'à 50 % de GBR dans les enrobés a été beaucoup étudiée et des chaussées contenant de 10 % à 50 % de GBR ont été posées dans tous les coins de la planète. Tant qu'il est inférieur à 50 %, le GBR est considéré comme un ajout aux granulats vierges dont la granulométrie doit être conforme aux recommandations de la norme. En revanche, dans cette étude, la granulométrie du GBR n'est pas modifiée, et une quantité minimale de granulats vierges sont ajoutés aux granulats vierges pour corriger la granulométrie. Les concepts de la méthode Bailey sont utilisés pour concevoir différents mélanges d'agrégats avec des structures rigides. Ensuite, des lignes directrices pour la préparation d'enrobés bitumineux à très haute teneur en matériaux recyclés (>50%) sont proposées, et une méthode de formulation basée sur des essais simples correspondant à différents aspects de la performance est développée pour trouver l'enrobé optimal. Étant donné que la méthode proposée est basée sur des essais simples, qui doivent être viables dans tous les laboratoires, il est nécessaire d'étudier plus en détail le comportement et les performances des mélanges et de vérifier l'efficacité de la conception du mélange. Tout d'abord, le comportement des mélanges bitumineux et de leurs liants correspondants a été étudié à l'aide d'essais dynamiques du module complexe, de la modélisation 2S2P1D et de la transformation Shift-Homothétie-Shift in Time-Shift (SHStS). Ensuite, des essais sur les liants ont été réalisés pour trouver le meilleur processus de mélange représentant le liant bitumineux afin de faciliter les études sur l'efficacité du rajeunisseur qui est indispensable dans les mélanges d'enrobés contenant de très grandes quantités de GBR. Enfin, la durée de vie en fatigue, principale préoccupation des mélanges bitumineux à très forte teneur en GBR, a été examinée à l'aide de méthodes classiques et de l'endommagement des milieux viscoélastiques (VECD). Les résultats indiquent la grande efficacité des concepts de la méthode Bailey dans l'amélioration de la résistance à l'orniérage. En outre, la conception du mélange s'est avérée efficace, bien qu'imparfaite, pour classer différents d'enrobés en ce qui concerne la performance en fatigue. Le cadre de la conception du mélange est solide, mais l'évaluation de la fatigue doit s'appuyer sur des tests et des analyses avancés, car il s'agit d'un phénomène complexe. Le VECD est une meilleure approche que l'approche classique pour analyser la résistance à la fatigue des enrobés contenant une très grande quantité de GBR. En ce qui concerne le processus de mélange, il

n'existe pas de conditions de mélange uniques qui puissent représenter exactement toutes les propriétés rhéologiques des bitumes extraits et récupérés dans les mélanges à très forte teneur en GBR. De même, le comportement du liant bitumineux n'est pas un indicateur du comportement d'un mélange bitumineux à très forte teneur en matériaux recyclés à toutes les températures et à toutes les fréquences ; il a plus d'impact et, par conséquent, est plus représentatif à des températures élevées et/ou à des fréquences faibles.

Mots clés: *La méthode Bailey, granulats bitumineux recyclés (GBR), modèle 2S2P1D, propriétés rhéologiques, formulation, endommagement des milieux viscoélastiques.*

Mix design guidelines development and performance evaluation of RAP-predominant asphalt mixtures

Reza IMANINASAB

ABSTRACT

Incorporation of higher percentages of RAP has always been favorable since it reduces use of raw materials including bitumen and aggregates. Consequently, not only are asphalt mixtures with higher RAP cheaper compared to the ones with lower RAP amount, but they are also more environmentally friendly. This thesis deals with the asphalt mixtures in which the amount of reclaimed asphalt pavement (RAP) prevails the virgin aggregates. So far, utilization of up to 50% RAP in asphalt mixtures has been studied a lot and pavements containing RAP from 10% to 50% have been laid in all corners of the globe. As long as it is less than 50%, RAP is considered as an addition to the virgin aggregates whose gradation must comply with the standard's recommendation. In contrast, in this study, RAP gradation remains as is in the stockpile and virgin aggregates are added in the minimal amount to correct the gradation. Concepts of Bailey method are used to design different aggregate blends with firm structures. Then, guidelines to prepare asphalt mixtures with very high RAP contents (>50%) is proposed and a mix design based upon simple tests corresponding to different aspects of performance is developed to find the optimum asphalt mixture among others. Since the proposed method is based on simple testing, which must be in order to be viable in all laboratories, it is required to further investigate the behavior and performance of the blends and verify the effectiveness of the mix design. First, behavior of asphalt mixtures and their corresponding binders were studied through dynamic complex modulus testing, 2S2P1D modeling and Shift-Homothety-Shift in time-Shift (SHStS) transformation. Then, binder tests were carried out to find the best blending process representing asphalt binder inside asphalt mixtures in order to facilitate studies on effectiveness of rejuvenator that is a must in asphalt mixtures containing very high RAP. Finally, fatigue life as the main concern of the asphalt mixtures with very high RAP content was examined using classical and visco-elastic continuum damage (VECD) approaches. Results indicate the high efficiency of Bailey method concepts in improving rutting resistance. Also, the mix design was found effective though not perfect in ranking different asphalt mixtures with respect to fatigue performance. The framework of the mix design is strong but the fatigue evaluation must be according to advanced testing and analysis since it is a complicated phenomenon. VECD is a better approach compared to classical one in analyzing fatigue life of asphalt mixtures containing very high RAP. With regard to blending process, there was no single blending conditions that can represent exactly all rheological properties of extracted and recovered bitumen from mixtures with very high RAP content. Also, asphalt binder is not an indicative of the behavior of asphalt mixture with very high RAP content at all temperatures and frequencies; it is more impactful and, subsequently, more representative at high temperatures and/or low frequencies.

Keywords: *Bailey method, reclaimed asphalt pavement (RAP), 2S2P1D model, rheological properties, mix design, visco-elastic continuum damage (VECD)*

TABLE OF CONTENTS

Page

LIST OF TABLES

Page

LIST OF FIGURES

Page

LIST OF ABREVIATIONS

2S2P1D	2 Springs, 2 Parabolics, and 1 Dashpot
AASHTO	American Association of State Highway and Transportation Officials
AFM	Atomic Force Microscopy
ASTM	American Society for Testing and Materials
CA	Coarse Aggregate
CDG	Coarse Dense-Graded
COS	Controlled On-specimen Strain
CRI	Cracking Resistance Index
CS	Controlled Stress
CX	Costant Crosshead
DBN	Di Benedetto and Neifar
DCT	Disk-shaped Compact Tension
DER	Dissipated Energy Ratio
DMR	Complex dynamic Modulus Ratio
DOT	Department Of Transportation
E&R	Extracted and Recovered
EMS	Epoxidized Methyl Soyate
ENTPE	École nationale des travaux publics de l'État
ESEM	Environmental Scanning Electron Microscope
ESO	Epoxidized Soybean Oil
FA_c	Coarse part of Fine Aggregates
FA_f	Fine part of Fine Aggregates
FE	Fracture Energy

FHWA	Federal Highway Administration
FI	Flexibility Index
FTIR	Fourier Transform Infrared
FDG	Fine Dense-Graded
GC-MS	Gas Chromatography-Mass Spectrometry
GM	Generalized Maxwell
HMA	Hot Mix Asphalt
HT	High Temparature
HT_e	Effective High Temparature
$HT_{e,unaged}$	Effective High Temperature corresponding to unaged binder
$HT_{e,ST\text{-}aged}$	Effective High Temperature corresponding to short term-aged binder
HWT	Hamburg Wheel Tracking
IB	Intense Blending
IDT	Indirect Tensile
LAS	Linear Amplitude Strain
LB	Low Blending
LC	Laboratoire Chaussées
LPC	Laboratoire des Ponts et Chaussées
LPPT	Long-term Pavement Performance Test
LT	Long Term
LT	Low Temperature
LT_e	Effective Low Temperature
LVE	Linear Visco-Elastic
MB	Moderate Blending

MDL	Maximum Density Line
MSCR	Multi Stress Creep Recovery
MSR	Marshall Stability Ratio
MTQ	Ministère des Transports du Québec
MTS	Material Testing System
$N_{des.}$	Design Number of Gyration
NMAS	Nominal Maximum Aggregate Size
OAC	Optimum Asphalt Content
OBC	Optimum Bitumen Content
OH	Hydroxyl
PAV	Pressure Aging Vessel
PG	Performance Grade
PI	Performance Index
PIDF	Proportional, Integral, Derivative and Future coefficients
PCS	Primary Control Sieve
RAP	Reclaimed Asphalt Pavement
rpm	revolutions per minute
RTFO	Rolling Thin Film Oven
SBO	Soybean Oil
SCB	Semi-Circular Bending
SCS	Secondary Control Sieve
SGC	Shear Gyratory Compactor
SHStS	Shift-Homothety-Shift in time-Shift
SMA	Stone Matrix Asphalt

ST	Short Term
S-VECD	Simplified Visco-Elastic Continuum Damage
T/C	Tension/Compression
TSC	Tertiary Control Sieve
TTSP	Time-Temperature Superposition Principle
V_a	Air Voids
VCA	Virgin Coarse Aggregate
VECD	Visco-Elastic Continuum Damage
VFA	Voids Filled with Asphalt
VFA	Virgin Fine Aggregates
VMA	Voids in Mineral Aggregates
VTS	Viscosity-Temperature Susceptibility
WEO	Waste Engine Oil
WLF	William-Landel-Ferry
WMA	Warm Mix Asphalt

LIST OF SYMBOLS

α	material constant relating to damage progress and is equal to 1 + (1/-m); fatigue life corresponding to strain level of 1 million
β	slope of fatigue life in log-log coordinates
γ_0	shear strain (%)
γ_{max}	maximum shear strain (%)
δ	phase angle of asphalt binder
δ_{max}	deformation at maximum load
$\Delta\varepsilon iax$	axial strain difference
$\Delta\varphi i$	phase angle difference
$\Delta\xi$	duration of the tensile part of the sinusoidal loading cycle
ΔHT_e	difference between $HT_{e,unaged}$ and $HT_{e,ST\text{-}aged}$
ε_{Aaxi}	axial strain of extensometer i
ε_{pp}	peak-to-peak strain of a sinusoidal loading cycle
$\varepsilon_{0,ta}^{R}$	maximum tensile of a sinusoidal loading cycle
ε^{R}	pseudo strain
η_0 and η_i	internal state variables for elastic response of Maxwell element i φ_E and φ phase angle of asphalt mixture
ν^*	complex Poisson's ratio
ξ_i	beginning time of the tensile loading cycle i
ξ_f	end time of the tensile loading cycle i
ρ_i	viscosity of Maxwell element i
$\sigma_{0,ta}$	maximum tensile stress
σ_{max}	maximum stress of a sinusoidal loading cycle
σ_{min}	minimum stress of a sinusoidal loading cycle

τ	characteristic time depending on temperature
$\varphi\varepsilon_{iax}$	phase angle based on extensometer i
φ_i	phase angle of cycle i
φ_G	complex shear modulus phase angle
φ_v	Poisson's ratio's phase angle
ω	angular speed
AI	normalized aging potential index
a_T	shift factor
A	fatigue life corresponding to strain level of 1 million
B	slope of fatigue curve
C	pseudo stiffness
CI	normalized cracking index
D	diameter; damage intensity
E_0	glassy modulus
E_{00}	static modulus
E*	dynamic complex modulus
E_R	reference modulus that is taken as one
f	frequency
F_i	magnitude of pseudo stiffness at cycle i
f_{req}	reduced frequencies
G*	complex shear modulus
G_{mm}	maximum theoretical Gravity of asphalt mixture
G^R	the rate of change of the averaged released pseudo-strain energy throughout entire test history
G_{sb}	bulk specific Gravity of aggregate

G_{se}	effective specific Gravity of aggregate
G_{mb}	bulk specific Gravities of asphalt mixture
G_{SSD}	bulk saturated surface dry specific gravity of aggregate
H	height
I_D	initial undamaged |G*|
j	imaginary unit in which j^2=-1
J_{nr}	MSCR high temperature parameter
m	the slope of the modulus vs time during relaxation in log-log coordinate
MI	normalized moisture damage index
N_f	fatigue life or number of cycles to failure in fatigue testing
P	load
RI	normalized rutting index
S_{LT}	SCB strength of LT specimens
S	damage
S_t	IDT strength
S_{ST}	SCB strength of ST specimens
t	time (s)
T	temperature
T_c	crystallization temperature
T_{ref}	reference temperature
T_m	valley melting points
W	work performed or dissipated energy
w_a	weight of aging index
w_c	weight of cracking index

XXX

w_m	weight of moisture damage index
w_r	weight of rutting index
W_i	dissipated energy of cycle i
W_N	dissipated energy at cycle N
W^R	pseudo strain energy density
W_C^R	total released pseudo strain energy

INTRODUCTION

There are economic and environmental reasons to include higher amount of reclaimed asphalt pavement (RAP) in new pavements. However, technical issues in production, performance deficiency, and insufficient available resource place restrictions on the increase of RAP in asphalt pavements.

With respect to the environment, RAP replaces the raw materials of asphalt mixtures and decelerates the consumption of natural resources. Also, using RAP is a solid waste recycling that contributes to cleaner environment. With respect to the economy, industries spend less on fossil fuel for procuring raw materials including bitumen and aggregates. Subsequently, the total price of producing asphalt mixture per metric tonne decreases with RAP content increase.

From the economic and environmental point of view, it is quite beneficial and justifiable to include as much RAP as possible in asphalt mixtures. Yet, currently, the maximum allowable RAP content is 15-25%, which is considered low, in the majority States of US and provinces of Canada (Williams, Willis & Ross, 2019). Few States increased the maximum allowable to approximately 50%, which is called high RAP content (Copeland, 2011; Aurangzeb, Al-Qadi, Abuawad, Pine & Trepanier, 2012; Hand & Aschenbrener, 2021). The tendency toward application of even more RAP, larger than 50% which is named very high RAP content here, is growing.

However, asphalt pavements with higher RAP contents are prone to early cracking that, consequently, shortens their service lives. Also, since there are no specific guidelines for mix design, production, and compaction of asphalt mixtures with very high amount of RAP that addresses their specific properties, the resultant asphalt mixtures with accordance to conventional volumetric-based mix design methods cannot be considered as the optimum with the best performance. Therefore, first, to reach the optimum performance, guidelines of performance-based mix design of asphalt mixture containing very high RAP are outlined. A

mix design is composed of different parts including: (a) materials' properties requirements, (b) guidelines for procurement and preparation of materials, (c) instruction for specimen fabrication, and (d) optimization criteria. Except part (a), other parts are included in this research.

Guidelines for procurement and preparation of materials contains rejuvenation of old bitumen of RAP and gradation. With respect to rejuvenation, the rich literature (chapter 1) is resorted but, due to lack of attention to gradation, chapter 3 is dedicated to gradation restoration of RAP with the aid of Bailey method concepts. Once the amount of RAP exceeds 50%, it can be claimed that the mixture is RAP dominant. So the aggregate blends is better to be designed based upon the existing gradation of RAP. This is the backbone of this thesis. Instruction for specimen fabrication along with optimization criteria is studied in chapter 4 in order to come up with the optimum asphalt mixture containing very high RAP.

The preliminary findings of chapter 4 are further investigated through chapter 5 to chapter 7. The mixtures with very high RAP contents from chapter 4 including the optimum and 100% RAP are studied deeply through thermomechanical characterization of bitumen and asphalt mixtures (chapter 5), bitumen grade and performance (chapter 6), and fatigue analysis (chapter 7). Since all mixtures meet the basic performance requirements proposed by standards, further investigation via advanced characterization and performance testing shed light on not only the effectiveness and validity of the proposed mix design guidelines and criteria, but also the behavior and performance of asphalt mixtures with very high RAP content. Finally, the conclusion is drawn based upon the results obtained in chapters 5, 6, and 7 on the mixtures designed in chapter 3 and 4. It is clarified if the rejuvenation, gradation, preparation, and optimization are valid and effective. Alongside, validity of current practices on asphalt mixtures testing and analysis is examined, required modifications are proposed, and insight toward behavior and performance of asphalt mixtures with very high percentages of RAP is provided.

The scheme of this thesis consists of problem evolution (Chapter 1 and 2), body of research (chapter 3, 4, 5, 6, and 7), and findings. Each chapter within the body of the research is a paper that has been published, accepted, or under review in scientific journals as of the now. Chapter 1 is dedicated to literature review in relation with the scope of this study. The gap in current studies, the introduction to the materials used and the justification of the methodology deployed can be found in this chapter. Chapter 2 outline the major and minor objectives of this study with the emphasis on the significance of it in the near future. Chapter 3 deals with the correction of the distorted gradation of the RAP via Bailey concepts. Chapter 4 develops guidelines for the design of the asphalt mixtures with very high RAP contents (>50%). It addresses the specific characteristics of this type of asphalt mixture. Chapter 5 investigates the characteristics of asphalt binder and asphalt mixture containing very high RAP and searches for any affinity between them. This gives better idea about the materials under study. Chapter 6 studies the rejuvenation and the effective ways to evaluate the efficiency of the rejuvenation through blended binder. Rejuvenation is mandatory once the amount of RAP increases. Chapter 7 analyses the main drawbacks of the asphalt mixture with very high RAP contents, Fatigue. It employed classical and linear visco-elastic continuum damage (VECD) approach to provide deep understanding of the mechanism of fatigue and come up with realistic fatigue resistance of this type of asphalt mixture. Finally, the conclusion is a short section that bring the former chapter into one for the conclusion. There is also the last part that provides recommendations for the future studies.

CHAPTER 1

LITERATURE REVIEW

1.1 Introduction

In the 1970's decade, it was the Arab countries oil embargo over the Western world that caused oil price skyrocket and brought RAP into use as a rich source of bitumen (West, Willis & Marasteanu, 2013). In early 90s, another oil crisis hit due to the first Gulf War and led to the increased ratio of the RAP recycled to the RAP produced to over 80%; i.e. 80% of the RAP produced was recycled (Copeland, 2011). In 2001, it was reported that 80-85% of the produced RAP in the US was consumed in the new asphalt mixtures containing low RAP contents (10 to 25%) (Asphalt Pavement Alliance, 2001; Chesner, Collins, MacKay, & Emery, J, 2002). Since then and until 2009, there had been almost the same portion of the milled and procured RAP that had been recycled and reused in the new pavements; it was between 80-85% (Hansen and Copeland, 2013; Williams, Willis, & Shacat, 2020). After substantial increase in bitumen price within 2007 to 2008 (300%), attention was drawn toward RAP once again. Since 2009, there has been an increasing trend of the RAP use in new pavements. The percentage of the RAP recycled to the RAP produced has escalated to 94% in 2019 (Williams et al., 2020) and, essentially, resulted in increased RAP content of asphalt mixtures. Figure 1.1 illustrates the increment of the average RAP percent in the asphalt mixtures in the US since 2009. From 2009 to 2020, the average RAP percent in asphalt pavements has increased by 59.3% (Williams et al., 2020).

It is evident that there has been a constant increasing demand to incorporate higher amount of RAP. Still, it is averagely 21.1% of the total 389.3 million tons of asphalt mixtures produced in 2018 in the US (Williams et al., 2019). As shown in Figure 1.2, very tiny numbers of states have adopted RAP content higher than 30%.

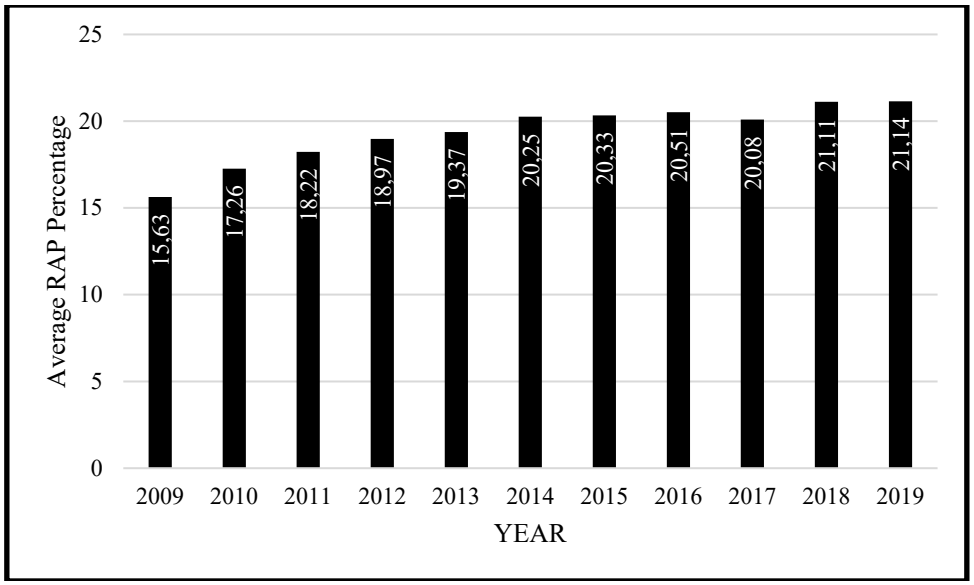

Figure 1.1 Average RAP content used in total new asphalt mixtures in USA
Adapted from Williams et al. (2020, p. 17)

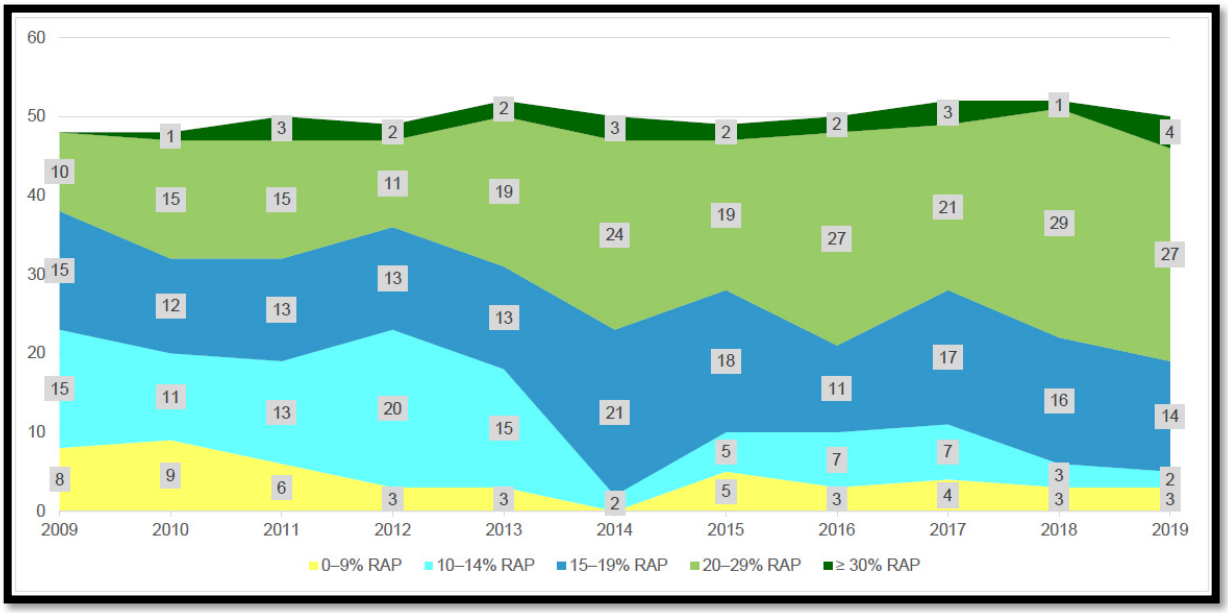

Figure 1.2 Average RAP content used by the number of States in the US
Taken from Williams et al., (2020, p. 20)

The annual amount of RAP production is rising steadily. It is faster than the increase rate of asphalt mixture production. It can be inferred from the RAP content increasing trend. Due to

the extended network needing regular milling and resurfacing and strict environmental regulations enforcing to recycle RAP, similar pattern as US can be observed in other developed countries. Developing countries with limited road networks, on the other hand, have far faster pace of construction and development than reconstruction. Thus, lower RAP contents are expected there. In short, application of high amount of RAP into the new pavements is a problem of the developed countries, whose extended old infrastructure requires reconstruction.

In the developed countries, as pavement reconstruction and resurfacing become more frequent, whether because of harsh weather and/or high traffic volume condition and/or providing better serviceability and pavement quality to road users, there will be, consequently, greater RAP production. In northern part of US and in Canada, RAP production has been accelerating, and mixtures containing more and more RAP are inexorable. Knowing the challenges ahead since 2009, there have been numerous research projects with the focus on incorporation of approximately 50% RAP (Loria-Salazar, 2011; Al-Qadi et al., 2012; Norouzi, Sabouri & Kim, 2014). Before that, in 2001, requirements and instruction for incorporating low RAP content (less than 25%) had been embedded in Superpave mix design (McDaniel and Anderson, 2001). Except 100% RAP asphalt mixture, there has not been much research on asphalt mixtures containing very high RAP content (RAP-predominant asphalt mixtures), i.e., more than 50%. Therefore, there is a gap of research in transition from less than 50% to 100% RAP (whole-RAP mixture) that needs to be filled. This research does not specifically aim to work on asphalt mixtures with RAP concentrations ranging 50-100% RAP but, due to the approach and premises adopted, it inevitably studies mixture falling with the aforementioned concentrations.

1.2 Mix design

Initially, Superpave mix design specifications required RAP and virgin aggregate blend have physical properties and gradation within the limits as virgin aggregate. Also, the asphalt mixture with RAP must comply the same volumetric properties as normal mixtures without RAP. Later in 2005, as the tendency to increase RAP content augmented, constructing blending chart was proposed and became important in order to determine RAP content range to achieve

a desirable performance grade (PG) once the virgin and RAP's bitumen blend (Anderson, 2005). Blending chart helps limiting the RAP content to avoid extremely stiff bitumen that are susceptible to cracking. But there is a major issue there as it also exists in American Association of State Highway and Transportation Officials code AASHTO M 323 (2001) and Federal Highway Administration (FHWA) report FHWA-HRT-11-021 (Copeland, 2011): none does take partial blending, which means remaining the inner layers of old bitumen intact (Shirodkar et al., 2011; Behnood, 2019), into account. For the virgin and RAP's bitumen blend, they took whether virgin bitumen's PG as constant and determine allowable RAP content, or RAP content as constant and determine virgin bitumen's PG to obtain desirable PG. Zhou Zhou, Hu, Das & Scullion (2011) considered the partial blending as a factor causing optimal bitumen increase with RAP percentage increase. So, in their balanced mix design, they advised on increasing virgin bitumen in the mixtures with higher RAP content, or else, elevating temperature with RAP concentration increase, as possible solutions to reach target %density. Both remedies negatively affect the environmental and economic benefits that higher amounts of RAP lead to. Thus, it is better whether to adopt different volumetric criteria or manipulate RAP gradation to accommodate less voids in mineral aggregates (VMA) or both.

While Zhou et al. (2011) dumped VMA limitation of AASHTO M 323 (2001) and took %density or target air void (V_a) as the criterion for performance evaluation, Aurangzeb et al. (2012) found VMA as the influential factor on performance. They deployed Bailey method for gradation to achieve desired volumetric properties in the mixtures containing high RAP. As recommended by Bailey in the case of RAP utilization (Vavrik, Pine & Carpenter , 2002), RAP was fractionated into coarse and fine and, then, blended so that the white curve of the RAP blend had approximately the same gradation as virgin blend, which was designed based upon Bailey method in. Also, within the mix design process, it was assumed that the RAP and virgin bitumen mingle 100%. It was proved that, having the same volumetric properties including V_a, VMA and voids filled with asphalt (VFA), stability and durability, asphalt mixtures containing different RAP percentages up to 50% pass the performance criteria of Illinois department of transportation (ILDOT). The research work did not modify Bailey method for high RAP content utilization; rather, it just endorsed the effectiveness and applicability of Bailey method

for high RAP content mixtures. In practice, fractionating RAP into stockpiles with different sizes is laborious and results in finer stockpiles pile-up.

West et al. (2013) advised against using effective specific gravity (G_{se}) to estimate RAP aggregate bulk specific gravity (G_{sb}), what Aurangzeb et al. (2012) did. They proposed using RAP bitumen to total bitumen ration as the criterion to distinguish high RAP content in lieu to the percentage of RAP by the total weight of mixture. Additionally, they developed protocols for RAP handling and management including heating and fractionating in order to better design high RAP content mixtures (25-55%). Mix design was still based upon volumetric requirements of AASHTO R 35 (2017a). The research work admitted that RAP and virgin bitumen mingle substantially. It was concluded that, although performance grade (PG) of the blend of virgin and RAP bitumen has substantial impact on performance, its effect on volumetric properties is negligible. The assumption of substantial degree of blending is not always true as Shirodkar et al. (2011) proved that it can be as low as 70% when stiffer virgin binder is used. Low degree of partial blending causes under-asphaltening and poor performance. It is more significant when higher amount of RAP and stiffer virgin binder is used (Shirodkar et al., 2013).

On the other hand, Copeland (2011) aimed at characterization of RAP material and constructing blending chart for the mixtures with RAP content of more than 25% before preparing Superpave mix design specimens. She placed emphasis on practices on procuring, stockpiling, plant mixing and placing mixtures containing high RAP content. Loria-Salazar (2011) evaluated physical properties of RAP's aggregate and bitumen and assessed the impact of high RAP content (50%) on the performance of mixture. Moreover, effect of high RAP (50%) on Superpave mix design parameters such as VMA and maximum theoretical gravity (G_{mm}) were examined. He found that the oven gives the most precise asphalt content of RAP. The study revealed that the low temperature PG of the bitumen extracted and recovered from mixtures containing 50% RAP, both field- and laboratory-prepared, fails satisfying Superpave's low temperatures specifications even when soft bitumen is used. Also, Izaks, Haritonovs, Klasa & Zaumanis (2015) proved, despite the negligible effect of 50% RAP on

volumetric and mechanical properties in comparison with 0 and 30% RAP, its detrimental effect on fatigue performance is significant. So, fatigue becomes the main concern of asphalt mixtures with high RAP content and, with RAP content increase, the negative impact on fatigue performance grows exponentially. The negative influences of RAP on low and intermediate temperatures clearly pronounce the dire need for recycling agents (rejuvenators) in high RAP content.

Barco Carrión, Lo Presti & Airey (2015) focused on bitumen and introduction of rejuvenator to see if increasing the amount of RAP in wearing course is feasible. The degree of partial blending was considered to construct the blending chart that was developed with respect to various important bitumen properties as recommended by European, American and Australian for bitumen-based blend design. It was found that it is possible for HMA and WMA to include up to 90% RAP using American and Australian models. The study did not include mix design according to volumetric properties of mixture. Moreover, no attempt was made to find optimal rejuvenator content. On the other hand, Im, Karki & Zhou (2016) developed a balanced mix design to find optimal bitumen and rejuvenator content. First, based upon rheological properties and Golver-Rowe damage parameter of the rejuvenator-RAP-virgin bitumen blend, the range of the rejuvenator content meeting specification requirements was determined. Then, optimal binder content of virgin mixture and those containing RAP was found using the balanced mix design that incorporates Hamburg wheel tracking test and overlay tester. Finally, the optimal rejuvenator content was determined by applying the same balanced analysis as mix design. The method was used for one mixture type incorporating 30% RAP and the gradations of virgin and RAP were almost the same. Thus, the balanced method, technically, deals with bitumen and rejuvenator content with no glance at the challenges such as poor gradation and low degree of partial blending that involves in high RAP content.

Bressi, Dumont & Partl (2016) developed a framework for mix designing asphalt mixture with RAP percentages of 10% to 90%. The influence of RAP's fine particle clustering on effective gradation and the impact of stiffened RAP bitumen on compactibility were taken into account in the mix design. The main drawbacks of the proposed method are (a) complexity and

advanced equipment and analysis utilization such as 3D image analysis of aggregates and environmental scanning electron microscope (ESEM) image analysis of filler, (b) absence of performance analysis for assessing mixture quality, and (c) only acknowledging air void content with regard to volumetric properties.

The literature review so far clarifies that there have been three major issues with regard to mix design of asphalt mixtures containing high RAP content:

(a) Gradation,

(b) Volumetric properties, and

(c) Performance.

These issues are interconnected. Solving one issue helps alleviate or even eliminate the other issues. There are remedies for each deficiency that can be practiced individually or along with others. The goal is good performance in the end.

Since aggregate skeleton is the main responsible of bearing loads, it is very important to readjust the gradation of RAP. To arrive at a good gradation as proposed by standards, fractionating RAP, as virgin aggregates, into fine and coarse stockpiles and, then, blending them with virgin aggregate in appropriate proportions has been rehearsed consensually. Also, there are different methods to build strong aggregate skeleton and/or high aggregate packing. Dominate aggregate size range (DASR) (Chun & Kim, 2016), Furnas void index (Olard &Perraton, 2010), and Bailey method (Vavrik et al., 2002) are among the methods that are used for aggregate gradation. In this study, however, concepts of Bailey method are deployed for correcting RAP distorted gradation and building up firm aggregate skeleton.

From the very early stage, it was found that RAP results in stiffer mixtures compared to those containing only virgin materials. As stated earlier, stiffness of the bitumen is not believed to impact the volumetric properties significantly as gradation does, but it makes RAP-containing mixtures prone to fatigue and thermal cracking (West et al., 2013; Norouzi et al., 2014). At low RAP concentration (up to 25%), application of softer virgin bitumen can maintain the

characteristics of the blend of the virgin and RAP bitumen within the allowable limits of low and intermediate temperatures (McDaniel and Anderson, 2001; Nazzal, Mogawer, Austerman, Qtaish & Kaya, 2015). However, with RAP content increment, the partial blending of RAP bitumen decreases (Shirodkar et al., 2013) and, subsequently, the stiffness condition exacerbates to an extent that the introduction of rejuvenators seem to become an inevitable complement to the application of soft bitumen (Nazzal et al., 2015; Zaumanis, Mallick, Poulikakos & Frank, 2014a). Up to 50% RAP, it is feasible to purge the downsides of stiff RAP bitumen through modifying mix design (Aurangzeb et al., 2012; West et al., 2013; Izaks et al., 2015; Ma, Huang, Zhao & Zhang, 2015). More than that, it is required to use rejuvenators in order to balance asphaltene/maltene ratio of RAP's bitumen more effectively (Elkashef, Williams & Cochran, 2018a). Therefore, since this study deals with very high RAP content (>50%), rejuvenator is used to soften the old bitumen of RAP. Consequently, cracking resistance is expected to improve with mitigating brittleness of asphalt mixtures with very high RAP content.

The last decade's efforts to tackle cracking problem involved with high RAP content mixtures can be summarized into (a) mix design modification, correction and enhancement, and (b) rejuvenating agent application were the two major solutions. Balanced mix design with consideration of performance has been studied in few research works (Aurangzeb et al., 2012; West et al., 2013; Izaks et al., 2015). On the other hand, studies have been conducted on degree of RAP binder blending with virgin one in the absence of additive (Shirodkar et al., 2011; Shirodkar et al., 2013), and subsequently, increasing the degree of blending in high RAP content mixtures were investigated by much research (Behnood, 2019).

With retrospect over the literatures on asphalt mixtures with high RAP content, the focus research of this research is on performance-based mix design of asphalt mixture with very high RAP content. Of course, rejuvenation is made by employing the findings of previous studies, which will be presented in sections 1.4 and 1.5, but the focus is on gradation correction through Bailey method concepts.

1.3 Thermomechanical characterization and performance evaluation

Once it comes to more than of about 50% RAP, 100% RAP and its rejuvenation process become what can be found the most in the literature. There are numerous studies devoted partially or totally to examining rejuvenated mixtures containing high RAP content (Zaumanis, Mallick & Frank, 2013; Zaumanis, Mallick & Frank, 2015; Ma et al., 2015; Elkashef & Williams, 2017a; Elkashef, Podolsky, Williams & Cochran , 2018b; Podolsky, Saw, Elkashef, Williams & Cochran, , 2020). In a research by Zaumanis et al. (2013), 100% RAP mixtures were rejuvenated by direct addition of nine different rejuvenators. They underwent low temperature performance tests including indirect tensile creep compliance at -10℃ and indirect tensile strength. Results indicates that five of the rejuvenators including waste engine oil (WEO) are contributive to thermal cracking improvement whereas organic rejuvenator failed to result in acceptable enhancement. In another study by Zaumanis et al. (2015), it was shown that organic and vegetable oils can significantly improve binder properties at far lower doses compared to a petroleum-based rejuvenator. They also results in better fatigue performance of bitumen and mixture compared to the petroleum-based rejuvenator. Ma et al. (2015) prepared asphalt mixtures with RAP contents up to 60% RAP. No rejuvenator was applied. From results of dynamic modulus, wheel tracking, bending beam at -10℃, freeze-thaw splitting, and 4-point beam fatigue tests, it was found that mixtures containing up to 50% can meet the standard requirements if properly mix-designed.

Elkashef et al. (2017a) conducted a research on the effect of soybean oil (SBO) on performance of the asphalt binder of the mixture containing 100% RAP. 0%, 1% and 2% SBO were added to asphalt binder composing of 1:5 neat (PG58-22) to RAP asphalt binder. PG testing, linear amplitude strain (LAS) and frequency sweep tests were performed on binders to determine critical low and high temperature, fatigue performance, and dynamic shear modulus over a wide frequency range, respectively, and compare the results of different binders. 1% SBO reduced high temperature PG of RAP by 6 grade[1] while neat binder (0%) did it by only one

[1] each grade is 6 ˚C

grade. It indicates how influential SBO is on softening RAP binder. LAS at different intermediate temperatures including 21, 28 and 31˚C showed that SBO increases fatigue life extensively at higher shear strains of about 4 to 5%. Fatigue life of asphalt binder at 5% strain rate can establish strong correlation with the fatigue life of mixture (Tran, Taylor & Willis, 2012). Another study indicated that N_f at 4% shear strain rate is a better indicator of real traffic once compared with long-term pavement performance test (LPPT) results (Hintz, Velasquez, Johnson & Bahia, 2011). Thus, SBO is effective in improving fatigue performance. As the temperature decreases, the positive influence of SBO, compared to adding only virgin asphalt binder, on enhancing the fatigue performance becomes more pronounced at lower temperatures; making it suitable for cold regions like Canada and north US. Additionally, dynamic modulus master curve and disc-shaped test (DCT) were carried out on the mixtures containing 100%RAP, 100%RAP+PG58-22, 100%RAP+PG58-22+1%SBO, and 100%RAP+PG58-22+2%SBO. The mixtures were prepared at 140˚C, like warm mix asphalt (WMA). It was found that SBO has no clear impact on dynamic modulus at different frequencies; notably high frequencies represent low temperature or fast traffic flow and low frequencies represents high temperature or slow traffic flow. It clarifies that there is lack of similarity between binder and mixture mechanical characteristics. Regarding DCT, which characterizes cracking resistance, although obtained results for mixture containing 2% SBO has higher cracking resistance, the uncertainty of results due to large error is a matter of concern.

Two studies have been conducted on neat asphalt binder and mixture modified by a SBO derivative in the absence of RAP (Elkashef, Podolsky, Williams & Cochran, 2017b; Elkashef et al., 2018b). These studies shed light on the fact that RAP binder is not like neat binder with respect to interaction with SBO derivatives. Asphalt binders of PG 64-28 and PG 58-28 and their corresponding mixtures soften as a result of the SBO derivative application at both high and low temperatures. The SBO derivative reduces the complex shear modulus of asphalt binders at any temperature, frequency, and aging level. The impact is greater at high temperature (3 grades or 18˚C drop for high temperature PG) compared to low temperatures (1 grade or 6˚C reduction for low temperature PG). Similarly, the stiffness reduction of asphalt

mixtures is more pronounced at higher temperatures, or interchangeably lower frequencies. Asphalt binders with higher high temperature PG (or larger PG span) enjoys the greater impact at low temperatures and fatigue resistance improvement more (Elkashef et al., 2017b; Elkashef et al., 2018b). Having very high temperature PG, sometimes as high as 108˚C, and large PG span, as large as about 120˚C (Elkashef et al., 2017a), RAP can benefit from the SBO derivative greatly regarding thermal and fatigue cracking resistance. It was found that the detrimental impact of the SBO derivative on rutting is not that significant (Elkashef et al., 2017b). All these changes take place at low dosage of 0.75% by the weight of bitumen (Elkashef et al., 2017a; Elkashef et al., 2017b). This makes the SBO derivative a promising rejuvenating agent for the stiff binder of RAP.

Apart from softening capability of rejuvenator, it is very important for a rejuvenator to have its impact last long. Hence, it must have good aging resistance. Aging causes upward shift and flattening of shear complex modulus master curve and such trend is observable for any type of binder. In short, it stiffens the binders. Phase angle master curve can be a good indicator of stiffness of asphalt binders. The SBO derivative leads to higher phase angles of RAP binder, which are more pronounced at lower temperatures. Since the SBO derivative modified RAP binders have greater drop in phase angle after aging compared to neat plus RAP binder. Therefore, they are susceptible to aging effect. Nonetheless, they have higher phase angle than the unmodified RAP and neat binder blend even after aging. Additionally, SBO derivative modified RAP binder has far better fatigue performance after long-term aging compared to neat plus RAP binder (Elkashef et al., 2017a). Therefore it can be concluded that SBO derivative abates aging.

Another promising feature of SBO-based rejuvenator is decreasing mixing temperature; it acts like a WMA agent. In order to be a good WMA agent, the SBO derivative rejuvenated mixtures ought not to be soft with low viscosity at high service temperatures as it contributes to rutting of all mixture types, draindown in stone matrix asphalt (SMA), and bleeding in dense-graded asphalt mixtures. Viscosity-temperature susceptibility (VTS) measures how the viscosity rate of a binder changes with temperature. High VTS shows low viscosity at high temperature

(draindown and bleeding problems) and high viscosity at low temperature (stiff and not good for thermal cracking); it is not preferable for a WMA agent. The viscosity vs. temperature proves that the SBO derivative can reduce the mixing and compaction temperature of neat binders by decreasing viscosity. But also, VTS proves that SBO derivative modified binders have lower VTS with less change due to temperature variation (Elkashef et al., 2018b). Both low viscosity at lower mixing temperature and low VTS are good attributes for a promising WMA agent. It was revealed that dynamic modulus of the unmodified mixtures is not impacted by mixing temperature reduction from 140˚C to 120˚C, but the cracking resistance does negatively (Elkashef et al., 2018b). However, the SBO-based rejuvenator is able to improve low and intermediate cracking resistance at both aforementioned temperatures, which is due to lowering stiffness.

Podosky et al. (2021) used an epoxidized soybean oil (ESO), namely epoxidized methyl soyate (EMS), as a rejuvenator to include 30% RAP in asphalt mixture. Inevitably, this type of ESO has to be treated as a WMA since it has boiling point of 147˚C. 3% and 6% EMS were blended with neat binder (PG58-28S) at 140˚C with rotational speed of 2000 rpm for one hour. The binder blends then were mixed with extracted and recovered RAP's binder to undergo binder testing and were used for preparing asphalt mixtures. After determining optimal bitumen content based upon mix design of high RAP content, it was found 24.5% of the total binder is made up of RAP's binder. Therefore, 24.5% of RAP's binder was mixed with 75.5% of the neat binder modified by EMS. PG testing proved that EMS does not improve low temperature PG of RAP and neat binder blend; which was claimed to be due to the shortcomings of PG testing and the need for advanced bitumen testing such as frequency sweep and LAS. Then, mixtures with 30% RAP were prepared in asphalt plant using neat binder containing 3% EMS and the samples obtained from the laid-down pavement underwent dynamic modulus, disk-shaped compact tension (DCT) and Hamburg wheel tracking (HWT) tests. For comparison, a control mixture with 20% RAP and neat binder was fabricated in the laboratory. With respect to complex dynamic modulus master curve, both mixtures, control and the EMS modified mixtures, have similar response to loading except that EMS has slightly lower dynamic modulus at intermediate temperatures, which means a bit greater resistance to fatigue cracking.

DCT results indicated that EMS modified mixture can narrowly satisfy the minimum requirement of 400 J/m^2 at -12℃ but not at -18℃. Plant-produced mixture has weaker rutting and moisture sensitivity performance than the control laboratory-produced mixture based on HWT results; the latter contains less RAP. That indicates the effectiveness of EMS in field. There are other research works that study plant production and provide recommendation for application of SBO-based rejuvenators (Zaumanis, Mallick & Frank, 2014c; Zaumanis, Boesiger, Kunz, Cavalli & Poulikakos, 2019; Rathore and Zaumanis, 2020, Zaumanis, Cavalli & Poulikakos, 2020). All confirms efficiency of this type of rejuvenator.

Fatigue performance is a main concern of asphalt mixtures with RAP. Fatigue cracking is a complex phenomenon and fatigue cracking potential of RAP-predominant asphalt mixtures must be studied. The fatigue performance of the rejuvenated high RAP content asphalt mixtures have been studied by indirect tensile strength (Subhy, Menegusso Pires, Jiménez del Barco Carrión, Lo Presti & Airey, 2019), four-point beam fatigue test (Jiao, Elkashef, Harvey, Rahman & Jones, 2022), indirect tensile fatigue test (Yan et al., 2021), flexibility index (FI) and cracking resistance index (CRI) of semi-circular bending test (kaseer etal., 2018) and Coaxial shear test (Zaumanis et al., 2014a). Some researchers evaluated fatigue performance by using LAS and visco-elastic continuum damage (VECD) on the fine aggregate matrix (Zhang, Ren, Qian & Wang, 2019 ; Jiao et al., 2022). But VECD has never been directly applied on the rejuvenated very high RAP content asphalt mixtures to be compared with empirical methods.

From the literature on SBO-based rejuvenators, it was found that they effectively soften RAP's binder, maintain adequate quality after aging, can work as WMA agent, improve cracking resistance, and produce plant asphalt mixtures. This research adopts SBO-based rejuvenator and uses the findings the previous studies for preparing rejuvenated asphalt binder and mixture containing high percentages of RAP. It does not deal with plant and field performance of rejuvenated. It focuses on laboratory-based thermomechanical characterization and performance of bitumen and asphalt mixture containing very high amount of RAP. Rutting,

cracking, aging, and moisture damage potential are examined and the influence of temperature and/or frequency on mechanical behavior are investigated.

1.4 Rejuvenation of bitumen and asphalt mixture

Zaumanis et al. (2014c) reviewed the technologies including RAP processing, handling, mix designing and performance examining that were available to fabricate %100 RAP since then. The study also includes environmental and economic analysis of %100 use, which, of course, was indicated favorable. Later, with challenges emerging within production phase, Zaumanis et al. (2019) proposed early addition of rejuvenator into RAP in order to provide sufficient reacting time between old binder of RAP and rejuvenator. Hence, closer results are likely to be obtained between plant- and laboratory- produced mixtures containing high RAP. Finally, Rathore and Zaumanis (2020) turned onto laboratory-produced mixture containing high RAP content and rejuvenator. They developed a mixing protocol including mixing time and temperature to avoid over-aging of RAP binder and the other subsequent side effect. Also, the goal of manipulating mixing process could be to have the most interaction between RAP's binder and rejuvenator. Consequently, the rejuvenator has the most effect on softening old RAP binder.

Rejuvenators are used to balance unproportioned asphaltene/maltene ration due to aging. Aging consists of mass loss of volatiles (short-term aging) and oxidation (long-term aging). Long term aging transforms chemical bonds such as Carbonyl (C=O) and sulfoxide (S=O) (Yang, You & Mills-Beale, 2015). Consequently, the portions of asphalt binder constituents including saturate, aromatics, resins (maltenes) and asphaltene change so that maltenes' aromatic with higher number of side chains transmute into asphaltene's aromatics with fewer side chains (Wei, Shull, Lee & Hawley, 1996). The resultant asphalt binder after long term aging (oxidation process) has bigger and/or more asphaltene micelle orderly dispersed within maltene phase (Wei et al., 1996). Rejuvenators add maltene into aged asphalt binder and correct the asphaltene/maltene ration. They are supposed to dissolve large asphaltene molecule into smaller size and let virgin binder diffuse in aged binder better (Zhao, Wang, Chen & Li,

2018). Additionally, in an efficient rejuvenation process, the rejuvenator is required to dilute aged asphalt binder of RAP (Behnood, 2019). Thus, colloidal structure of binder can be revived.

Most bio-based rejuvenators are well capable of diluting in binder (Cai et al., 2019) but they do not bond with binder through chemical reaction sufficiently (Sun, Yi, Huang, Feng & Guo, 2016). Diluting only leads to early loss of gained properties during rejuvenation; i.e. not stable against aging (Cai et al., 2019). Though Elkashef et al. (2017b; 2018a) indicated well-reacted and low aging potential of RAP binder rejuvenated by SBO derivative, it should be noted that the aged binder of RAP was rejuvenated under severe blending conditions (2000 rpm @160 ˚C for 45 min), which are unlikely to take place in plant mixtures production. Ma et al. (2015) applied a rejuvenator in two ways: (a) directly adding rejuvenator into asphalt mixture containing high RAP and (b) blending it with aged binder. It was revealed that, due to the non-uniform diffusion and distribution of rejuvenator throughout the RAP, poor moisture damage, cracking, and rutting resistance are observed. Increasing temperature and mixing time are the most common remedies for a higher degree of blending, uniformity and diffusion (Zhao, Huang, Shu & Woods, 2016). They are not green solutions and it is required to develop or use more efficient rejuvenators, which are capable of mingling with old binder of RAP at normal or even lower temperature and mixing time.

As mentioned before, study of rejuvenator has always been intertwined with aging. Regaining sufficient initial softness and maintaining it to an acceptable level through service life are the main issues in effectiveness of rejuvenating. Long-term aging is a chemical reaction of asphalt binder in the presence of oxygen (Oxidation) that occurs within pavements service life. It accelerates with temperature increase and decelerates with depth of asphaltic layer of pavements (Kim et al., 2018). There have been many protocols developed to simulate asphalt mixture aging (Braham, Buttlar, Clyne, Marasteanu & Turos, 2009; Yin, F., Arámbula-Mercado, Epps Martin, Newcomb & Tran , 2017; Kim et al., 2018), however, there is almost consensus on how to short- (ASTM, 2019a) and long-term (ASTM, 2019b) age asphalt binder.

Aged asphalt binder has been studied rheologically and chemically to examine effect of aging on their behavior and functional groups, respectively.

Influence of rejuvenators on RAP's aged binder before and after re-aging artificially has been studied through PG grading system (Zaumanis, Mallick & Frank, 2014b; Osmari et al., 2017; Elkashef and Williams, 2017a; Elkashef et al., 2017b; Podolsky et al., 2021). It was indicated that rejuvenators lower the viscosity of aged binder significantly (Zaumanis at al., 2015) and shift PG into lower grade; both high and low temperature grade. Complementary rheological tests incorporating traffic effects such as linear amplitude strain (LAS) (Elkashef & Williams, 2017a; Zaumanis at al., 2015), shear complex modulus master curve (Elkashef and Williams, 2017a; Elkashef et al., 2017b), multi stress creep recovery (MSCR) (Osmari et al., 2017) tests have also been performed on rejuvenated asphalt binders. Using LAS, rejuvenating aged binder by a SBO derivative showed significantly improved fatigue life compared to the binder rejuvenated by adding soft binder only (Elkashef & Williams, 2017a). It shows that, by using severe blending conditions, they arrived at stable rejuvenated binders. Organic oils have greater influence on fatigue life compared to waste engine oil (WEO) and aromatic extract (Zaumanis at al., 2015). It's also been proven by shear complex modulus master curve that rejuvenators softens binder at all frequencies or interchangeably temperatures (Osmari et al., 2017; Elkashef & Williams, 2017a; Elkashef et al., 2017b). Regarding high temperature performance, increased J_{nr} (MSCR high temperature parameter) of aged binder, similar to that of virgin binder, was obtained by rejuvenation (Osmari et al., 2017).

Apart from rheological evaluation involving aging, chemical analysis before and after aging has been carried out by researchers (Yang et al., 2015; Osmari et al., 2017; Elkashef 2018a; Cai et al., 2019). Fourier transform infrared (FTIR) has been found a handy tool to determine functional groups and chemical fingerprints in binder before and after aging. It is well-established that carbonyl (C=O @ ~ 1740 cm-1 wavenumber) index and sulfoxide (S=O @ ~1030 cm-1 wavenumber) index are indicators of asphalt binder aging (Yang et al., 2015; Elkashef et al., 2018b; Cai et al., 2019). Addition of a SBO oil derivative leads to the sudden increase of carbonyl content due to the existence of ester in it. Consequently, aging potential

of virgin and the rejuvenated aged binder were approximately the same (Elkashef et al., 2018b). Similar results by using summed up carbonyl and sulfoxide indices were obtained, which shows no different aging potential between bio-rejuvenated old binder and virgin one (Cai et al., 2019). FTIR is a very basic tool to distinguish functional groups variation and nothing can be revealed with regard to bonding of chemical components. Although, in a study by Elkashef et al. (2018a), pyrolysis gas chromatography-mass spectrometry (GC-MS) was used in lieu to FTIR for aging analysis of rejuvenated binder, the ability of this test to perform fractionated spectrometry using LC-transform and construct molecular weight distribution curve so as to determine amount of reacted rejuvenator was not used. They only realized that the SBO-based rejuvenator has good stability against aging based upon retention time (Elkashef et al., 2018a).

There are very few who turn to GC-MS for aging analysis; rather, there are quite many who utilized atomic force microscopy (AFM) to study aging of asphalt binder. It is surface analysis method that can be applied for asphalt binder before and after aging. As indicated in Figure 1.3, asphalt binder's surface topography is made up of three zones: (a) bee structure representing asphaltene, (b) transition zone representing polars like resin, and (c) flat matrix representing oily phase consisting of aromatics and saturates (Das, Baaj, Tighe & Kringos, 2016). With aging progress, the bee structure grows and expands (Das et al., 2016). Application of rejuvenator is supposed to shrink the size of the bee structure. Osmari et al. (2017) employed a digital image technique for microstructural analysis in order to compute each zone's area before and after aging. They used three rejuvenators including a commercial, namely AR, waste cooking oil and castor oil. They took bee size larger than 5 μm into account for aging potential analysis. It was found that AR has favorable capacity to prevent aging than the other rejuvenators. Yet, it has faster aging progression compared to virgin binder. Chen et al. (2018) also deployed AFM for finding impact of two rejuvenators, namely RA 100 and RA 102, on microstructure with regard to both softening and aging. They found that the rejuvenators had physical reaction with binder and did not change the bee size once introduced. Apparently, they were not capable of withstanding aging as it was not dissolved. In general, AFM is a practical, visual and effective tool to observe efficiency of rejuvenation (i.e. dissolving vs diluting) and aging process after rejuvenation.

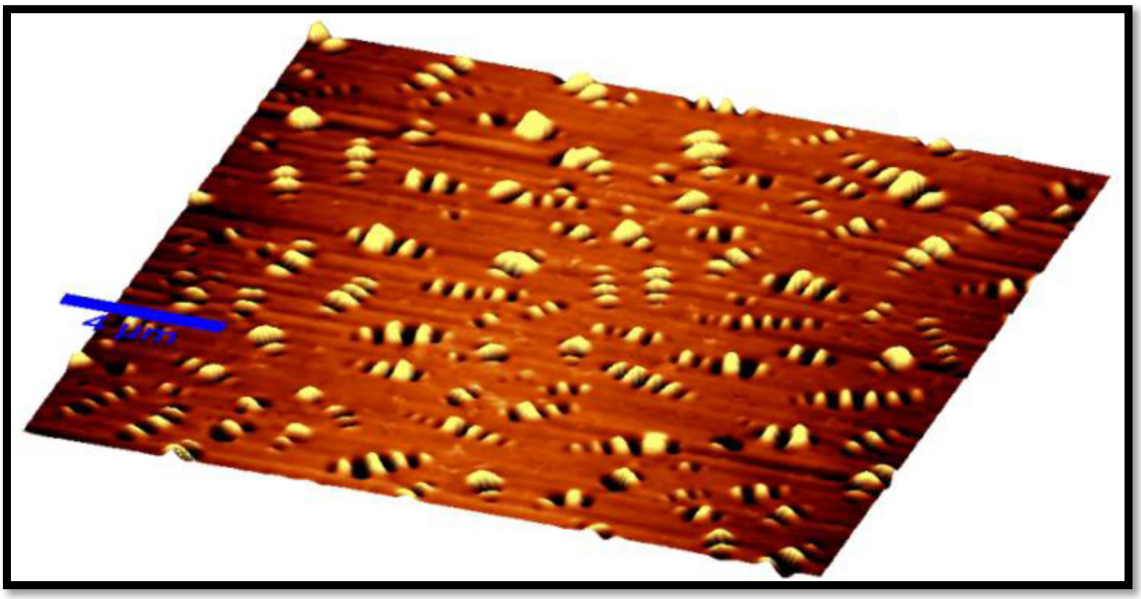

Figure 1.3 Bitumen topography of AFM taken from Villegas-Villegas & Loría-Salazar (2012, p 8)

This section elaborated on aging mechanism, protocols of short- and long-term aging of binders and mixtures, effect of aging on rheology, chemical and microscopy. It was discussed that it is important to have rejuvenator diluted and dissolved in the binders. Almost all studies used some severe blending conditions to prepare rejuvenated asphalt binder that is unlikely to take place within plant production. On the other hand, there have been studies that focused on the optimization of rejuvenation within plant production. As of now, there is no proposal for blending process of rejuvenator and binder, old and new binder, to best represent real mingling during mixing. The similarity between the binder blended and the binder inside rejuvenated mixture rheological behavior and chemical components of has not been investigated. It is essential to have a binder blending condition most representative the binder inside mixture because it can reveal the efficiency of a rejuvenator authentically. Then, the rheological and chemical analysis of modified binder reflects the reality and evolution of rejuvenators is valid.

In this research, after finding the proper blending procedure, the study of rejuvenation and its impact of asphalt binder properties can be carried out. Evaluation of rejuvenated bitumen was

done by rheological analysis. Although chemical analysis using FTIR and GC-MS is valuable for understanding the underlying reason of rheological behavior, the scope of this research is not discovering the origin of behavior. Instead, it is examining the behavior and finding the best practices of analysis.

1.5 Evolution of soybean oil (SBO) derivatives as rejuvenator

Apart from its favorable influence on rejuvenation, like bitumen, soybean is in abundance. US and Brazil are major producer of soybean. US alone accounts for one third of the total world production (Elkashef et al., 2018b). The profuse soybean has led scientists to process it for other purposes such as biodiesel (Elkashef et al., 2018b) and recycling agent of old pavements. It is renewable, bio-degradable, auspicious rejuvenator with no carbon footprint in nature. Therefore, it is worth studying and modifying it for the widespread use as a rejuvenator.

From the literature review, it is obvious that pavement engineers has been so much reliant on the materials that they received as rejuvenator rather than developing it or, at least, look for the most appropriate derivatives. There are couple of SBO-based bio-products that were developed for the target pavement application (Kurth, Nivens, Stevermer & Tabatabaee, 2019a; Kurth, Nivens, Stevermer & Tabatabaee, 2019b). Also, it was stated that bio-based rejuvenator has low dissolving capability; they mostly dilute in asphalt binder. Hence, bearing in mind that SBO has great potential to be modified and upgraded, its derivatives development apt to rejuvenation purposes so as to more dissolve in asphalt binder during mixing.

1.5.1 Soybean oil (SBO)

SBO is a triglyceride (three branches of acid) with two dominant fatty acid: Linoleic acid (-OOC(CH2)7CH=CHCH2CH=CH(CH2)4CH3) with two double-bond (about 50%) and Oleic acid (-OOC(CH2)7CH=CH(CH2)7CH3) with one double-bond (about 25%). Also, there can be found acids such as Palmitic (-OOC(CH2)14CH3) and Stearic (-OOC(CH2)16CH3) with no double-bond or Linolenic (-OOC(CH2)7CH=CHCH2CH=CHCH2CH=CHCH2CH3) with

three double-bond in the triglyceride molecules of a SBO (Guo, Cho & Petrović , 2000). Figure 1.4 illustrates the chemical structure of a typical triglyceride.

The average number of double bond per molecule (or per acid branch) is called functionality (Guo et al., 2000). Acid branches with no double-bond are called saturated acid. They are not chemically reactive since the bond between SBO and the other reactant forms via double bonds. They do not participate in chemical reactions such as gelation and epoxidization (Petrović & Cvetković, 2012). Hence, SBOs with greater average functionality are more likely to crosslink in the network of asphalt binder and using them as rejuvenator is more preferable. Furthermore, SBO with higher functionality leads to derivatives such as ESO and soy polyol with more functionality to crosslink with reactants (Guo et al., 2000).

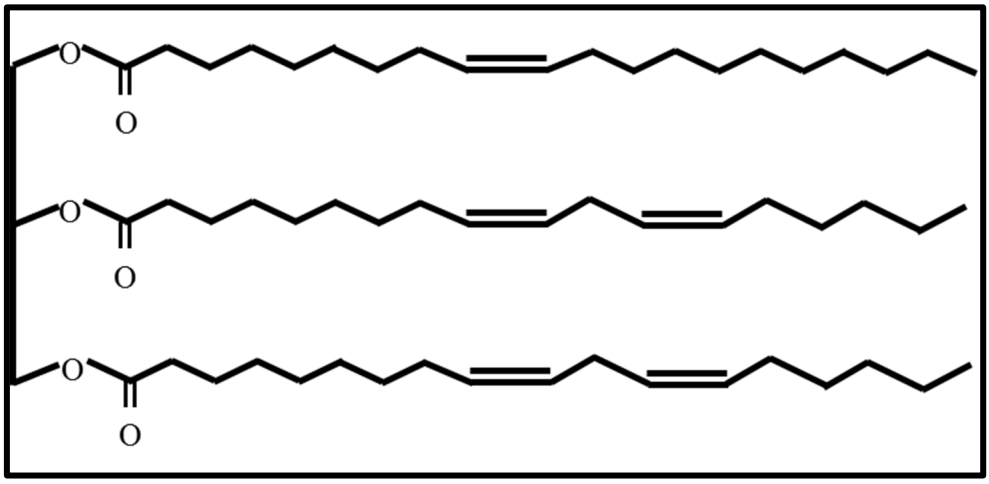

Figure 1.4 SBO chemical structure

1.5.2 Epoxidized soybean oil (ESO)

ESO is the product of oxidation of SBO by hydrogen peroxide and acetic/formic acid. The product, as depicted in Figure 1.5, is transformation of double bonds into oxirane ring, which is more chemically reactive than double bond with more compatibility with asphalt binders (Tang et al., 2018; Apostolidis, Liu, Erkens & Scarpas, 2019). Rejuvenating RAP binder involves increasing aromatic content in which colloidal asphaltene suspension stabilizes. There

can be other dispersant agent that can better dissolve asphaltene in molecular scale and stabilize asphaltene colloids (Hashmi & Firoozabadi, 2013). ESO thanks to its polar epoxy group (Kuang et al., 2018) can facilitate asphaltene dispersion (Si et al., 2020). ESO, because of its polarity, can penetrate into asphalt, dissolve asphaltene, react with unsaturated bond by its oxirane rings being opened and, consequently, render a 3D network inside asphalt binder. Thus, the asphalt binder is practically rejuvenated by oil content of ESO which leads to high thermal stability and aging performance (Yin, Wang & Lv , 2013).

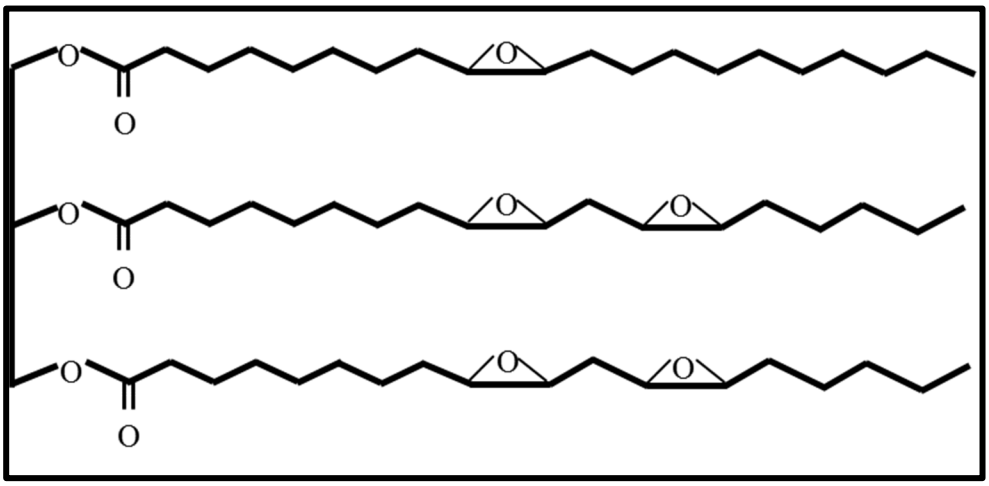

Figure 1.5 EBO Chemical Structure

1.5.3 Soy polyol

Catalyst can transform ESO into polyol to make it even more reactive. But, ESO can also be converted to polyols as an independent product by oxirane ring opening. Soy polyol is ESO oxirane ring transition to hydroxyl group (OH functional group). Fig 1.6 depicts how the polyols' chemical structure is like. The conversion of ESO into soy polyol can be done by (a) catalytic hydrogenation; (b) a reaction with hydrochloric or hydrobromic acid, resulting in halogenated polyols; or (c) an acid-catalyzed ring-opening reaction with methanol, yielding methoxylated polyol. Still, SBO itself can directly transforms into polyols. It can be hydroformylated and the resultant Aldehyde is reduced to hydroxyls (water, forming vicinal

hydroxy groups). Obviously, the polyols obtained from each approach impacts the structure-properties of any product they are going to be part of (Guo et al., 2000).

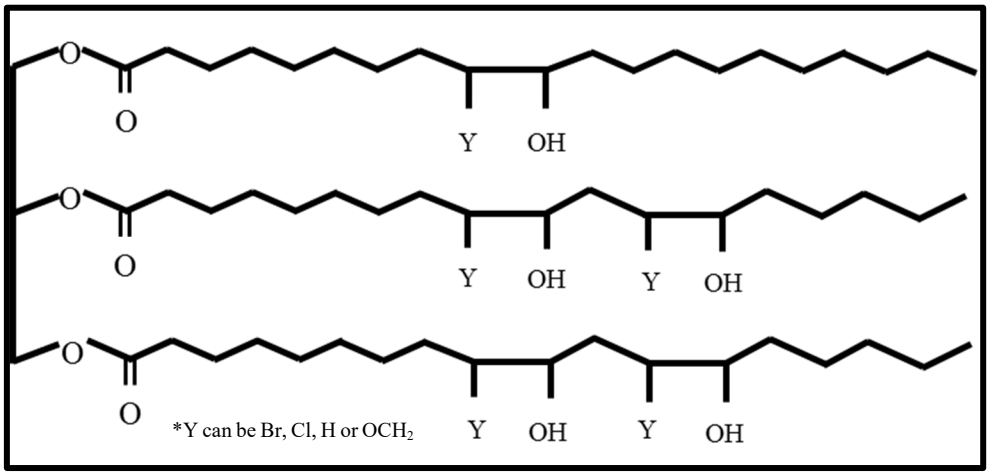

Figure 1.6 Soy polyol Chemical Structure

Halogen[2] in the structure (i.e. hydrochloric and hydrobromic acid) increases polarity, which is a desired attribute for adhesive properties as well as dissolution and dispersion of asphaltene, and lowers thermal stability[3]. Thermal stability is of great importance for asphalt modification purposes and having the greatest difference between Tg and Tc (d=Tg-Tc) is preferable. The minimum d must be equal to the span of the service temperatures. It is probably achievable. Consequently, the asphalt binder modified by soy polyol supposedly have proper thermal stability to impart both high and low temperature performance.

After crosslinking with asphalt binder, the saturated acid chains of polyol remain as pendent in the structure of modified binder and do not contribute to bear stress under load. Instead they act as plasticizer. Hence, the less the SBO has saturated acid, the better the modifier (Guo et al., 2000). It is noteworthy that oils with more saturated acid are better food stuff with regard

[2] the polar bond of hydrogen with another atom like Cl or Br is called halogen.

[3] How closely the phase change due to heating from glass transition (T_g), crystallization transition (T_c) and melting point (T_m) occurs.

to health and oils with less saturated acid are better binder modifier, but not necessarily better rejuvenator.

Table 1.1 gives the properties of polyols processed through different reagents. The processes of making these polyols are explained by Guo et al. (2000) and Petrović & Cvetković (2012).

The reaction of methanol with ESO requires catalyst acid while, for the rest, use of a catalyst is arbitrary. Fluoboric acid was found to give the most OH in the polyol. The higher the OH, the better for reactivity and adhesive properties, and the lower viscosity, which is preferred for the modification of aged asphalt binder. On the other hand, the reactions between oxirane rings and hydrochloric or hydrobromic acids is self-catalyzed, yet, since these inorganic reagents are unsolvable in ESO, organic solvent such as acetone or dioxane can be deployed. Hydrogenation of ESO oxirane ring can be catalyzed by Raney nickel (Guo et al., 2000).

Table 1.1 Polyols properties taken from Guo et al. (2000, p. 3903)

Polyol	reagent	Conversion Yield (%)[4]	Hydroxyl Number (mg KOH/g)[5]	Equivalent Weight (g/Equival-ent)[6]	Functionality[7]	Polyol M_n[8]	Physical state at room temp.
Soy-H_2	H_2	89	212	265	3.5	983	Grease
Soy-Met	CH_3OH	93	199	282	3.7	1053	Liquid

[4] Conversion means the amount of initial material (ESBO here) reacted to products while conversion yield means the amount of desired product produced from the initial material. Some papers uses selectivity which means how much of desired product was obtained in ratio to undesired one(s).
[5] hydroxyl value (or number) is the amount of Potassium hydroxide (KOH) required for neutralizing the free OH of a substance
[6] For acid-bade reactions, equivalent weight of an acid or base is the mass which supplies or react with one mole of hydrogen cations (H+). Here, it means how much ESBO is required for one mole of reagent
[7] Average double bond remained in each molecule after polyols was made.
[8] Molar weight. Each mole is $6.022*10^{23}$ molecules.

Polyol	reagent	Conversion Yield (%)[4]	Hydroxyl Number (mg KOH/g)[5]	Equivalent Weight (g/Equival-ent)[6]	Functionality[7]	Polyol M_n[8]	Physical state at room temp.
Soy-HCl	HCl	94	197	285	3.8	1071	Grease
Soy-HBr	HBr	100	182	308	4.1	1274	Grease

As expected, soy-HBr has the highest density followed by soy-HCl. This is because Cl and Br are heavy atoms and their existence in the structure weighs the molecular weight. In differential scanning calorimetry thermogravimetry, the peaks indicates the crystallization temperature (T_c) and the valley melting points (T_m). Several peaks show crystalline polymorphs. It reveals that soy-HBr and soy-HCl have more than one crystalline structure that appear one after another (Guo et al., 2000). It is a good characteristic for asphalt binders because it helps them to benefit from different crystalline structures at different temperatures. If one fades away, the others exist. Furthermore, it is known that at mid-temperature, for instance, there are both cracking and rutting so the crystalline structure that preserves its structure at mid-temperature resists against rutting while the one that is not crystal anymore contributes to the fatigue cracking resistance.

Methaxylated polyols (Soy-Met) has crystalline form at low temperatures only (-17˚C and -3˚C). So it cannot be helpful for high temperature rutting resistance of asphalt (Guo et al., 2000). Still, it can be considered quite beneficial as it is supposed to be used as rejuvenator and be mixed with an aged and hardened binder. It can be perceived that the result can give high workability of asphalt at low temperatures. With all valleys below the room temperature, i.e. all crystalline structures reaches melting temperature before room temperature, Soy-Met is liquid at room.

Hydrogenations seems promising for high temperature performance of asphalt as it preserves one of its crystalline structure in the high temperature of 50˚C. Hence, it might result in

rejuvenation with minor negative impact on high temperature performance. Yet, its capability as rejuvenator for improving fatigue and thermal cracking resistance is required to be investigated.

Chlorinated polyols seems the best for all temperatures of asphalt performance as it has peaks, i.e. crystalline forms, at low (-21˚C), intermediate (8˚C) and high (65˚C) temperatures. Yet, it does not have thermal stability because the structure changes quite often. Brominated polyol, on the other hand, behaves the same as Chlorinated polyols but within smaller temperature range; crystalline forms at low (-18˚C), intermediate (1˚C) and high (43˚C) temperatures (Guo et al., 2000). They might not stabilize in asphalt binder phase due to their heavy molecular weight as it has been proved that they do not have high thermal stability. Additionally, Chlorinated and Brominated polyols have the highest OH content that imparts higher viscosity and grease-like state at room temperature. Another important feature of these polyols is that they still act very well in the absence of crystallization since bromine and chlorine tends to form inter molecular bonds, which increase the softening point. So, they can also increase the softening point of asphalt binder and contributes to rutting resistance, which rejuvenators are not supposed to do, but if they do, it is definitely a desirable feature. In spite of not deeming as potent rejuvenators at first glance, if they stabilized in asphalt binder phase, Chlorinated and Brominated polyols may worth to be evaluated because of their crystalline structure at various temperatures and their seemingly potential positive effect on rutting performance.

Soy polyols have never been used in asphalt, though they are far more chemically reactive than ESO. Soy polys seems to be auspicious candidates as rejuvenator, especially Methaxylated polyols (Soy-Met) and Soy-H2. Cautions need to be taken as low degree of yield conversion may result in oligomerization, which Soy-Met slightly possesses. This may lead to OH functional group to be involved in ring-opening of existing oxirane rather than crosslinking with asphalt binder unsaturates.

Although soy polyols are promising, but there is no previous study on their application as recycling agent of RAP. Here, a detailed introduction to soy polyols, their weaknesses and

potentials, is provided for future studies. But, in this study, epoxidized soybean oil (ESO) as a popular derivative of soybean oil (SBO) was used since the scope of research cannot contain studying soy polyols. ESO is more chemically reactive than SBO and many studies have proved its efficiency in rejuvenating old RAP bitumen. Findings of previous research were deployed for its application.

1.6 Summary

The feasibility to increase RAP content in asphalt mixtures without compromised performance relies on (a) balanced mix and (b) recycling agents (Cantrell, Wen & Wang, 2022). Some States DOTs such as NJDOT and WSDOT allow application of higher RAP contents in condition that balanced mix design is used (Hand & Aschenbrener, 2021). Therefore, this study begins with developing guidelines for a balanced mix design dedicated, but not limited, to asphalt mixtures with very high RAP contents.

Recycling agent is a must once the amount of RAP increases. As stated within the literature, there have been many studies on recycling agents and this research has deployed one of the well-proved one. It is epoxidized soybean oil (ESO) that is bio-sourced and in abundance in the nature. Although the efficiency of ESO has been studied a lot (Elkashef et al., 2017a; Elkashef et al., 2017b; Elkashef et al., 2018a, Elkashef et al., 2018b, Podolsky et al., 2021), the main focus of the studies so far were on bitumen. This study focuses more on mixture and similarity of the binders inside the mixtures and those blended.

The advanced testing and analysis for characterization and fatigue life analysis of asphalt mixtures prepared based upon the developed balanced mix design guidelines will reveals not only the effectiveness of the mix design but also the ESO.

CHAPTER 2

RESEARCH OBJECTIVE AND PLAN

2.1 Problem statement

Within the previous chapter, the findings and gaps in the research works focusing on asphalt binders and mixtures containing high RAP content was laid out. Mostly, studies aimed at softening RAP's binder via rejuvenation. Achieving soft enough asphalt binder means solving the main concern of asphalt mixtures with high RAP content: cracking. There have been achievements on it that is deployed in this study. However, gradation is another influential aspect of asphalt mixtures performance that not only does it impact cracking, but, most importantly, it also has major effects on rutting potential. It has been less under scrutiny for the mixtures with high RAP contents.

Once the amount of RAP increases, it becomes less efficient to, first, sieve it into fine and coarse stockpiles and, then, apply them in proportions that less deteriorates the target gradation. Therefore, this thesis set the goal to rectify the gradation of RAP, as is, in the asphalt mixtures in which the amount of RAP is predominant; i.e. more the 50%. In other words, the RAP is not fractionated into fine and coarse in asphalt mixtures with very high RAP contents (>50%); rather, the gradation of RAP is corrected through introduction of virgin aggregates. This is the efficient approach of treating very high RAP content asphalt mixture. Fractionation of RAP is laborious and results in huge fine RAP leftovers.

Gradation vary depending on the aggregate blend type and gradation of RAP. Aggregate blend type can be fine dense-graded (FDG), coarse dense-graded (CDG), stone matrix asphalt (SMA), and open graded. Gradation of RAP can be taken as black curve (RAP gradation), white curve (RAP aggregate gradation), or the average of the formers. Subsequently, there can be different aggregate blends that all can be favorable. Mix design standards takes binder content as variable to arrive at specific volumetric properties. In this thesis, after arrival at the

specific volumetric properties for each gradation, it is the gradation that is taken as variable. The literature on mix design place emphasis on the balanced mix within which the performance determines the optimum mixture. Yet, current balanced mix design procedures are more qualitative rather than quantitative. Also, the high RAP inclusion requires taking aging potential into account. It was clarified in the literature review that aging is a primary concern of asphalt mixtures with high RAP content. Therefore, although the aggregate blends are designed to give good gradation with firm aggregate structure, their performance need to be evaluated in order to find the best with regard to all aspects of performance. This requires an index incorporating all aspects of performance.

The gradation and mix design are the initial steps of any research. There are advanced characterization and performance testing and analysis that reveals a lot about mixtures. Aligned with the gradation evaluation, it is important to know if asphalt binder behavior can reflect the mixture behavior. It shed light on the effect of gradation on behavior. There are studies that attribute the behavior of asphalt mixture to asphalt binder (Mangiafico et al., 2013). If asphalt binder projects the behavior of the total mixture, the role of gradation is negligible. So, it is a big problem to find whether or not the gradation is impactful on asphalt mixture's behavior.
It was stated that a big portion of studies on asphalt mixtures with high RAP content focuses on asphalt binder. The investigation of the effectiveness of rejuvenation requires virgin asphalt binders combined with RAP binder and rejuvenator. That combination is a matter of study that has not been inspected sufficiently. The combination of rejuvenator, virgin and RAP binder must be representative of their combination inside asphalt mixtures. Then, the study of rejuvenated binder is authentic.

Finally, asphalt mixtures containing high RAP contents are prone to early cracking. Once it comes to very high RAP content, the deficiency, of course, exacerbates. Any study dealing with RAP involvement should look into cracking resistance. Fatigue cracking is the most complicated distress in asphalt mixtures. Analyzing it can be done by simple analysis of Wöhler curve or the advanced approach of visco-elastic continuum damage (VECD). Both can

be applied to see how influential the gradation can be on fatigue life as the primary concern of asphalt mixtures containing very high RAP content.

2.2 Research objective

The main objective of this thesis is development of a mix design guidelines for high performance asphalt mixtures containing very high amount of RAP (>50%). Five problems have been outlined within the former section. These problems are the backbones of the research objectives of this thesis. As a result, the objectives of this thesis are:

(a) Correction of RAP gradation to restore the aggregate structure by adding virgin aggregates
(b) After finding the optimum asphalt content (OAC) for different aggregate blends, determining the optimum aggregate blend based upon all aspects of performance using an integrated performance index (PI)
(c) Comparing mechanical characteristic of asphalt binder and mixture to observe if the gradation has impact on behavior of asphalt mixture containing high amount of RAP
(d) Finding the blending conditions within which the combination of rejuvenator, virgin and RAP binder represents the asphalt binder in the mixture with high RAP content the most
(e) Investigating the fatigue performance of asphalt mixtures with very high RAP contents using classical and visco-elastic continuum damage (VECD) analysis to see the impact of gradation and rejuvenation on fatigue life and, also, find which method is more compatible for analyzing fatigue performance of this type of mixture

Each of the following chapter is dedicated to one objective above. All subsequent chapters deal with rejuvenated asphalt mixtures with very high RAP contents: from design to performance. Each chapter is a paper that is published or accepted in a scientific journal, or submitted to one.

2.3 Research plan

This thesis can be divided into two parts: (a) mix design and (b) evaluation the mix design. The first two chapters (chapter 3 and 4) are for designing asphalt mixtures with very high RAP content. Then, chapter 5, 6, and 7 evaluates the characteristics and performance of asphalt binders and mixtures.

The first step of mix design after controlling material properties is particle size distribution of aggregate. RAP contains mostly fine aggregates due to coarse aggregates break-down under traffic load during service as well as being scratched for removal. Simply, the gradation of RAP is not good. It requires restoration and restoration requires virgin aggregates. Adding virgin aggregate is made using Bailey method concept. Bailey method is well-established method for aggregate blend design so as to build up a firm aggregate skeleton that is capable of bearing and distributing load properly. The problem with Bailey method is that it is not devised for asphalt mixtures with very high RAP content. In other words, it is not used for correcting an existing distorted aggregate blend. It is for blend design from the beginning by proportioning aggregate stockpiles. Still, its concepts can be used for restoring a bad gradation. So chapter 3 is dedicated to apply Bailey concepts to rectify the gradation of RAP. Several aggregate blends based upon different assumptions are designed and the effectiveness of the Bailey method concepts for restoring gradation is examined through indirect tensile (IDT) strength and laboratoire des ponts et chaussées (LPC) wheel tracking tests.

Once the preliminary evaluation of the aggregates blends proves efficiency of the method. An integrated performance index (PI) incorporating different performance aspects of asphalt mixtures containing very high amount of RAP is introduced in chapter 4. The performance aspects include rutting, moisture damage, cracking and aging resistance. Simple tests of LPC wheel tracking, Marshall stability, semi-circular bending (SCB) strength are deployed and performed on different specimen types. The PI ranks the mixture types based upon their general performance and is used to find the best mixture among others performance wise.

The performance evaluation done by simple testing program requires deeper and more advanced examination. First and foremost, it should be verified that the difference in performance is also rooted in the variation in gradation; not only as a result of variation in RAP binder. Therefore, dynamic complex modulus test is performed on both asphalt binders and mixtures. In chapter 5, comparison between Cole-Cole, Black space, phase angle and complex modulus master curves of binder and mixture is made to find the origin of the behavior of mixture.

Performance and rheological characteristics of asphalt binder is studied in chapter 6. The binder of the asphalt mixture with the best performance and characteristic from previous chapters is taken for rheological analysis. Asphalt binder extracted and recovered and the one prepared under different blending conditions are compared to find the blending condition that results in the rheological properties most similar to the asphalt binder extracted and recovered form asphalt mixture. As a result, not only does the rheological properties of the rejuvenated asphalt binder containing very high amount of RAP is examined, but the best blending condition that represent the asphalt binder inside asphalt mixture is also found. The testing program comprises PG tests, MSCR, LAS, linear visco-elastic (LVE) limit and complex dynamic modulus frequency and temperature sweep.

Since cracking is the main concern when the percentage of RAP increases, chapter 7 is dedicated to fatigue life of different asphalt mixtures containing different percentages of RAP. There are classical and VECD approach for fatigue life analysis. After determining the LVE limit of different asphalt mixtures at the frequency of 10 Hz and the temperature of 10˚C, the frequency and temperature at which tension/compression (T/C) fatigue test is usually performed (Perraton, Baaj & Carter, 2010), the T/C fatigue test was performed on different mixture types. Classical approach defines the fatigue life based upon any of the followings:

(a) 50% reduction in initial stiffness,
(b) maximum of phase angle (φ_i)
(c) phase angle difference ($\Delta\varphi_i$),

(d) axial strain difference ($\Delta\varepsilon_{iax}$), and
(e) accumulated viscous dissipated energy ratio (DER)

On the other hand, VECD is the analysis based upon intrinsic fatigue property of visco-elastic materials. In addition to classical approach, VECD analysis is conducted on T/C fatigue test results to gain deeper insight toward fatigue performance of asphalt mixtures with very high RAP contents. Also, it is possible to understand which method is more compatible with this type of mixture.

All the attempts of this thesis are focused on the mix design of RAP-dominant asphalt mixture. Aggregate blends are designed according to Bailey method concepts. Optimum asphalt contents (OAC) of the aggregate blends are determined based upon volumetric properties and, then, ranked with accordance to general performance expressed by PI. Comparison the behavior of asphalt binders and mixtures is made through SHStS transformation to check if the variation in performance is due to variation in gradation. Rheological behavior and performance of asphalt binder are also studied to find the impact of rejuvenation on them. Furthermore, the best blending conditions of rejuvenator, RAP and virgin asphalt binder are found for future works on rejuvenation. Fatigue life as the primary weakness of RAP-predominant asphalt mixture is investigated using classical and VECD methods. Figure 2.1 summarizes the structure of this thesis and how the objectives of this research work is carried out.

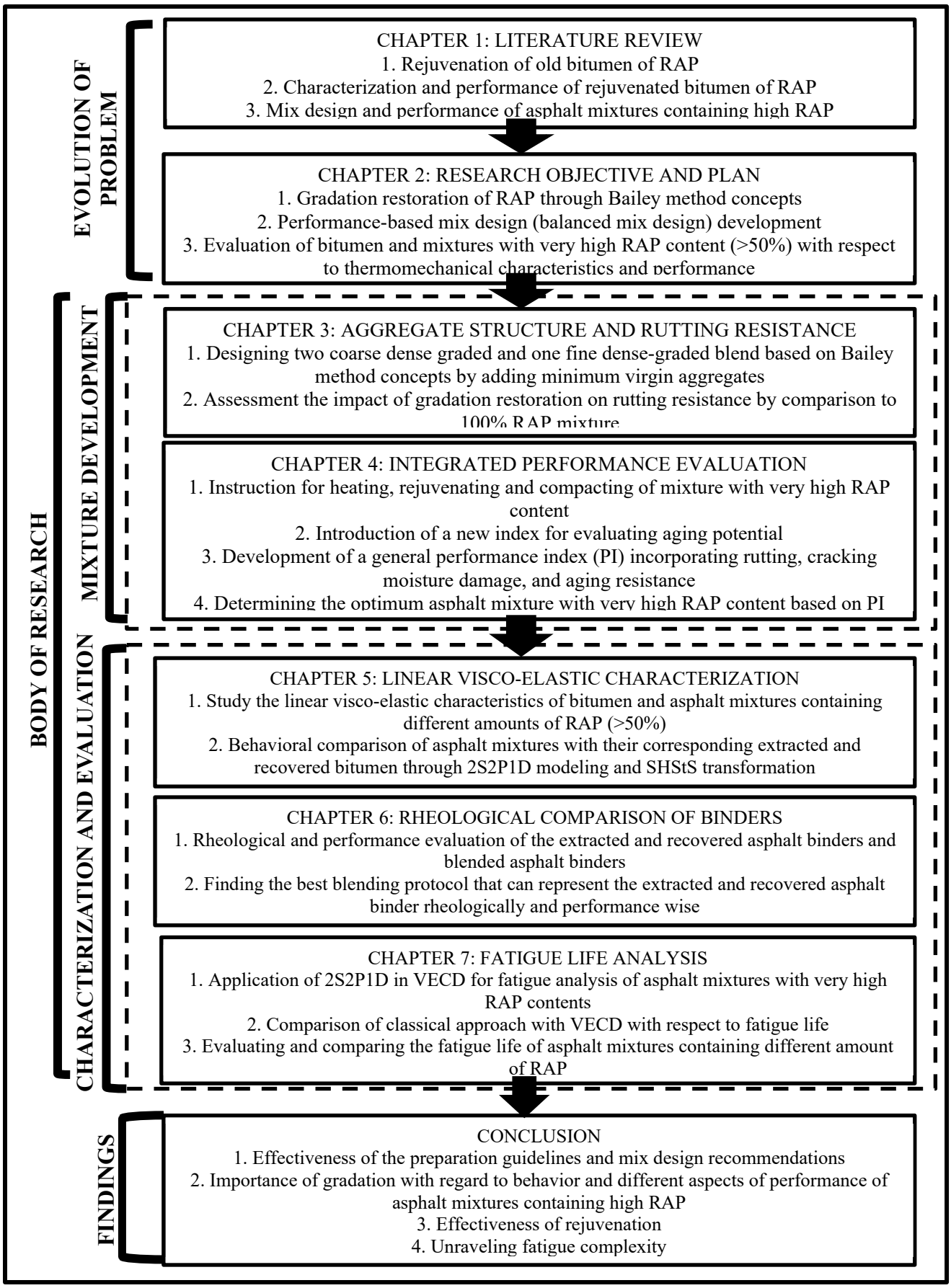

Figure 2.1 Scheme of thesis

CHAPTER 3

IMPACT OF AGGREGATE STRUCTURE RESTORATION ON RUTTING RESISTANCE OF ASPHALT MIXTURES WITH VERY HIGH PERCENTAGES OF RAP

Reza Imaninasab[a], Luis Loria-Salazar[b], Alan Carter[a]

[a] Construction Engineering Department, École de technologie supérieure, 1100 Notre-Dame St W, Montreal, QC H3C 1K3, Canada.
[b] Universidad Isaac Newton, Av. 7 13, Paso De La Vaca, San José, Costa Rica.

Paper published in the Journal of Road Materials and Pavement Design, March 24, 2023, 1-17.

3.1 Abstract

Bailey method is a well-proved method to build strong aggregate structure, but it is originally devised to do so by proportioning the fractionated virgin aggregate stockpiles. Yet, the concepts of strong aggregate structure in the Bailey method stand true in any type of aggregate. This study develops a method for correcting the bad gradation of RAP by utilising Bailey's concepts. The virgin aggregate stockpiles are added minimally into RAP to establish a firm aggregate skeleton. This changes the philosophy of aggregate blend design from the RAP following an existing good gradation to the RAP gradation correction. The effectiveness of the method was evaluated by the indirect tensile (IDT) strength and laboratoire des ponts et chaussées (LPC) wheel tracking tests. The mixtures whose gradations were rectified by this method, whether coarse dense-graded (CDG) or fine dense-graded (FDG), have significantly higher rutting resistance than 100% RAP mixture.

3.2 Introduction

Increasing the amount of reclaimed asphalt pavements (RAP) in new pavements is favorable (Norouzi et al., 2014). However, high RAP content can decrease cracking resistance (Norouzi, Sabouri et al., 2014) and it can also result in a weak aggregate skeleton in asphalt mixtures.

Many studies have been conducted to alleviate the detrimental impact of high RAP on cracking (Al-Qadi, Aurangzeb, Carpenter, Pine & Trepanier, 2012; Hajj, Souliman, Alavi, & Salazar, 2013; Zaumanis et al., 2015). Effective rejuvenation, as the most popular solution to tackle the cracking deficiency of asphalt mixture with very high RAP content, has been investigated through different recycling agents and methods of application (Zaumanis et al., 2015; Elkashef et al., 2017b). The findings of previous studies on rejuvenation of high RAP content mixtures were applied for rejuvenating the asphalt mixtures of this study and the focus was placed on the development of a method that can restore the strong aggregate structure with the minimal effort and use of raw resources (virgin bitumen and aggregates).

The majority of pavement researchers believes that rutting is not of any concern in asphalt mixtures with high RAP content (Gong, Huang & Shu, 2018). This is mostly true because the bitumen of this mixture type is stiffer than the conventional mixtures with low RAP content; it is due to the higher portion of RAP's bitumen in total bitumen (Al-Qadi et al., 2012). But it must also be taken into account that aggregate skeleton is the main load bearer and paying attention to it can further improve rutting resistance of asphalt mixtures containing high RAP. Sufficient stone-on-stone contacts are required in order to construct a firm aggregate skeleton that is capable of distributing loads properly (Coenen, Kutay, Sefidmazgi & Bahia, 2012).

The Bailey method has been developed to combine virgin fine and coarse stockpiles to ensure proper gradation with sufficient stone-on-stone contacts. However, it does not recommend the application of (i) RAP content greater than 40% and (ii) RAP with gradation different from the aggregate blend designed based on virgin aggregate stockpiles (Vavrik et al., 2002). In other words, prior to introduction into the already designed virgin aggregate blend, RAP stockpile must be first sieved and, then, mixed in a proportion that results in the gradation close to the existing blend (Aurangzeb et al., 2012). The blend design in Bailey's method is always based on virgin aggregates and RAP follows the gradation. Not only is this practice laborious, but it is also inaccurate since RAP is a different aggregate type with different volumetric properties. Additionally, deviation from the gradation of the blend designed based upon Bailey method exacerbates once it reaches 50% (Aurangzeb et al., 2012). In short, the Bailey method cannot be applied to a RAP-predominant asphalt mixture to fix the gradation problem, although it has

a strong philosophy and good reputation. Bearing in mind that the amount of RAP is exceeding in asphalt mixtures, this study mainly focuses on the development of a method that rectifies the gradation of RAP with no need for fractioning and with the least amount of virgin aggregates used as possible. The philosophy behind the Bailey method is deployed in the new method but the focus is on RAP instead of virgin aggregate. The examination of the effectiveness of the method limits to rutting performance. More results that prove the efficiency of the methodology developed here can be found in the research work by Imaninasab, Loria-Salazar & Carter (2022).

3.3 Materials and Methodology

In addition to 100% RAP, aggregate blends including two coarse dense-graded (CDG) and one fine dense-graded (FDG) based upon the Bailey concepts were designed out of the available RAP by adding virgin aggregates. Then, optimal bitumen contents (OBC) were determined according to volumetric properties. The details on how volumetric design must be modified for the asphalt mixtures with very high RAP content (>50%) is given in the research work by Imaninasab et al. (2022). Finally, the rutting performance of different mixtures containing very high RAP was evaluated by the Laboratoire des Ponts et Chaussées (LPC) wheel tracking test and indirect tensile (IDT) strength tests. As a result, it can be understood that the correction of RAP's gradation by the new approach based upon Bailey concepts is effective.

3.3.1 Aggregates, RAP, and bitumen

Table 3.1 presents the physical properties of the virgin and RAP aggregates used in this study. In addition to coarse (5-14 mm) and fine (0-5 mm) virgin aggregates, a fine modifier aggregate sizing 0-2.5 mm was extracted from the fine (0-5 mm) to further correct the gradation of RAP (0-10 mm).

The bitumen content of RAP was found to be 4.9% using ignition oven as per ASTM D6307-19 (2019c). Also, using extraction and recovery as per ASTM D8159-19 (2019d) and ASTM

D5404/D5404M (2021), respectively, the PG+ of RAP bitumen was determined as a PG88S-16. A soybean oil derivative was utilized as recycling agent and a PG58S-28 was the virgin bitumen used for fabricating asphalt mixtures with very high RAP content. The ratio of recycling agent to RAP bitumen (by weight) was calculated as 1.154%. This dosage leads to recycling agent to total bitumen ratio of 1% at 100% RAP mixture, which has been proved effective for rejuvenating old bitumen of RAP (Elkashef et al., 2017b).

Table 3.1 Physical properties of the virgin and RAP aggregates

	RAP			Virgin aggregates		
	Coarse (5-10 mm)	Fine (2.5-5 mm)	Fine (0-2.5 mm)	Coarse (5-10 mm)	Fine (2.5-5 mm)	Fine (0-2.5 mm)
G_{sb}[1]	2.694	2.667	2.660	2.714	2.707	2.694
G_{SSD}[1]	2.721	2.704	2.693	2.734	2.728	2.720
G_{se}[1]	2.769	2.769	2.749	2.770	2.766	2.766
Absorption (%)	1.00	1.38	1.22	0.74	0.79	0.97

[1] **G_{sb}: bulk specific gravity, G_{SSD}: bulk saturated surface dry specific gravity, G_{se}: effective specific gravity**

3.3.2 Aggregate blends design

The aggregate blend design was done based on coarse dense-graded (CDG) and fine dense-graded (FDG) presented in the Bailey method, but the approach to arrive at them from 100% RAP by adding virgin aggregates is devised in this study.

3.3.2.1 Coarse dense-graded (CDG)

Design of the CDG blend is done in two steps. Step one consists in proportioning stockpiles and the step two is checking if the blend obtained satisfies the ratio limits of coarse and fine parts. For better understanding, Figure 1.1 shows the algorithm developed for the CDG blend design once RAP is dominant. It conforms to the Bailey definitions and will be explained in details within steps #1 and #2. Notably, correction based on Bailey method (Vavriket al., 2002) is required if coarse stockpile contains fine aggregates and/or fine stockpile contains coarse aggregates.

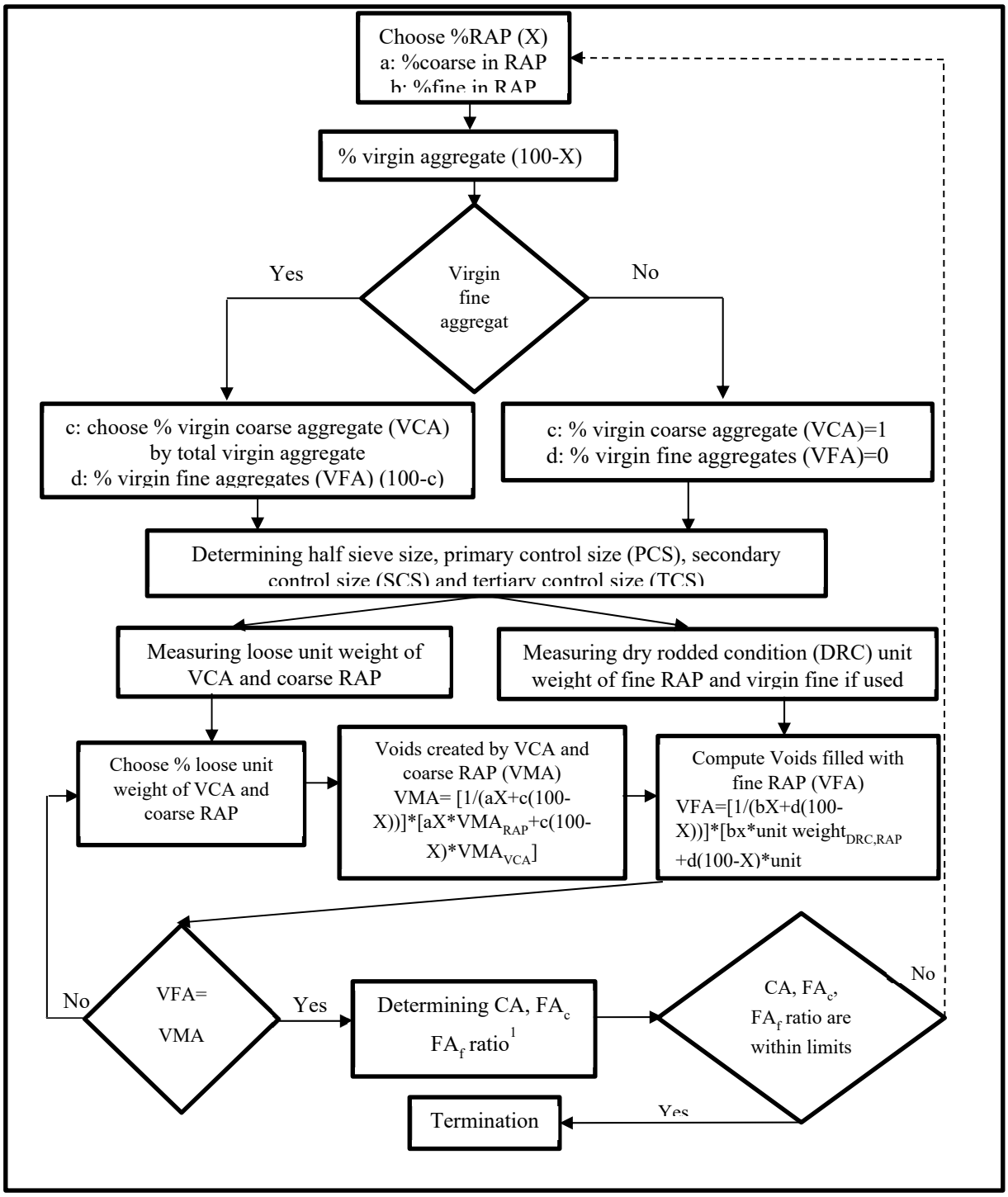

[1] **CA: Coarse aggregate, FA_c: coarse part of fine aggregate, and FA_f: fine part of fine aggregates**

Figure 3.1 Algorithm of design of coarse-dense graded (CDG) containing very high RAP

Step#1:

In CDG, coarse aggregates form a skeleton whose space (voids) is filled with finer portions. Based on the Bailey method, coarse aggregates are particles larger than 22% of the nominal maximum aggregate size (NMAS) in an aggregate blend (Vavrik et al., 2002). The closest sieve size to 22% NMAS is called primary control sieve (PCS). The voids created by coarse portion of an aggregate blend can be determined by Equation (3.1):

$$VMA = a_1\left(1 - \left(\frac{chosen\ unit\ weight}{G_{sb,1}}\right)\right) + a_2\left(1 - \left(\frac{chosen\ unit\ weight}{G_{sb,2}}\right)\right) + \cdots + a_n\left(1 - \left(\frac{chosen\ unit\ weight}{G_{sb,n}}\right)\right) \quad (3.1)$$

Where: VMA is void in mineral aggregates of the coarse part of the blend, G_{sb} is bulk specific gravity; a_1, a_2, … a_n is the percentages of each coarse aggregate stockpile by the total weight of coarse aggregates; and chosen unit weight is a percentage of loose unit weight of coarse aggregate (Equation (3.2)) that is selected by the designer within the design procedure. It must be between 95-105% to ensure the sufficient interlock of coarse aggregates (Vavrik et al., 2002).

$$chosen\ unit\ weight = \%chosen \times loose\ unit\ weight\ (Coarse) \quad (3.2)$$

Apparently, the higher the chosen unit weight, the higher the compacted blend, the less voids in coarse aggregate, and, subsequently, the less fine aggregate requirement for filling voids. Finding the correct chosen unit weight does not mean that the final mixture has the same unit weight of coarse aggregate as the chosen unit weight is an iterative process (Figure 1.1) and it does not necessarily equals the unit of coarse aggregate in asphalt mixture.

The dry rodded condition (DRC) unit weight of the fine portion is used for determining the amount of fine needed for filling the void created by the coarse portion (Equation (3.3)).

$$fine\ aggregate\ amount = VMA \times (a_1 \times DRC\ unit\ weight\ (Fine_1) + a_2 \times DRC\ unit\ weight\ (Fine_2) + \cdots + a_n \times DRC\ unit\ weight\ (Fine_n)) \quad (3.3)$$

Where: a_1, a_2, a_n are the percentages of each fine aggregate stockpile by the total weight of fine aggregates.

Unlike the Bailey method, since this study deals with correction of RAP gradation, there is no fine and coarse stockpiles in which one(s) creates voids and the other(s) occupies it. Instead, there is a distorted gradation containing both coarse and fine particles that requires virgin coarse aggregates (VCA) and fine ones (if used) to help generate firm aggregate structure. So, the following steps are taken:

1) Measuring the loose unit weight of VCA (Table 2).
2) Fractionating RAP into coarse and fine aggregate, so the loose unit weights of the coarse fraction of RAP and the DCR unit weight of the fine fraction of RAP stockpile can be measured (Table 3.2).
3) Choose a proportion of RAP, VCA, and virgin fine aggregates if used.
4) In the first trial, an arbitrary percentage between 95-105% is chosen to compute unit weights for both coarse fraction of RAP and VCA using Equation (3.2).
5) Using Equation (1), the VMA created by VCA and coarse RAP is calculated.
6) It is checked if the fine portion of RAP and virgin fine aggregate (if used) exactly fills the voids created by VCA and RAP's coarse fraction.
7) If not, which is very likely for the first trial, another percentage between 95 to 105% is chosen until, if any, the fine fraction of RAP becomes the amount that is capable of filling voids created by virgin and coarse RAP at the proportion of RAP, VCA and virgin fine aggregates, if used.
8) Once the proper percentage is found, steps 3 through 7 are done for another blend with another proportion of RAP, VCA and virgin fine aggregates if used.

9) Finally, possible combinations of RAP, VCA and virgin fine aggregates (if used) with a chosen unit weight satisfying conditions in step 6 can be plotted and the desired RAP content can be selected (Figure 3.2).

Figure 3.2 shows percentage of fine and coarse particles including virgin aggregates and RAP together (total 100%), along with the percentage of RAP and virgin aggregate (total 100%) vs chosen unit weight for one of the CDG blends. It can be observed that the RAP content decreases when chosen unit weight increase. Since all chosen unit weights meet the requirements of step #1 and the aim is inclusion of maximum RAP possible, 96% of the loose unit weight is selected in order to have highest possible RAP content for CDG. Although 95% of the loose unit weight has higher RAP, it is the boundary of limits and it is better to avoid boundaries, especially once the variation is not significant. However, the chosen unit weight for the other CDG blend was found 105% of loose unit weight since it was the only one that fulfills the Bailey requirements the best.

Table 3.2 Loose and DRC unit weights

Unit weight	Fine RAP (0-2.5 mm)	Coarse RAP (2.5-10 mm)	Coarse agg. (5-10 mm)	Fine agg. (2.5-5 mm)	Fine agg. modifier (0-2.5 mm)
Loose (kg/m^3)	-	1394.3	1470.5	1400.3	-
DRC (kg/m^3)	1302.6	1495.8	1595.2	1533.6	1747.1

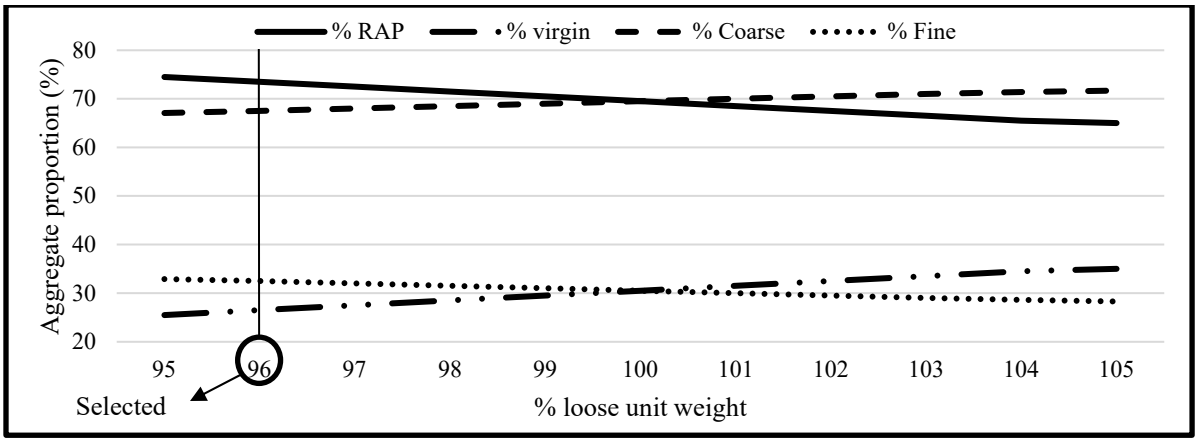

Figure 3.2 Aggregate proportioning based on % chosen unit weight for one of the CDG blends

Step#2:

The Bailey method divides fine particles into two categories of coarse and fine for further analysis and control. So, technically, there are three parts in an aggregate blend: Coarse aggregate (CA), coarse part of fine aggregate (FA_c), and fine part of fine aggregates (FA_f). The boundaries of these three parts are defined by two sizes, namely primary control sieve (PCS) and secondary control sieve (SCS), respectively. Moreover, there are tertiary control sieve (TSC) and half sieve that is used for ratio analysis within FA_f and CA, respectively (Vavrik et al., 2002). Through Equations (3.4) to (3.7) PCS, SCS, TCS and half sieve can be determined, respectively.

$$PCS = 0.22 \times NMAS \tag{3.4}$$

$$SCS = 0.22 \times PCS \tag{3.5}$$

$$TCS = 0.22 \times SCS \tag{3.6}$$

$$Half\ sieve = 0.5 \times NMAS \tag{3.7}$$

Since PCS, SCS and TCS do not yield exactly the standard sieve sizes, the closest sieve sizes to these values are taken into account. In order to examine balanced proportioning within CA, FA_c, and FA_f parts, ratios for each part are calculated through Equations (3.8) to (3.10). For FA_c and FA_f ratio, the limit range is 0.3-0.5 and, for CA ratio, it depends on the blend's NMAS (Vavrik et al., 2002). These limit ranges ensure that finer particles of each part, namely interceptors, are not too abundant to use the space among coarser ones and, consequently, hinder firm skeleton formation.

$$CA\ ratio = \frac{\%passing\ half\ size - \%passing\ PCS}{100 - \%passing\ half\ size} \tag{3.8}$$

$$FA_c ratio = \frac{\%passing\ SCS}{\%passing\ PCS} \tag{3.9}$$

$$FA_f ratio = \frac{\%passing\ TCS}{\%passing\ SCS} \tag{3.10}$$

Since the Bailey method deals with virgin aggregate, there is only one gradation curve, but the use of RAP involves two gradations: white curves (RAP aggregate gradation after bitumen extraction) and black curve (RAP gradation). The ratios above can be calculated based upon (i) white curves, (ii) black curves and (iii) the average of (i) and (ii). In this study, (i) and (iii) were only used since (ii) represents the state that RAP acts as rocks and does not let other aggregates indent through old bitumen film during mixing in plant. This is unlikely to take place. Therefore, in this study, it must be decided which gradation must be considered for the ratios proposed by the Bailey method in order to have the highest rutting performance.

Figure 3.3 shows that, using the average of black and white curves (namely RAP in Figure 3.3), the specifications regarding FA_c and FA_f proposed by Vavrik et al. (2002) are met whereas using the white curve (namely RAP agg. in Figure 3.3) does not work at all. Therefore, for the blend design based on the white curve, fine aggregate modifier (0-2.5 mm) was deployed to correct the gradation of the fine part. Figure 3.3 indicates, in the absence of fine

aggregate modifier, how far out of the limit range FA_c ratio can be, even though CA and FA_f ratios are OK. Table 3 gives the final CDG blends design and it can be observed the fine modifiers alleviate the outlying FA_c ratio significantly.

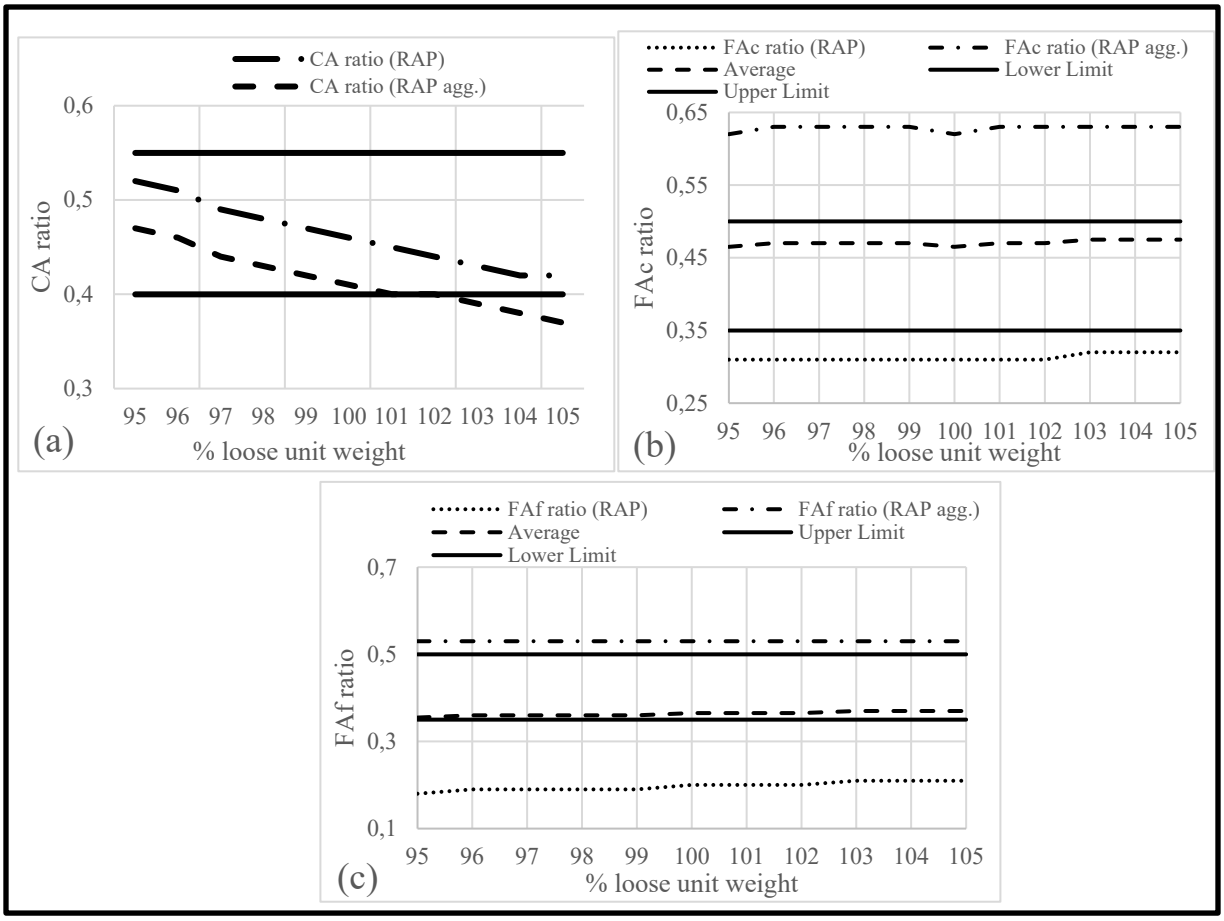

Figure 3.3 (a) CA, (b) FA_c, and (c) FA_f ratio vs. %loose unit weight

Table 3.3 Bailey characteristics of CDG blends

	Selected % loose unit weight	CA ratio	Limits[1]	FAc ratio	Limits[1]	FAf ratio	Limits[1]
Average gradation based (black and curve)	96	0.51	0.40-0.55	0.47	0.35-0.50	0.36	0.35-0.50
RAP agg. gradation based (white curve)	105	0.46		0.53		0.53	

[1] Vavrik et al. (2002)

3.3.2.2 Fine-dense graded (FDG)

Fine-dense graded (FDG) is another popular aggregate blend that the Bailey method introduces. In FDG, coarse aggregates are dispersed in the sea of fine portions. It was found that chosen unit weight of less than 90% of loose unit weight of coarse aggregates is low enough for missing coarse aggregate skeleton and formation of FDG. Lower chosen unit weight means more fine particles (Vavrik et al, 2002) and the aim here is to incorporate the most coarse aggregate for rutting potential purposes; i.e. highest chosen unit weight possible. It has a fine part dominance and no calculation is required for assuring coarse part skeleton, i.e. no step #1 as for CDG. Instead, in addition to checking CA, FA_c, and FA_f ratios of the whole aggregate blend, the fine part is taken as an independent blend and CA, FA_c, and FA_f ratios of the fine part is also checked with proposed limits. This type of blend is easier with regard to calculation but harder to achieve. For FDG, only average of black and white curve was considered. Table 3.4 shows the final results of ratios with respect to the total blend and fine part for the designed FDG. It includes ratios of black and white curve based ratios along with the averages that only the average have all ratios fell within the proposed limits by Vavrik et al. (2002). So, for FDG, only the average of black and white curve was considered. Good to note that it was impossible with the available stockpile to arrive at the proposed ratios by the

Bailey method. It is 85% of loose unit weight as the highest chosen unit weight of coarse aggregate possible that satisfies Bailey method requirements.

Table 3.4 Bailey characteristics of FDG blends

Selected % loose unit weight	85					
	Coarse portion			Fine portion		
	CA ratio	FA_c ratio	FA_f ratio	CA ratio	FA_c ratio	FA_f ratio
RAP gradation based (black curve)	0.56	0.30	0.26	0.99	0.36	-
RAP agg. gradation based (white curve)	0.53	0.56	0.53	1.09	0.51	-
Average	0.54	0.43	0.40	1.04	0.44	-
Limits[1]	0.4-0.55	0.35-0.50	0.35-0.50	0.6-1.0	0.35-0.50	0.35-0.50

[1] Vavrik et al. (2002)

3.3.2.3 Aggregate blends gradations

Table 3.5 gives the proportions for two types of CDG and one FDG type that yields the final gradations depicted in Figure 3.4. Restoration of aggregate structure gives closer gradation to maximum density line (MDL).

Table 3.5 Type of blends along with percentages of stockpiles used

	RAP %	Coarse (5-14 mm) %	Fine (0-5 mm) %	Fine modifier (0-2.5 mm) %
Whole-RAP	100	0	0	0
CDG (average-based)	73	27	0	0
CDG (white curve-based)	65	23	0	12
FDG	57	30	13	0

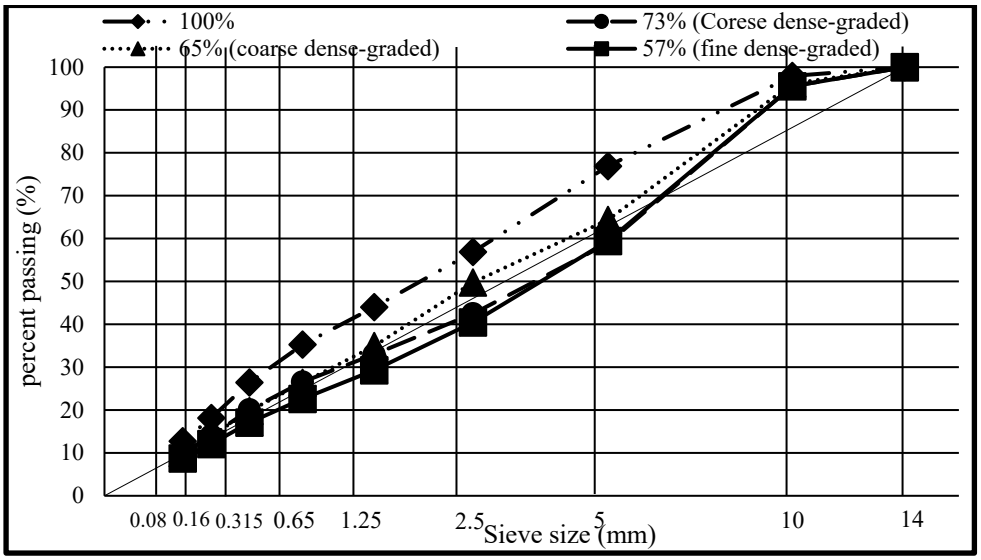

Figure 3.4 Particle size distribution of aggregate blends

3.3.3 Volumetric properties and optimal bitumen content (OBC)

Based upon the LC method, optimal bitumen content (OBC) defines as the one that gives 4-7% air voids after the design number of gyrations ($N_{des.}$) by a shear gyratory compactor (SGC). As shown in the research work by Imaninasab et al. (2022), 4% does not provide sufficient coating for mixtures containing 73%, 65% and 57% RAP, so 3% air voids at $N_{des.}$ was chosen for them. On the other hand, 3% air voids results in bleeding in 100% RAP mixture. Given the

fact that the negative effect of extra bitumen on rutting resistance is greater than air voids (Sreedhar & Coleri, 2018), 4% air voids at $N_{des.}$ is selected for 100% RAP mixture. Also, voids in mineral aggregates (VMA) is the key volumetric properly affecting the rutting performance of asphalt mixtures (Kandhal & Mallick, 2001; Zhang et al., 2019). Hence, the focus was shifted onto the VMA rather than air voids. This way, it can be assured that, regardless of air voids, the rutting performance of each mixture type is tried to be at its best. The mixing temperatures of 100% RAP and the other mixtures including 57%, 65% and 73% RAP mixtures were 100±5˚C and 110±5˚C, respectively. These were the minimum temperatures where insufficient coating and clustering were not observed. Heating up RAP was done using microwave so as not to induce further aging (Basueny, Perraton, & Carter, 2014). This practice better represents real mixing plant procedure where RAP is added at the mid-section of the drum. Also, compaction temperatures for 100% RAP and the other mixtures were set 90˚C and 110˚C, respectively. The mixtures had approximately the same compactibility (compaction slope) at these temperatures.

3.3.4 Rutting performance

3.3.4.1 Indirect tensile (IDT) strength test

IDT strength is a simple but practical test to preliminary assessment of the general performance of asphalt mixtures. It is an indicator of both rutting and cracking resistance. High strength represents high rutting resistance according to ASTM D6931 (2017a). Still, the decision on rutting performance cannot be made solely based upon IDT strength.

The test was conducted according to ASTM D6931 (2017a) on two replicates for each mixture type. The 101.6-mm diameter cylindrical specimens were compacted by applying 50 blows of Marshall Hammer per side. The air void contents of specimens were measured before testing and, in order to adjust the temperature of specimens, they were kept in the water bath of 25˚C for 2 hours right before running the test. The peak load can be converted to IDT strength (S_t) by using Equation (3.11).

$$S_t = \frac{2000 \times P}{\pi \times H \times D} \quad (3.11)$$

Where: H is height (mm); D is diameter (mm); P = load (N); S_t = IDT strength (kPa).

In addition to IDT strength, total fracture energy (FE) can provide deeper insight with regard to cracking resistance. It is an energy-based criteria that is the area under the load-deformation curve up to absolute failure (total rupture). Equation (3.12) can be used to calculate it. Higher FE means higher cracking resistance (Ziari, Moniri, Imaninasab & Nakhaei, 2019).

$$FE = \frac{\int_0^{\delta max} P(\delta) d\delta}{H \times D} \quad (3.12)$$

Where: δ_{max} is the deformation corresponding to load zero (mm).

3.3.4.2 Laboratoire des ponts et chaussées (LPC) wheel tracking test

LPC wheel tracking is simulative test for rutting resistance of asphalt mixtures. Rectangular moulds of 500×180×50 mm were used to compact and prepare asphalt slabs for LPC rutting test. Mixing materials was carried out using high capacity (30 L) thermoregulated mixer. Based on maximum theoretical density (G_{mm}), the amount of hot loose mixture (Equation (3.13)) is calculated to yield 5% air voids at the brimful condition in the mould as per LC 26-410 (2020). But the slab usually has a greater height than the mould's height; i.e higher air voids than the target one. This is because the LPC compactor used in this study (Figure 3.5) applies the same compaction effort to all mixtures rather than compacting them to a specific height. LPC compactor was devised to simulate both pneumatic and steel roller compactor from the field.

$$Asphalt\ mixture\ mass = G_{mm} \times \frac{500 \times 180 \times 50}{1000} \times 0.95 \quad (3.13)$$

Eight slabs were fabricated (two specimens for each mixture type) for LPC wheel tracking test. After compaction, they were kept in the mould for two days to cool down. After compaction, the slabs remained inside the mould for 2 days to cool down and, then, their bulk specific gravities (G_{mb}) were measured by submerging them into the water bath. Having both G_{mb} and G_{mm}, the air voids of the slabs were computed. These air void contents are very close to those of in-field right after compaction. Notably, air voids have a significant impact on rutting potential but not as much as bitumen (Sreedhar & Coleri, 2018). The higher the air voids and the greater the bitumen content, the greater the rut depth.

The testing temperature was 58±2˚C and was monitored by a probe drilled inside the slabs. Prior to testing, the slabs were placed into the mould again and underwent 1,000 cycles by LPC wheel tracker at room temperature so as to settle inside the mould. The rut depth was measured after 1,000, 3,000, 10,000, and 30,000 at 5 equal intervals along wheelpath with 3 readings for each: one at the centreline, one at left and one at right. The average of the measurements is expressed as the rut depth. Based on LC 26-410 (2020), %rut depths at 1,000 and 3,000 cycles must be less than 10% and 15%, respectively. %rut depth can be calculated usig Equation (3.14).

$$\%rut\ depth = \frac{rut\ depth}{initial\ thickness\ of\ slab} \times 100 \qquad (3.14)$$

Figure 3.5 LPC compactor

3.4 Result and discussion

3.4.1 Volumetric properties analysis

Figure 3.6 shows the main volumetric properties including air void (Va), VMA, and VFA vs binder content. Each mixture type contains 6 datapoints and each point is the average of two replicates. It can be observed that 57%, 65%, and 73% RAP mixtures have better packing than 100% RAP mixture because higher VFA, lower Va, and VMA are always achieved at the same bitumen content. At the bitumen contents of 5.2% and 5.4%, VMA curves of 57% and 73% RAP mixtures, respectively, move upward. It indicates the abundance of bitumen that prevents the aggregates packing and makes space between them which, consequently, causes VMA to increase. Both 57% (FDG) and 73% (CDG) RAP mixtures were designed based upon the average black and white curves. That explains their similar volumetric behavior.

Table 3.6 presents the OBC along with volumetric properties of different mixtures. With RAP content decrease, the OBC decreases but the amount of virgin bitumen increases. Still, the amount of virgin bitumen is significantly low when very high RAP content is utilized. Since current volumetric mix design procedure such as Superpave (AASHTO R 35, 2017) and LC method (Ministère des Transports du Québec, 2006) were not devised for RAP contents greater than 40%, the focus on the mix design here is on VMA as the main volumetric property that impacts the rutting performance (Aurangzeb et al., 2012). In conventional mixtures, there is variation in VMA and VFA with RAP content increase and it does not show any pattern (Aurangzeb et al., 2012; Yang et al., 2022). The Bailey method helps control VMA and makes different mixtures with approximately the same VMA. True Bailey aggregate blends must have approximately the same VMA (Aurangzeb et al., 2012). It can be observed that the mixtures containing 57%, 65%, and 73% RAP have almost the same VMA. This has been achieved not through using the Bailey method but by the approach developed in this study.

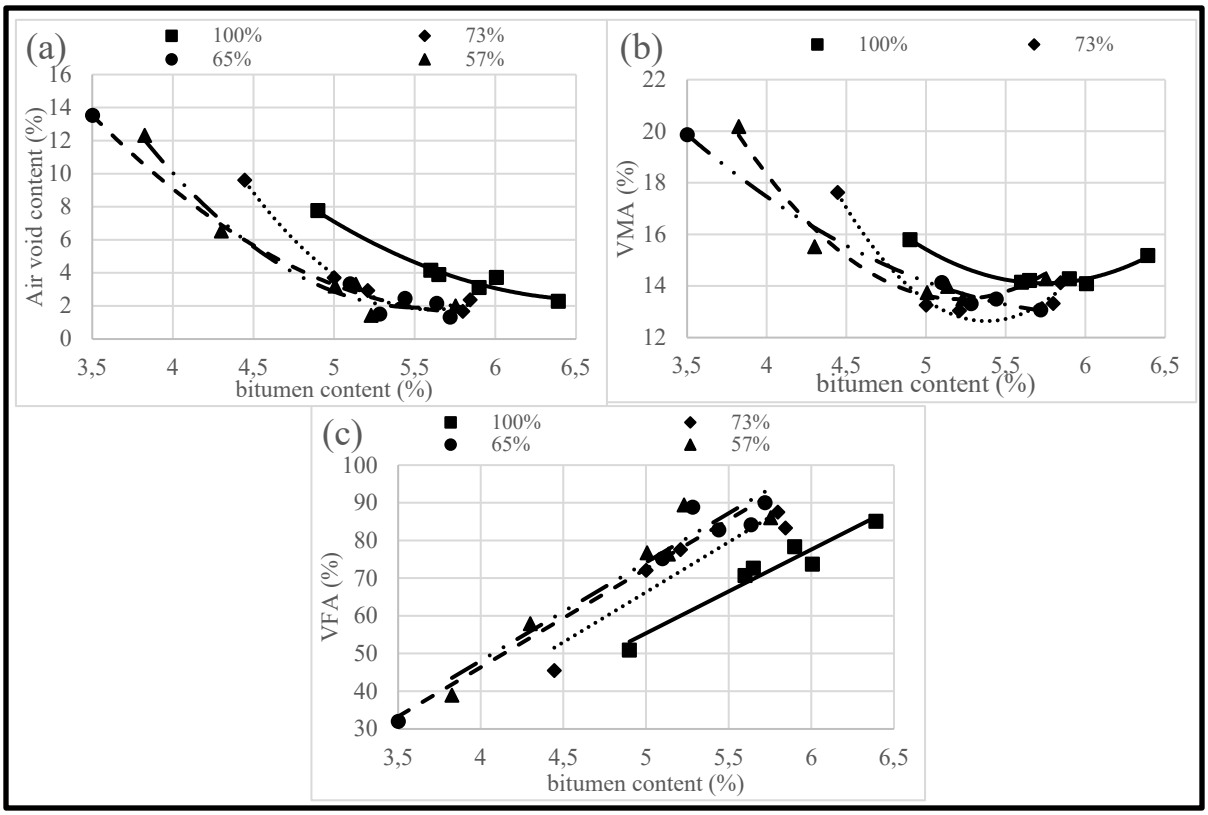

Figure 3.6 Volumetric properties including (a) air void, (b) VMA, and (c) VFA vs. bitumen content

Table 3.6 Mix design data

	Optimal Bitumen content (Total)	Optimal Bitumen content (virgin)	Maximum specific gravity	Air void @ $N_{des.}$	Air void @ $N_{ini.}$	Air void @ $N_{Max.}$	VMA	VFA
100%	5.65	0.71	2.534	4.08	11.41	2.59	14.20	72.65
73%	5.15	1.63	2.546	2.98	10.76	1.85	13.03	77.57
65%	5.10	1.99	2.535	2.92	10.68	2.04	13.34	75.12
57%	4.95	2.25	2.537	3.06	10.92	1.42	13.73	76.76

3.4.2 Rutting performance

3.4.2.1 Indirect tensile (IDT) strength test

Table 3.7 presents the air voids of different mixture types. 100% RAP has very high air voids compared to other mixtures. It can be attributed to its poor gradation that impacts its compactibility. Due to the high amount of fine particles that are way more than the amount to fill the space created by coarse particle, deficiency in compaction occurs. This can, consequently, influences the rutting performance negatively. Overall, the air voids vs %RAP trend is similar with the trend observed for the SGC specimens.

Table 3.7 Average air void content of IDT specimens

RAP content	100%	73%	65%	57%
Air voids (%)	7.9	4.7	4.5	3.8

Figure 3.7 illustrates the load vs deformation curves obtained from IDT strength test. The test was continued up to full rupture where the specimens do not bear any load. As it can be seen, mixtures with more RAP content deform less before full rupture. However, mixtures with more RAP do not necessarily have the larger peak load.

Figure 3.8 presents IDT strength of each mixture with the standard deviation shown on it. As depicted, 100% RAP has the lowest IDT strength in spite of having stiffest bitumen due to greater amount of old RAP bitumen. On the other hand, 57%, 65%, and 73% RAP mixture have almost the same IDT strength that slowly increases with RAP content increase. Since smaller IDT strength is an indicator of lower rutting resistance, it can be concluded that 100% RAP mixture has higher rutting potential than other mixture types. Simulative rutting test like LPC wheel tracking can reveal more, especially once it comes to less distinguishable mixtures of 57%, 65%, and 73% RAP.

Figure 3.9 shows that 100% RAP mixture has lower cracking resistance compared to other mixture types as it has the lowest fracture energy. Similar to IDT strength, 57%, 65%, and 73% RAP mixtures seem to have approximately the same cracking resistance. Further study is required to discern cracking potential of these mixtures.

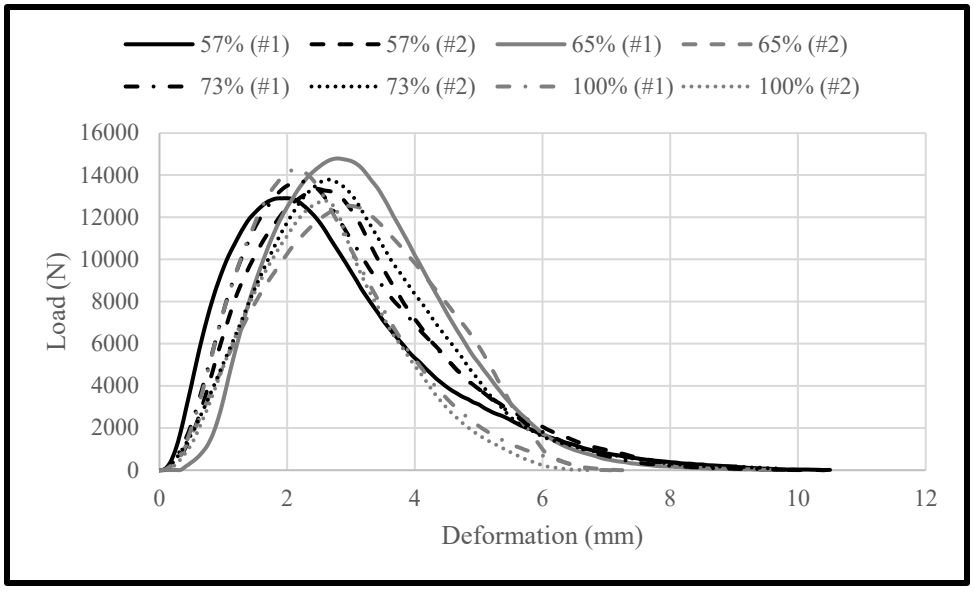

Figure 3.7 Load vs. deformation curves of different mixtures

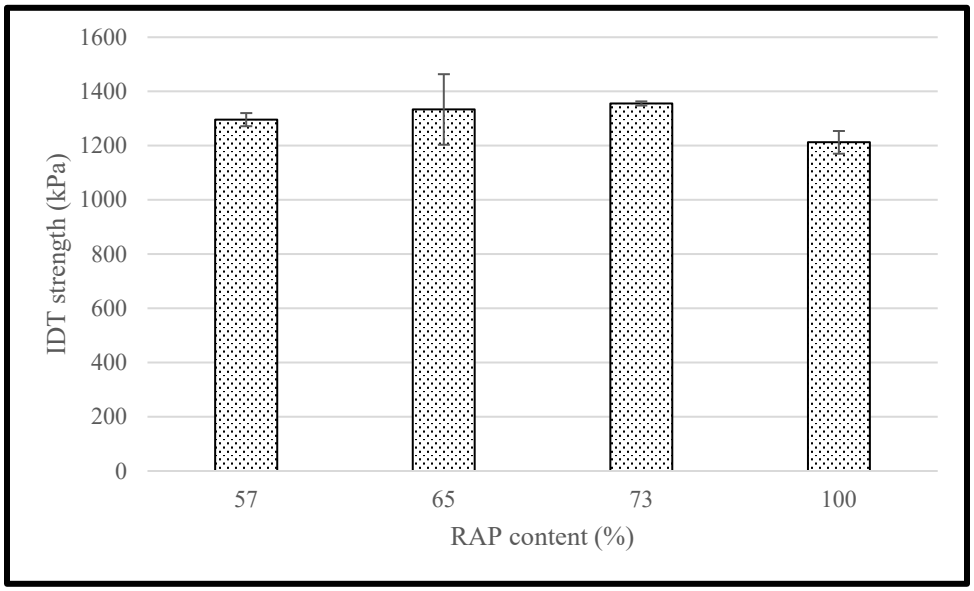

Figure 3.8 IDT strength of different mixtures

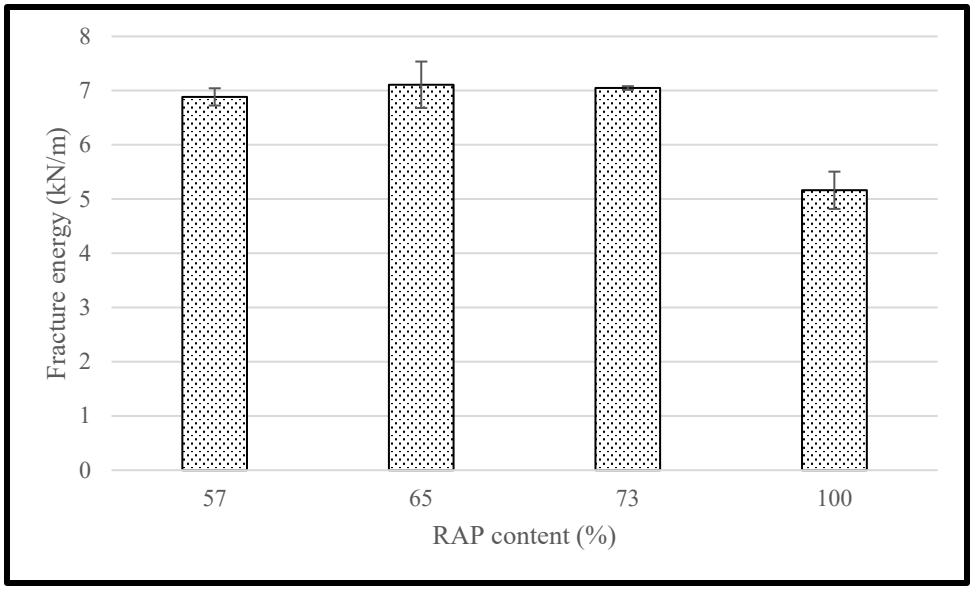

Figure 3.9 Fracture energy of different mixtures

3.4.2.2 Laboratoire des ponts et chaussées (LPC) wheel tracking

As given in Table 3.8, the air void content of 100% RAP mixture is significantly higher than the others. On the other hand, except one of the 73% RAP slabs that is an outlier, the Bailey aggregate blends have approximately the same air voids. The variation in air voids and OBC of the Bailey and non-Bailey aggregate blends is an intrinsic property of them and inevitable. This is as it must be since similar volumetric properties means controlling the gradation to be the same (Aurangzeb et al., 2012). The aim of this study is to evaluate the effect of the gradation.

Bearing in mind that the compaction energy is the same for all mixtures, poor gradation of 100% RAP due to the abundance of fine particles leads to high air voids. Too many fine particles fill the space between the coarse particles and do not allow them slide on each others.

Table 3.8 Air voids content of the prepared slabs by LPC compactor

	100% RAP		73% RAP		65% RAP		57% RAP	
Slab	1	2	1	2	1	2	1	2
Air voids	14.09	13.18	8.11	11.29	7.82	8.13	7.69	8.38
Average	13.63		9.70		7.97		8.03	

The results of performing LPC wheel tracking indicate the key role of aggregate skeleton in rutting resistance (Figure 3.10). It is well-established that higher amount of RAP in a mixture leads to greater rutting resistance. This is due to the fact that the RAP is added to the virgin aggregates complying their gradations. The approach in this study is virgin aggregates added to the RAP for correction. As a result, although 100% RAP mixture has stiffer asphalt binder due to higher RAP content (Table 3.9), 57%, 65%, and 73% RAP mixtures are more rutting resistant. Building firm aggregate skeleton using the method proposed in this study to reach Bailey aggregate blends contributes to rutting resistance. This corroborates the results of IDT strength test.

Table 3.9 PG+ designations of different mixtures' binders

Mixture type	Binder PG+
RAP	88S-16
100% RAP	82S-16
73% RAP	76S-22
65% RAP	76S-22
57% RAP	70H-22

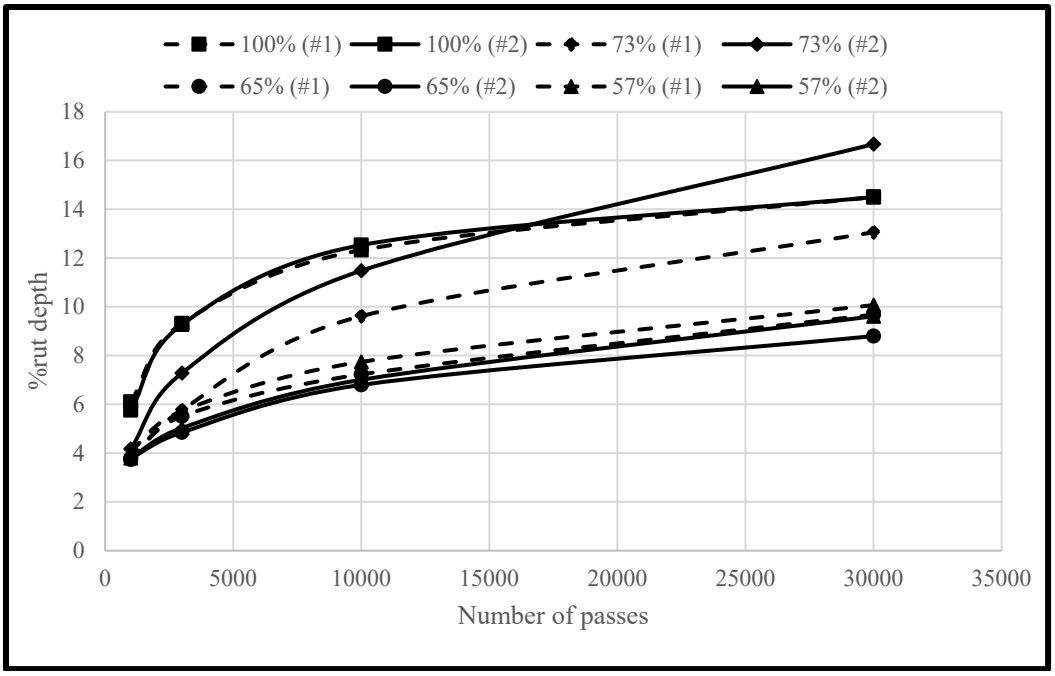

Figure 3.10 %rut depth vs. number of passes

As depicted in Figure 3.11, the improvement of rutting resistance varies not only by the mixture type, but also by the number of passes. The improvement can be as high as 44.3% (65% RAP @ 3000 passes) and as low as 9.9% (73% RAP @ 30000 passes). It can be observed that the maximum percentage of improvement always takes place at 3000 passes for all mixture types. Before and after it, there is decline. For 65% and 57% RAP, the percentages of improvement are almost the same at 1000 and 30000 passes whereas, for 73% RAP, the percentage of improvement at 30000 is far less than that at 1000. It indicates that, compared to 57% and 65% RAP, 73% RAP tend to deform faster as the number of passes increases. Bearing in mind that both 65% and 73% RAP are CDG, the reason for significantly less rutting potential of 73% RAP lies in the gradation difference. 65% RAP was designed based upon white curve (RAP aggregate gradation) while 73% RAP was designed based upon the average white and black (RAP gradation) curves. Such difference in gradation selection of RAP resulted in different blends. In 65% RAP, the gradation of the fine part of RAP is modified through addition of virgin fine aggregate whereas the fine part of the RAP remained intact in 73% RAP mixture. This shows that, not only does the skeleton of coarse part contribute to rutting performance improvement, but that of the fine part also does. So, it pronounces the necessity of paying

attention to both fine and coarse part of the RAP in gradation restoration and correction to maximize the rutting resistance of asphalt mixtures with very high RAP content.

The 65% RAP mixture has the highest rutting resistance. At any number of passes, it has the lowest %rut depth and highest percentage of improvement. Once compared with 57% RAP mixture, there might be one or both of the following reasons behind it: (i) higher amount of RAP in 65% RAP mixture that leads to stiffer mixture, and (ii) designing 65% RAP mixture as CDG blend that is supposed to have greater rutting resistance compared to FDG blend (57% RAP).

The rutting resistance difference between 57% and 65% RAP mixtures is insignificant as suggested by LPC wheel tracking test results. It cannot be concluded that gradation does not play any role since the effect of gradation on rutting resistance is generally significant (Ghuzlan, Bara'W, & Al-Momani, 2020). The higher amount of RAP in 65% RAP mixture resulted in slightly greater rutting resistance than 57% RAP mixture. Thus, it can be inferred that designing CDG and FDG blends with very high RAP content according to Bailey method leads to the same rutting performance if the amount of RAP remains approximately the same.

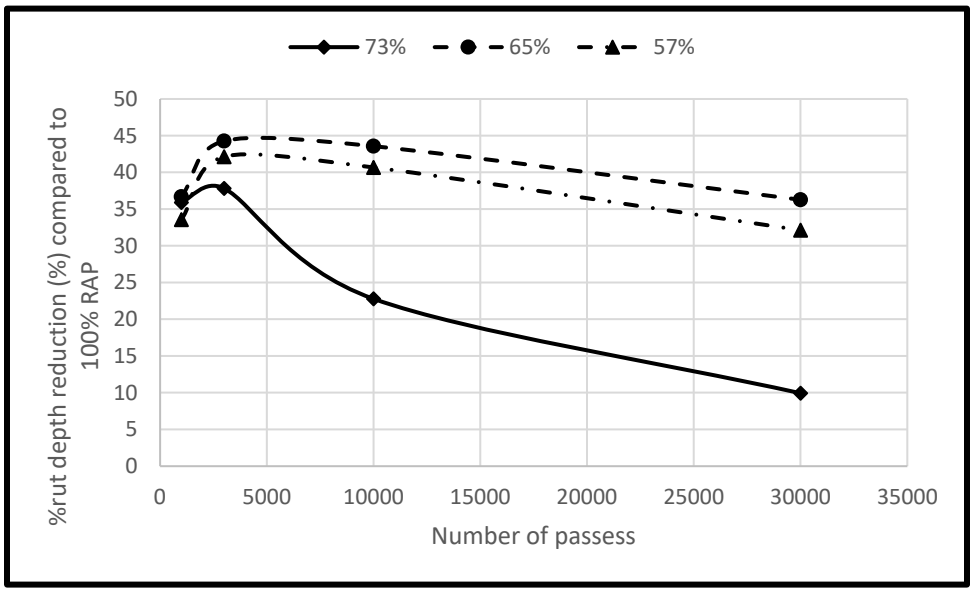

Figure 3.11 Reduction (%) in %rut depth with respect to 100% RAP mixture

3.5 Conclusion

This study focuses on the gradation of asphalt mixtures with very high RAP content (>50%) in order to enhance rutting resistance to the most. A new method was proposed for gradation correction of RAP to obtain Bailey aggregate blends. Consequently, Bailey aggregate blends became feasible for asphalt mixtures with very high RAP content. The effectiveness of the proposed method on building strong aggregate structure was evaluated through volumetric analysis and rutting resistance. The air voids, VMAs, and VFAs of the Bailey aggregate blends are approximately the same. These are the fingerprints of true Baily blends. From the results obtained from indirect tensile (IDT) strength, the difference between Bailey and non-Bailey (100% RAP) aggregate blends is distinguishable. It is required to perform simulated tests like Laboratoire des ponts et chaussées (LPC) wheel tracking test to appreciate the rutting performance differences among Bailey aggregate blends.

It was observed that the design of the coarse dense-graded (CDG) mixtures is better to be carried out based upon the white curve (RAP aggregate gradation) since fine part of the RAP is considered and revised using it. Subsequently, greater rutting resistance is obtained. Fine dense-graded (FDG) and CDG mixtures with very high RAP contents can have the same rutting resistance in condition that both contain the same amount of RAP and CDG was designed based upon white curves of RAP. It can also be derived that aggregate structure can have greater influence on rutting performance than bitumen because 100% RAP, in spite of having stiffer bitumen, has lower rutting resistance compared to other mixtures with far less RAP contents.

In addition to rutting resistance, there are moisture damage sensitivity and cracking. While rutting is due to compression, cracking is believed to be the act of tension (Underwood, 2006). Thus, stone-on-stone contacts of aggregate structure, which bear compressive loads, is not expected to directly impact cracking resistance of any kind. Yet, it is good to examine its indirect impact as a result of changing the amount of virgin binder and volumetric properties on cracking.

CHAPTER 4

INTEGRATED PERFORMANCE EVALUATION OF ASPHALT MIXTURES WITH VERY HIGH RECLAIMED ASPHALT PAVEMENT (RAP) CONTENT

Reza Imaninasab[a], Luis Loria-Salazar[b], Alan Carter[a]

[a] Construction Engineering Department, École de technologie supérieure, 1100 Notre-Dame St W, Montreal, QC H3C 1K3, Canada.
[b] Universidad Isaac Newton, Av. 7 13, Paso De La Vaca, San José, Costa Rica.

Paper published in the Journal of Construction and Building Materials, Volume 347, September 12, 2022, 128607.

4.1 Abstract

Conventional mix design methods are incapable of making the most of RAP, especially in very high content (>50%). RAP is not the kind of waste to just get rid of, but it has the potential to build better asphalt pavements. Therefore, the aim of this research is to modify practices and criteria within mix design and develop a ranking system in order to better fabricate and evaluate asphalt mixtures containing very high RAP, respectively. The specific challenges of this mixture type including gradation, production, compaction, volumetric properties and optimal asphalt content (AOC) were handled in this study. Also, a general performance index integrating essential performance aspects including rutting, cracking, aging and moisture sensitivity was developed. It had been found that rejuvenation and aging potential are important in mixtures with very high RAP content, so rejuvenation was made based upon previous studies and aging potential was included in the performance evaluation. Paying more attention to gradation within mix design was proved very important and Bailey method was found impactful on improving aggregate structure of mixtures with high RAP content. It was observed that the target air void of 3% leads to better coating of virgin aggregates of this mixture type.

4.2 Introduction

Aged infrastructures in developed countries call for renewal and governments are now determined to rebuild them. United States just approved the historical budget of 2 trillion dollars for that purpose and roads are taking the big share. Consequently, soon or late, landfills will be filled with waste asphalt pavements and, subsequently, the reclaimed asphalt pavement (RAP) content in new pavements will increase substantially. However, there are mix design, production, construction and, consequently, performance challenges with RAP content increase. As shown in Figure 1, the three elements of mix design, production and construction are interconnected and mutually influential; together, they impact performance. Since high performance is the goal, there has been a shift from conventional (volumetric) mix design to balanced mix design (Newcomb, Brown & Epps, 2007; Copeland, 2011; West et al., 2013). While mix design, whether conventional or balanced, of asphalt mixtures with up to about 50% RAP is well established (McDaniel and Anderson, 2001; AASHTO, 2017a), the mix design of asphalt mixtures with very high RAP content (>50%) is still prone to investigation.

Inhomogeneity and high stiffness of asphalt binder in the mixtures with very high RAP content are the research areas that have attracted the researchers' attention the most. Weak fatigue performance of these mixtures is attributed to the old asphalt binder of RAP that becomes predominant (Norouzi et al., 2014). Although it is true and the achievements of previous studies for softening and homogenizing the old asphalt binder must be deployed, it is also very important to revise the mix design of asphalt mixtures with very high RAP in order to take the specific characteristics of these mixtures into account. One of these specific characteristics is the gradation. It is vital to restore the distorted particle size distribution within mix design process since the structure formed by aggregates is the main load bearer of asphalt pavement (Vavrik et al., 2002).

Furthermore, volumetric properties recommended by conventional mix design procedure might not lead to the best performance because the large portion of aggregates is the RAP that is covered by a film of old asphalt binder. Once dealing with this aggregate type, it is better to

be directly reliant on performance rather than volumetric properties. So, a framework to rank very high RAP asphalt mixtures is required. The framework must include various aspects of performance. In the meanwhile, in order to avoid over-aging and consider rejuvenator introduction, the instructions of production and construction need to be adjusted. So very high RAP asphalt mixture specimens can be fabricated more efficiently.

Therefore, the objective of this study is to marginalize the volumetric properties and focus more on performance aspects within mix design. Gradation restoration and building firm aggregate structure, proper production and compaction, and introduction of a comprehensive performance-based index based on which the best mixture among several mixtures with very high RAP content can be chosen are the means to achieve the objective.

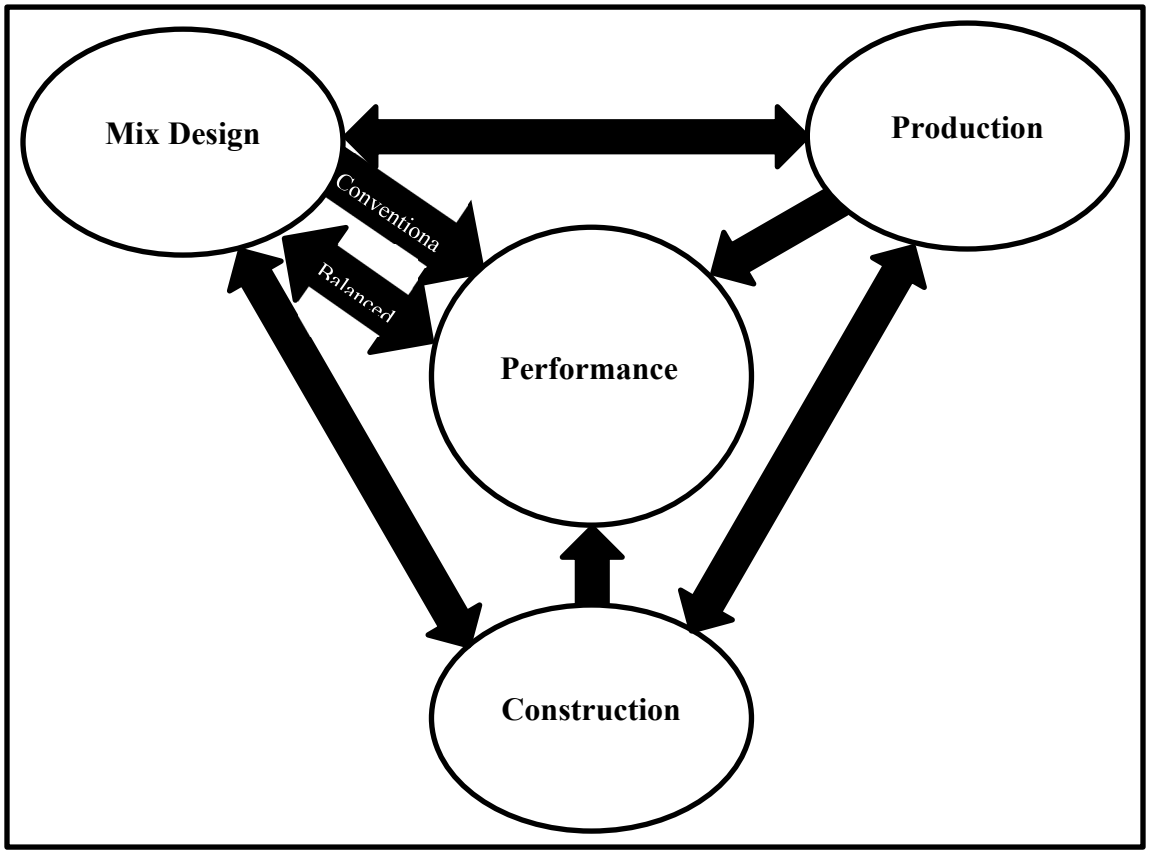

Figure 4.1 The mutual relationship between mix design, production, construction and performance

4.3 Materials

4.3.1 Aggregates, RAP and asphalt binder

The virgin aggregates used in this study are fine (0-5 mm) and coarse (5-14 mm) limestone. Additionally, a finer size range (0-2.5 mm) was extracted from the virgin fine aggregates. The RAP source contains 0-10 mm particles. Table 4.1 gives the specific gravities of RAP and virgin aggregates. The virgin asphalt binder was a PG 58S-28 that is typical in cold regions. Its specifications are shown in Table 4.2.

Table 4.1 Virgin and RAP aggregate gravities and water absorption

	RAP agg. (5-10mm)	RAP agg. (2.5-5mm)	RAP agg. (0-2.5mm)	Coarse agg. (5-14mm)	Fine agg. (2.5-5mm)	Fine agg. (0-2.5mm)
G_{sb}	2.694	2.667	2.660	2.714	2.707	2.694
G_{SSD}	2.721	2.704	2.693	2.734	2.728	2.720
G_{se}	2.769	2.769	2.749	2.770	2.766	2.766
Absorption (%)	1.00	1.379	1.215	0.738	0.793	0.968

Table 4.2 Virgin bitumen properties

Property	Value	Standard
Viscosity @ 135℃ (Pa.s)	0.309	AASHTO T 316
Viscosity @ 165℃ (Pa.s)	0.092	AASHTO T 316
Density @ 25℃ (g/cm^3)	1.021	AASHTO T 228
Flash point (℃)	273	ASTM D 29
Softening point (℃)	44.2	AASHTO T 53
G*/sin δ of unaged bitumen @ 58℃ (kPa)	1.54	AASHTO MP 1
Mass loss after RTFO (%)	0.351	AASHTO MP 1

Property	Value	Standard
Jnr (3.2) of RTFO aged bitumen @ 58℃ (kPa^{-1})	2.12	AASHTO T 301
Jnr (diff.) (%)	13	AASHTO T 301
R (3.2) (%)	1.4	AASHTO T 301
Stiffness after PAV @ -18℃ & 60 s (MPa)	187	AASHTO MP 1
Slope @ -18℃ & 60 s	0.313	AASHTO MP 1

4.3.2 Rejuvenator

Because of abundance (Elkashef et al., 2018b), effectiveness and efficiency of soybean oil derivatives (Hajj et al., 2013; Elkashef et al., 2017b), one was used in this research for rejuvenating old asphalt binder of RAP and facilitating its mingling with virgin binder. It has been proven that 1-2% of soybean oil derivative by total weight of bitumen (old and new bitumen) in 100% RAP mixture is capable of softening the old binder as the virgin one (Elkashef et al., 2017b; Elkashef et al., 2018a; Elkashef et al., 2018b; Podolsky et al., 2020). Since there is no study proposing the percentage of the rejuvenator for mixtures containing RAP percentages other than 100%, in this research, 1% rejuvenator by the total binder weight in 100% RAP mixture was transformed and expressed based upon the precentage by the weight of RAP binder. So, it can be applied for mixtures other than 100% RAP. 1% rejuvenator by the total binder weight was found to be equivalent to 1.154% rejuvenator by the weight of RAP binder in 100% RAP mixture. Therefore, all mixtures in this study, regardless of the amount of RAP, have 1.154% rejuvenator to RAP binder ratio.

4.4 Methodology

The big picture of this research is depicted in Figure 4.2. The three main steps are according to the objective of this study as (a) gradation restoration through Bailey method concepts, (b) optimal bitumen determination, and (c) selecting the best mix based upon performance aspects. The focus here is on aggregate blends rather than asphalt binder designation and rejuvenator

content since much research has been conducted on rejuvenation and, for now, it is assumed that the best aggregate blend skeleton leads to the best mixture performance (Golalipour, Jamshidi, Niazi, Afsharikia & Khadem, 2012). Also, it has been proved that volumetric properties have good correlation with performance for asphalt mixtures containing high RAP (Aurangzeb et al., 2012). So the optimal asphalt content (OAC) was determined according to volumetric properties proposed by Superpave mix design (AASHTO, 2017a) and LC method (MTQ, 2006) with minor modification. Finally, the best very high RAP content mixture was chosen among the mixtures with different gradations based upon integrated performance.

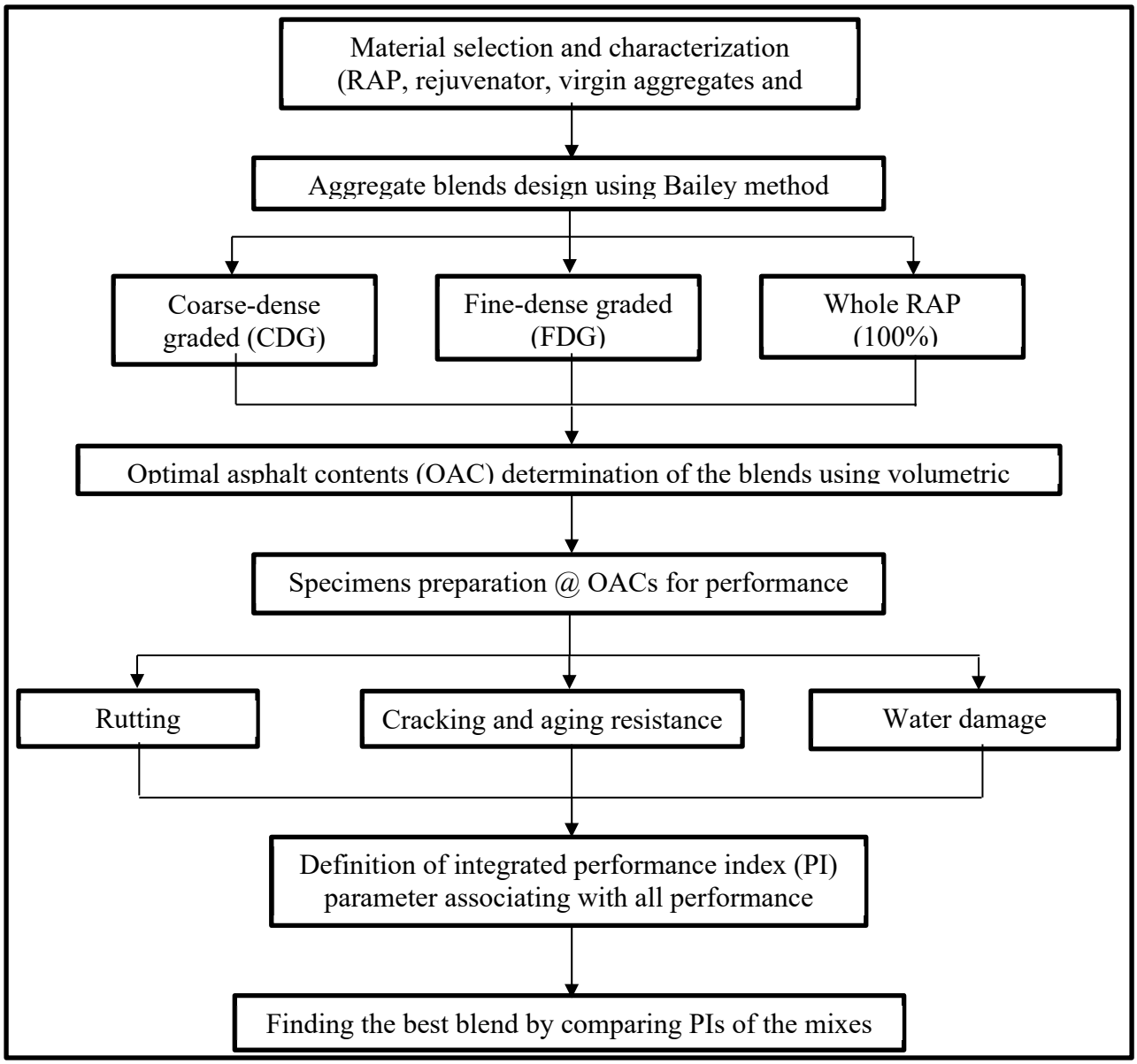

Figure 4.2 Research program for developing the balanced mix design

4.4.1 RAP and virgin aggregates

In the first step, RAP specifications including asphalt binder content and RAP aggregate gradation and specific gravities (Table 4.1) were determined. Ignition oven was used as the most accurate tool for finding RAP asphalt binder content (Loria-Salazar, 2011; West et al., 2013; Rodezno & Grant, 2018); it was 4.9%.

4.4.2 Aggregate blend design

Although stiffer asphalt of RAP decrease rutting potential, the lack of stone-on-stone contact aggravates it in greater extent since aggregate structure is the main responsible for rutting resistance (Golalipour et al., 2012). Therefore, as expected from a good mix design, RAP gradation is rectified through Bailey method concepts. Since Bailey method does not allow introduction of high RAP content (>40%) and requires RAP having similar gradation as the designed gradation (Vavrik et al., 2002), modification in this method was made for applicability with regard to very high RAP content.

Firstly, no fractioning of RAP was made and the desired aggregate size distribution was attained by proportioning RAP and virgin aggregate stockpiles. Virgin aggregates were added in the least possible portions in order to achieve coarse-dense graded (CDG) and fine-dense graded (FDG) blends containing the most possible RAP. Compared to fractionation of RAP and weighting each fraction in the total aggregate blend, this practice is more labor-saving and RAP aggregate gradation (white curve), instead of RAP gradation (black curve), can be taken into account. With respect to fine portion, there is significant variation between white and black curve and white curve is believed to be closer to the real gradation of RAP (Saliani, Carter, Baaj & Tavassoti, 2019).

Also, design of CDG was carried out based on the white curve as well as the average of black and white curves. By using the white curve, it is assumed that the old bitumen film of RAP is soft enough, during mixing and compaction, to let hard cores of RAP, i.e. RAP aggregates, touch each other. This is an ideal state and worth studying if takes place. Using only black curves means that the old bitumen film of RAP is as hard as aggregate and does not allow any indentation into old bitumen film around RAP. This is unlikely to occur in HMA and WMA, especially when an efficient rejuvenator is applied. Often, partial blending takes place, which implies partial softening of the old bitumen film (Behnood, 2019; Shirodkar et al., 2011). Hence, using the average of black and white curves is justifiable, though not perfectly representative of the real state. Regarding FDG, the average of black and white curves were

only taken into account. Based on the gradations of fine (0-5 mm) and coarse (5-14 mm) virgin aggregates, the fine derived from fine virgin aggregates (0-2.5 mm), RAP and RAP aggregates obtained from ignition oven (Table 4.3) , the proportions of RAP, fine(0-2.5 mm), fine (0-5 mm) and coarse (5-14 mm) aggregate were computed as presented in Table 4.4 for different blend types including two CDGs (one white curve based and the other average white and black curve based), one FDG and a whole-RAP (100% RAP).

The proportionings of Table 4.4 yield the gradations demonstrated in Figure 4.3. They are constructed utilizing the white curve. It can be observed that 57% RAP (FDG) has coarser gradation than CDGs. It is because the blends do not contain all the same stockpiles. Otherwise, if the same aggregate stockpiles had been utilized, CDGs must have been coarser than FDG. Notably application of Bailey method concepts brought the whole-RAP gradation closer to maximum density line (MDL).

Table 4.3 RAP, coarse and fine gradation

Sieve size (mm)	RAP gradation (black curve)	RAP agg. gradation (white curve)	Coarse agg. (5-14 mm)	Fine agg. (0-5 mm)	Fine agg. (0-2.5 mm)
14	100.0	100.0	100.0	100.0	100
10	97	98	89	100.0	100
5	71	77	10	96.0	100
2.5	45	57	3	54	100
1.25	27	44.0	3	25	47
0.630	13	35	3.0	12	23.0
0.315	5	26	3	9	16
0.160	2	18	3	7	12
0.080	0.6	12.7	2.7	4.9	9.2

Table 4.4 Type of blends along with percentages of stockpiles used

	RAP %	Coarse (5-14 mm) %	Fine (0-5 mm) %	Fine (0-2.5 mm) %
Whole-RAP	100	0	0	0
CDG (average-based)	73	27	0	0
CDG (white curve-based)	65	23	0	12
FDG	57	30	13	0

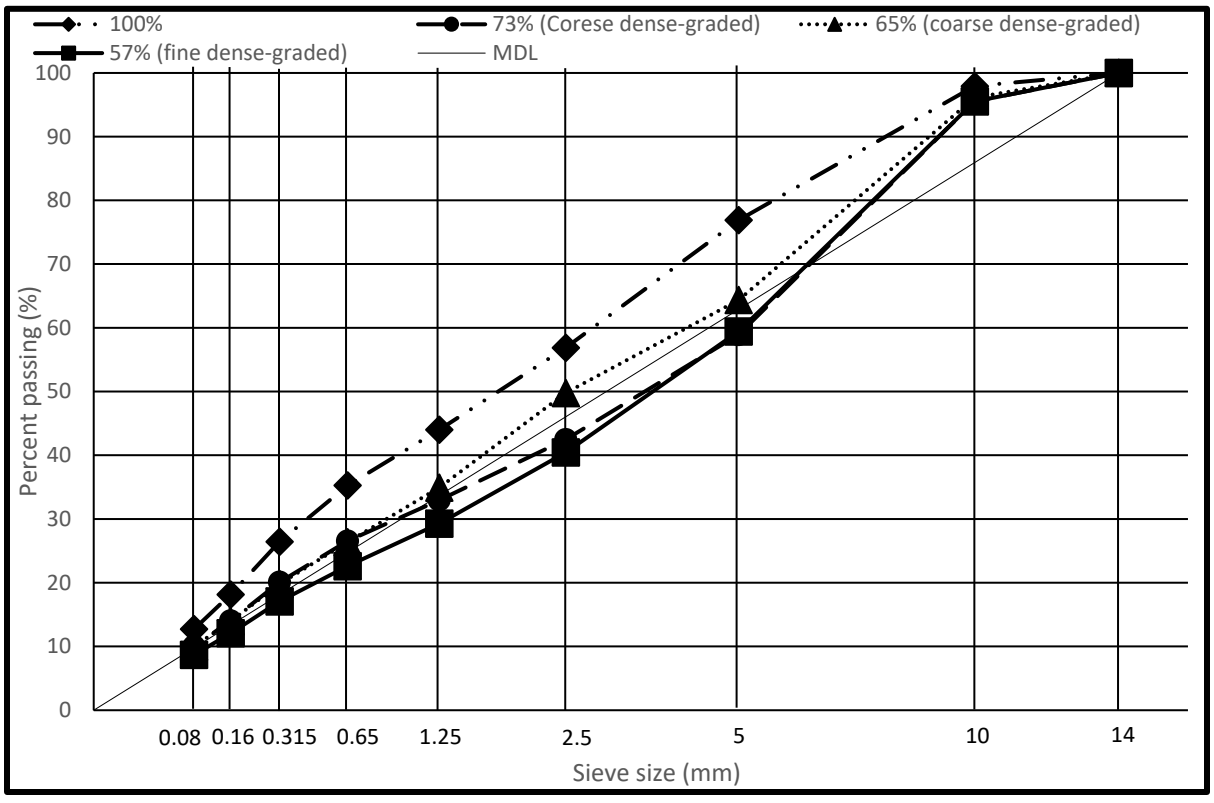

Figure 4.3 Particle size distribution of aggregate blends

4.4.3 Sample preparation

Neither Superpave nor LC was devised for OAC determination of mixture with very high RAP content (AASHTO, 2017a; MTQ, 2006). So, there are challenges and unknowns to be handled when designing mixes with very high RAP contents. First, it comes to specimen preparation. Heating up RAP for mixing was done using a microwave to avoid over-aging of RAP binder. In asphalt plants, RAP is added, at least, in the mid-section of the drum to avoid burning the old RAP binder. Therefore, RAP must not stay at high temperatures for long. In condition of higher RAP content, it is better to reach the desired temperature in the least possible time. So as recommended by Basueny et al. (2014), microwave was used to least damage hydrocarbons of RAP binder.

The heating procedure is to pour RAP into standard cardboard and measure its temperature by thermometer at short intervals until the target temperature is reached (Figure 4.4). The time required for reaching a desired temperature depends on the amount of RAP and microwave type. For 5200 g RAP, for example, it took 6±0.25 min reaching 100±5 ˚C. This is the mixing temperature of whole-RAP. It is the lowest temperature that, as depicted in Fig 4.5, no conglomeration and clustering were observed. For other mixture types containing virgin aggregates, the virgin aggregate's temperature was 165 ˚C (15 ˚C higher than the bitumen temperature) and the RAP temperature was increased to 110±5 ˚C in order to avoid conglomeration and clustering.

Compaction temperature must reflect real temperature drops from mixing until laying and compaction. Thus, 90 ˚C for whole-RAP mix and 110 ˚C for the other mixtures were selected. As given in Figure 4.6, compactibility was negligibly impacted by the temperature drop from conventional 135 to 90 ˚C; it is less than 1%. Also, Figure 4.7 shows the compaction curves of specimens prepared at the target air voids of 7%. As can be seen, 90 ˚C for whole-RAP mix and 110 ˚C for the other mixtures yields almost the same compaction slope, meaning the compactibility of both are approximately the same at their compaction temperatures.

Figure 4.4 Temperature measurement after intervals

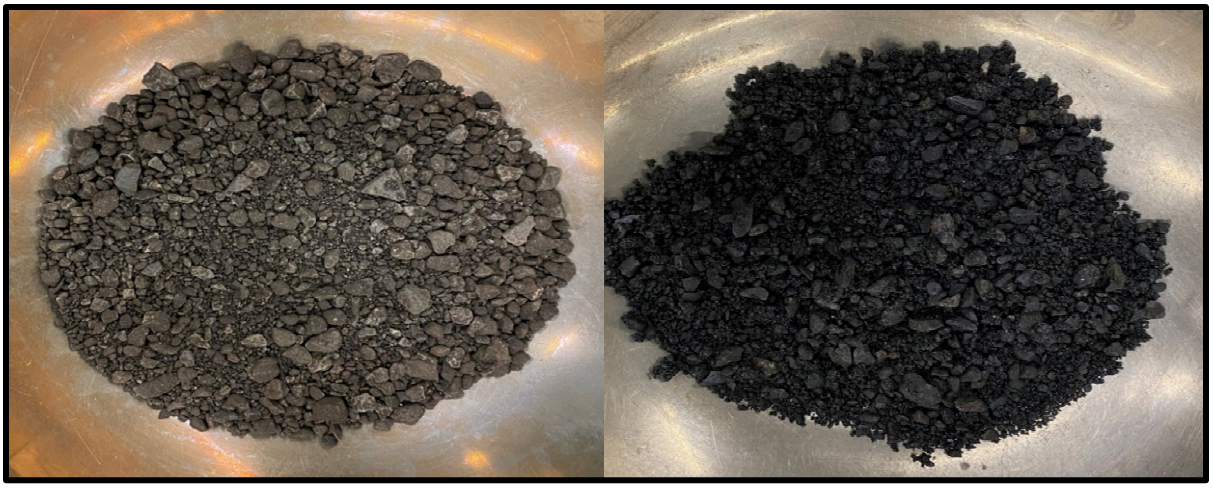

Figure 4.5 RAP (left) and rejuvenated whole-RAP loose mixture prepared at 100 ˚C (right)

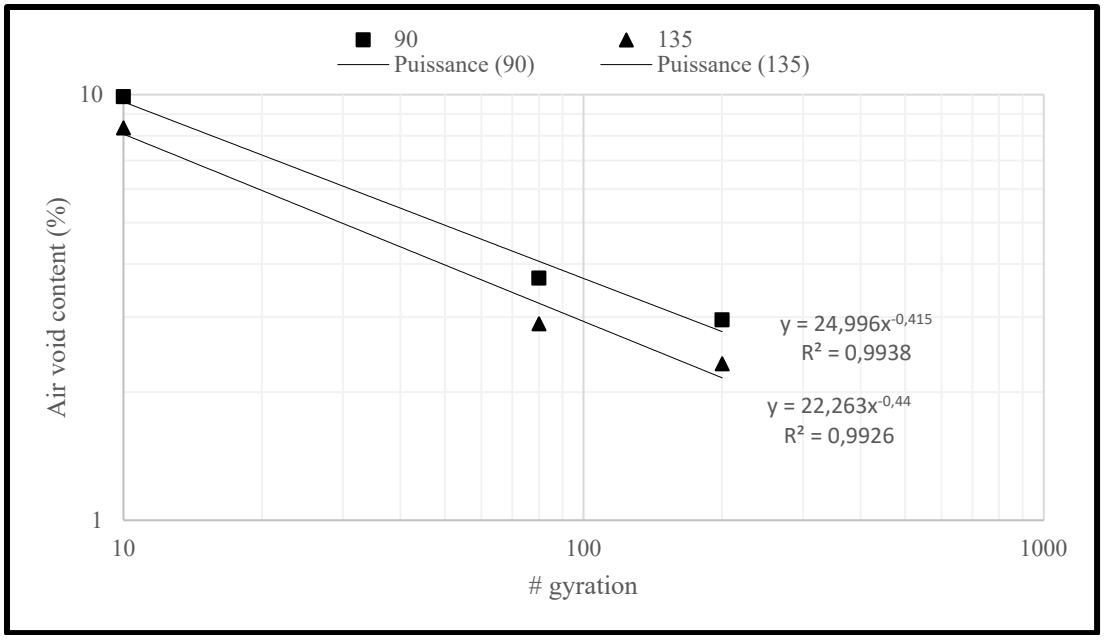

Figure 4.6 Compactibility of the whole-RAP mixture

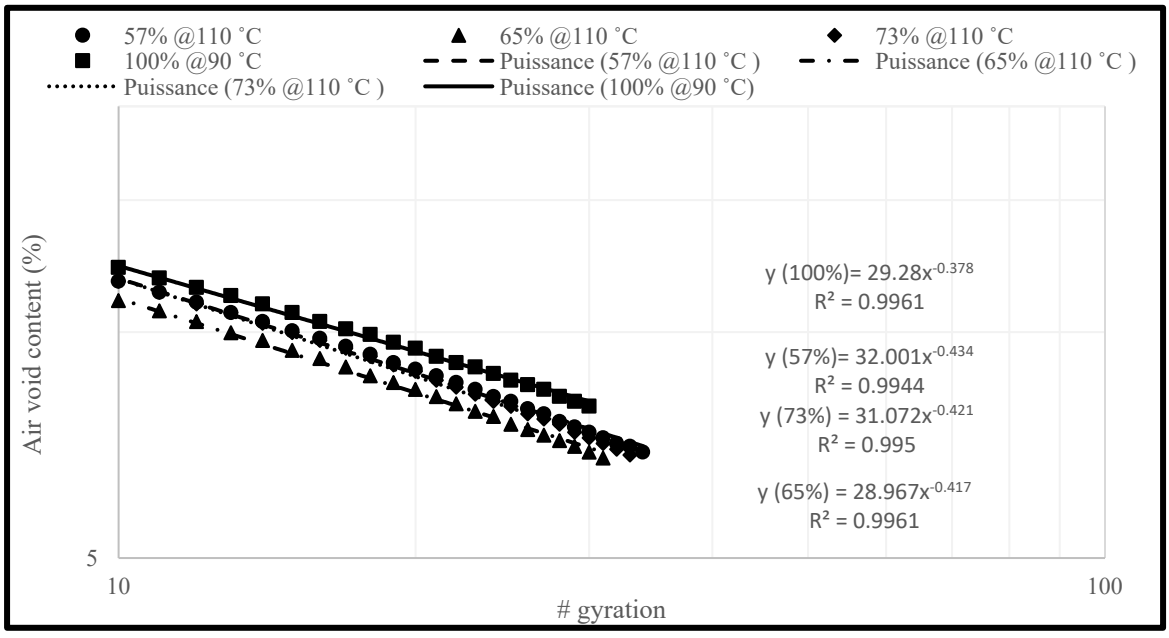

Figure 4.7 Compactibility of the different mixture types

4.4.4 Optimal asphalt content (OAC)

The LC and Superpave method adopt different paths to arrive at 4% air voids at the design number of gyration ($N_{des.}$). While both approaches have been proved to be effective in designing mixes with no or low RAP content, none may be appropriate for the unconventional mixtures under study in this research. In this study, first, LC method was utilized because it provides shortcuts to OAC. After a few trials, it was revealed that LC was suggesting either very high or low asphalt content. So, having enough data points in the air voids vs. asphalt content coordinate, it became possible to find the asphalt content corresponding to 4% air voids by interpolation. While this asphalt content can be considered as OAC for the whole-RAP mixture, it cannot be for the other mixtures. As depicted in Figure 4.8, such asphalt content results in insufficient coating for the mixtures containing virgin aggregates compared to whole-RAP mixture. Subsequently, 3% air voids was set as the target air voids for 57, 65 and 73% RAP mixtures. On the other hand, in order to have all mixtures containing the same air voids for a fair comparison, whole-RAP mixture was also fabricated at 3% air voids. But, as also depicted in Figure 8, 3% air voids results in obvious bleeding in it as if the mixture cannot contain more asphalt binder. Since the detrimental effect of too much asphalt binder on rutting is greater than higher air voids (Sreedhar & Coleri, 2018), the decision to determine OAC at 4% air voids for whole-RAP mixture was made. It is believed that the OAC at 4% air voids gives a better whole-RAP mixture than that at 3% air voids.

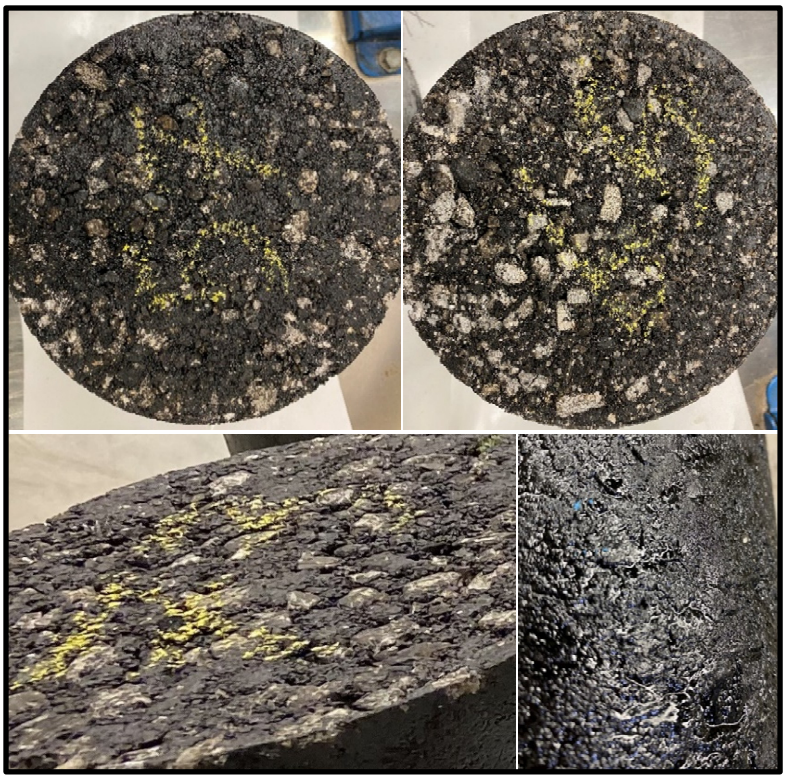

Figure 4.8 (From top left to bottom right) mixtures containing 57, 65 (top view), 73% RAP (angled top view) at 4% air voids and 100% RAP at 3% air voids (side view)

4.4.5 Performance testing

Performance is the criterion based on which asphalt mixtures are judged. Even the credibility of volumetric-based mix design procedures is mainly derived from performance. So, in this study, an additional and important step is taken to assess the performance of mixtures with different RAP contents. The RAP contents were not chosen tentatively; instead, they were designed based upon two aggregates structures and two assumptions regarding permeability of old binder layer over RAP.

Performance itself has different aspects that relate to different distresses. Rutting, moisture damages, fatigue and thermal cracking resistance are among the most common behavioral

performance that can be assessed through wheel tracking, strength ratio of conditioned and unconditioned specimens and semi-circular bending (SCB) testing.

4.4.5.1 LPC wheel tracking test

Laboratoire des Ponts et Chaussées (LPC) wheel tracking test was performed on different mixtures as per LC 26-410 using rectangular moulds of 500×180×50 mm (LC, 2020b). The asphalt mixtures were prepared using high capacity (30 L) thermoregulated mixer. Then, they were poured into the mould and compacted using LPC compactor whose schematic is shown in Fig 4.9. This compactor is designed to simulate both pneumatic and steel roller compactor.

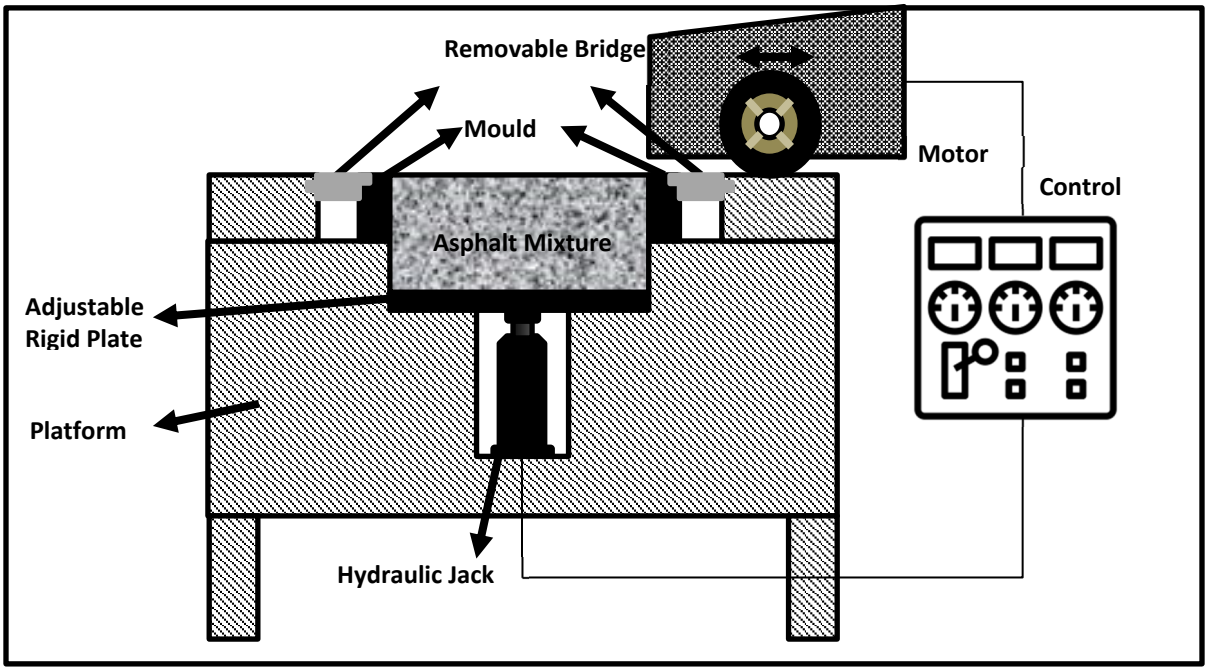

Figure 4.9 Schematic of LPC compactor (side view)

After compaction, the asphalt mixture slabs remained inside the mould for 2 days to cool down and, then, their bulk specific gravities (G_{mb}) were measured by submerging them into a water bath. Having both G_{mb} and G_{mm}, the air voids of the slabs were computed. This air voids is

very close to that in-field right after compaction. Notably, air voids have a significant impact on rutting potential. The higher the air voids, the greater the rut depth.

LPC wheel tracking test was done on 8 slabs (2 for each mixture type, 57%, 65%, 73% and 100% RAP). The rut depth was measured after 1,000, 3,000, 10,000 and 30,000 at 5 equally distanced points along wheelpath. The rut depth of each point is the average of 3 readings including one at the centreline, one at left and one at right of the wheelpath. Finally, the average of all measurements is expressed as the rut depth. Based on LC 26-410, %rut depths at 1,000 and 3,000 cycles must be less than 10% and 15%, respectively (LC method, 2020b). %rut depth can be calculated usig Equation (4.1).

$$\%rut\ depth = \frac{rut\ depth}{initial\ thickness\ of\ slab} \times 100 \quad (4.1)$$

The testing temperature was 58±2 ˚C and was monitored by a probe drilled inside the slabs. Prior to testing, the slabs were placed into the mould again and underwent 1,000 cycles by LPC wheel tracker at room temperature so as to settle inside the mould.

4.4.5.2 Semi circular bending (SCB) test

The SCB test is one of the most common tests for evaluating cracking resistance at the design stage as it is easy and quick to perform (Elseifi, Mohammad, Ying & Cooper III, 2012). Different variants of the SCB testing have been developed for intermediate and low temperatures (ASTM, 2018; AASHTO, 2020a; AASHTO, 2020b), however, due to its simplicity, ASTM D 8044 was selected in this research. The SCB specimens were prepared at target air voids of 7±0.5% using a Shear Gyratory Compactor (SGC) in which two slices with thickness of 57±4 mm were cut from each cylindrical specimens, and each slice cut into hlaf to have two SCB specimens that were, then, notched at the center. Simple Marshall testing apparatus with SCB testing frame, which can be found in any laboratory, can be used for this testing procedure. Since the mixtures were rejuvenated and this study investigates the durability of rejuvenation, the test was performed on both short term (ST) and long term (LT)

aged specimens to assess and compare aging resistance of mixtures. The testing temperature was 23±2℃. A new criteria based on ST aged to LT aged strength ratio (Equation (4.2)) is introduced with that regard to rank aging resistance.

$$SCB\ strength\ ratio = \frac{S_{ST}}{S_{LT}} \quad (4.2)$$

Where: S_{ST} and S_{LT} are the average SCB strength of ST and LT aged specimens, respectively. The closer the ratio to 1, the higher aging resistant the mixture.

By placing loose mixtures in forced-draft oven for at least 2 h, ST aging was implemented on all samples. After compaction, for LT aging, sawed and notched samples were kept at 95 ˚C in forced-draft oven for 3 days (Al-Qadi et al., 2019). Figure 4.10 indicates the difference between ST and LT aged specimens containing 57% RAP.

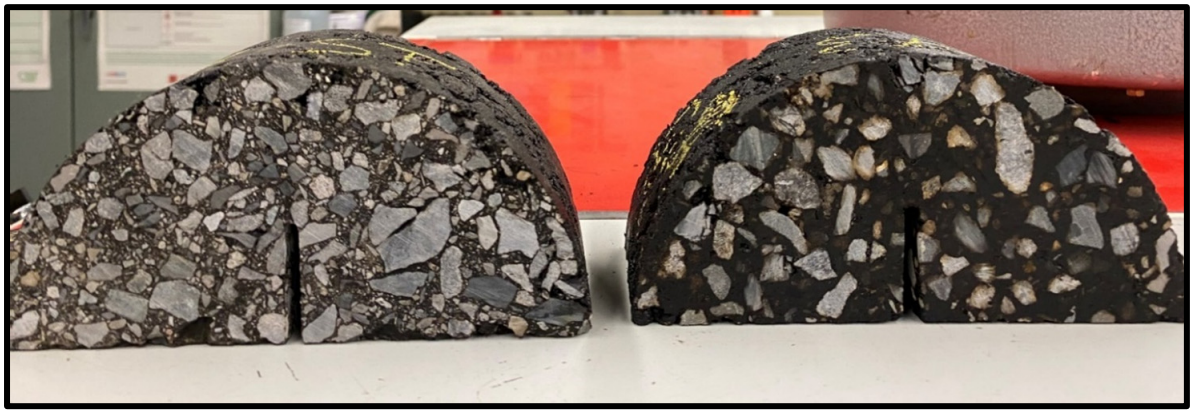

Figure 4.10 SCB sample before (left) and after (right) LT aging

In addition to the peak load, load vs vertical displacement curve gives slope (m) and strain energy to failure, namely fracture energy (U). U is the area under load vs vertical displacement curve and represents energy absorption before failure and m is the stiffness of the specimen. ASTM D 8044 recommends taking U as the area until the maximum load. However, since the post-peak portion is also important with regard to cracking resistance (AASHTO, 2020b), the test was terminated when %5 of the peak load is reached. Then, it is possible to well extrapolate

the tail of the curve and compute U as the whole area under load vs vertical displacement curve. This is a more trustworthy assessment of cracking resistance as it takes the energy until full rupture rather than the initiation of rupture; the way the area until the maximum load suggests. It should be noted that the higher U and lower m are preferable with respect to cracking resistance.

4.4.5.3 LC method for moisture damage resistance testing

Complying LC method (2020a), a batch of about 10 kg loose asphalt mixture was prepared at OAC and, then, splited 3 times to give 8 samples of approximately 1200±50 g. By applying 40 blows of Marshall hammer at each side, 8 compacted samples were fabricated. Among them, the two sets of three samples that have the closest bulk specific gravity were chosen for moisture damage resistance test.

One set (conditioned) underwnet dry vacuuming for 30 min followed by slow water introduction under vacuuming for another 30 min or until the samples get immersed. Then, samples transferred into 60 ˚C water bath without being exposed to air and remain there for 24 h before Marshall Stability testing. The other set (unconditioned) stays in 60 ˚C water bath for 30-40 min before Marshall Stability test. The ratio of average conditioned to unconditioned Marshall Stability is an indicator of moisture damage resistance. The closer the ratio to 1, the more water damage resistant the mixture.

4.4.6 Integrated performance index

Cracking and rutting are the most common distresses that occur in flexible pavements. Moisture damages are regarded as conditions that causes premature cracking, ravelling or even rutting to occur. Moreover, aging potential can be considered as an important factor with respect to premature cracking occurrence, especially in rejuvenated mixtures. Therefore, in this study, four indicators corresponding to cracking, rutting, moisture damages and aging potential were taken into account for comparing and ranking different types of mixtures containing

different concentrations of RAP. Energy absorption, %rut depth, Marshall Stability ratio (MSR) and SCB strength ratio were the indicators deployed for cracking, rutting, moisture damages and aging potential, respectively. These indicators can be determined via simple testing equipment and procedures. That simplicity was the reason of selecting them for performance evaluation.

Equation (4.3) was developed to integrate all the indicators of performance into one index, namely performance index (PI). For calculating PI, first indicators are normalized using Equation (4.3) to (4.7) to determine performance indexes. Then, they get weighted based upon their importance and summed up to yield PI. The summation of indexes' weights is equal 1, i.e. $w_c + w_r + w_m + w_a = 1$, and in this study, they were equally weighted, i.e. $w_c = w_r = w_m = w_a = 0.25$. These weights can change based upon experts' opinion. The weighting requires considering pavement distress pattern in the region under study. Traffic loading and climatic conditions decree on the weight of each performance aspect. Here, the framework is presented and more local studies must be done for finding the pertinent weights to a region.

$$PI = w_c \times CI + w_r \times RI + w_m \times MI + w_a \times AI \tag{4.3}$$

$$CI = \frac{U_{mix}}{U_{best}} \tag{4.4}$$

$$RI = \frac{1-\frac{\%rut_{mix}}{100}}{1-\frac{\%rut_{best}}{100}} \tag{4.5}$$

$$MI = \frac{MSR_{mix}}{MSR_{best}} \tag{4.6}$$

$$AI = \frac{SCB\ strength\ ratio_{mix}}{SCB\ strength\ ratio_{best}} \tag{4.7}$$

Where: CI is normalized cracking index; RI is normalized rutting index; MI is normalized moisture damage index; and AI is normalized aging potential index; ws are corresponding

weights of each index. For rutting index (RI), the %rut depth at 30,000 is used because it is long enough to show how much shear rutting occurs. The subscript “mix” represents the mix whose index is under calculation and the subscript “best” represents the best performance among the mixtures under study. Nominators and denominators of RI, MI and AI can have values between 0 and 1. The closer to 1 means the better performance. Notably, for each index, there is always a mixture having the value of 1. It is the best mix regarding that specific performance.

Finding PIs of different mixtures under study makes it possible to determine the mixture with best performance. The one with highest PI has the best general performance among the rest and can be selected as the optimal in a balanced mix design.

4.5 Results and discussion

4.5.1 Optimal asphalt content (OAC)

Table 4.5 presents OACs and volumetric properties of different mixtures along with the PG+ designation of the extracted and recovered bitumen from them. PG+ includes the traffic designation into PG as standard “S”, high “H”, very high “V” and extremely high “E” traffic volume. It is evident that the asphalt binder from mixtures containing virgin aggregates have almost the same PG+ designation. Also, rejuvenation deems effective in improving PG grades of RAP binder. AOC decreases with RAP content decrease, yet, virgin binder content increases. There is significant reduction in amount of virgin binder once compared to conventional mixtures. It can be a feat respecting environmental resources preservation and fuel consumption reduction for procurement of raw materials. Although, air voids of mixtures with virgin aggregates do not meet LC and Superpave specifications, the voids in mineral aggregate (VMA) and voids filled with asphalt (VFA) almost all meet. Aurangzeb et al. (2012) proved that controlling VMA is the key factor to preserve the performance of mixtures with high RAP content.

Table 4.5 PG+ designation and mix design properties

Mixture type	Binder PG+	AOC	Virgin binder content	V_a (%)	VMA (%)	VFA (%)
Virgin binder	58S-28	-	-	-	-	-
RAP	88S-16	-	-	-	-	-
100%	82S-16	5.65	0.71	4.08	14.20	72.65
73%	76S-22	5.15	1.63	2.98	13.03	77.57
65%	76S-22	5.10	1.99	2.92	13.34	75.12
57%	70H-22	4.95	2.25	3.06	13.73	76.76

4.5.2 Performance evaluation

4.5.2.1 Rutting

Air voids content is an important factor in rut depth. The LPC compactor applies the same compaction effort on all mixture types. So, the air voids content of a prepared slab by LPC can be an indication of in-field compactibility since the same compaction energy was used for all the slabs. Additionally, the rutting potential of these slabs can well represent asphalt pavement rutting potential. Table 4.6 gives the air voids contents of different mixtures fabricated at their OACs. The second slab of 73% RAP seems to be an outlier. 100% RAP has far greater air voids than 57%, 65% and 73% RAP. It is as expected since the design air voids of 100% RAP was greater than the other mixture types. This relates to intrinsic property of a badly graded mixture: at lower air void content, particles do not provide enough space to accommodate binder, rather they force binder out and cause bleeding. As a result of higher air voids due to bad gradation, as shown in Figure 4.11, 100% RAP has poorer rutting performance compared to other mixture types, even though it has stiffer asphalt binder. However, 100% RAP along with other mixture types securely satisfy maximum %rut depth at 1000 and 3000 passes criteria proposed by LC method (2020b); in fact, they all outperform conventional mixtures.

For a better visualization, profiles of different mixture types after rutting test are depicted in Figure 4.12. Distinguishable difference between 100% RAP and others exists. 100% RAP does not have strong aggregate skeleton and coarse particles are dispersed within finer particles. In contrast, 57%, 65% and 73% RAP look to have similar strong aggregate structure. It indicates another reason for higher rutting performance of 57%, 65% and 73% RAP compared to 100% RAP and magnifies the significant role of aggregate structure and the importance of restoring messed-up gradation of RAP in the mixtures with very high RAP content.

On the other hand, 65% and 73% RAP are both CDG, but 65% RAP, as a result of using white curves, had its fine particles part modified. As mentioned earlier white and black curves deviates significantly within fine particle sizes domain. 73% RAP has poorer rutting performance compared to 65% RAP. It indicates the important role of fine aggregates in rutting performance. Therefore, the stone-on-stone contact count analysis developed by Golalipour et al. (2012) for rutting potential assessment seems insufficient here since another finer level of particle sizes and its structure must be considered. It can be concluded that paying attention to both fine and coarse portion of blend is pivotal to reach a rut resistant mixture containing very high amount of RAP.

Table 4.6 Air voids content of the prepared slabs by LPC compactor

	100% RAP		73% RAP		65% RAP		57% RAP	
	Slab 1	Slab 2	Slab 1	Slab 2	Slab 1	Slab 2	Slab 1	Slab 2
Air voids	14.09	13.18	8.11	11.29	7.82	8.13	7.69	8.38
Average	13.63		9.70		7.97		8.03	

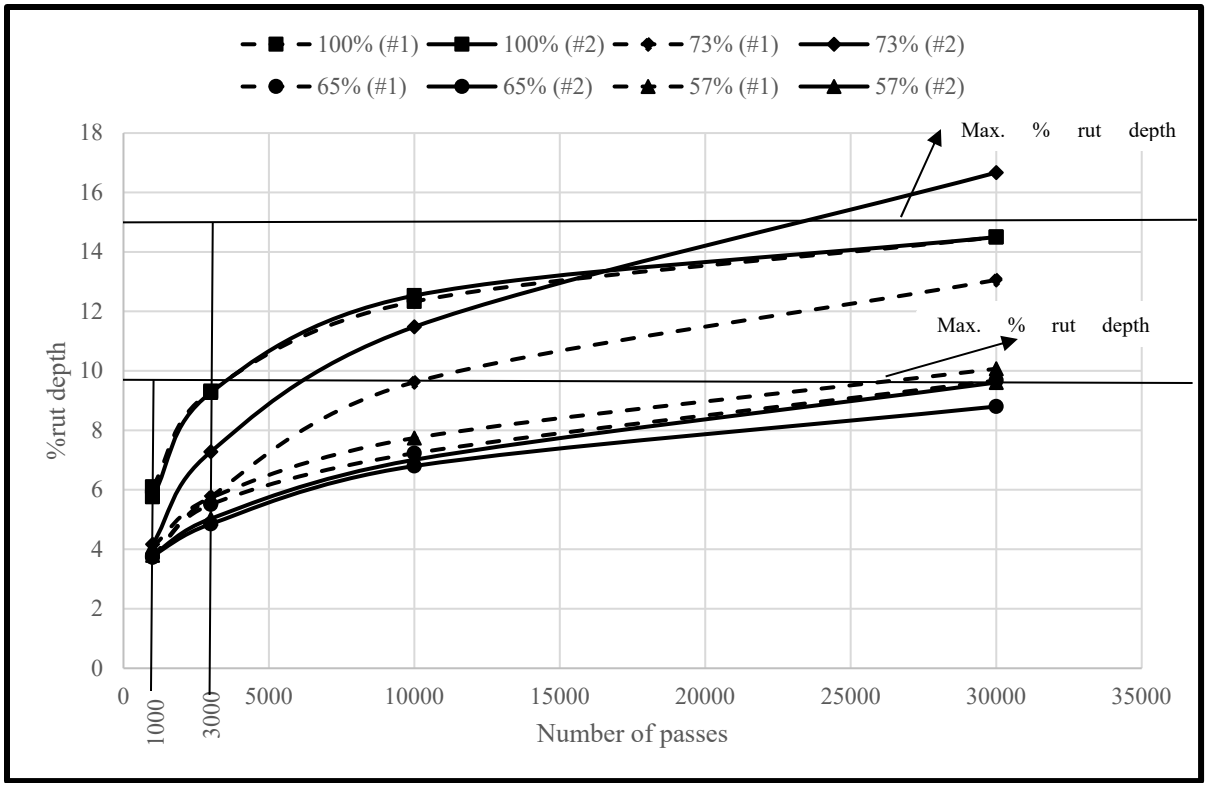

Figure 4.11 %rut depth vs. number of passes

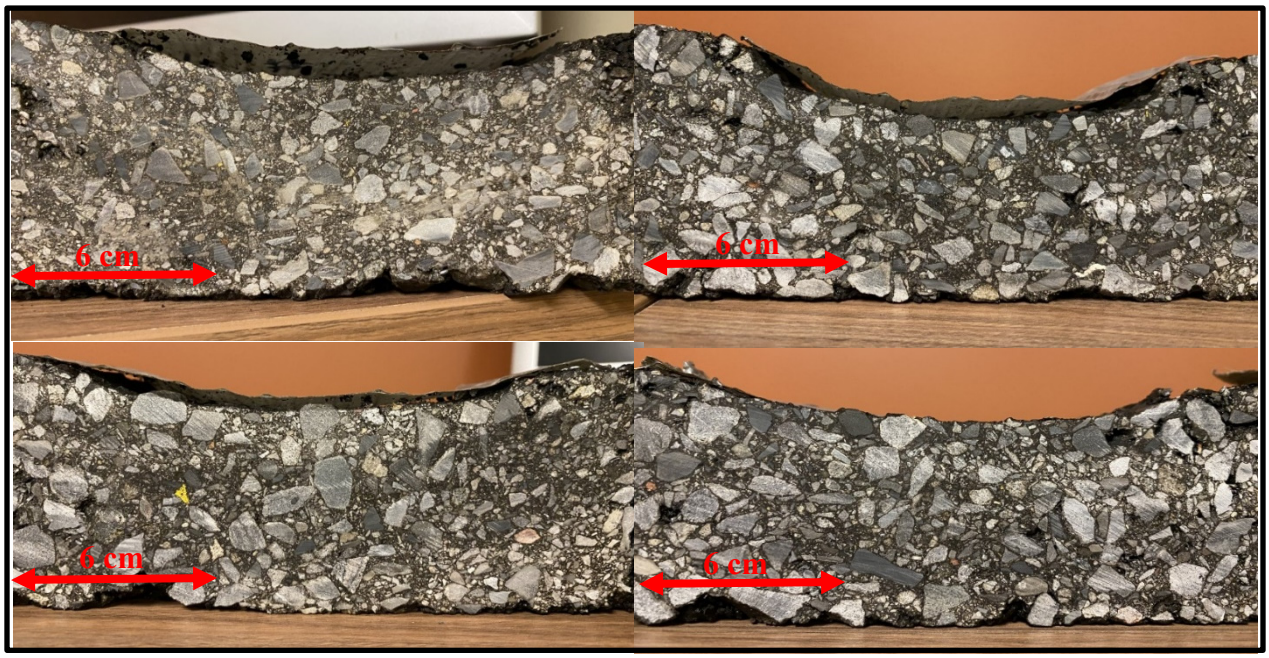

Figure 4.12 Profile of 100% (top left), 73% (top right), 65% (bottom left) and 57% (bottom right)

4.5.2.2 Aging

The amount of asphalt mixture poured into SGC mold was set to have 7% air void at the height of 135 mm. However, due to irregularity, as presented in Table 4.7, the average measured air void of two specimens is less than that. 100% RAP resulted in the highest air void content, which is expected to have a negative effect on its SCB strength.

Table 4.7 Air void content of SGC specimens prepared for extracting SCB

	100%	73%	65%	57%
Air void (%)	5.27	4.29	4.67	4.48

Figure 4.13 shows the cracking strength of short- and long-term (ST and LT) aged SCB specimens. The results are the average of three specimens with standard deviation depicted on them. Strength gain after LT aging can be an indicator of aging potential; the more the strength gain, the more intense the oxidation, the higher the aging potential with greater SCB strength ratio. At the same time, strength gain shows that oxidation can still take place and stiffen asphalt binder; i.e. there has been rejuvenation.

100% RAP has very small amount of virgin binder, however, it gains as much strength as 65% RAP does after LT aging. Furthermore, 57% RAP, with the most virgin binder, has the most strength gain. Thus, virgin binder is more prone to aging in comparison with rejuvenated binder and mixtures with higher amount of virgin binder are more susceptible to aging. Still, 73% RAP with highest SCB strength ratio has the least aging potential, not 100% RAP. That is due to the higher air voids and finer gradation of 100% RAP. These make binder more exposed to air and, subsequently, aging potential. Therefore, higher exposure to air can explain greater aging potential of 100% RAP compared to 73% RAP, and it is still true that the more virgin binder (lower RAP content here), the more aging potential.

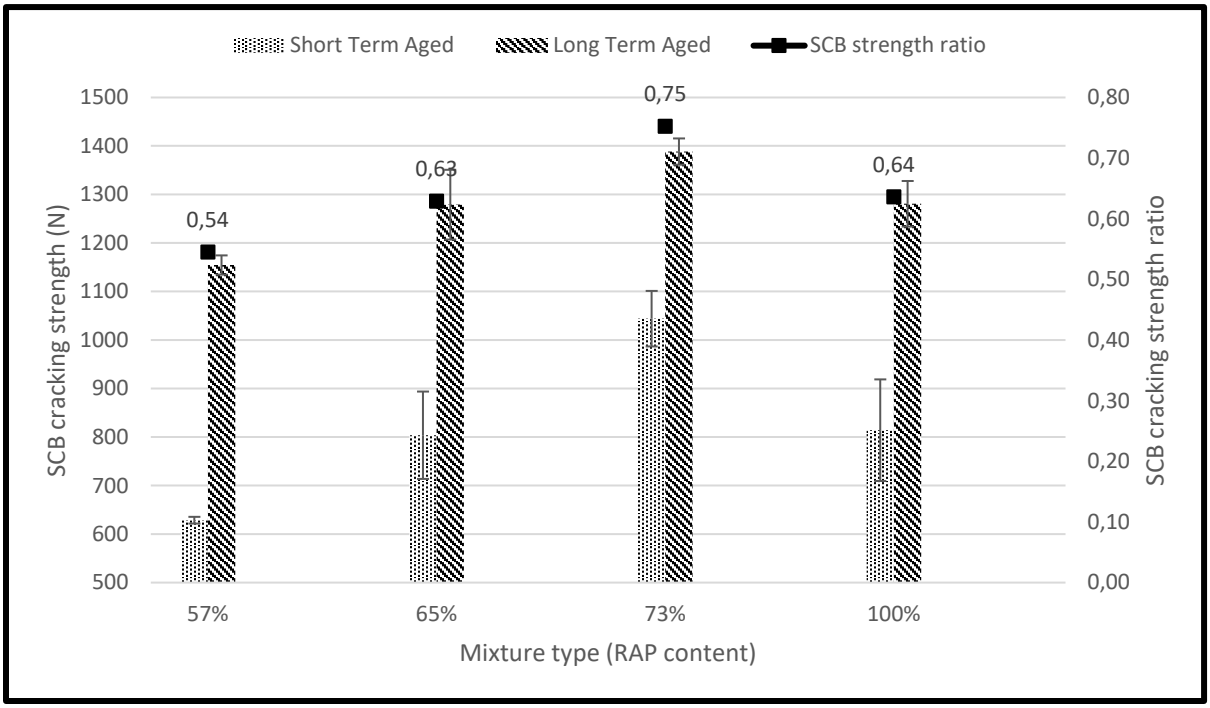

Figure 4.13 SCB cracking resistance along with short- to long-term cracking strength ratios

4.5.2.3 Cracking

As shown in Figure 4.14, total fracture energy until full rupture (U), i.e. the area under load vs displacement curve including post-peak, is not sensitive to aging. The standard deviations of Fig 14 indicates that there is no significant change between total fracture energy of short- and long-term (ST and LT) aged samples. Therefore, this indicator is not suitable for aging analysis. However, it is a good indicator of cracking resistance of mixture. Technically, embrittlement evolution by aging advancement makes asphalt mixtures more susceptible to cracking. Hence, it is wise to consider LT aged fracture energy for cracking resistance analysis. Consequently, 100% RAP has the least fracture energy showing the least cracking resistance. On the other hand, 73%, 65% and 57% RAP have almost the same cracking resistance.

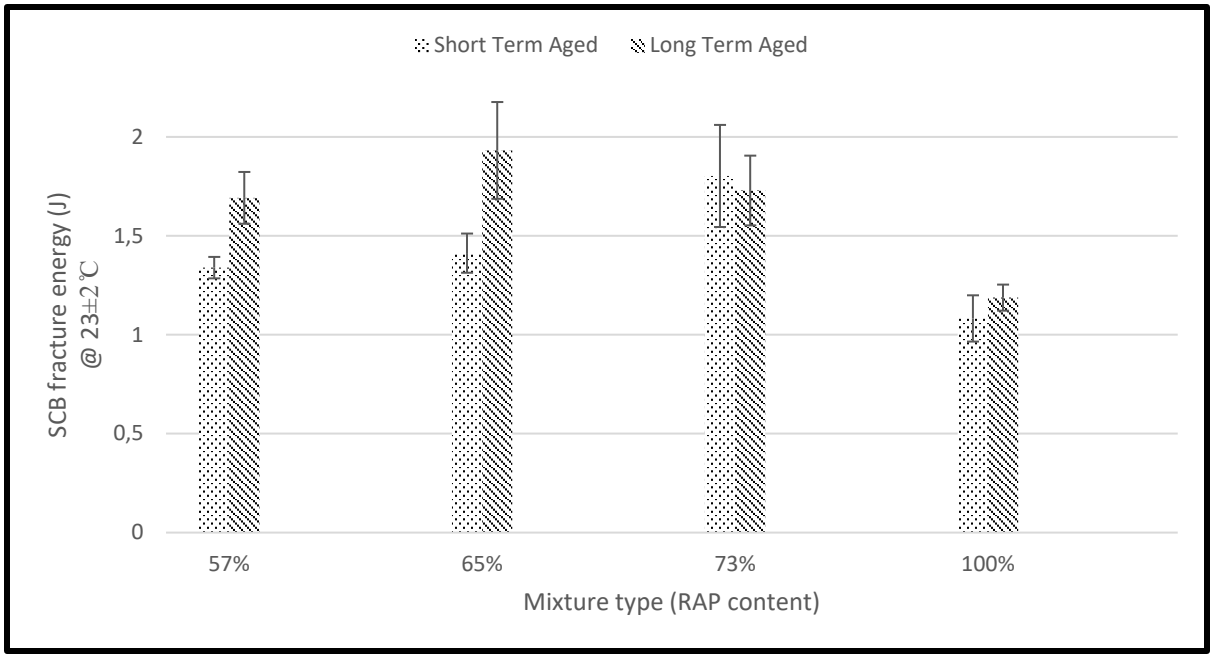

Figure 4.14 Fracture energy of the mixture types

4.5.2.4 Moisture damage

LC method proposes a defined compaction effort for all samples of moisture damage testing, both conditioned and unconditioned. So, as presented in Table 4.8, 100% RAP has greater air voids than other mixture types due to its compactibility deficiency. That intrinsic characteristic of 100% RAP certainly has a negative impact on moisture damage resistance of 100% RAP.

Table 4.8 Air voids contents of moisture sensitivity samples

	100% RAP	73% RAP	65% RAP	57% RAP
Average air void (unconditioned)	8.13	4.63	4.43	4.13
Average air void (conditioned)	7.83	4.37	4.47	4.20

Figure 4.15 reveals that the increasing trend of moisture damage resistance with RAP content reverses once it comes to 100% RAP. 73% RAP has the highest Marshall Stability ratio (MSR),

i.e. the most moisture damage resistant mixture, while 100% RAP has the highest Marshall Stability in both unconditioned and conditioned state.

Moisture damage is due to two failure mechanisms: adhesion and cohesion. Adhesive failure is due to the lack of adhesion at the interface of bitumen and aggregate while cohesive failure is due to the loss of integrity of the bitumen. For 100% RAP, the weakness does not originate in lack of adhesion because aggregate and binder of RAP has become one stance after many years of natural curing during the pavement service life. Cohesive failure, on the other hand, can be as a result of high air voids and/or lack of bitumen; 100% RAP suffers from both. In condition of adding more virgin binder into 100% RAP, lower air voids and the preservation of the increasing trend of MSR with RAP content is expected. Notably, all mixtures have outstanding moisture damage resistance. They securely meet the requirement of LC method.

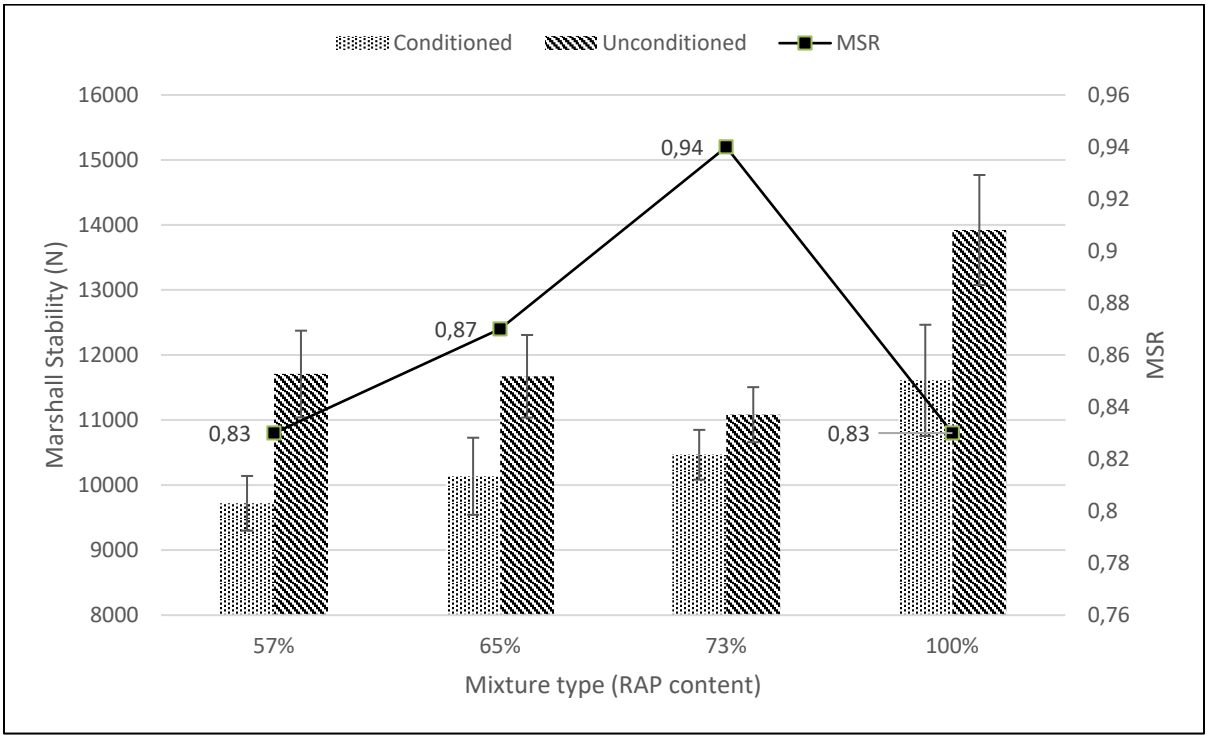

Figure 4.15 Marshall Stability and MSR of the mixture types

4.5.3 Integrated performance ranking

Several mixtures may meet criteria and requirements with respect to resistance against all distress types. In this study, all mixtures meet the criteria; both rutting and moisture damage resistance criteria. So, the judgement among different acceptable mixtures to choose the best one with respect to general performance is tough and generally very qualitative. Hence, the development of an integrated performance index (PI) is very important for a balanced mix design in order to include all performance aspects of mixtures. The PI formulated in this study can help ranking asphalt mixtures containing very high RAP fairly if the weight of each performance aspect is properly given; i.e. based upon the prevalence of distresses in a region. Table 4.10 summarizes the PIs of different mixture types along with each specific performance index.

On the basis of equal occurrence potential of all distresses, 73% RAP is ranked first; narrowly followed by 65% RAP. 73% RAP has the best performance regarding aging and moisture damage resistance whereas 65% RAP is the best regarding cracking and rutting resistance. 57% RAP lags behind 65% and 73% RAP mainly due to the weakest aging and moisture damage resistance. 100% RAP has the lowest PI indicating the worst overall performance among all. It should be noted that this specific results are due to the specific weight allocations to performance aspects.

In addition to PI, it is highly recommended to calculate standard deviation for each mixture type. Regardless the very good overall performance, poor performance regarding one or two distress types can easily eradicate all very good aspects of performance and leads to early failure of the pavement. Therefore, it is very important to consider how centralized the performance indexes including RI, CI, AI and MI are so as not to choose a mixture that has a short service life due to a single failure. Table 9 indicates 73% has the lowest standard deviation and 100% has the highest. This corroborates the first rank of 73% and the lowest rank of 100% and, all in all, it pronounces the necessity of correcting gradation to have better quality mixture.

Table 4.9 Performance indices of mixture types

	57% RAP	**65% RAP**	**73% RAP**	**100% RAP**
%rut depth @ 30,000	9.84	9.24	13.6	14.5
RI	0.993	1	0.952	0.942
fracture energy after long-term aging	1.691968	1.932	1.729	1.188
CI	0.876	1	0.895	0.615
SCB strength ratio	0.5444	0.628	0.752	0.636
AI	0.724	0.835	1	0.845
MSR	0.830	0.868	0.944	0.834
MI	0.879	0.919	1	0.883
PI	0.868	0.939	0.962	0.821
Standard deviation	0.111	0.078	0.050	0.143

4.6 Conclusion

This research provided guidance to particle size grading, producing, compacting, finding optimal asphalt content (OAC) and systematic ranking of rejuvenated asphalt mixtures with very high RAP content (>50%). These are essential means of a balanced mix design. Using coarse dense-graded (CDG) and fine-dens-graded (FDG) concepts of Bailey method, gradation of 100% RAP was rectified. The resultants were mixtures containing 73%, 65% (CDG) and 57% (FDG) RAP. Subsequently, the impact of gradation restoration on performance including rutting, cracking, aging and moisture damage resistance was evaluated. Based on the obtained results, following conclusions can be drawn:

- Any design system dealing with mixtures containing very high RAP must take gradation, rejuvenation, optimal asphalt content (AOC) determination and performance into account.

- Bailey concepts can be successfully applied to correct gradation of 100% RAP. The gradation correction improves performance, especially rutting and cracking resistance, and compactibility.

- Volumetric properties based on which conventional mixtures are designed cannot be strictly followed when it comes to mixtures with very high RAP content. A more flexible approach with regard to volumetric properties is recommended for determining AOC. Using 3% as the target air voids, instead of 4%, is recommended for mixtures with very high RAP content if bleeding does not take place.

- RAP is a rich source of aggregate and bitumen that have been naturally procured together during service life of pavements. Its application in very high amount can result in mixture with good performance satisfying all performance requirements.

Since rejuvenation is a must for mixtures with very high amount RAP, aging potential of rejuvenated mixture becomes important. The rejuvenation that does not last for long is a waste of investment. Hence, in this study, a simple but effective method to evaluate aging potential was proposed that can discriminate mixtures before and aging. Aging is an important performance aspect for mixture with very high RAP content that is required to be, somewhat, embedded in any balanced mix design for these mixtures.

CHAPTER 5

LINEAR VISCO-ELASTIC BEHAVIOR OF ASPHALT BINDERS AND MIXTURES CONTAINING VERY HIGH PERCENTAGES OF RAP

Reza Imaninasab*[a], Luis Loria-Salazar[b], Alan Carter[a]

[a] Construction Engineering Department, École de technologie supérieure, 1100 Notre-Dame St W, Montreal, QC H3C 1K3, Canada.
[b] Universidad Isaac Newton, Av. 7 13, Paso De La Vaca, San José, Costa Rica.

Paper accepted for publication in the Journal of Frontiers of Structural and Civil Engineering, February 10, 2023

5.1 Abstract

The primary aim of this study is to correlate the impact of aggregates, if any, on the viscoelastic behavior of rejuvenated asphalt mixtures containing very high amounts of reclaimed asphalt pavement (RAP) (> 50%). First, gradation of 100% RAP was rectified, using a modified Bailey method by adding virgin aggregates to achieve two coarse dense-graded and one fine dense-graded blends. Complex modulus test was then performed from -35 to +35℃ and 0.01–10 Hz. In addition to performance grade (PG) testing, extracted and recovered binders from different asphalt mixtures underwent shear complex modulus test within -8℃ to high temperature PG and frequencies from 0.001–30 Hz. Cole-Cole, Black space, complex modulus and phase angle master curves were constructed and Shift-Homothety-Shift in time-Shift (SHStS) transformation was used to compare the linear viscoelastic behavior of asphalt binders and mixtures. The influence of aggregates on the viscoelastic behavior of asphalt mixtures depends on temperature and/or frequency. The role of asphalt binders in the behavior of asphalt mixtures is more pronounced at high temperatures and the effect of the aggregate structure increases as the temperature falls. The maximum difference (60% to 70%) in the viscoelastic behavior of the binder and mixture based on SHStS transformed Cole-Cole curves is within the phase angle of 15–20°.

5.2 Introduction

The introduction of reclaimed asphalt pavement (RAP) into new asphalt pavements has economic and environmental implications. In 1973, 1990, and 2009, the oil crises forced western countries to use RAP as a rich source of bitumen. It is now used more owing to environmental concerns (West et al., 2013). Although RAP had been used before, it was in 2001 that Superpave included a mix design of asphalt mixtures containing up to 25% RAP (McDaniel & Anderson, 2001). This was the first fundamental step, because mix design is the first stage of research on asphalt mixtures.

Research on high RAP content (25–50%) has accelerated in recent decades because there has been a move to deploy increasingly more RAP in industry; there are sufficient RAP resources, and RAP is a cheaper raw material than virgin asphalt binder and aggregate. In parallel to many studies on different asphalt mixtures with low and high RAP content (Xiao, Amirkhanian & Juang, 2007; Hill, 2011; Kim, Mohammad & Elseifi, 2012), the idea of using a 100% RAP mixture has attracted interest (Zaumanis et al., 2013; Orosa, Pérez & Pasandín, 2022). Several studies have been conducted on this since 2013, but there have been very few studies on the transition from 50–100% RAP (very high RAP content mixtures).

It is evident from studies on 100% RAP mixtures that researchers have been too focused on the stiffness (Zaumanis et al., 2013; Zaumanis et al., 2014a; Zaumanis et al., 2014b; Elkashef & Williams, 2017a; Elkashef et al., 2017b; Elkashef et al., 2018b; Portugal et al., 2018a; Portugal et al., 2018b; Podolsky et al., 2021), aging potential (Elkashef et al., 2018a; Elkashef et al., 2018b) and mobilization (Zhao, Huang, Shu & Woods, 2015a; Zhao, Huang & Shu, 2015b; Zhao et al., 2016; Zhao et al., 2018; Kuang et al., 2018) of RAP binder. Similarly, binder rejuvenation is being investigated more than aggregates to enhance the performance of asphalt mixtures (Zaumanis et al., 2013; Zaumanis et al., 2014a; Zaumanis et al., 2014b; Elkashef & Williams, 2017a; Elkashef et al., 2017b; Elkashef et al., 2018b; Portugal et al., 2018a; Portugal et al., 2018b; Podolsky et al., 2021; Elkashef et al., 2018a; Kuang et al., 2018). The main reason for so much focus on the binder can be attributed to the belief that it is the

viscoelastic characteristics and behavior of the binder that imparts the viscoelastic characteristics and behavior to the asphalt mixture. It is claimed that for conventional asphalt mixtures containing zero to high RAP content, the aggregate skeleton plays no role in the linear viscoelastic behavior of asphalt mixtures (Olard & Di Benedetto, 2003; Possebon, Specht, Di Benedetto, Schuster & Pereira, 2022; Mangiafico, Di Benedetto, Sauzéat, Olard, Pouget & Planque, 2013). More precisely, the linear viscoelastic behavior of the asphalt mixture is the same as that of the asphalt binder and aggregates simply scale up their properties. This study investigates mixtures containing very high amounts of RAP (> 50%), and aims to verify whether the role of aggregates in the viscoelastic behavior of asphalt mixtures is insignificant. Verification was performed by establishing a correlation between the linear viscoelastic behavior of the asphalt binder and the mixture.

Using different aggregate gradations skeletons improves the certainty of the aggregate impact, if any, on the viscoelastic behavior of asphalt mixtures. Hence, four asphalt mixtures with different gradations were designed. The design of aggregate blends was based on Bailey's concepts to have a firm aggregate skeleton. In addition, minimal amounts of virgin aggregates are added to obtain coarse dense-graded (CDG) and fine dense-graded (FDG) blends to obtain asphalt mixtures with very high RAP contents. Complex modulus tests were then performed on both the asphalt mixtures and their corresponding binders that were extracted and recovered from the mixtures. The Shift-Homothety-Shift in time-Shift (SHStS) transformation was used to understand if the behavior of the asphalt binder can represent the behavior of the asphalt mixture on a smaller scale and to verify if the role of gradation is negligible.

As this study deals with rejuvenated asphalt mixtures with different percentages of RAP, its scope cannot be limited to the primary objective explained above. Comparison of different asphalt mixtures and binders with regard to viscoelastic behavior, as well as effectiveness of the rejuvenation are the secondary objectives of this study that accompany the primary objective.

5.3 Materials and methodology

As shown in Figure 5.1, the methodology is devised to assess how the asphalt binder imparts thermomechanical properties to asphalt mixtures that have a very high RAP content. A complex modulus test was performed on both asphalt binders and mixtures to construct characterization curves such as Cole-Cole, Black space, complex modulus, and phase angle master curves. Finally, SHStS transformation was performed on the Cole-Cole curves of the binder and mixture to determine the similarities between the two sets of curves.

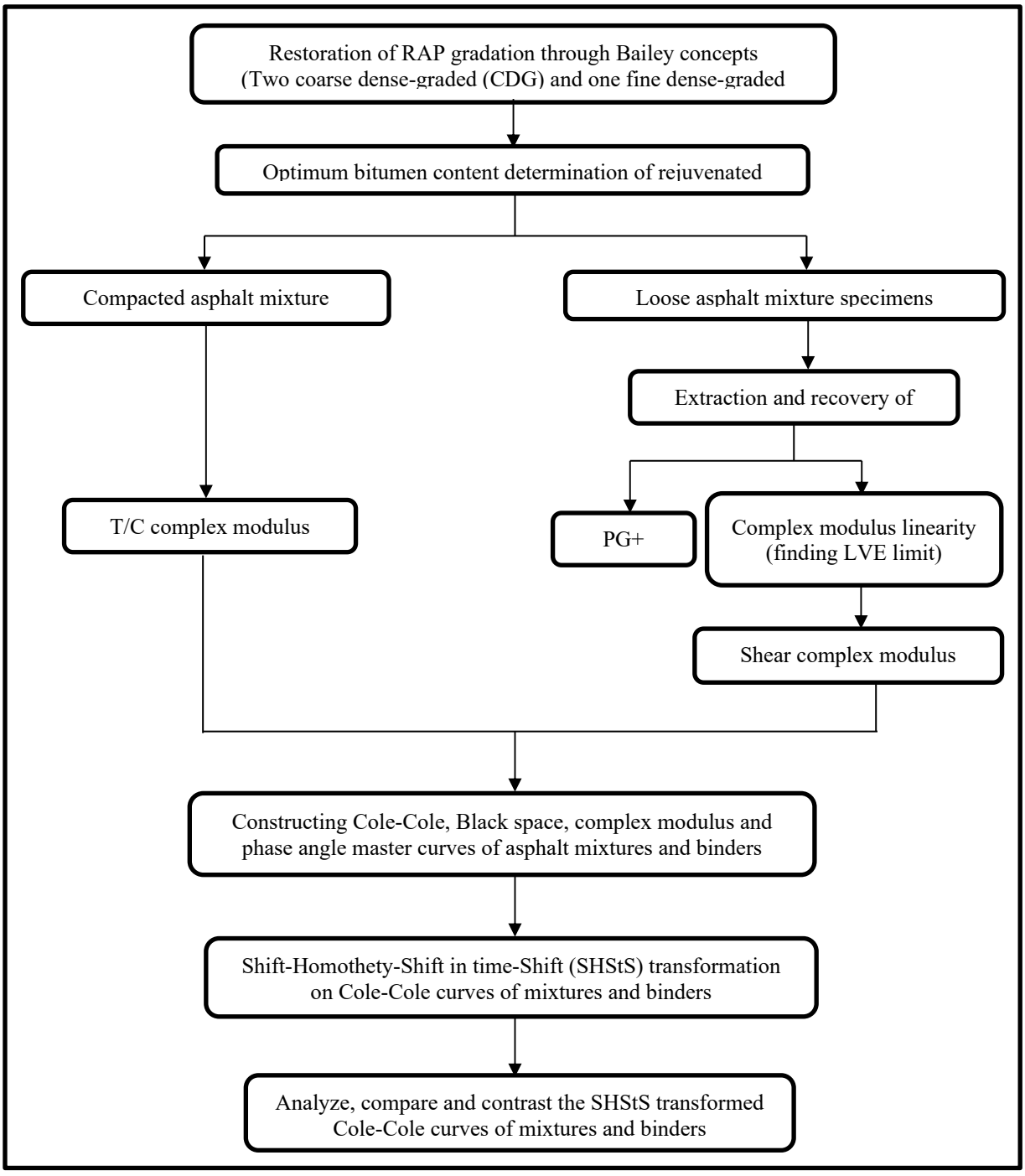

Figure 5.1 Research plan and testing program

5.3.1 Aggregates, RAP, and bitumen

The virgin aggregates used in this study were limestone that were fractionated into two stockpiles: 0–5 mm (fine) and 5–10 mm (coarse). To achieve finer gradation to rectify the RAP gradation, a finer size range (0–2.5 mm) was derived from the fine virgin aggregate. RAP contained 0–10 mm of aggregate size and was not fractionated to produce mixes because the aggregate size distributions of the blends were manipulated by proportioning the virgin aggregate stockpile. However, the RAP stockpile was fractionated to more precisely evaluate its properties. This practice is more efficient, labor-saving, and accurate because the fractionation of RAP is based on the black curve, which does not represent the real gradation, especially with respect to the fine portion. Table 5.1 lists the specific gravities of the RAP and virgin aggregates. Based on laboratoire chaussée (LC) method (MTQ, 2006), the bulk specific gravity (Gsb) and water absorption of aggregate blends were determined in the size ranges 0–2.5, 2.5–5, and > 5 mm separately, and differently. In all size ranges, the virgin aggregates had higher bulk specific gravities and less absorption. This was mainly because the RAP aggregates were a mix of different aggregate types, including granite, limestone, and siliceous aggregates, with some having more pores and cavities than the limestone.

The virgin bitumen was PG 58S-28, which is typical in cold regions. The specifications are presented in Table 5.2.

Table 5.1 Virgin and RAP aggregate gravities and water absorption

	RAP agg. (5-10mm)	RAP agg. (2.5-5mm)	RAP agg. (0-2.5mm)	Coarse agg. (5-10mm)	Fine agg. (2.5-5mm)	Fine agg. (0-2.5mm)
G_{sb}	2.694	2.667	2.660	2.714	2.707	2.694
G_{SSD}	2.721	2.704	2.693	2.734	2.728	2.720
G_{se}	2.769	2.769	2.749	2.770	2.766	2.766
Absorption (%)	1.00	1.379	1.215	0.738	0.793	0.968

Table 5.2 Virgin bitumen properties

Property	Value	Standard
Viscosity @ 135℃ (Pa.s)	0.309	AASHTO T 316
Viscosity @ 165℃ (Pa.s)	0.092	AASHTO T 316
Density @ 25℃ (g/cm^3)	1.021	AASHTO T 228
Flash point (℃)	273	ASTM D 29
Softening point (℃)	44.2	AASHTO T 53
G*/sin δ of unaged bitumen @ 58℃ (kPa)	1.54	AASHTO T 315
Mass loss after RTFO (%)	0.351	AASHTO MP 1
Jnr (3.2) of RTFO aged bitumen @ 58℃ (kPa^{-1})	2.12	AASHTO T 350
Jnr (diff.) (%)	13	AASHTO T 350
R (3.2) (%)	1.4	AASHTO T 350
Stiffness after PAV @ -18℃ & 60 s (MPa)	187	AASHTO T 313
Slope @ -18℃ & 60 s	0.313	AASHTO T 313

5.3.2 Rejuvenator

For 100% RAP mixtures, there is consensus on the necessity of rejuvenation (Zaumanis et al., 2013; Zaumanis et al., 2014a; Zaumanis et al., 2014b; Elkashef & Williams, 2017a; Elkashef et al., 2017b; Elkashef et al., 2018a; Elkashef et al., 2018b; Portugal et al., 2018a; Portugal et al., 2018b; Podolsky et al., 2021). Zaumanis et al. (2014a) indicated that bio-based rejuvenators are better than petroleum-based rejuvenators. In addition, the use of bio-based materials reduces the carbon footprint. Therefore, the application of bio-based rejuvenators has become popular.

Soybean oil derivatives are the most commonly used bio-based rejuvenators in the US, mainly because of their properties and abundance, particularly in North and Latin America (Elkashef et al., 2018b). Asphalt binders and mixtures modified by commercial soybean derivatives have been evaluated rheologically and performance-wise in several studies (Portugal et al., 2018a; Portugal et al., 2018b; Podolsky et al., 2020). In addition, the diffusibility of epoxidized soybean oil (ESO) into aged binder (Kuang et al., 2018), its chemical and rheological resistance to aging, (Elkashef et al., 2018a), and its effectiveness were studied and verified. It has been proved that 1–2% of soybean oil derivatives by total weight of asphalt binder (old plus new asphalt binder) in a 100% RAP mixture is capable of softening the old binder to be similar to the virgin binder (Elkashef et al.,2017;b Elkashef et al., 2018a; Elkashef et al., 2018b; Podolsky et al., 2020). Thus, in this study, 1% of ESO in a 100% RAP mix was converted and expressed as a percentage of the old RAP binder for application in asphalt mixes containing less than 100% RAP. All mixtures with different RAP concentrations then had the same old binder-to-rejuvenator ratio.

As a side objective, this study evaluates the efficiency of ESO inside mixtures because it is very important for asphalt mixtures with very high RAP contents. However, unlike other studies conducted that blend the rejuvenator, virgin, and RAP binders using high shear (Zaumanis et al., 2013; Zaumanis et al., 2014a; Zaumanis et al., 2014b; Elkashef & Williams, 2017a; Elkashef et al., 2017b; Elkashef et al., 2018a; Elkashef et al., 2018b; Portugal et al.,

2018a; Portugal et al., 2018b; Podolsky et al., 2021), rheological tests were performed on extracted and recovered binders from asphalt mixtures to obtain a binder with properties closer to those inside the mixture.

5.3.3 Gradation

To obtain a CDG blend of RAP, virgin coarse aggregates (5–10 mm) were added to create more space for accommodating the fine aggregates of RAP. Then, the coarse aggregate (CA), coarse part of fine aggregate (FAc), and fine part of fine aggregate (FAf) ratios were checked to satisfy the limits proposed by the Bailey method (Vavrik et al., 2002).

One of the challenges in using RAP is its gradation. The type of RAP gradation, whether black curve (RAP gradation), white curve (RAP aggregate gradation), or their average, which is used for calculation of the CA, FAc, and FAf ratios, impacts the gradation of the blend. In this study, the white curve and the average of the white and black curves were the two gradations deployed to build the CDG. Consequently, as shown in Table 5.3, two different CDG blends were obtained by combining RAP and virgin stockpiles. However, the FDG blend was designed solely based on the average of the white and black curves because, with the available virgin stockpiles, it was impossible to have an FDG blend according to the white curve that meets the CA, FAc, and FAf ratio limits proposed by the Bailey method for FDG (Vavrik et al., 2002).

Figure 5.2 shows the particle size distribution of all blend types. It can be seen that FDG has coarser gradation than CDG. This is because different stockpiles were used to correct 100% gradation, whereas if the same stockpiles had been used, CDGs would have the coarser gradations.

Table 5.3 Proportion of stockpiles for CDG, FDG and 100% RAP blends

Blend ID	RAP %	Coarse (5-10 mm) %	Fine (0-5 mm) %	Fine modifier (0-2.5 mm) %	Based on
100% RAP	100	0	0	0	
CDG (73%)	73	27	0	0	ave. black and white curve
CDG (65%)	65	23	0	12	white curve
FDG (57%)	57	30	13	0	ave. black and white curve

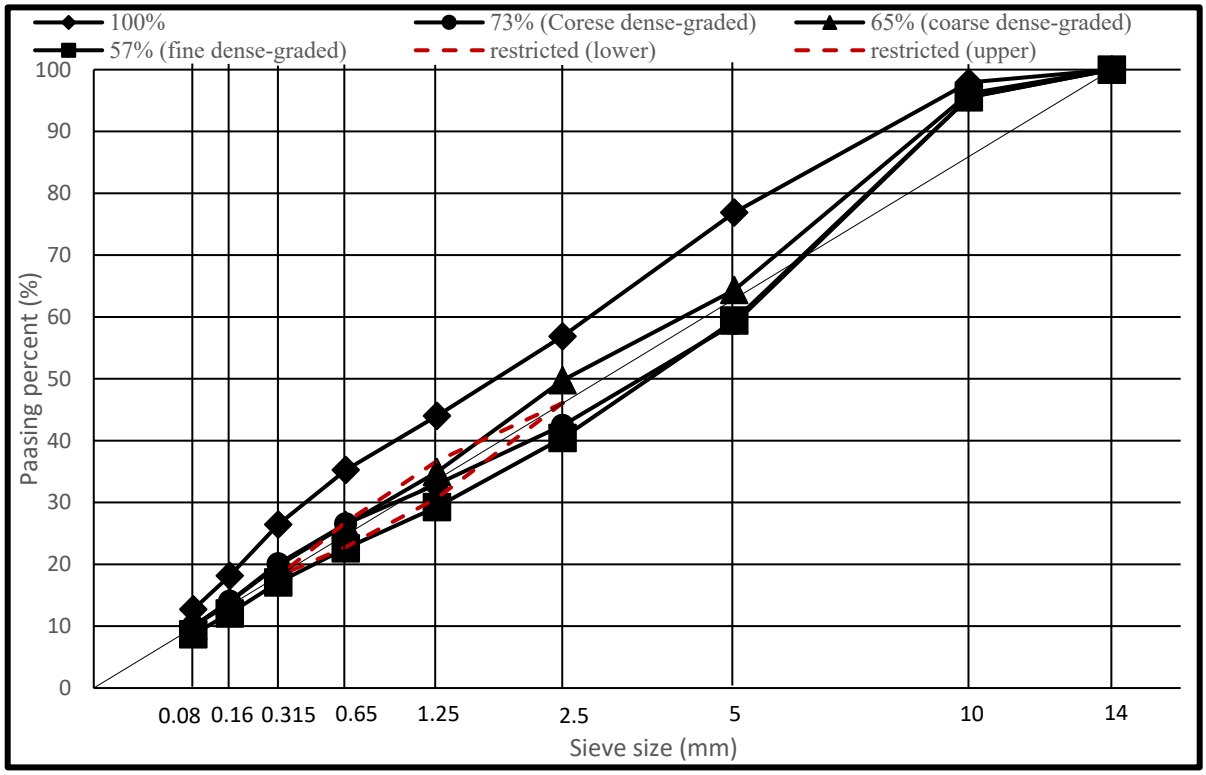

Figure 5.2 Particle size distribution of blends

5.3.4 Mix design and sample preparation

It has been proven that heating RAP using a forced-draft oven, and microwaves, results in similar mixture characteristic (Basueny et al., 2014). Therefore, to save time, microwaves were used to heat the RAP and reach the desired temperatures of 100 °C and 110 °C for 100% RAP and the other mixture types, respectively. Using a rejuvenator made it possible to decrease the mixing temperature to the aforementioned values with no negative impact on the coating and negligible clustering formation (see Figure 5.3).

Table 5.4 shows the optimum binder content (OBC) of the mixtures with different very high RAP contents, along with other important mix design properties. As recommended by Imaninasab et al. (2022), except for 100% RAP, the target air voids for asphalt mixtures containing very high amounts of RAP must be 3% to have sufficient coating. For 100% RAP, 4% target air voids were recommended (Imaninasab et al., 2022). It can be seen that a very high RAP content significantly reduces the amount of virgin binder, which not only benefits the environment, but also decreases the cost of asphalt mixture production.

Loose specimens with 57%, 65%, 73%, and 100% RAP content were prepared with OBCs and compacted at 7±0.5% air void content with a height of 150 mm to obtain 75 mm cores with 5±0.5% air voids, as recommended by Clyne, Li, Marasteanu & Skok (2003).

Table 5.4 Mix design data

	Optimal Bitumen content (Total)	Optimal Bitumen content (virgin)	Maximum specific gravity	Air void @ $N_{des.}$	Air void @ $N_{ini.}$	Air void @ $N_{Max.}$	Voids in mineral aggregates (VMA)	Voids filled with asphalt (VFA)
100%	5.65	0.71	2.534	4.08	11.41	2.59	14.20	72.65
73%	5.15	1.63	2.546	2.98	10.76	1.85	13.03	77.57
65%	5.1	1.99	2.535	2.92	10.68	2.04	13.34	75.12
57%	4.95	2.25	2.537	3.06	10.92	1.42	13.73	76.76

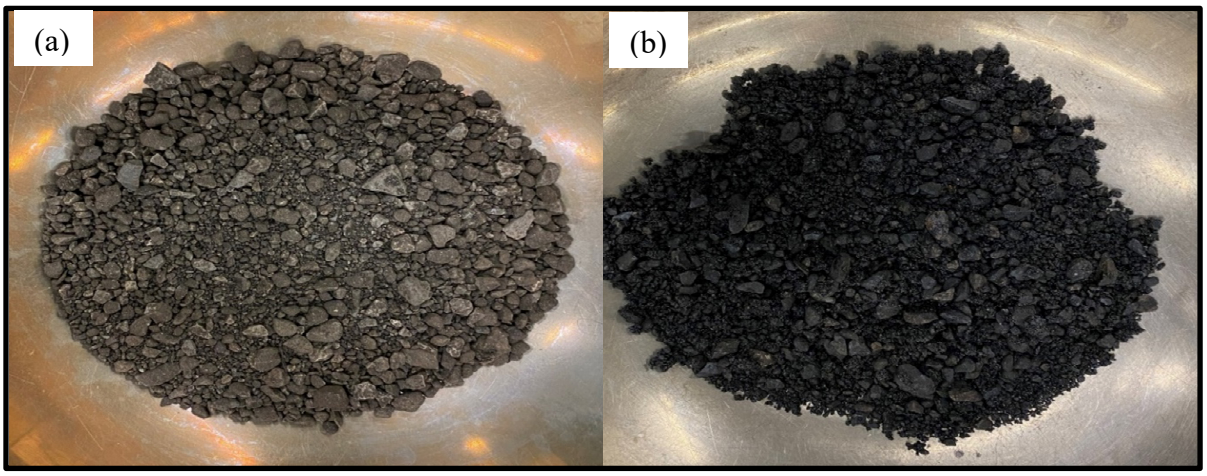

Figure 5.3 (a) RAP and (b) rejuvenated whole-RAP loose mixture prepared at 100 ˚C

5.3.5 Complex modulus of mixtures

Tension/compression complex modulus tests were performed at temperatures of -35, -25, -15, -5, 5, 15, 25, and 35 °C and frequencies of 0.01, 0.03, 0.1, 0.3, 1, 3, and 10 Hz with a strain amplitude of 50 µm/m (Di Benedetto et al., 2013). The complex modulus and phase angle were then both measured for all combinations of temperature and frequency. The useful curves that such testing provides are Cole-Cole, Black space, phase angle, and complex modulus master curves (Carret, 2018). Cole-Cole plots the real vs. imaginary complex modulus of asphalt

mixtures that can be well modeled by two springs, two parabolic elements, and one dashpot (2S2P1D). As shown in Figure 5.4, this model contains two parallel springs for elastic behavior, one dashpot for viscous behavior, and two parabolic elements (k and h) for creep behavior that subsequently address the impact of temperature on behavior. The 2S2P1D is a continuous model and cannot be used for finite element analysis; however, it is the best model for calibrating discrete models, such as Maxwell or Kelvin-Voigt, for further finite element analysis (Di Benedetto et al., 2013). Equation (5.1) yields the formulation of 2S2P1D, which is plotted in Figure 5.5 (Cole-Cole curve).

$$E^*(\omega) = E_{00} + \frac{E_0 - E_{00}}{1+\delta(j\omega\tau)^{-k}+(j\omega\tau)^{-h}+(j\omega\beta\tau)^{-1}} \quad (5.1)$$

where j2 = -1; E* is the complex modulus modelled by 2S2P1D; ω is the angular speed (ω = 2πf and f is the frequency); τ is the characteristic time depending on temperature; E0 is the glassy modulus when ω→+∞; E00 is the static modulus when ω→0; k and h are constants and, as depicted in Fig. 4, multiplied by π/2, they yield the initial and terminal slopes of the Cole-Cole curve, respectively (0 < k < h < 1); δ is a dimensionless constant; and β is a constant relating to the Newtonian viscosity of the dashpot (η = (E0 - E00)βτ).

While the Cole-Cole curve is useful for low temperatures (high frequencies) representation, the Black curve (phase angle against complex modulus curve) is suitable for high temperature (low frequencies) (Carret, 2018).

The complex modulus master curve is probably the most important curve used to interpret complex modulus test results. This provides the complex modulus (E*) of the asphalt mixtures over a wide range of frequencies at any temperature. This curve can be obtained if two conditions are satisfied: (a) the material is thermo-rheologically simple, and (b) it shows linear viscoelastic (LVE) behavior under loading (Di Benedetto & Corté, 2005). The unique Cole-Cole and black curve for a material, regardless of frequency and temperature, indicate that the two conditions are met. As a result, there is equivalency between pairs of temperatures and frequencies, that is, E* of a specific temperature (T) at different frequencies is equal to E*s of

a different arbitrary temperature (reference temperature (T_{ref})) at the frequencies (reduced frequencies (freq.)) obtained by multiplying the frequencies of T with a constant (shift factor (aT)). This concept, namely the Time-Temperature Superposition Principle (TTSP), can be expressed as Equation (5.2):

$$E^*(f,T) = E^*(f.a_T(T), T_{ref}) \tag{5.2}$$

The shift factor itself depends on the temperature (T), and each selected reference temperature yields a unique shift factor vs. T curve. This unique curve can be found using the William-Landel-Ferry (WLF) equation (Equation (5.3)) (Williams, Landel & J. D. Ferry , 1955):

$$Log(a_T) = \frac{-C_1(T-T_{ref})}{C_2+T-T_{ref}} \tag{5.3}$$

where C1 and C2 are constants that vary with respect to T_{ref}. In this study, T_{ref} was set as 15 °C.

With the same shift factors as those obtained for E*, the master curve of the phase angle can also be drawn to see how the response is delayed with frequency variation. The phase angle reveals the viscous properties of a material at different frequencies.

The goodness of fit of the 2S2P1D model in fitting the data points obtained from the complex modulus testing, was verified using statistical analysis. First, S_e (standard error of estimation) and S_y (standard error of deviation) are calculated using Equation (5.4) and Equation (5.5), and, then, R^2 (the coefficient of correlation) is determined using Equation (5.6) (Yusoff & Airey, 2010).

$$S_e = \sqrt{\frac{\sum(X-x)^2}{(n-k)}} \tag{5.4}$$

$$S_y = \sqrt{\frac{\sum(X-\bar{X})^2}{(n-1)}} \tag{5.5}$$

$$R^2 = 1 - \frac{(n-k)}{(n-1)} \times (\frac{S_e}{S_y})^2 \tag{5.6}$$

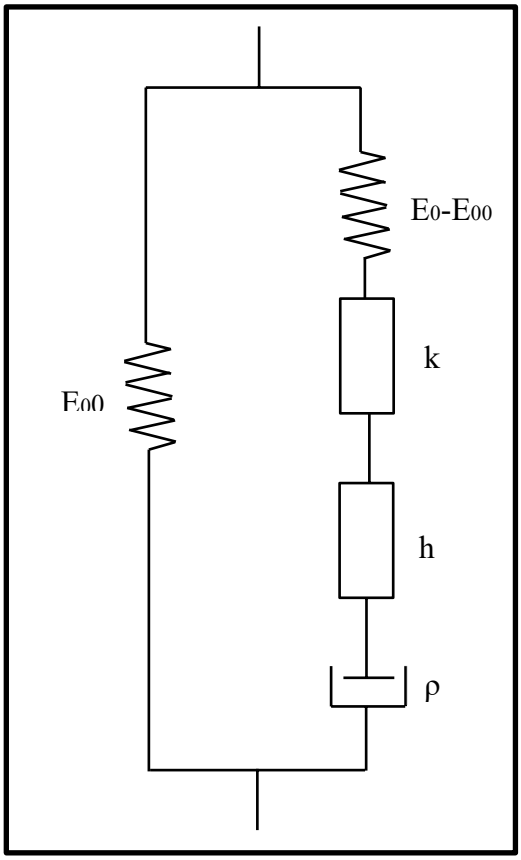

Figure 5.4 2S2P1D model schematic

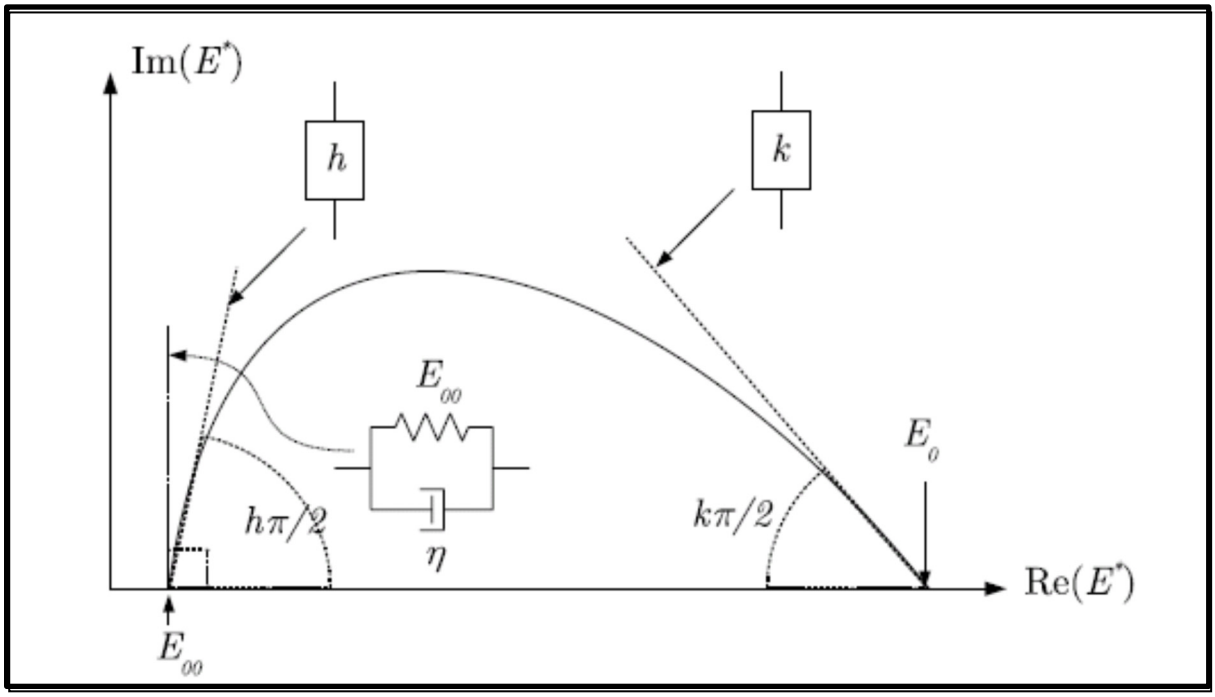

Figure 5.5 Cole-Cole curve

5.3.6 Performance grade testing and shear complex modulus master curve

In addition to the compacted specimens, loose asphalt mixtures containing 57%, 65%, 73%, and 100% RAP were prepared at their OBCs using a procedure similar to that described in the previous section. After mixing with the virgin binder, they were maintained at their compacting temperature for at least 2 h and no more than 4 h to induce short-term aging. Subsequently, the asphalt binders of these mixtures were extracted and recovered according to ASTM D8159-19 (2019d) and ASTM D5404/D5404M (2017b), respectively, for rheological testing.

First, PG testing was performed to determine the high- and low-temperature (HT and LT) PG (AASHTO T 313, 2019a; AASHTO T 315, 2020c). Because the extracted binders had already been short-term aged, they were taken as rolling thin film oven (RTFO)-aged binders. Hence, RTFO aging was not performed, and only the criteria of $G^*/\sin(\delta) < 2.2$ kPa was used to determine the HT PG. Additionally, multiple stress creep recovery (MSCR) based on

AASHTO T 350 (2019b) was performed to determine the traffic designation of asphalt binders, such as standard (S), heavy (H), very heavy (V), and extremely heavy (E).

A complex shear modulus test was performed on intact asphalt binders (non-pressure vessel aging (PAV)-aged) within a temperature range of -8 °C to the HT PG temperature in increments of 6 °C at 0.1–1 Hz frequency in increments of 0.1 Hz, and at 1–10 Hz in increments of 1 Hz. From -8 to 34 °C, an 8 mm diameter and 2 mm gap geometry was used, whereas a 25 mm diameter and 1 mm gap was used for 40 °C upward.

Prior to running the shear complex tests, a linearity test was performed for each geometry to ensure that the specimens remained within the LVE domain. Shear strain amplitude sweeps at -2 °C and 10 Hz (except 100% that was 4 °C and 1 Hz) were conducted for the 8 mm spindle while 40 °C and 10 Hz (except 100% that was 46 °C and 10 Hz) was conducted for the 25 mm spindle. To determine the linearity limit, the applied shear strain was increased, and the complex modulus was measured. With an increase in shear strain, the complex modulus decreases. The shear strain increase continues to a 5% reduction in the shear complex modulus. The shear strain corresponding to 95% of the initial shear complex modulus was set as the LVE strain limit and used to determine the shear complex modulus (Airey, Rahimzadeh & Collop , 2004). It is well known that, as the temperature increases and the frequency decreases, the shear complex modulus decreases. A decrease in the complex modulus results in an increase in the LVE strain limit (Bahia, Zhai, Onnetti & Kose, 1999; Airey et al, 2004). Therefore, for each geometry, the lowest possible temperature and highest possible frequency were used to determine the LVE strain limit for use throughout the temperature and frequency sweep.

To construct the shear modulus master curves, the same equation (WLF) was used to determine the shift factor for the asphalt binder, and the mixture behaved similarly. The reference temperature (T_{ref}) was set to 16 °C to be closest to the Tref of the mixture master curve (15 °C). Using Equation (5.7), the complex modulus of the asphalt binders can then be derived, which can subsequently be used for fitting in the 2S2P1D model.

$$E^* = 2G^*(1 + \nu^*) \quad (5.7)$$

Where G* is shear complex modulus and ν* is complex Poisson's ratio.

5.3.7 Shift-Homothety-Shift in time-Shift transformation

The SHStS transformation involves one shift along the horizontal axis, followed by a homothetic transformation, and then one shift of the characteristic time and another shift along the horizontal axis. In a study by Mangiafico et al. (2013), the SHStS transformation was successfully used to transform the Cole-Cole of the asphalt binder into the Cole-Cole of the asphalt mixture by assuming ν* = 0.5, which results in the E* binder being equal to 3G*. Although successful, setting ν* = 0.5 is not a precise assumption because ν* is a complex number (Equation (5.8)). The master curve of ν* has the same shift factor as that of E* for asphalt mixtures (Di Benedetto et al., 2013) it is believed that the same is true for asphalt binders. Combining Equation (5.8) and Equation (5.7) yields Equation (5.9).

$$\nu^* = |\nu^*|e^{j\varphi_\upsilon} \quad (5.8)$$

$$E^* = 2\ (|G^*|e^{j\varphi_G} + |G^*||\nu^*|e^{j(\varphi_G+\varphi_\upsilon)}) \quad (5.9)$$

Where φ_G and φ_ν are shear complex modulus and Poisson's ratio's phase angle, respectively.

The transformation of E_{binder}* = 3G* for the E* of mixtures reveals that the lag of the lateral response (φν) must be negligible for the asphalt materials they studied. So, Equation (5.9) could have been rewritten as Equation (5.10) in the research they carried out.

$$E^* = 2\left(|G^*|e^{j\varphi_G} + |G^*||\nu^*|e^{j(\varphi_G)}\right) = 2|G^*|e^{j\varphi_G}(1 + |\nu^*|) \quad (5.10)$$

As a result, it does not matter whether E* or G* of asphalt binder are used for SHStS transformation; the Cole-Cole of both complex modulus can establish a relationship with the Cole-Cole of the asphalt mixture, so G* was used in this study to assess whether it works.

5.4 Results and analysis

5.4.1 Performance grade (PG)

As shown in Table 5.5, the HT and LT PG of asphalt binders extracted from 57%, 65%, and 73% RAP mixtures is one level (6 °C) lower than that of the 100% RAP mixture; that is, 57%, 65%, and 73% of RAP can shift the PG of 100% RAP one level down. The rejuvenator and/or a small amount of virgin binder (12.6%) in the 100% RAP mixture resulted in a one-level shift down of the HT PG of the RAP binder (88 °C to 82 °C). The PG span of all the rejuvenated binders remains as high as 98 °C, which is reasonably high and comparable to that of the modified binders. This proves the high value of the RAP binder rather than the waste. In addition, unlike the others, 57% RAP cannot satisfy the criteria of a standard binder at its HT PG (76 °C), when it comes to PG+ designation. However, at 70 °C (one level lower than the original HT PG), it meets the requirement for a high-traffic binder, that is, H.

As shown in Figure 5.6, the effective HTs (HT_e) and LTs (LT_e) linearly decrease as the virgin binder content increases. This is consistent with the general concept of the blending chart in the NCHRP-452 report developed for determining the RAP percentage corresponding to a desired PG (McDaniel & Anderson, 2001). However, it was found that the linear correlation can be well established by using the virgin to total binder ratio rather than the percentage of RAP.

ΔTc, on the other hand, is the difference between the stiffness- and m-value-based effective LT (LT_e) and is an indicator of the aging potential (Elkashef et al., 2017b). Most aged asphalt binders have a stiffness-based LT_e smaller than the m-value-based LT_e (Elkashef et al., 2017b). Therefore, LT is generally controlled by m-value and ΔTc is generally negative. It can be

inferred that a higher value of ΔT_c indicates a higher ability to relax stress and less aging potential. Table 5.5 shows that 65% RAP results in the lowest aging potential, whereas 57%, 73%, and 100% RAP have almost the same sensitivity to aging. Compared to virgin binders, these ΔT_c values are quite promising and show the high potential of rejuvenated binders against aging.

Table 5.5 PG, PG+ and ΔT_c specifications

RAP content of mixture	100%	73%	65%	57%	RAP binder
%virgin binder in total binder	12.6	31.6	39.0	45.4	0
PG	82-16	76-22	76-22	76-22	88-16
PG+	82S-16	76S-22	76S-22	70H-22	88S-16
ΔT_c	-3.33	-2.36	-0.07	-3.28	-

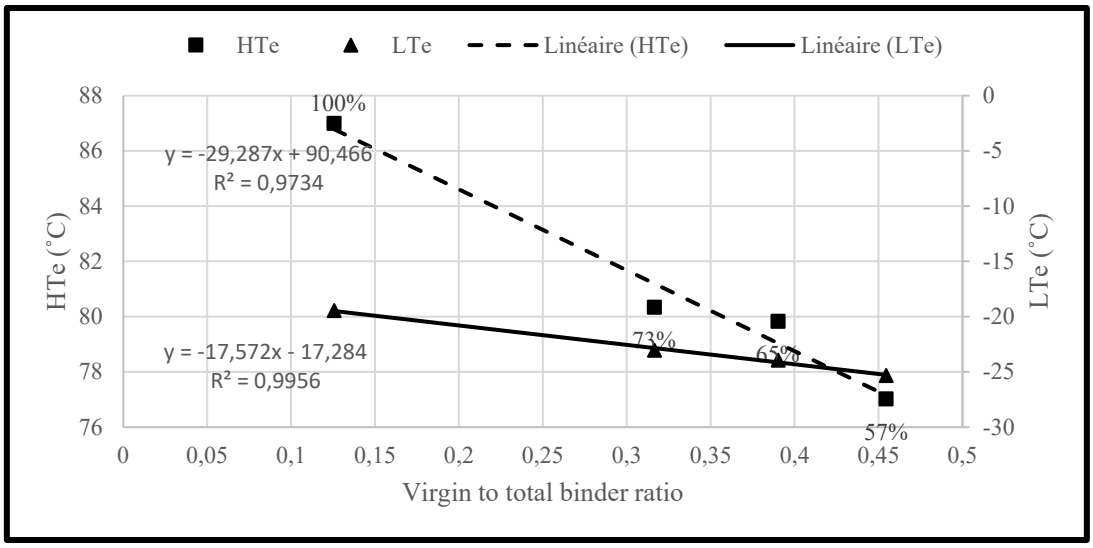

Figure 5.6 Effective high and low temperature variation with virgin to total binder ratio

5.4.2 Linearity and complex modulus of asphalt binders

Before conducting the shear complex modulus tests, linearity tests were performed on 25 mm diameter and 1 mm gap geometry (high-temperature geometry), and with 8 mm diameter and

2 mm gap geometry (low- and intermediate-temperature geometry) to determine the LVE limits of the asphalt binders. As shown in Figure 5.7, for each geometry, the LVE limits of the different binder types were approximately the same. For low- and intermediate-temperature geometries, a shear strain of 1% guarantees the LVE domain, whereas it is approximately 3% for high-temperature geometry. In addition, as shown in Fig. 8, for both geometries, the phase angles of the different binders are fairly close (less than 6° difference).

Figure 5.9 and Figure 5.10 show the Cole-Cole and Black space curves, respectively, based on the 2S2P1D model, whose calibration is given in Table 5.6. Table 5.7 evaluates the closeness of fit of the model for the data obtained from the shear complex modulus testing. Because R^2 is greater than 0.9 and S_e/S_y is greater than 0.35, the 2S2P1D model is confirmed as an excellent fit for the data (Yusoff & Airey, 2010). They indicate that 100% RAP clearly possesses stiffer characteristics at low temperatures (dashed circle in Figure 5.9) and high temperatures (dashed circle in Figure 5.10) compared to the others. The asphalt binders extracted and recovered from 57%, 65%, and 73% RAP have approximately the same stiffness characteristics as can be seen through Cole-Cole, Black space, shear complex modulus, and phase angle master curves.

Table 5.6 calibrated parameters of 2S2P1D model for asphalt binders

	E0 (MPa)	E00 (MPa)	k	h	δ	τ_0	B
100%	0	720000	0.28	0.60	4.30	0.00080000000	1000
73%	0	610000	0.30	0.62	3.50	0.00040000000	500
65%	0	670000	0.30	0.62	3.50	0.00030000000	500
57%	0	610000	0.30	0.62	3.25	0.00020000000	500

Table 5.7 Goodness of fitting statistical analysis of binders

	R^2	S_e/S_y	Criteria
100%	0.9968	0.0606	Excellent
73%	0.9976	0.0518	Excellent
65%	0.9915	0.0984	Excellent
57%	0.9940	0.0825	Excellent

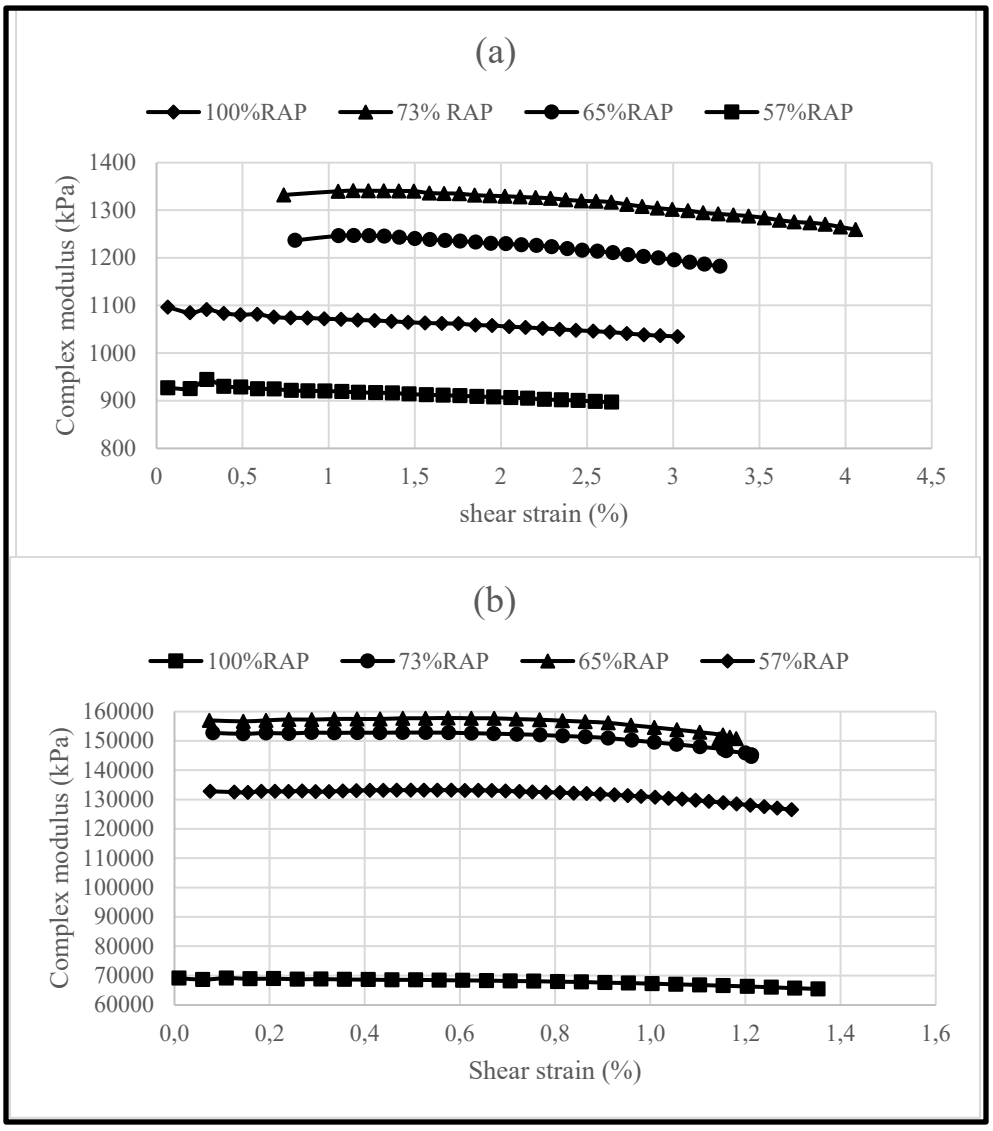

Figure 5.7 Linearity test for (a) 25 mm diameter and 1 mm gap and (b) 8 mm diameter and 2 mm gap geometry

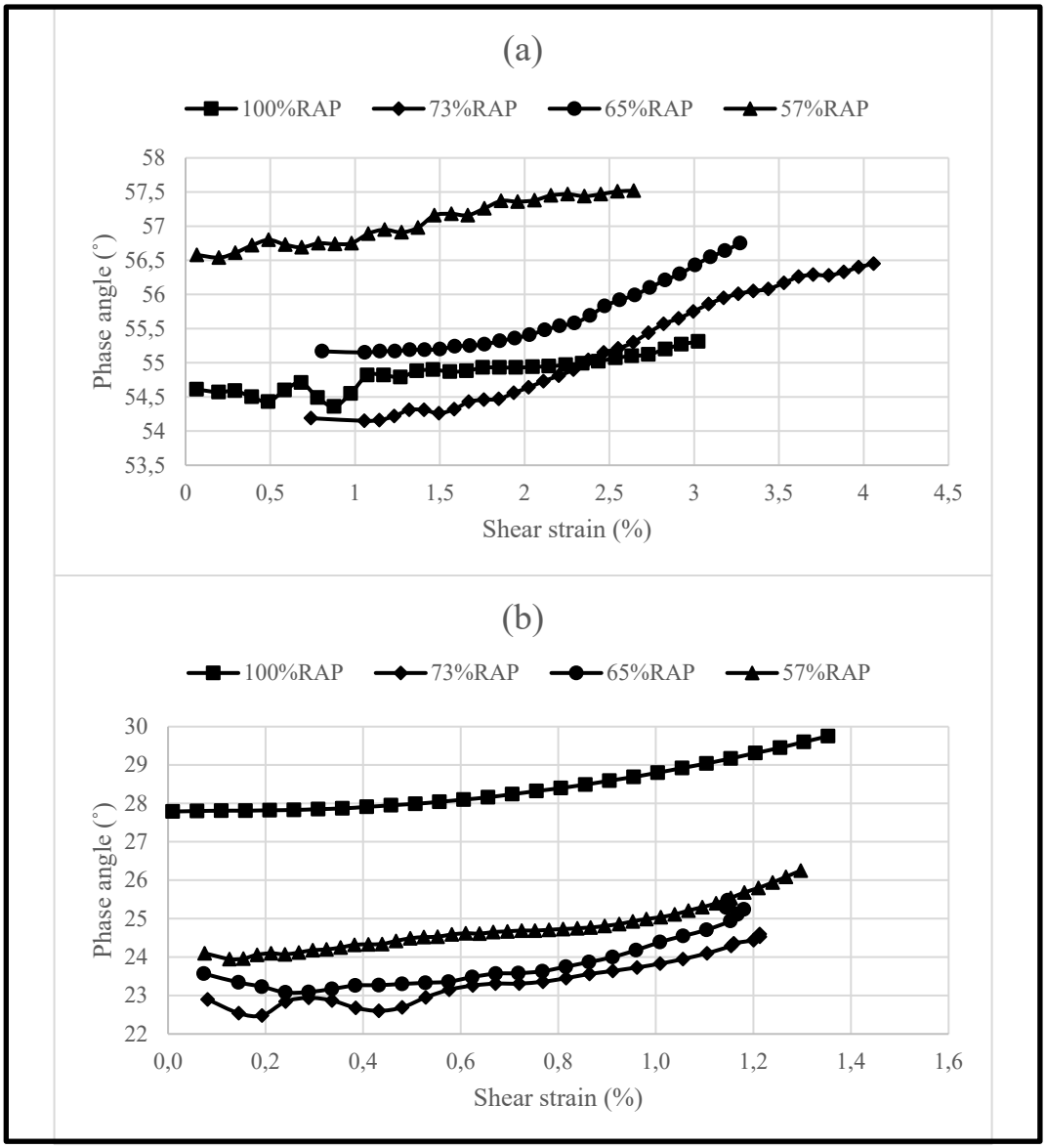

Figure 5.8 Phase angle variation during linearity test for (a) 25 mm and (b) 8 mm geometry

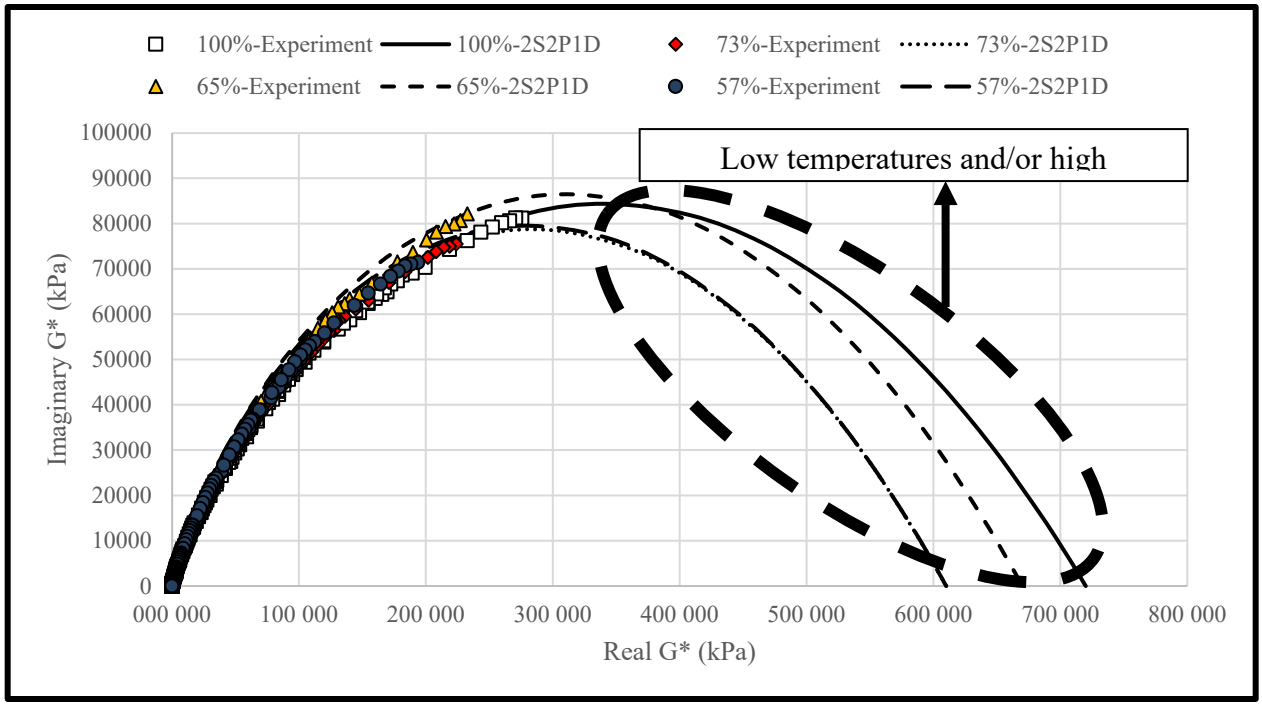

Figure 5.9 Cole-Cole diagrams of asphalt binders

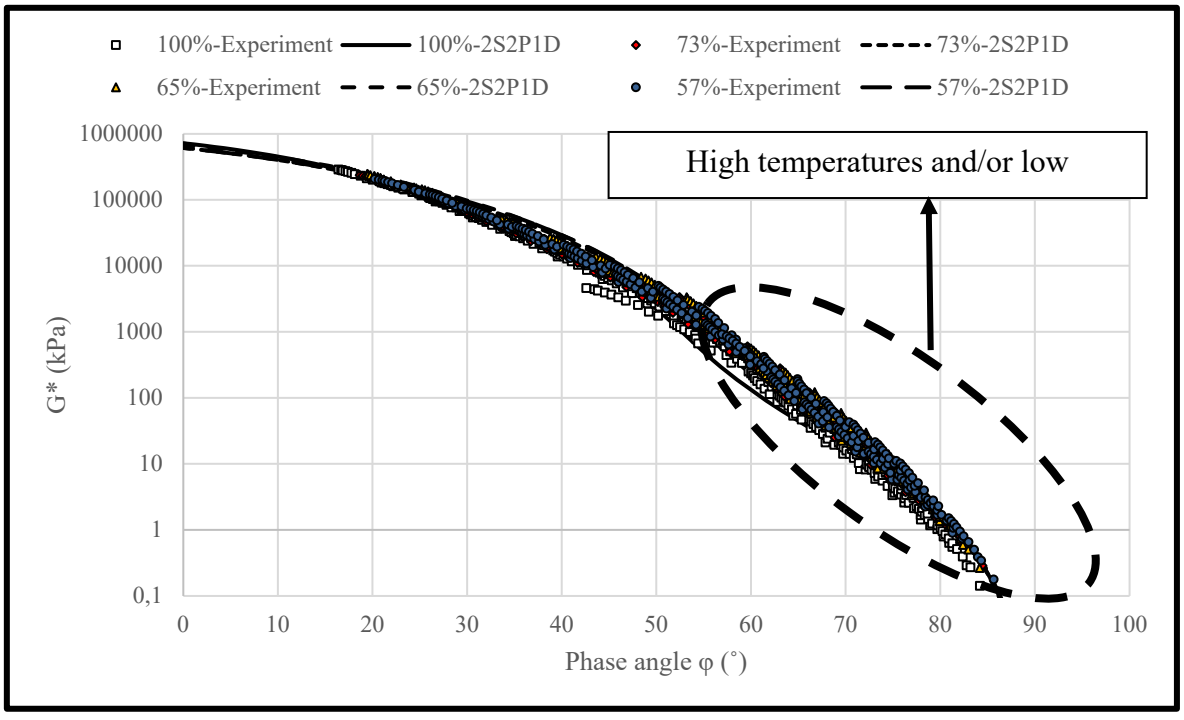

Figure 5.10 Black space diagrams of asphalt binders

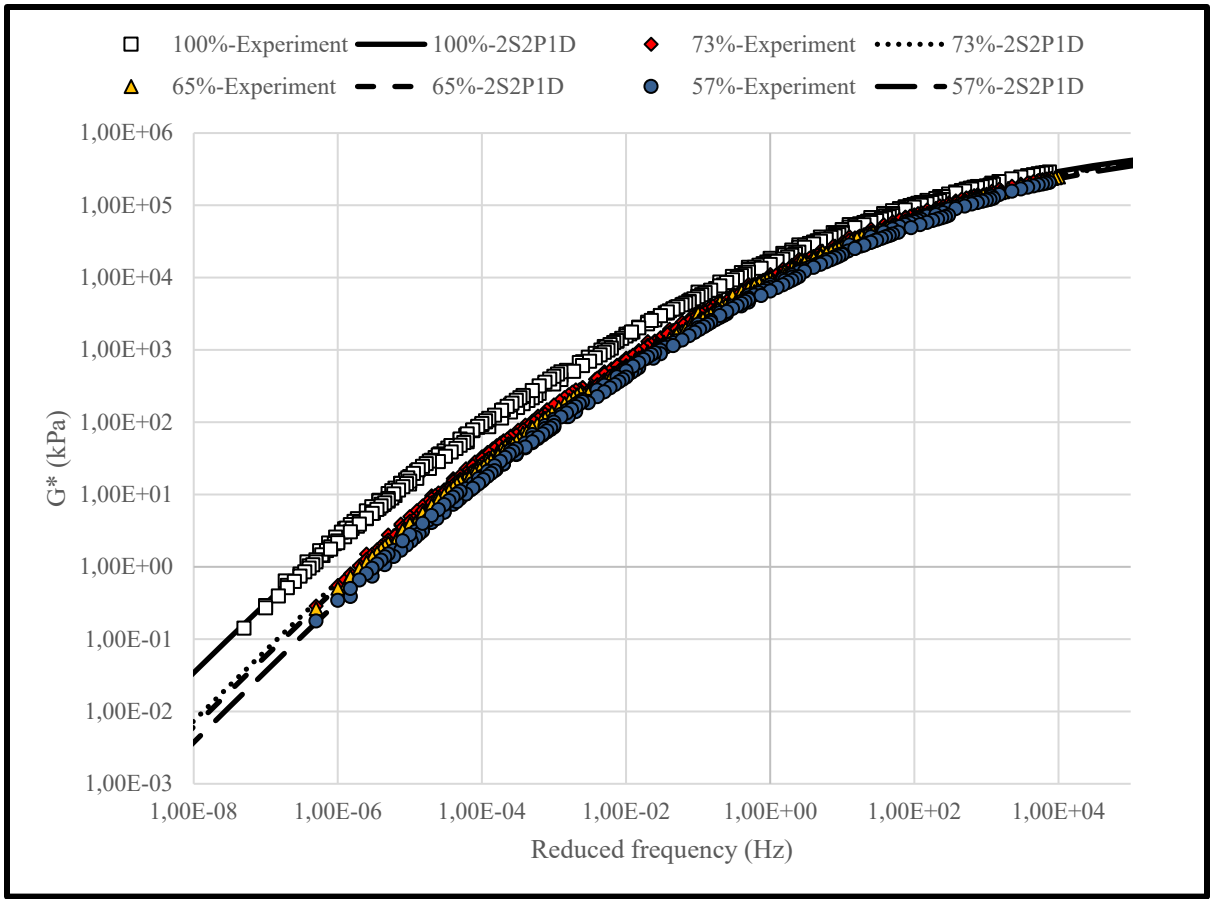

Figure 5.11 Shear complex modulus master curves of asphalt binders at reference temperature of 16 ˚C

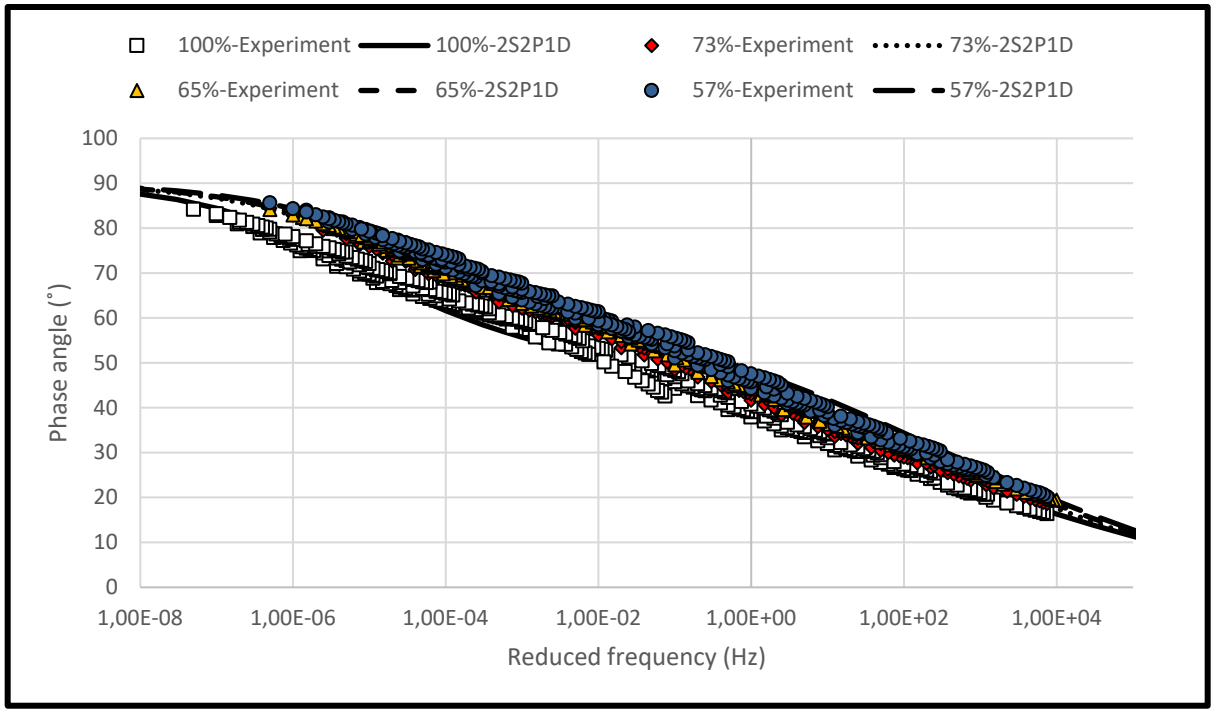

Figure 5.12 Phase angle master curves of asphalt binders at reference temperature of 16 ˚C

5.4.3 Complex modulus of mixtures

Table 5.8 shows the calibrated parameters of 2S2P1D for the asphalt mixtures under investigation. Table 5.9 indicates that the modeling has been done perfectly and the model is an excellent fit for the data. All asphalt mixtures have approximately the same E_0, k, h and δ but different E_{00}. The difference in E_{00} mainly makes the Cole-Cole plot illustrated in Figure 5.13 different from mixture to mixture. Considering the right side of the post-peak, which represents low and intermediate temperatures, 57%, 65%, and 73% RAP are stiffer than 100% RAP mixture even though 100% RAP contains stiffer asphalt binder. This signifies the importance of the aggregate skeleton in imparting characteristics to asphalt mixtures. While 57% and 65% RAP have almost the same Cole-Cole curve, 73% RAP shows a slightly stiffer curve. This can be attributed to higher RAP binder compared to 57% and 65% RAP rather than a significant difference in aggregate structure. Also, black space curves confirm the same pattern for high temperatures, that is 57%, 65%, and 73% RAP are stiffer than 100% RAP (Figure 5.14). Therefore, as shown in Figure 5.15 and can be inferred from the Cole-Cole and

Black curves, the complex modulus master curves of 57%, 65%, and 73% indicate stiffer asphalt mixtures compared to 100% RAP. Similarly, 73% RAP's complex modulus master curve stands above the 57% and 65% RAP curves. Phase angle master curves, as depicted in Figure 5.16, are consistent with former curves corresponding to Cole-Cole, Black space, and complex modulus master curves. These results contradict those obtained from binder testing. There, asphalt binder extracted and recovered from 100% RAP stands stiffer than the others, both at high and low temperatures. Although extracted and recovered binders may not represent the exact binders inside the asphalt mixtures, the stiffness comparison is valid since all binders underwent the same extraction and recovery procedure. Hence, a conclusion can be drawn that, from whole RAP to partial RAP (57%, 65%, and 73%), the contributive impact of aggregate structure on asphalt mixture's stiffness takes over the reverse impact of binder stiffness on asphalt mixture's stiffness and causes stiffer asphalt mixtures for partial than whole RAP mixtures.

Table 5.8 calibrated parameters of 2S2P1D model for asphalt mixtures

	%void	E0 (MPa)	E00 (MPa)	k	H	δ	τ_0	B
100%	5.6	35	37000	0.17	0.55	2.45	0.10000	6000
73%	4.1	35	39500	0.17	0.55	2.35	0.15000	6000
65%	4.7	35	38000	0.16	0.56	2.50	0.09000	6000
57%	4.5	35	37000	0.17	0.55	2.45	0.10000	6000

Table 5.9 Goodness of fitting statistical analysis of mixtures

	R^2	S_e/S_y	Criteria
100%	0.9984	0.0423	Excellent
73%	0.9991	0.0313	Excellent
65%	0.9988	0.0364	Excellent
57%	0.9975	0.0533	Excellent

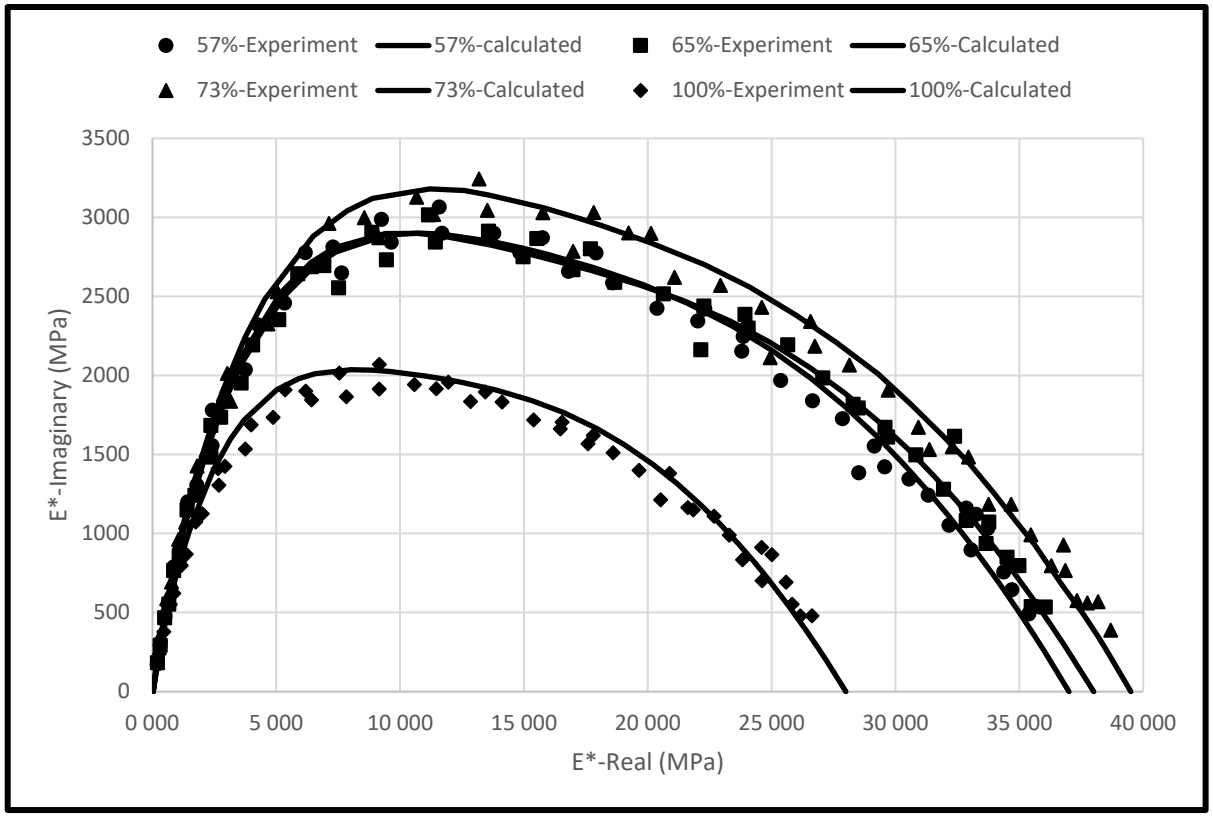

Figure 5.13 Cole-Cole diagrams of asphalt mixtures

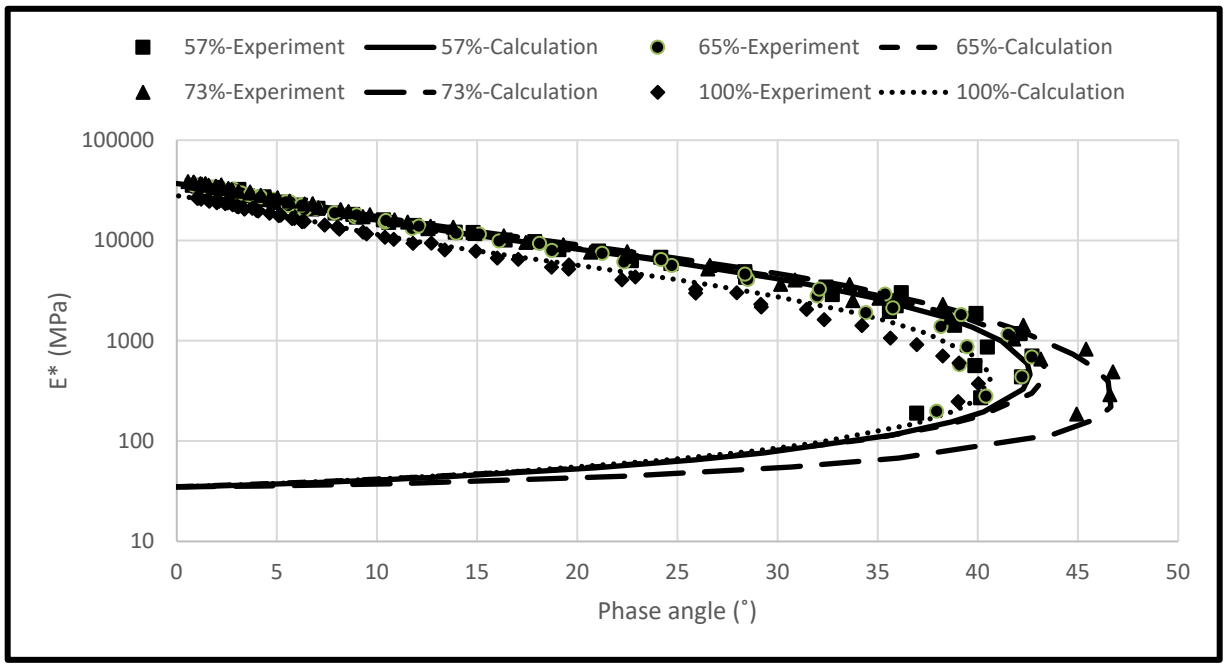

Figure 5.14 Black space diagrams of asphalt mixtures

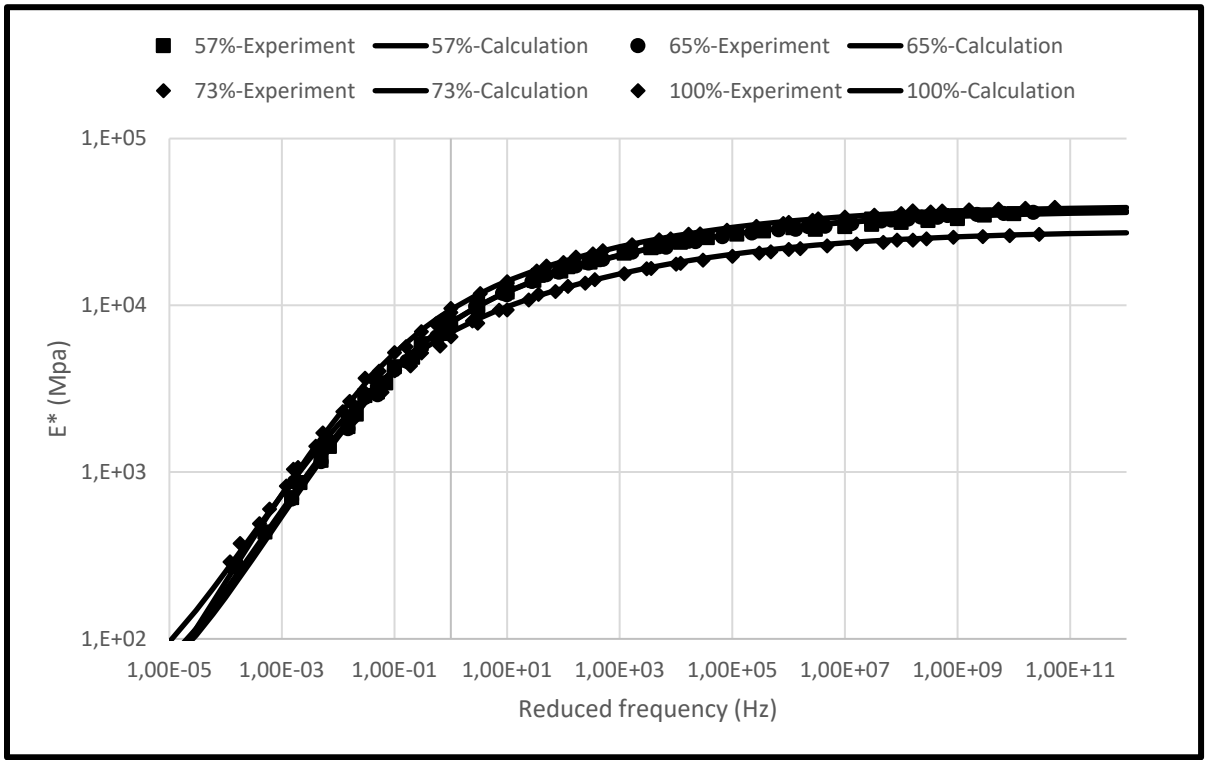

Figure 5.15 Complex modulus master curves of asphalt mixtures at reference temperature of 15 ˚C

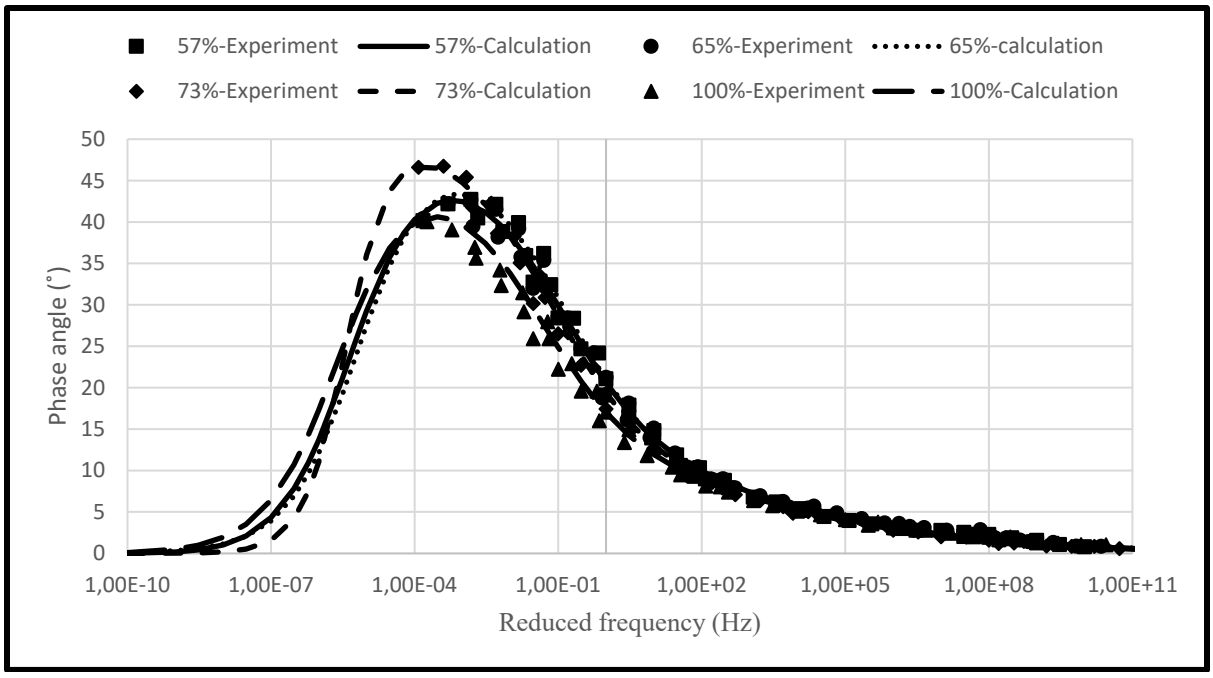

Figure 5.16 Phase angle master curves of asphalt mixtures at reference temperature of 15 ˚C

5.4.4 SHStS transformation

To understand if the aggregate gradation has an impact on the behavior of asphalt mixtures, the SHStS transformation was `conducted. The SHStS transformation provides curves with their basic shapes. As a result, it is a useful tool for assessing the similarity of material behavior regardless of the scale of their properties. The SHStS transformed Cole-Cole curves of the asphalt binder and asphalt mixture can be compared and, if approximately the same, the asphalt binder imparts viscoelastic properties to the asphalt mixture.

Figure 5.17 indicates that they are not the same within a wide domain, ending with the temperature and frequency corresponding to the lowest and highest, respectively. At the same real E*, the normalized Cole-Cole diagrams of binders have a greater loss modulus (imaginary E*) than the normalized Cole-Cole diagrams of the asphalt mixtures. Hence, within this temperature and/or frequency domain, aggregates lessen the viscous properties of binders that can be imparted to asphalt mixtures. On the other hand, asphalt binders and mixtures behave similarly at higher temperatures and lower frequencies, as the SHStS-transformed Cole-Cole diagrams are almost the same within a domain starting from the origin and ending somewhere before the peak.

Figure 5.18 shows the complex modulus vs. the phase angle of the asphalt mixtures. There are two curves for each mixture type: one is based on real results and the other is the prediction or estimation based on asphalt binder results. The two curves converge at phase angles between 25° and 35°. These correspond to higher temperatures and lower frequencies, respectively. Within the domain corresponding to low temperatures and/or high frequencies, the prediction based on the asphalt binder overestimated the complex modulus.

Thus, at high temperatures, the asphalt binder becomes more representative of the complex modulus and phase angle of the asphalt mixtures, where the asphalt binder deforms more because of less cohesion. In other words, as the temperature increases, the asphalt binder becomes more predictive of the complex modulus of the asphalt mixture (|E*|) and phase angle.

Between the phase angle of 15–20°, which corresponds to the intermediate temperature of 5 °C with a frequency range of 0.01–0.3 Hz to 15 °C with a frequency range of 1–10 Hz, the viscoelastic behavioral dependency of the asphalt binder and mixture based upon |E*| is minimized because, as depicted in Figure 5.19, the percentage difference between the normalized |E*| of the asphalt binder and mixture is at a maximum. Figure 5.20 shows that the maximum percentage difference can reach as high as 60–70%. This means that in asphalt mixtures with very high RAP content, the impact of the aggregate on the reduction of the complex modulus of the asphalt binder is between 60% and 70%. In addition, for 57%, 73%, and 100% RAP mixtures, the aggregates decreased both the real and imaginary parts of the complex modulus of the asphalt binder by approximately 60–70%. It was approximately 75–80% for a 65% RAP mixture. However, from Fig. 20, the difference between the percentage reduction of the real and imaginary parts of the complex modulus of the asphalt binder < 5%; that is, aggregates reduce both the real and imaginary parts of the complex modulus of the asphalt binder almost equally. Thus, it can be inferred that the impact of the aggregate on the phase angle of asphalt mixtures with a very high RAP content is negligible, and their effect is on the magnitude of E*.

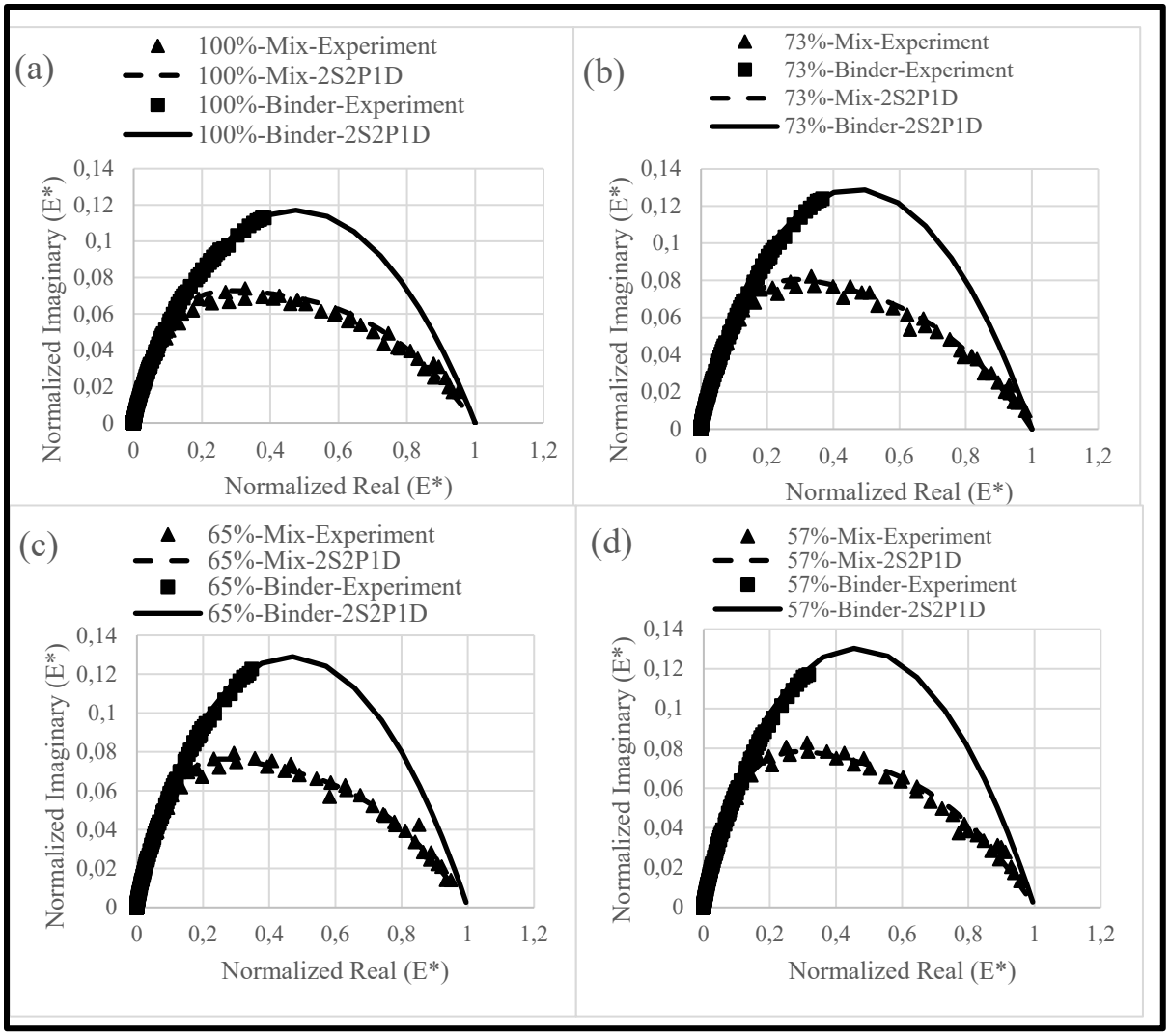

Figure 5.17 Normalized Cole-Cole diagram of asphalt mixtures and binders containing (a) 100%, (b) 73%, (c) 65% and (d) 57% RAP

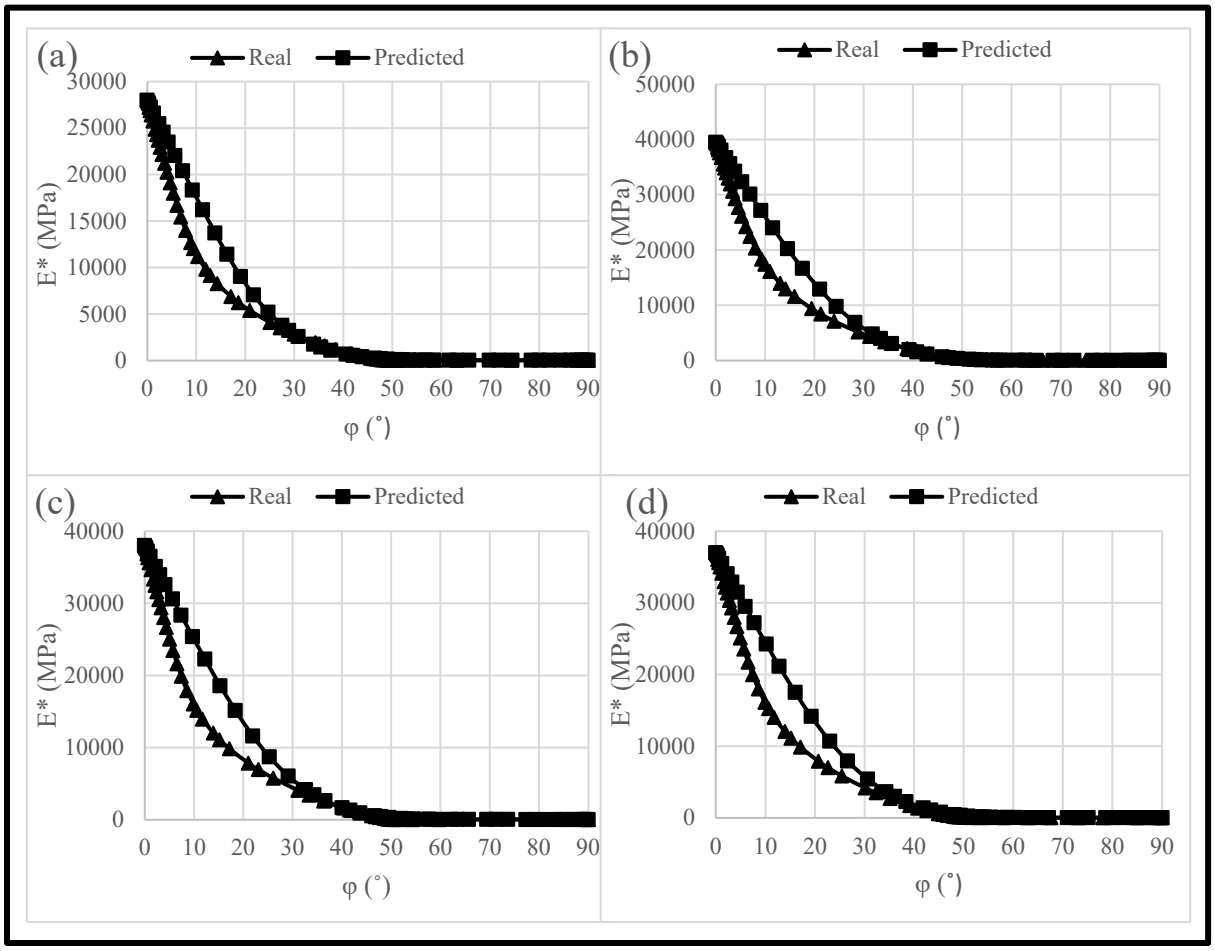

Figure 5.18 Results of SHStS traformation of asphalt binders' G* to predict asphalt mixtures' E* of (a) 100%, (b) 73%, (c) 65% and (d) 57% RAP

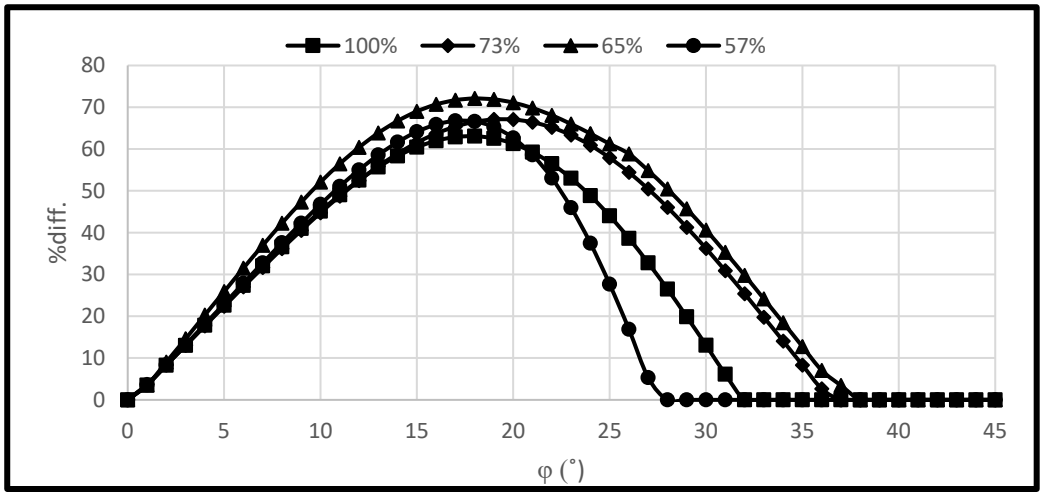

Figure 5.19 Percent difference between real and predicted E* for various mixtures

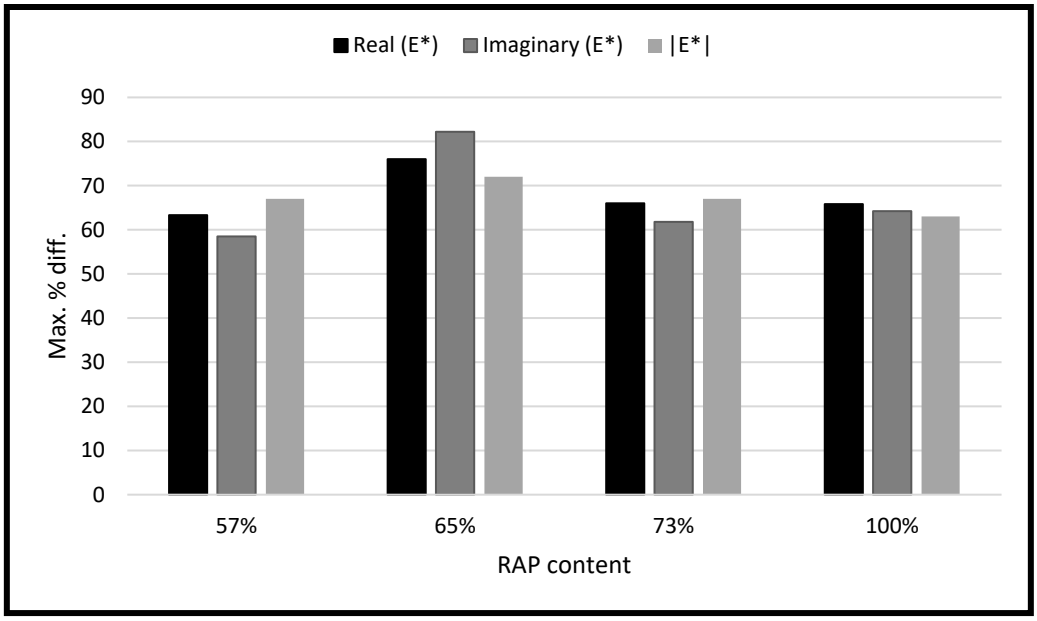

Figure 5.20 Maximum percent difference between real and imaginary part of E*

5.5 Discussion

In this study, ESO was applied in proportion to the RAP percentage of the mixtures so that all mixtures contained the same ESO to RAP binder ratio. However, the viscoelastic characteristics of asphalt binders extracted and recovered from different mixtures are not the same. On the other hand, the PG and PG+ of the binder extracted and recovered from 57%, 65%, and 73% RAP were the same, even though the amount of virgin binder in them changed. Thus, there is a high probability that the ESO partially softened the old RAP binder. This can be due to one or more of the following: (a) evaporation or modification of the ESO during the extraction and recovery process, (b) inefficiency of the ESO or the method of application, and (c) insufficient amount. This is subject to further study beyond the scope of this research.

Furthermore, previous studies have shown that the aggregate skeleton does not impart viscoelastic properties to asphalt mixtures; rather, it simply scales up the viscoelastic properties of asphalt binder (Olard & Di Benedetto, 2003; Possebon et al., 2022; Mangiafico et al., 2013). This study finds that for asphalt mixtures with very high RAP contents (> 50%), this claim is a matter of temperature and/or frequency. At high temperatures that correspond to rutting

performance, the binder imparts viscoelastic properties, and the aggregate skeleton simply scales up the viscoelastic properties. This does not mean that the aggregate skeleton does not contribute to the rutting resistance of asphalt mixtures; it does contribute, but by scaling up, not by shaping the viscoelastic behavior. However, at intermediate and low temperatures, the role of the aggregate skeleton in shaping viscoelastic behavior signifies that the asphalt mixture acts more like a composite material. In contrast, its impact on the thermal and fatigue resistance as a low and intermediate phenomenon is negligible (Underwood, 2006). This negligible impact occurs because cracking is an act of tension, and the aggregate structure engages in compressive loading rather than tensile loading.

5.6 Conclusion

In this study, PG, linearity, and complex modulus tests were performed on asphalt binders. Linearity and complex modulus were also determined for asphalt mixtures containing very high RAP content (> 50%), whose gradation was modified through the Bailey method concepts. The main purpose was to correlate the linear viscoelastic behavior of asphalt mixtures with that of their corresponding binders to determine whether aggregates affect the viscoelastic properties of asphalt mixtures. In addition, as a side objective, the rejuvenation efficiency was investigated through PG testing and characterization of the asphalt binders extracted and recovered from the asphalt mixtures. From the obtained results, the following conclusions can be drawn:

- - The asphalt binder cannot predict the behavior of the asphalt mixture at all temperatures because it is not the only element that depends on it. At high and partially intermediate temperatures, the viscoelastic characteristics of asphalt binders and mixtures are aligned, whereas at low and partially intermediate temperatures, asphalt mixtures tend to behave like a composite material with both their elements effectively contributing to the behavioral characteristics.

- Viscoelastic behavior corresponds to the non-destructive domain of a material, whereas rutting or cracking performance is related to its destructive domain. The influence of the aggregate structure on imparting viscoelastic behavior to the asphalt mixture (non-destructive domain) has nothing to do with the influence of the aggregate structure on rutting or cracking resistance (destructive domain). Rather, the impact of aggregates on rutting or cracking resistance depends on the effective type of loading (compressive or tensile) that corresponds to the resistance.

- The asphalt binder extracted and recovered from the 100% RAP mixture is stiffer than the others, but the viscoelastic characterization of the asphalt mixtures proves that it is less stiff than the others. This indicates that the effect of the aggregate structure on the viscoelastic characteristics of the asphalt mixtures is significant.

- The effect of aggregates on the linear viscoelastic properties of asphalt mixtures is limited by the magnitude of E*, and its influence on the phase angle is negligible.

- The rejuvenator and/or virgin binder used in this study, namely ESO, softened the old asphalt binder of RAP.

- Coupling rejuvenation with a firm aggregate structure leads to marginalization of the RAP percentage effect. The 57%, 65%, and 73% RAP mixtures behaved similarly, even though they contained different amounts of RAP. This is an achievement for increasing the RAP content without compromising viscoelastic characteristics. However, further investigation is required in this respect.

The viscoelastic characteristics of asphalt mixtures were measured based on both tensile and compressive action, while the rutting and cracking resistance were investigated based on

compressive and tensile action, respectively. Consequently, rutting and cracking resistance cannot be evaluated via viscoelastic characterization. In future work, it is recommended that compressive loading be applied at high temperatures and/or low frequencies, tensile loading at low temperatures and/or high frequencies, and tensile/compressive loading at intermediate temperatures and frequencies.

In addition, the findings of this study limit the materials used. A round-robin testing campaign with different RAP and virgin aggregate sources is suggested for further verification.

CHAPTER 6

RHEOLOGICAL COMPARISON BETWEEN BLENDED ASPHALT BINDERS AND EXTRACTED AND RECOVERED ASPHALT BINDER FROM REJUVENATED ASPHALT MIXTURE WITH VERY HIGH RAP CONTENT

Reza Imaninasab[a], Luis Loria-Salazar[b], Alan Carter[a]

[a] Construction Engineering Department, École de technologie supérieure, 1100 Notre-Dame St W, Montreal, QC H3C 1K3, Canada.
[b] Universidad Isaac Newton, Av. 7 13, Paso De La Vaca, San José, Costa Rica.

Paper submitted for publication in the Journal of Materials in Civil Engineering, February 2023

6.1 Abstract

Efficient rejuvenation of the RAP's binder facilitates the use of higher RAP contents. Assessing the efficiency requires evaluating the right blend of the rejuvenator, new and old binder that represents the real binder blend inside the asphalt mixture. Extracted and recovered (E&R) binder from the rejuvenated asphalt mixtures containing RAP is the best practice to obtain the existing blend of the rejuvenator, new and old binder. However, Extraction and recovery is not a common practice to study rejuvenation efficiency since it is time-consuming and energy-demanding with exposure to hazardous chemicals. Instead, blending rejuvenator, new binder and the E&R binder from RAP under appropriate blending conditions limits the extraction and recovery to RAP, and minimizes efforts for studying rejuvenation efficiency. This study aims to find the blending conditions under which the blend of the rejuvenator, new and RAP binder resembles the E&R binder from asphalt mixture rheologically. The rheological properties of three binder blends prepared under intense (IB), medium (MB) and low blending (LB) conditions were compared with those of the E&R binder. Performance grade (PG), rutting potential, fatigue resistance and behavioral characteristics are the rheological properties for making comparison. It was found that IB and MB are good representative of the E&R binder

with regard to PG and PG+ designation. In addition to IB and MB, LB can be a surrogate for the PAV-aged E&R binder. Also, any blending conditions between MB and IB for rutting potential and characterization are recommended.

6.2 Introduction

Incorporation of more reclaimed asphalt pavements (RAP) in new asphalt mixtures is desirable because it contributes to the environment (Sabouri & Kim, 2014). But, due to the higher amount of the immobilized RAP binder in the asphalt mixtures with higher RAP contents, inhomogeneity within the asphalt binder phase increases (Zhao et al., 2015a). To mitigate the problem, rejuvenators are generally introduced into the mixtures with high RAP contents. Rejuvenators diffuse the RAP binder and soften it (Zhao et al., 2018). Still, inhomogeneity exists. Staged or progressive extraction using trichloroethylene is deployed to determine inhomogeneity. It is defined as the ratio of the immobilized RAP binder to the total binder in an asphalt mixture containing RAP (Zhao et al., 2015b; Zhao et al., 2016). This ratio is also an indicator of the rejuvenator's efficiency in mobilizing RAP binder; the lower the rate; the higher the efficiency of the rejuvenator.

There is a consensus on the fact that it is impractical, and somewhat impossible, to achieve a fully uniform asphalt binder in an asphalt mixture with very high RAP content (>50%). As a result, while some studies stuck to the concepts of staged extraction of asphalt binder from asphalt mixture with high RAP content for evaluating the efficiency of a rejuvenator (Rathore & Zaumanis, 2020; Zhao et al., 2018), others, for the same purpose, turned to the average mechanical and rheological properties as a representation, rather than a reproduction, of the asphalt binder inside the asphalt mixture with very high RAP content. They deployed different mixing conditions to blend rejuvenator, old and new binder together in order to analyze and evaluate the rheological properties (Chen, Leng, Wu & Sang, 2014; Elkashef et al., 2017a). This approach is less laborious to obtain binder blends. Yet, there are different sets of conditions deployed for mixing the rejuvenator, new and old binders and all aimed to reach a homogeneous and stable blend (Zaumanis et al. ,2020). The temperature varies from 130℃ (Li

et al., 2021) to 160℃ (Elkashef et al., 2018a; Pradhan & Sahoo, 2020; Abdelaziz, Masad, Epps Martin, Mercado & Bajaj, 2021); the mixing was done by high shear (Elkashef et al., 2017a; Elkashef et al., 2018a), mechanical mixer (Pradhan & Sahoo, 2020) and hand stirring (Yu, Zaumanis, Dos Santos & Poulikakos, 2014; Abdelaziz et al., 2021); and, of course, the mixing time (15 min to 2 h) and rotational speed are prone to much variation. So, the main concern of this study is finding the set of mixing conditions that gives an asphalt binder blend representing the asphalt binder inside the asphalt mixture with very high RAP content.

The binder extracted and recovered (E&R) from the mixture with high RAP content is the basis of comparison. Although it is not exactly the asphalt binder blend inside the rejuvenated asphalt mixture containing very high RAP, it represents the average properties of it. Finding the blending conditions under which the blend of rejuvenator, old and new binder rheologically resembles the E&R binder makes the evaluation of the rejuvenation effectiveness more realistic. Because it is not simply a set blending conditions that supposedly leads to a uniform well-bonded asphalt binder blend, but it is a set of blending conditions that correlates to the real mixture.

6.3 Materials

In this study, a single source of virgin aggregates, one type of RAP, one type of virgin binder and a bio-sourced rejuvenator were used. The properties of the four materials are explained in this section.

6.3.1 RAP, aggregates and asphalt binder

The aggregate stockpiles include RAP (0–10 mm), virgin fine (0–2.5 mm) and virgin coarse aggregate (5–10 mm). Minimum amount of virgin aggregates was added to rectify the distorted gradation of RAP's (Figure 6.1). To determine the minimum percentages of virgin fine and coarse aggregates, Bailey concepts were deployed. The gradation shown in Figure 6.1 satisfies the Bailey method specification for the coarse dense graded aggregate blend (Vavrik et al.,

2002). It contains 65% RAP, 23% virgin coarse aggregates and 12% virgin fine aggregates. Since the scope of this study is not mixture, the details of the aggregate blend are not presented here, but they can be found in a research conducted by Imaninasab et al. (2022). Also, the virgin binder used in this study is a PG 58S-28. It is commonly used in north US and Canada.

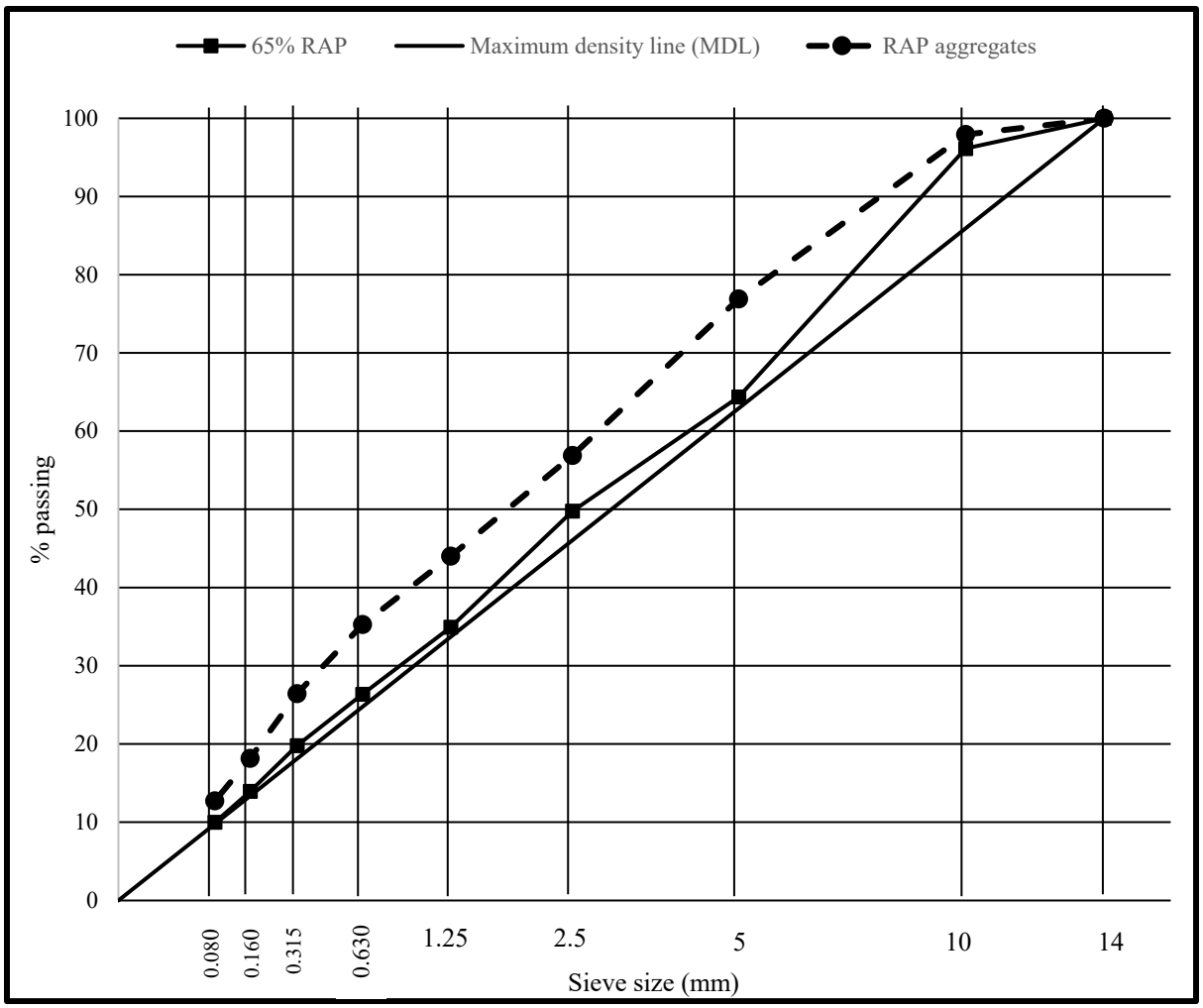

Figure 6.1 Particle size distribution of asphalt mixture with high RAP content

6.3.2 Rejuvenator

It was found that bio-based rejuvenators have better rejuvenating capability compared to petroleum-based ones (Zaumanis et al., 2015). They have been applied successfully for

rejuvenating asphalt mixtures containing high RAP (Hajj et al., 2013) and 100% RAP (Elkashef et al., 2017). Among bio-based rejuvenators, soybean oil derivatives are popular because of the abundance of soybeans in north and Latin America as well as the efficiency in rejuvenation (Elkashef et al., 2017). In this research, epoxidised soybean oil (ESO) was deployed as the rejuvenating agent. ESO is the product of soybean oil oxidation, within which the double bonds transform into the more chemically reactive agent of oxirane ring (Yin et al., 2013) (Figure 6.2). Consequently, it is quicker and easier for the soybean oil-based rejuvenator to react and crosslink with the aged molecules of the RAP binder. Also, this may help dissolution of rejuvenator into the asphalt binder phase instead of its dilution in it (Zhao et al., 2018).

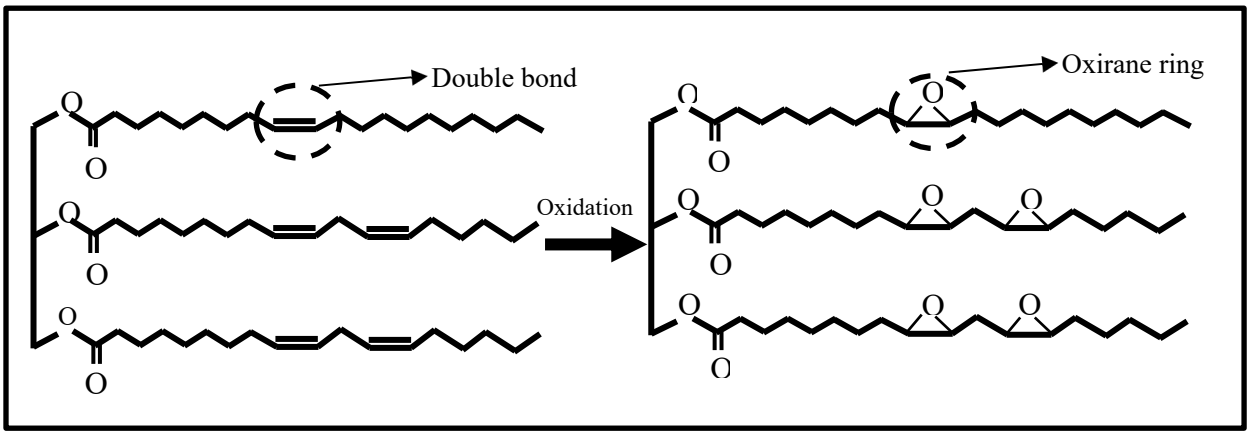

Figure 6.2 Epoxidised soybean oil (ESO) formation from soybean oil

6.3.3 Specimen preparation

Optimal asphalt content (OAC) was determined as 5.1%. This OAC results in satisfactory volumetric properties and moisture damage resistance as recommended by Superpave volumetric design for asphalt mixtures (AASHTO, 2017a). It also constitutes virgin to total asphalt binder ratio of 39%; considering 100% of the RAP binder effective. It also leads to virgin asphalt binder constituting 39% of the total binder content, considering that 100% of the RAP binder is effective.

Previous studies indicated that, for the mixtures with 100% RAP, 1% to 2% soybean oil derivatives by the weight of the total binder (including RAP and virgin binder) is a good dose for rejuvenation (Elkashef et al., 2017a).

The rejuvenator, old and new asphalt binder were then mixed based upon the above-mentioned proportions at three blending levels including:

- Intense blending (IB) conditions: rotational speed of 2000 rpm @ 150 ˚C for 60 min under the flow of nitrogen on top with a flow rate of 1 ± 0.05 L/min to avoid oxidation;

- Moderate blending (MB) conditions: rotational speed of 400 rpm @ 150 ˚C for 12 min, which is one fifth of IB regarding rotational speed and mixing time, under the flow of nitrogen on top with a flow rate of 1 ± 0.05 L/min;

- Low blending (LB) conditions: hand stirring @ 150 ˚C for 1 min.

6.4 Methodology

In order to obtain the reference asphalt binder, based on which the binders obtained from different blending conditions are assessed, loose asphalt mixtures containing 65% RAP were fabricated and short-term aged. Short-term (ST) aging was done by placing the loose mixture in a forced-drafted oven for at least 2 h and no more than 4 h at 135 ˚C (SHRP, 1994). Then, extraction was carried out using automatic asphalt analyzer (ASTM D8159-19). Following extraction, the asphalt binder was recovered by rotary evaporator (ASTM D5404). Since the loose asphalt mixtures were kept inside a force-drafted oven for at least 2 h, the extracted and recovered (E&R) asphalt binder is assumed to be short-term aged.

RAP binder was also obtained using the same extraction and recovery protocols as the loose asphalt mixtures. It was blended with new asphalt binder and rejuvenator under three different sets of blending conditions. The comparison was made between the blended asphalt binders

and the E&R binder to find the set of blending conditions that resembles the E&R binder rheologically the most. Performance grade (PG), multiple stress creep and recovery (MSCR), linear amplitude sweep (LAS), linearity, and complex modulus were performed on the binders using a dynamic shear rheometer (DSR) and a bending beam rheometer (BBR). Figure 6.3 summarizes the research plan for the goal of this study.

The PG testing for determining high (HT) and low temperature (LT) limits was conducted in accordance with AASHTO T 315. Additionally, MSCR based on AASHTO T 350 was carried out for rutting resistance evaluation. It is used to determine the traffic-level designation in PG+ grading system.

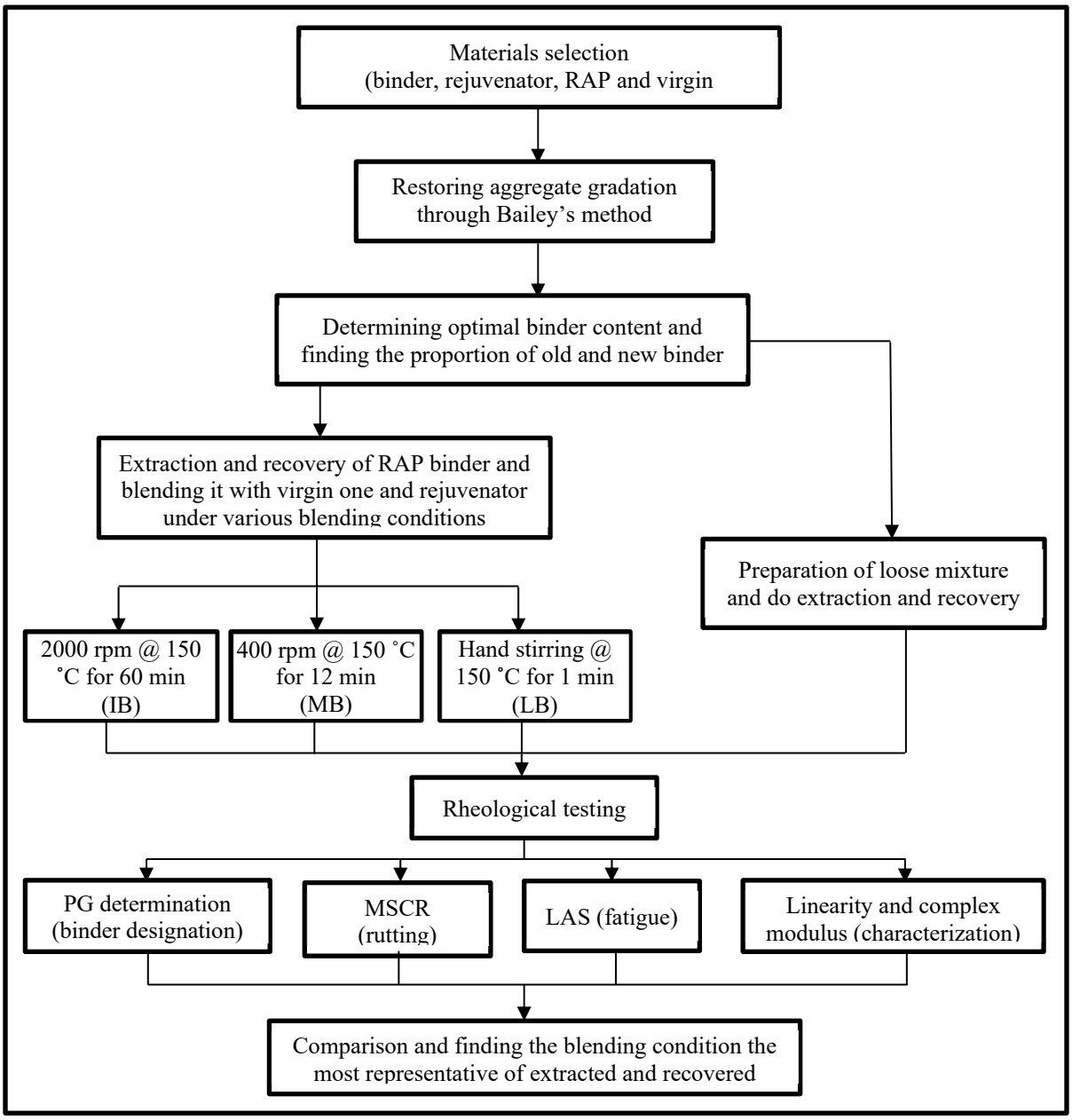

Figure 6.3 Research program

6.4.1 Linear amplitude sweep (LAS)

Linear amplitude sweep (LAS) test is a surrogate for strain-controlled time sweep test that is used to evaluate fatigue cracking resistance of asphalt binders (Hintz et al., 2011). LAS analysis

is based on visco-elastic continuum damage (VECD) that follows Schapery's theory for modelling damage growth. The LAS was performed according to AASHTO TP 101 at 23 ˚C in order to construct the fatigue life vs shear strain curve in the log-log coordinate. Equation 6.1 is the basic form used for the curve fitting of fatigue life.

$$N_f = A(\gamma_{max})^{-B} \tag{6.1}$$

Where: N_f is the fatigue life, which is the number of cycles to 35% reduction in the initial complex shear modulus; A is the intercept; $-B$ is the slope which corresponds to the deterioration rate; and γ_{max} is the maximum shear strain.

Additionally, integrity of the asphalt binder vs damage intensity can be plotted using the results of LAS (Hintz et al., 2011). Integrity is defined as |G*|×sin δ. Damage intensity, on the other hand, can be calculated by combining Equation 6.2 and Equation 6.3 to arrive at Equation 6.4 and, then, fitting the experimental data into the formulation that is given in Equation 6.5.

$$\frac{dD}{dt} = (\frac{\partial W}{\partial D})^{\alpha} \tag{6.2}$$

$$W = \pi \times \gamma_0 \times |G^*| \times sin\delta \tag{6.3}$$

$$D(t) \cong \sum_{i=1}^{N} [\pi I_D \gamma_0^2 (|G^*| sin\delta_i - |G^*| sin\delta_{i-1})]^{\frac{\alpha}{1+\alpha}} (t_i - t_{i-1})^{\frac{\alpha}{1+\alpha}} \tag{6.4}$$

$$C = C_0 - C_1 (D)^{C_2} \tag{6.5}$$

Where: D is the damage intensity; W is the work performed or dissipated energy; T is time (s); A is material constant relating to damage progress and is equal to 1 + (1/-m) where m is the slope of the modulus vs time during relaxation in log-log coordinate; γ_0 is shear strain (%); G^* is complex modulus (MPa); δ is the phase angle; I_D is the initial undamaged |G*|; and C_0, C_1, C_2 are coefficients of the model (Equation 6.5).

6.4.2 Linearity and complex shear modulus

Linearity test was performed on all asphalt binders in order to determine their linear visco-elastic (LVE) limits. The LVE limit is defined as the shear stain corresponding to 95% of the initial complex modulus (Airey et al., 2004). The decrease in temperature and the increase in frequency lead to the LVE limit decrease (Airey et al., 2004). Hence, for a geometry, using the LVE limit determined at the lowest temperature and the highest frequency for higher temperatures and lower frequencies guarantees the resting within LVE domain.

For the temperatures above 40 ˚C, 25 mm diameter and 1 mm gap geometry was used and, for temperatures below 40 ˚C, 8 mm diameter and 2 mm gap geometry was used. In order to determine the LVE limit for each geometry, the LVE limit was only measured at the lowest temperature and the highest frequency. Consequently, for the geometry of the high temperatures, the LVE limit was determined at 40 ˚C and 10 Hz and, for the geometry of the intermediate temperatures, it was determined at -2 ˚C and 10 Hz. It is good to note that the LVE limit of -2 ˚C and 10 Hz is also valid for -8 ˚C because, at low temperatures, the variation of LVE limits are negligible (Bahia et al., 1999).

Using the LVE limit of each geometry, the complex shear modulus test was carried out from -8 ˚C to the high temperature (HT) PG of the asphalt binder under study in 6 ˚C increments. The frequency range was 0.1-10 Hz; within 0.1 to 1 Hz in 0.1 Hz increments and, within 1 to 10 Hz in 1 Hz increments. The complex shear modulus results were then used to calibrate 2S2P1D model (Equation 6.6), which is made up of 2 springs, 2 parabolic elements and 1 dashpot (Figure 6.4).

$$E^*(\omega) = E_{00} + \frac{E_0 - E_{00}}{1+\delta(j\omega\tau)^{-k}+(j\omega\tau)^{-h}+(j\omega\beta\tau)^{-1}} \quad (6.6)$$

Where: j^2 is equal to -1; E^* is complex modulus modelled by 2S2P1D; ω is angular speed which is equal to 2 πf; τ is characteristic time depending on temperature; E_0 is glassy modulus when ω→+∞; E_{00} is static modulus when ω→0; h and k are dimensionless constants for the

parabolic elements as depicted in Figure 4 (0 <k <h <1); δ is dimensionless constant; and β is coefficient relating to Newtonian viscosity of dashpot ($\eta=(E_0-E_{00})\beta\tau$).

Also, Black space, Cole-Cole curves, complex shear modulus and phase angle master curves were constructed for further analysis. Black space curve is phase angle vs complex shear modulus value. It is helpful for high temperatures' behavioral assessment. Complex shear modulus and phase angle master curves reveal an asphalt binder's responses over a wide range of frequencies at a reference temperature. Constructing master curves is based on Time-Temperature superposition principle (TTSP). It assumes that the effect of time (frequency) and temperature on asphalt binder's complex shear modulus can be used interchangeably. Therefore, by having complex modulus values at different temperatures over a limited frequency range, it is possible to extend the complex shear modulus vs frequency curve at a specific temperature, namely reference temperature. Complex shear modulus vs frequency curves at other temperatures can slide horizontally into the position of the complex shear modulus vs frequency curve at reference temperature to form a curve over a wide frequency range. The reference temperature in this study is 16 ˚C and the shift factors for sliding the curves of different temperatures into the reference temperature is calculated using Equation 6.7, known as William-Landel-Ferry (WLF) equation (Williams et al., 1955).

$$Log(a_T) = \frac{-C_1(T-T_{ref})}{C_2+T-T_{ref}} \tag{6.7}$$

Where: a_T is shift factor; T is the temperature whose curve is sliding horizontally into constructing reference temperature master curve; T_{ref} is reference temperature; and C_1, C_2 is coefficients of the model.

The shift factors of the complex shear modulus master curve can be used for constructing the phase angle master curve.

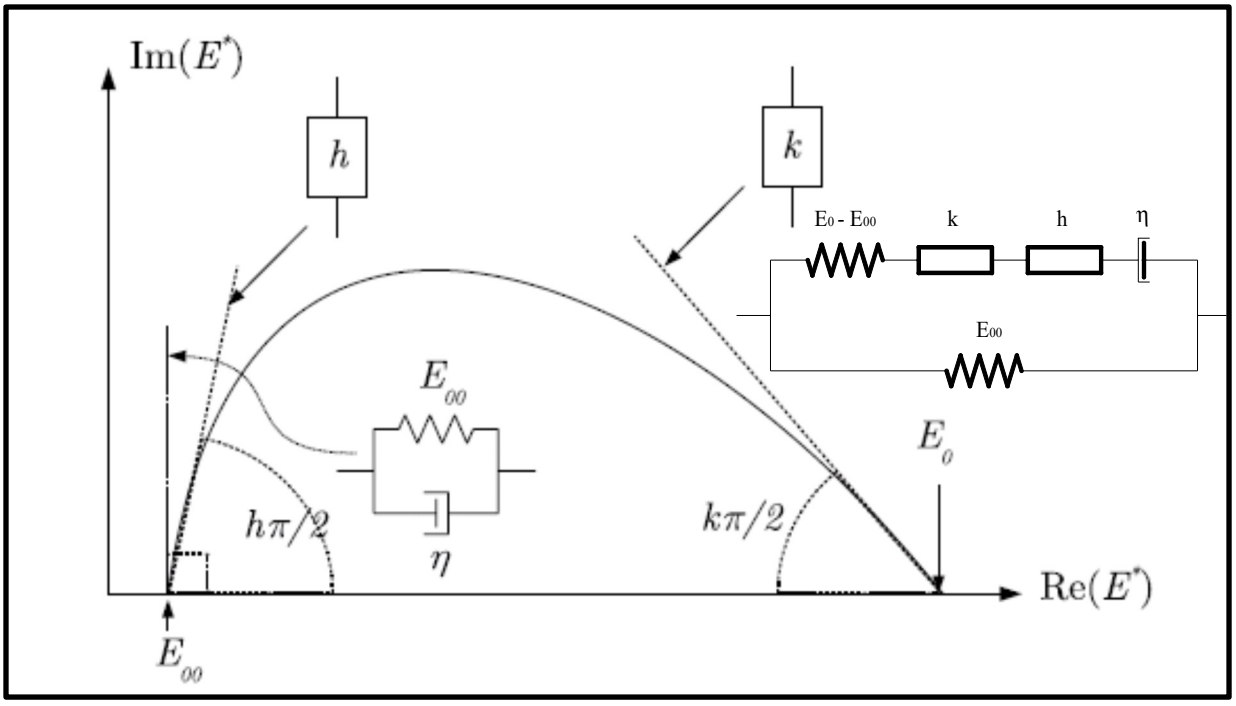

Figure 6.4 2S2P1D model

6.5 Results and discussion

Comparison was made between blended binders and the extracted and recovered (E&R) binder based upon results of rheological tests including the PG designations, rutting performance, fatigue life and characterization. They determine the set of blending conditions, if any, that results in a blended binder with the most rheological affinity to the E&R binder. Subsequently, the assessment of the rejuvenating efficiency is more realistic. The rheological tests' results along with the comparisons are presented within this section.

6.5.1 Performance grade (PG)

Since the E&R asphalt binder was treated as short term (ST) or rolling thin film oven (RTFO) aged binder, the high temperature (HT) PG was determined only based upon G*/sin (δ)≥2.2 kPa (RTFO criterion). As shown in Figure 6.5(a), the HT_e according to the unaged blended binder (G*/sin (δ) ≥1 kPa), namely $HT_{e,unaged}$, decreases with blending severity increases; i.e.

intense blending (IB) results in the lowest $HT_{e,unaged}$ while low blending (LB) gives the highest. In contrast, the trend of the HT_e based upon RTFO-aged blended binder, namely $HT_{e,st\text{-}aged}$, reverses and, with blending severity increases, there is increase in $HT_{e,ST\text{-}aged}$; i.e. intense blending (IB) results in the highest $HT_{e,unaged}$ while low blending (LB) gives the lowest. Table 6.1 reveals that, with blending condition severity increase, the difference between $HT_{e,unaged}$ and $HT_{e,ST\text{-}aged}$, namely ΔHT_e, decreases; i.e. IB has the lowest and ΔHT_e and LB has the highest. Rejuvenation using bio-rejuvenator is an intermolecular interactions between asphaltene dimers and amide groups in bio-rejuvenators (Zadshir, Oldham, Hosseinnezhad & Fini 2018; Behnood, 2019). Time, temperature and rotational speed are the effective factors of the interaction's progress and completion (Behnood, 2019). ΔHT_e can be an indicator showing the completion of the rejuvenation process for a set of blending conditions. It can be concluded that, since the blending conditions of LB including time and rotational speed are not long and fast enough, respectively, to complete the interaction of rejuvenation process, it continued during RTFO aging and, after RTFO aging, there is a rejuvenated binder that is evaluated based upon ST-aged criterion. As a result, ΔHT_e is large; $HT_{e,,unaged}$ is high; $HT_{e,ST\text{-}aged}$ is very low; and the HT PG of LB is, subsequently, quite lower than IB and MB.

However, finding the blended asphalt binder with the most similarity to E&R binder is more important as it deals with reality of the blend inside the mixture. From Figure 6.5(a), it is evident that medium blending (MB) has approximately the same G*/sin (δ) vs temperature curve as the E&R. Consequently, both MB and E&R have the same HT PG designation.

With respect to low temperatures criteria (stiffness and m-value from BBR test), all asphalt binders behave approximately the same (Figure 6.5(b)). It indicates that, regardless of blending conditions, PAV aging results in almost the same thermal cracking resistance for all rejuvenated asphalt binders. This could mean that the PAV process eradicates the rejuvenation impact in all binders equally. Yet, it does not mean that all asphalt binders have equal aging potential. It is evident from Table 6.1 that the E&R has the lowest aging potential because, with respect to absolute value, its ΔTc is the lowest. ΔTc is the difference between stiffness- and m-value-based effective LT (LTe) and is an indicator of aging potential (Elkashef et al.,

2017a). Most aged asphalt binders have stiffness-based LTe smaller than the m-value-based LTe (Elkashef et al., 2017a). So, LT PG is generally controlled by m-value and ΔTc is generally negative. It can be inferred that higher value of ΔTc shows higher ability to relax stresses and less aging potential. E&R is less prone to aging because the major aging probably takes place during extraction and recovery. Consequently, the E&R has already done its aging and it is less prone to further aging.

After determining the LT and HT PG, there is an intermediate temperature control (G*.sin (δ)≤5000 kPa). As shown in Figure 6.5 (c), all asphalt binders securely pass the criterion. The E&R's temperature vs G*.sin (δ) curve is the same as the IB's curve. While, with respect to performance grading, MB mimics ST-aged E&R and IB mimics PAV-aged E&R, LB manifests a very different behavior compared to E&R binder. Thus, IB or MB is recommended for PG determination as both yield the same PG as E&R. Also, since HT PG under any blending condition is controlled by RTFO-aged criteria, performing PG testing on the unaged blended binders can be considered optional.

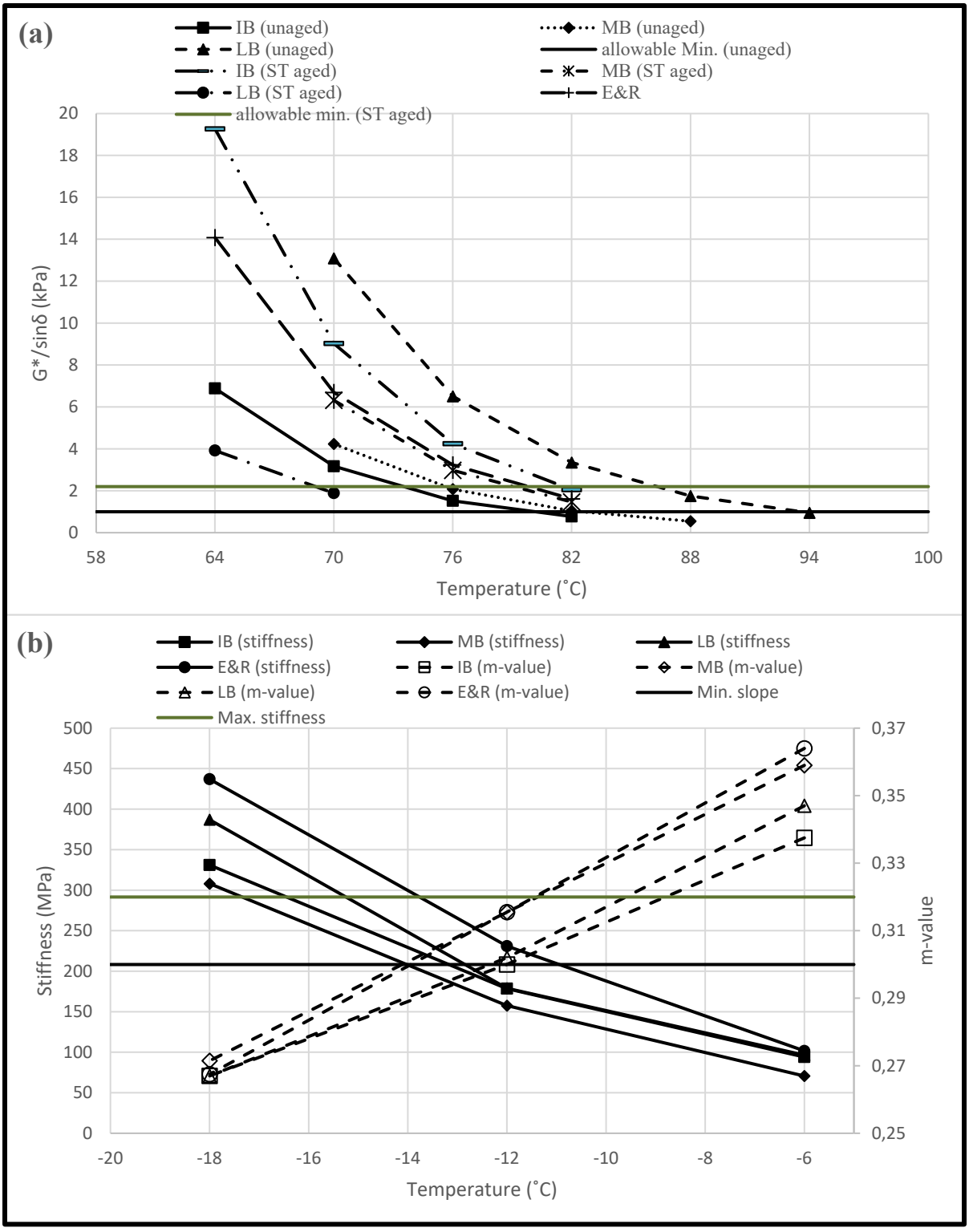

Figure 6.5 PG testing results: (a) G*/sin (δ) of original binders and ST-aged binders, (b) stiffness and m-value of RTFO- and PAV-aged binders, and (c) G*. sin (δ) of RTFO- and PAV-aged binders

Table 6.1 PG Properties

	IB	MB	LB	E&R	RAP binder
HT_e corresponding to unaged ($HT_{e,unaged}$) (℃)	80.1	82.5	93.6	NA	96.6
HT_e corresponding to ST-aged ($HT_{e,ST\text{-}aged}$) (℃)	81.6	79.1	69.1	79.8	89.1
$\Delta HT_e = HT_{e,unaged} - HT_{e,ST\text{-}aged}$	-1.5	3.4	24.5	NA	7.5
LT_e (˚C)	-22.17	-24.11	-22.29	-23.94	-16.2
PG	76-22	76-22	64-22	76-22	88-16
ΔT_c (˚C)	-4.61	-3.57	-3.2	-0.07	-6.2

6.5.2 Multiple stress creep and recovery (MSCR)

Based on PG designation, IB and MB show the closest behavior to E&R. But, due to the shortcomings of the PG grading system in addressing traffic impact on rutting potential, MSCR was adopted in PG+ (Harman, Youtcheff & Bukowski, 2011). Based upon non-recoverable creep compliance (Jnr) at 3.2 kPa stress level and the percent difference between Jnr at 3.2 kPa and 0.1 kPa stress levels, all asphalt binders have standard traffic designation letter “S”. From Figure 6.6, it can be seen that the Jnr values of the E&R at 3.2 kPa stress level fall between the Jnr values of the IB and MB. The E&R has greater percent difference between Jnrs compared to the blended binders. Still, it can be inferred that IB, MB and E&R are in the same PG category, namely PG 76S-22, whereas LB is PG 64S-22. It corroborates the similarity of the IB and MB with the E&R, and the discrepancy between the LB and the E&R.

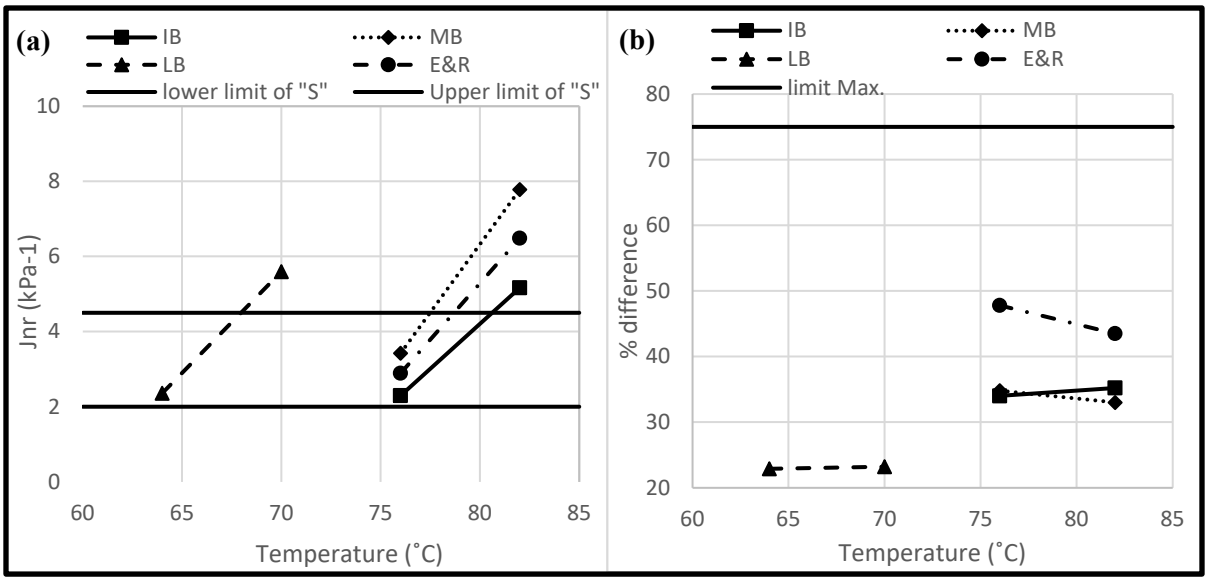

Figure 6.6 MSCR testing results: (a) J_{nr} at 3.2 kPa stress level, and (b) % difference between J_{nr} at 3.2 kPa and 0.1 kPa stress levels

6.5.3 Linear amplitude sweep (LAS)

Fatigue analysis is essential for asphalt binders and mixtures containing very high RAP since fatigue performance is the primary concern of these types of asphalt mixtures (Sabouri & Kim, 2014). It is common to perform tension/compression (T/C) fatigue test at 10 ˚C in Canada for asphalt mixture fatigue performance (Perraton et al., 2010). But, as given Table 2, performing LAS at 10 ˚C gave G*s at the frequency of 10 Hz which are higher than the limit recommended by Teymourpour and Bahia (2014) (G*s greater than 60 MPa). Therefore, as recommended by Safaei and Castetorena (2016), LAS was performed at the average climatic PG temperature minus 4 ˚C as recommended by Safaei and Castetorena (2016). For PG 76S-22, it is 23 ˚C. The same was applied for LB (PG 64S-22) because of comparison purposes. LAS was performed on two replicates for each binder.

Figure 6.7(a) and Figure 6.7(b) show the curves derived from LAS testing for fatigue life and damage growth, respectively. It can be observed that the binders have more or less the same damage characteristic curve, whereas fatigue life curves vary. If fatigue life is considered, there

is differences between the extracted and recovered (E&R) binder and the blended ones; i.e. IB, MB and LB. The E&R shows higher fatigue life. However, the blended binders have intertwined fatigue lives over the strain levels (Figure 6.7(b)). Taking the shear strain level of 5% as the one most representing the mixture (Tran et al., 2012), it can be observed that the fatigue lives of the binders blended under different blending conditions are close.

Figure 6.7 shows that damage and fatigue life have different results with regard to the fatigue performance of the binders. Damage is an intrinsic property of a material that is not impacted by the shear strain level. Here, fatigue life is an estimation based upon damage characteristics curves.

Considering the damage resistance (Figure 6.7 (a)), LB has a very close integrity parameter (C) vs damage intensity curve to E&R's one. However, all the binders have almost the same damage endurance. Thus, regardless the fatigue life, all binder blends can represent E&R with respect to fatigue performance. It can be inferred that the blending conditions do not maintain much of their influence on the binders after PAV aging. Perhaps, PAV totally releases the rejuvenation impacts on all binders and leaves them in a same non-rejuvenated state. Further studies are required on it.

Table 6.2 G* of binders at 10 ˚C

Binder	G* @ 10 ˚C and 10 Hz (MPa)
IB	79.3
MB	67.0
LB	74.3
E&R	88.0

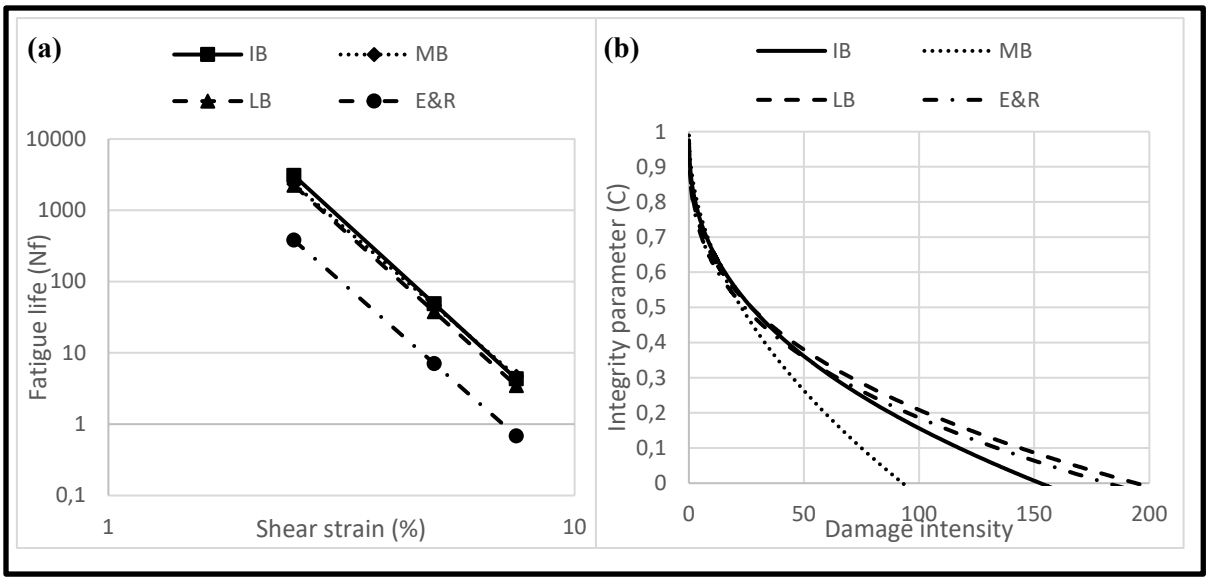

Figure 6.7 LAS testing results: (a) fatigue life, and (b) damage characteristics

6.5.4 Linearity and complex shear modulus

The characterization of binders was conducted through linearity and complex shear modulus testing on the RTFO-aged binders. So, the results are limited to the short term (ST) aged state of the binders. LB is the softest asphalt binder with the highest LVE limit at both intermediate and high temperature (Figure 6.8). Except the Cole-Cole curve, E&R curves always fall between IB and MB (Figures 6.8 to 6.12). This complies with the results obtained from DSR testing on the ST-aged binder; i.e. G*/sin (δ) and Jnr. Cole-Cole curves indicate that the LB and MB have roughly the same curve, which is between E&R and IB.

As given in Table 6.3, parameters such as “h” and “k” of the 2S2P1D model are roughly the same for all binder types. “h” along with the static modulus (E00=0) shape the very left part of the Cole-Cole curves. This part represents the high temperatures behavior of binders. Figure 6.9 proves that all asphalt binders, regardless the blending conditions, behave more or less the same at high temperatures.

As the temperature decreases, the IB, E&R, MB and LB curves tend to diverge. This is due to the parameter "δ" and glassy modulus (E0). Comparing the Cole-Cole curves of the MB and LB indicates that the influence of the E0 is far greater than "δ". Also, because of the constant value for the parameter "k", there are almost constant distances between curves within the post-peak domain. Therefore, the origin of the difference among the Cole-Cole curves is the glassy modulus.

The complex shear modulus master curves at the reference temperature of 16 ˚C confirms that IB is the stiffest and LB is the softest asphalt binder type (Figure 6.11). The results of the phase angle master curves comply with complex shear modulus one. As shown in Figure 12, the difference between the curves can be as large as 10 ˚. Phase angle tends toward 90 ˚ and 0 ˚ with the frequency tending to infinitive low and high asymptote, respectively.

Table 6.3 2S2P1D parameters

	E_{00} (kPa)	**E_0 (kPa)**	**k**	**H**	**δ**	**τ_E (s)**	**β**
E&R	0	670000	0.30	0.62	3.50	0.00030	500
IB	0	610000	0.30	0.62	4.00	0.00080	500
MB	0	650000	0.29	0.62	3.50	0.00015	350
LB	0	650000	0.29	0.63	3.20	0.00010	250

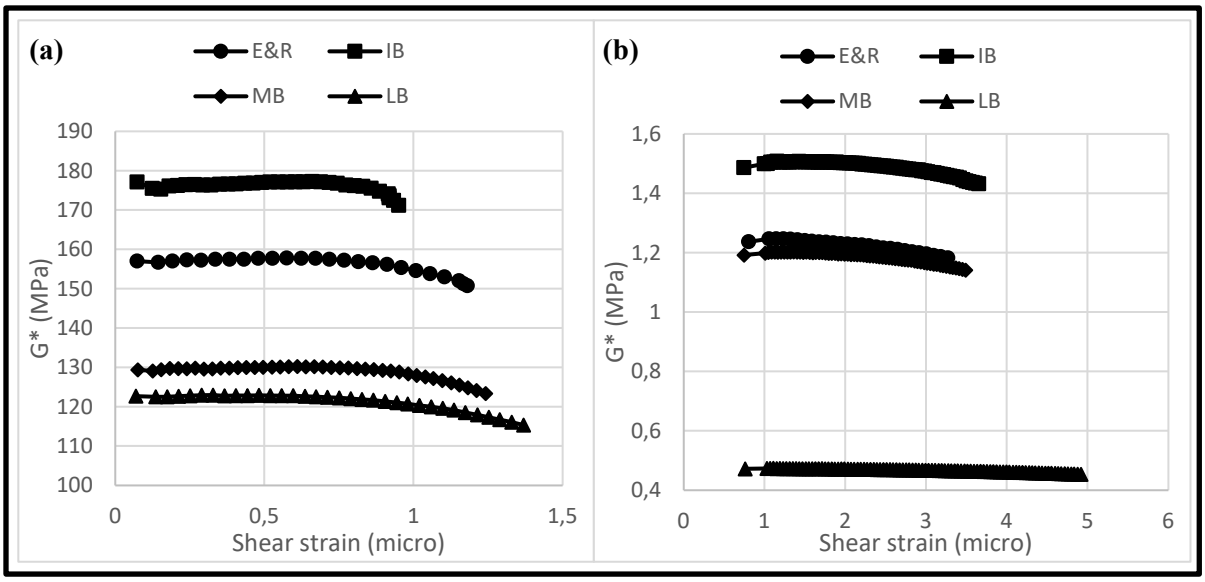

Figure 6.8 Linearity results for: (a) 8 mm diameter and 2 mm gap geometry, and (b) 25 mm diameter and 1 mm gap geometry

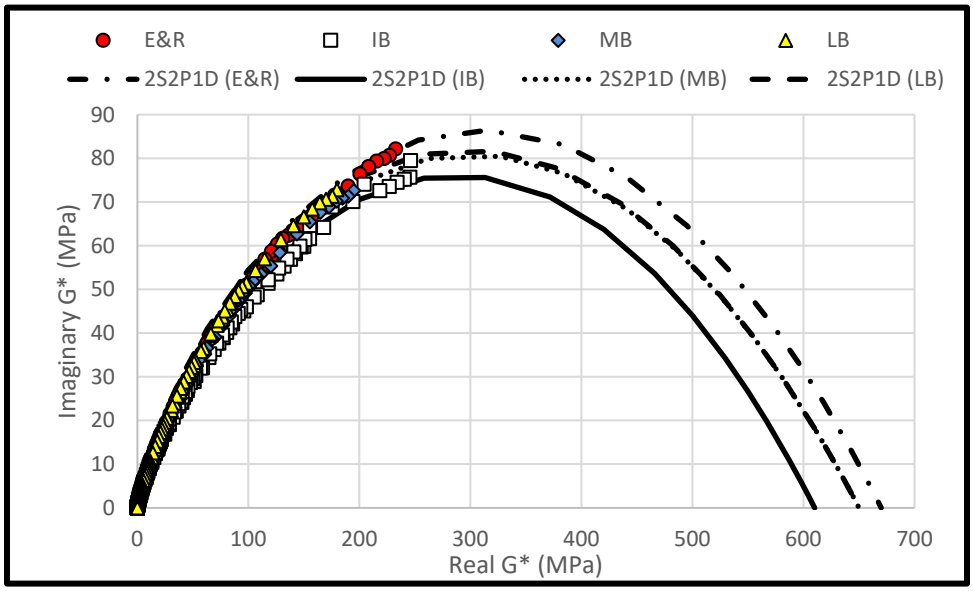

Figure 6.9 Cole-Cole curves

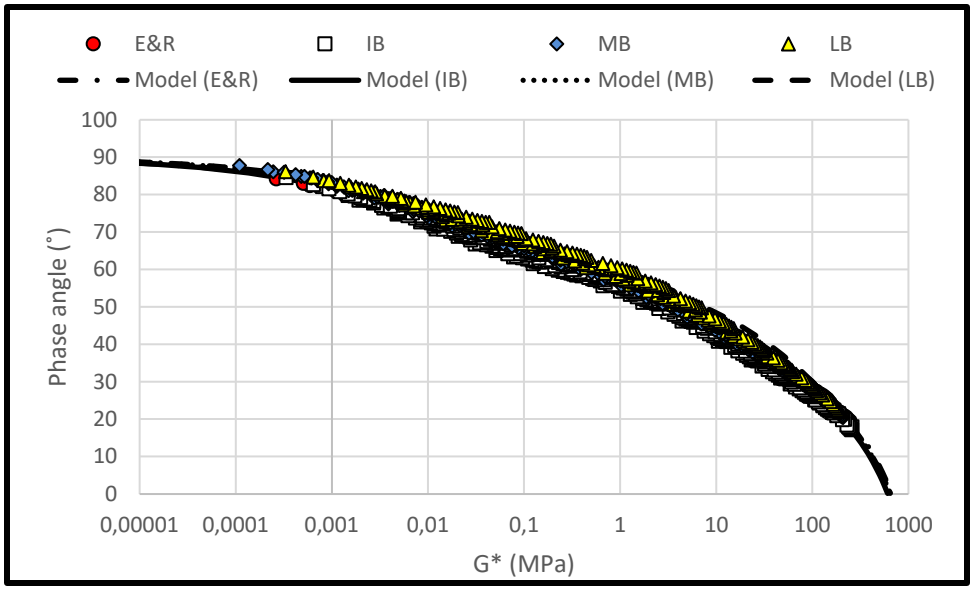

Figure 6.10 Black space curves

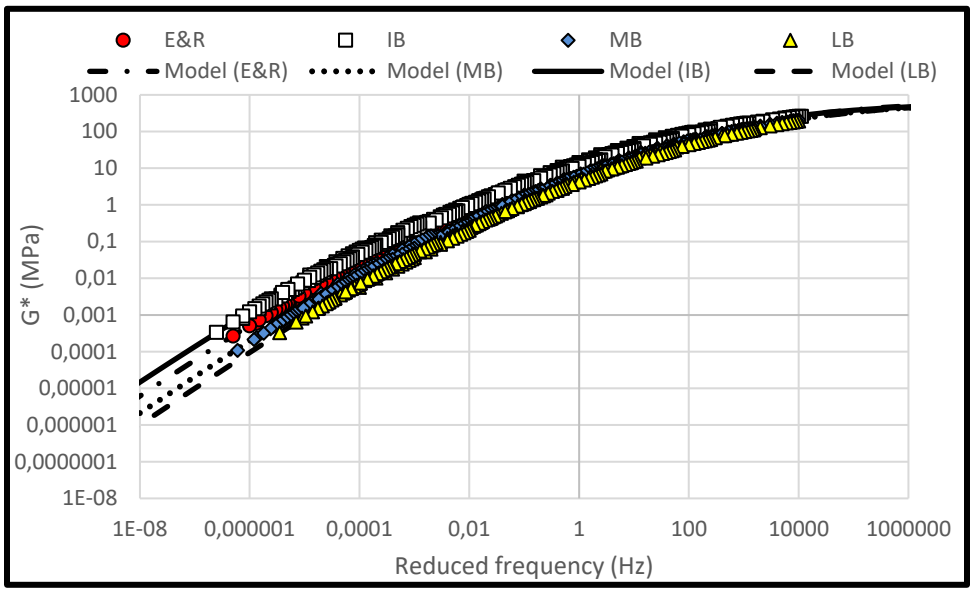

Figure 6.11 Complex shear modulus master curves

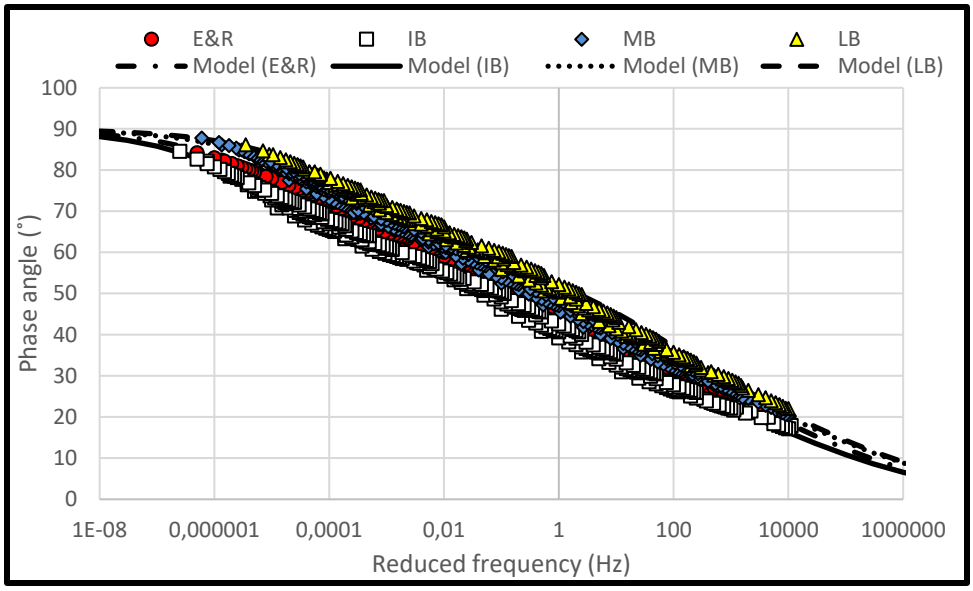

Figure 6.12 Phase angle master curves of RTFO-aged binders

6.6 Conclusion

This paper aimed to find the best blending condition that can represent rheological properties of the asphalt binder extracted and recovered (E&R) from the asphalt mixture containing very high RAP (>50%). According to the results of PG designation, characterization, rutting, and fatigue cracking resistance, following conclusions can be drawn:

- The original state of the asphalt binders with high RAP contents does not control high temperature PG. Therefore, it is recommended to limit testing on RTFO- and PAV-aged asphalt binders.

- Low blending (LB) conditions are not recommended for the analysis relating to the unaged and RTFO-aged binder since the rejuvenation process is not completed within blending and the RTFO aging acts as the continuation of blending. Also, the results of RTFO-aged LB are not anywhere close to the E&R binder.

- Both intense (IB) and medium blending (MB) conditions are good enough to replicate ST-aged E&R asphalt binder. Hence, any blending conditions between IB and MB works.

- For determining low temperature PG or evaluating the thermal cracking resistance, any set of blending conditions can be employed since PAV aging brings all of the asphalt binders rejuvenated by epoxidized soybean oil (ESO) into the same state regardless of their RTFO state. Thus, LB is enough for representing PAV-aged E&R asphalt binder.

- Any set of blending conditions between IB and MB can be used for characterization and multiple stress creep and recovery (MSCR) testing of the E&R binder. It can be stated that both RTFO-aged IB and MB can be a representative of the ST-aged E&R binder and any blending conditions between them suits for the purpose.

CHAPTER 7

FATIGUE LIFE ANALYSIS OF ASPHALT MIXTURES WITH VERY HIGH RAP CONTENTS USING CLASSICAL AND VISCO-ELASTIC CONTINUUM DAMAGE (VECD) APPROACHES

Reza Imaninasab[a], Luis Loria-Salazar[b], Alan Carter[a]

[a] Construction Engineering Department, École de technologie supérieure, 1100 Notre-Dame St W, Montreal, QC H3C 1K3, Canada.
[b] Universidad Isaac Newton, Av. 7 13, Paso De La Vaca, San José, Costa Rica.

Paper submitted for publication in the Fatigue and Fracture of Engineering Materials and Structures, March, 2023.

7.1 Abstract

This study focuses on the fatigue life of asphalt mixtures with very high RAP contents (>50%). The classical and visco-elastic continuum damage (VECD) approaches were employed for analysis of four mixture types designed according to Bailey method with 57, 65, 73 and 100% RAP. Within characterization phase of VECD, 2S2P1D model was used to calibrate generalized Maxwell (GM). Wöhler curves based upon classical and VECD prediction approach were constructed and compared to find the better method for this type of asphalt mixtures. Classical approach establish strong relationship between fatigue life and strain level but a thorough comparison between the mixtures regarding the fatigue life is not possible. It is because of the strain level. However, VECD effectively removes the strain impact and makes the comparison viable. Also, the averaged released pseudo-strain energy throughout entire test history (G^R) was found useful to compare fatigue characteristics of very high RAP content mixtures.

7.2 Introduction

Inclusion of higher amount of RAP is favorable and there have always been growing trend of incorporating more RAP in new asphalt pavements (Williams et al., 2020). It is environmentally friendly and economically beneficial. RAP is a rich source of bitumen and aggregate that can substitute the virgin bitumen and aggregate. Hence, not only does it decrease the need for raw materials, it also reduce the cost of procuring them.

Although higher RAP content contributes to moisture damage (Ghabchi, Singh & Zaman, 2014) and rutting resistance (Carter & Stroup-Gardiner, 2007), it weakens the resistance against cracking (Norouzi et al., 2014). Rejuvenation can mitigate the negative effect of high RAP content on cracking susceptibility. Rejuvenation involves softening the stiff bitumen of RAP and makes it more mingled with the virgin bitumen.

This study deals with fatigue evaluation of rejuvenated asphalt mixtures containing very high RAP (>50%). Fatigue is a common type of cracking and, with respect to analysis, it can be quite complicated due to visco-elastic behavior of asphalt mixtures. Fatigue is stiffness reduction of a material as a result of damage that load repetition causes. The stiffness reduction can be considered as fatigue effect once it is irreversible; i.e. the stiffness reduction due to the damage is because of permanent crack formation, whether micro or macro. Artefacts such as thixotropy and self-heating reduce stiffness during fatigue testing but such stiffness reduction can be recovered because of self-healing (Di Benedetto et al., 2004). Different studies deployed different methods to remove the artefact effects from fatigue test results to arrive at pure fatigue (Di Benedetto et al., 2004; Underwood, 2006).

A damage evolution model was developed in École nationale des travaux publics de l'État (ENTPE) by Di Benedetto, Ashayer Soltani & Chaverot (1996). They conducted analysis on complex dynamic modulus (|E*|) vs number of cycles curve obtained from tension/compression (T/C) fatigue test. The phase II of the curve was divided into four intervals and linear regression was utilized to eliminate artefact effects and find pure fatigue damage.

Later, ENTPE used generalized non-linear fatigue damage law that was developed by Di Benedetto and Neifar (DBN) (Di Benedetto et al., 2004). It incorporates viscous properties. DBN is a characterization model that has never caught on for fatigue analysis. Some of the damage fatigue laws based on non-viscous behavior like the one proposed by Laboratoire central des ponts et chaussées (LCPC) (Bodin, de La Roche, Piau & Pijaudier-Cabot, 2002) became more wide-spread for fatigue analysis of asphalt mixtures. On the other hand, visco-elastic continuum damage (VECD) has become dominant for fatigue life assessment since its introduction to asphalt pavement in 1990 (Kim & Little, 1990). Within VECD analysis, the characterization of a material with visco-elastic behavior is made through the concept of pseudo strain in order to exclude the artefact effects, which can be healed with rest, from fatigue test. This removes time effects in the damage growth analysis of a visco-elastic material. The damage evolution is, then, modelled based upon Schapery's nonlinear viscoelastic constitutive theory (Schapery, 1982). This approach for fatigue damage modelling of asphalt mixtures has been the basis of numerous studies (Kim, Daniel & Wen, 2002; Chehab, Kim, Schapery, Witczak & Bonaquist, 2003; Lundstrom & Isacsson, 2003; Underwood, 2006; Hou, 2009; Sabouri & kim, 2014; Hernandez-Fernandez, Underwood & Ossa-Lopez, 2020). The main advantage of VECD coupled with Schapery's damage evolution modelling is constructing a unique damage characteristic curve for a visco-elastic material that represents its intrinsic damage growth properties regardless of the strain level (Underwood, Kim & Guddati, 2010).

In this study, VECD method is employed to model damage growth in the asphalt mixtures with very high RAP contents (>50%). However, the fatigue life curves (Wöhler curves) are constructed based on the classical approach and the VECD predictions. Although both classical and VECD methods have been separately and successfully applied for fatigue life evaluation of asphalt mixtures with high RAP content (<50%) (Tapsoba et al., 2014; Sabouri & kim, 2014), in this research, a comparison between them is made to assess which method gives more consistent results with regard to the fatigue life of the rejuvenated asphalt mixtures containing very high amount of RAP (>50%). As a result, not only is the fatigue performance evaluation

of asphalt mixtures containing very high RAP including 100% RAP done, the best fatigue analysis method is also found.

Also, the rate of change of the averaged released pseudo-strain energy throughout entire test history (G^R) criterion is investigated. The G^R vs fatigue life (N_f) can be used as a surrogate to the conventional Wöhler curve plotting N_f vs strain level. G^R vs N_f yields a unique curve for a visco-elastic material regardless of the loading mode (Zhang, Sabouri, Guddati & Kim, 2013; Sabouri & kim, 2014).

7.3 Materials

7.3.1 RAP, aggregates and bitumen

The RAP (0-10 mm) used in this study was mixed with the coarse (5-10 mm) and fine (0-5 mm and 0-2.5 mm) aggregates to yield three Bailey aggregate blends (Vavrik et al, 2002). They are two coarse dense-graded (CDG), one fine dense-graded (FDG). 100% RAP is the control mixture. Table 7.1 lists the virgin aggregates and RAP proportions in different blends and the corresponding gradations are illustrated in Figure 7.1. In CDG #1, the black curve (RAP gradation) is used whereas, in CDG #2, the white curve (RAP aggregate gradation) is deployed. As a results, there is difference in the gradation. Also, the virgin bitumen used in this study is PG 58S-28, which is commonly-used in north US and Canada.

Table 7.1 Percentages aggregates and RAP in blends of stockpiles used

	RAP %	Coarse (5-10 mm) %	Fine (0-5 mm) %	Fine (0-2.5 mm) %
100% RAP	100	0	0	0
CDG #1	73	27	0	0
CDG #2	65	23	0	12

	RAP %	Coarse (5-10 mm) %	Fine (0-5 mm) %	Fine (0-2.5 mm) %
FDG	57	30	13	0

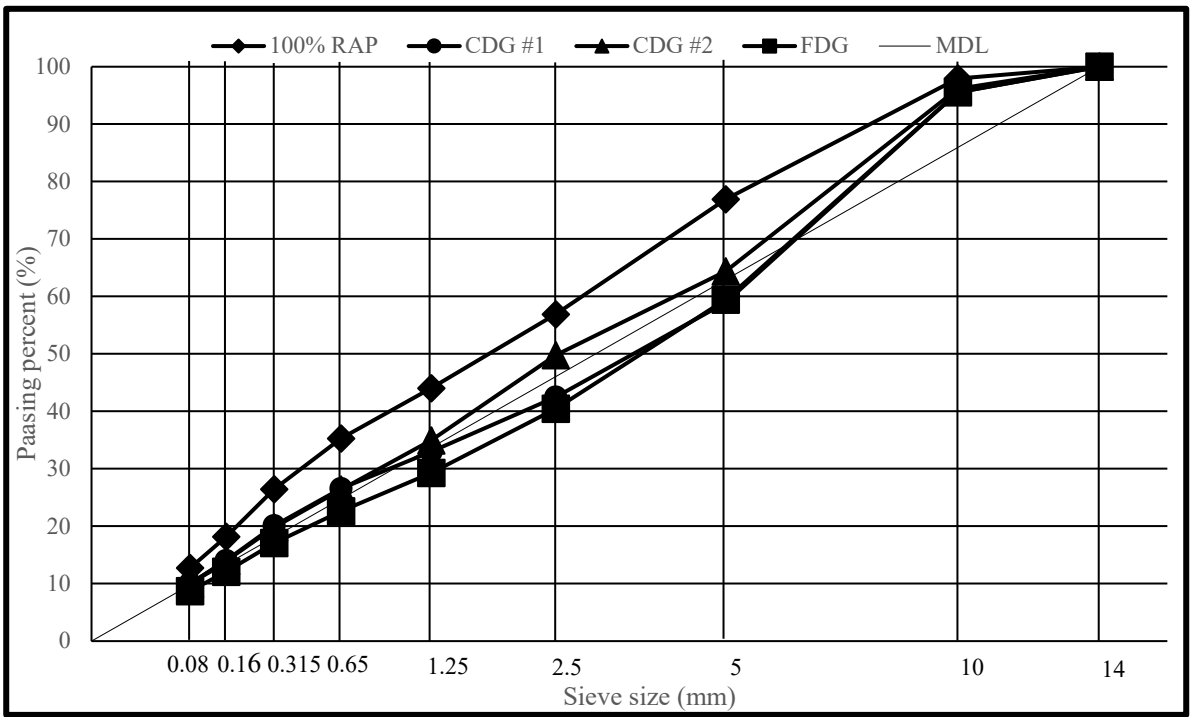

Figure 7.1 Gradations of blends

7.3.2 Rejuvenator

Soybean oil is abundant (Elkashef et al., 2018b) and, more importantly, its derivatives are effective in the rejuvenation of RAP binder (Hajj et al., 2013; Elkashef et al., 2017b). Hence, one was used in this research. It has been proven that 1-2% of the soybean oil derivative by the total weight of the bitumen (old and new bitumen) in 100% RAP mixture is capable of softening the old bitumen of RAP as the virgin one (Elkashef et al., 2017b; Elkashef et al., 2018a; Elkashef et al., 2018b). 1% rejuvenator by the total weight of bitumen is equivalent to 1.154% rejuvenator by the weight of RAP bitumen. Therefore, 1.154% rejuvenator by the weight of RAP bitumen was used for all very high RAP content asphalt mixtures.

7.4 Methodology

7.4.1 Mix design

The optimum asphalt content (OAC) was determined based upon volumetric properties. For 100% RAP, the target air voids (V_a) of 4% at the design number of gyration was used while it was set 3% for CDGs and FDG. It was observed that 4% air voids results in insufficient aggregate coating for CDGs and FDG. On the other hand, 3% lead to bleeding for 100% RAP asphalt mixture. Table 7.2 provides the mix design properties for different mixture types.

Table 7.2 PG+ designation and mix design properties

Mixture type	Bitumen PG+	AOC	Virgin bitumen content	V_a (%)	VMA (%)	VFA (%)
RAP	88S-16	-	-	-	-	-
100%	82S-16	5.65	0.71	4.08	14.20	72.65
CDG #1	76S-22	5.15	1.63	2.98	13.03	77.57
CDG #2	76S-22	5.10	1.99	2.92	13.34	75.12
FDG	70H-22	4.95	2.25	3.06	13.73	76.76

7.4.2 Sample preparation

Superpave gyratory compactor (SGC) was used to prepare cylinderical asphalt specimens at the AOC. Cylinderical cores of 75 mm by diameter were then extracted and the top and bottom of them were polished to remove surface irregularity. The specimens were 135±10 mm high after polishing. 100% RAP asphalt mixture specimens contained 5.5±0.5 air voids and the others had 5.5±0.5 air voids. These are as expected since the air void contents of the mix design phase are not the ones after compaction (Ali, 2019).

7.4.3 Fatigue life testing program

Before running T/C fatigue test, specimens underwent the complex dynamic modulus test. The test was performed at 50 μ strain level, and temperature range of -35 to 35℃ with 10℃ increment and the frequencies of 0.01, 0.03, 0.1, 0.3, 1, 3, 10 Hz. This testing procedure for complex dynamic modulus do not dmage specimens and provide enough data points to construct master curves of complex dynamic modulus and phase angle.

Before running tension/compression (T/C) fatigue test, it is good to perfrome linear visco-elastic (LVE) limits test on different mixtures to determine LVE limits. The LVE test was performed at 10℃ and 10Hz, which are the common temperature and frequecy of T/C test (Perraton et al., 2010). The LVE limit is defined as the maximum strain level before the complex dynamic modulus becomes less than 95% of initial complex dynamic modulus (Airy, 2004). The initial complex dynamic modulus was determined as the average of the first five initial strain levels (10, 20, 30, 40 and 50 μ). Then, the starin level increase was made at 5 μ strain rate from 55 μ. The complex dynamic modulus at each strain level was reported as the average of the closest five complex dynamic modulus values among the one hundred logged. This is because, in the beginning of testing at each strain level, the complex dynamic modulus tends to be high and, gradually, it gets stable and almost constant. Between the starin increase intervals, there was 10 min rest for the asphalt specimens to recover. Determination of LVE limit before running fatigue test is important. The strain levels at which T/C is performed must not exceed the LVE limit to make sure the hypothesis of VECD analysis is valid.

The strain-controlled on-specimen (COS) T/C fatigue test was carried out at various strain levels falling between 50 μ and the LVE limit. The axial deformation due to sinusoidal loading was measured and controlled via three 5-cm-long extesometers that were placed on the mid-height of the cylindrical specimens with equal angular distance of 120 ˚ (Figure 7.2). Since this testing setup controls strains within the middle of the specimens, based on Saint-Venant's principle, the stress is uniform and the VECD analysis is valid. Before carrying out the test, proportional, integral, derivative and future coefficients, known as PIDF, of the material testing

system (MTS) were adjusted for each mixture type. Therefore, the average displacement of the three extesometers as a result of acuator loading became as commanded. The test was terminated when the specimens ruptured. So all failure criteria has been surely met.

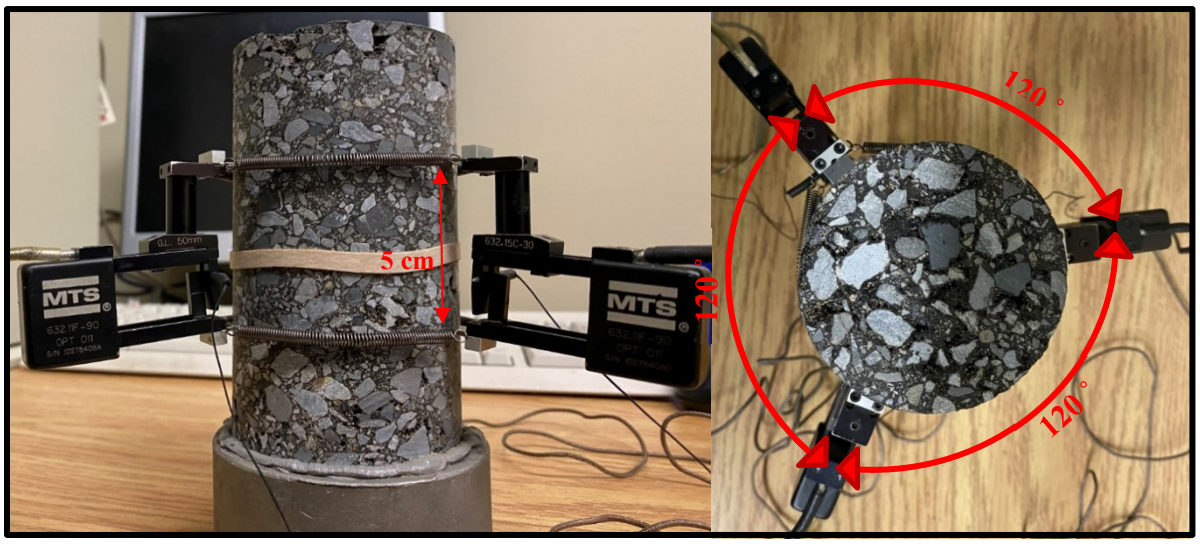

Figure 7.2 T/C fatigue specimen with extesometers attached; (left) side view (right) top view

7.4.4 Fatigue life classical criteria

50% stiffness reduction is a classical criterion that has been long and widely used by pavement researchers to assess fatigue life (N_f) of the asphalt mixtures (Monismith & Deacon, 1969). This criterion is mainly utilized for 4-point bending beam fatigue test (Monismith, Epps & Finn, 1985) but it is also consensually acceptable for T/C fatigue test (Tapsoba et al., 2014). Also, maximum phase angle in Black curve (phase angle vs complex dynamic modulus) can represent the localization of microcarcks and the initiation of macro-crack propagation (phase III) (Reese, 1997; Bodin et al., 2002; Di Benedetto et al., 2004). Hence, the number of cycles corresponding to the maximum phase angle can be taken as N_f. Specimen integrity can also be the criterion of N_f determination. It can be phase angle- or axial strain-based. For phase angle, the phase angle difference ($\Delta\varphi_i$ in Equatio 7.1) of 5 ˚ and, for axial strain, the percent of axial strain difference ($\Delta\varepsilon_{iax}$ in Equation 7.2) of 25%, are assumed as the fatigue failure (Sauzéat, Di Benedetto, Baaj & Ech, 2014, 2014) and the number of cycles corresponding to them are N_f.

The last criterioan is based on viscous energy dissipation. The accumulated viscous dissipated energy ratio (DER) (Equation 7.3) vs number of cycles curve has two stages with different tangential slopes. The number of cycles corresponding to the intersection of the two tangential lines represents N_f (Tapsoba et al., 2014).

$$\Delta\varphi_i = \varphi\varepsilon_{iax} - \varphi_E \tag{7.1}$$

$$\Delta\varepsilon_{iax} = \frac{\varepsilon_{Aaxi} - \varepsilon_{Aax}}{\varepsilon_{Aax}} \times 100 \tag{7.2}$$

$$DER = \sum_{i=1}^{N} \frac{W_i}{W_N} \tag{7.3}$$

Where: $\varphi\varepsilon_{iax}$ is the phase angle based on extensometer i; φ_E is the phase angle; ε_{Aaxi} is the axial strain of extensometer i; ε_{Aax} is the axial starin; W_i is the dissipated energy (Equation 7.4) of cycle i; and W_N is the dissipated energy at cycle N.

$$W_i = \pi\varepsilon_{Aax}\sigma_{Aax}sin\varphi_E \tag{7.4}$$

After determining fatigue lives (N_f) at, at least, three starin levels within the LVE domain, Wöhler curves were plotted. For each mixture type, five Wöhler curves were constructed according to the different criteria. Wöhler curve is a straight line with two constants of B (slope) and A (fatigue life corresponding to strain level of 1 million) in the log-log coordinates (Equation 7.5).

$$N_f = A(\varepsilon)^{-B} \tag{7.5}$$

7.4.5 Visco-elastic continuum damage (VECD)

Visco-elastic continuum damage (VECD) has two steps: (1) LVE characterization and (2) damage growth modelling. With regard to LVE characterization, generalized-maxwell (GM)

(Figure 7.3) is generally used (Equation 7.6) to model the behavior of the asphalt mixture; more precisely estimating complex dynamic modulus in time domain. As the number of elements in the GM model increases, the complex dynamic modulus estimation gets closer to the continuous spectrum of the complex dynamic modulus modelled by Sigmoid function or 2S2P1D. In most studies, twenty-five elements were found satisfactory to reproduce continuous models (Underwood, 2006; Tiouajni, Di Benedetto, Sauzéat & Pouget, 2011). As shown in Figure 7.4, unlike Sigmoid function which is a mathematical representation, 2S2P1D is a physical model with two springs, two parabolics and one dashpot. Hence, it can be used instead of GM for VECD analysis if it is transformed into the time domain. The superiority of 2S2P1D over GM is the precision of the model by using only one element (Olard & Di Benedetto, 2003). However, as given in Equation 7.7, 2S2P1D was developed in frequency domain and, to be transformed into the time domain, inverse Laplace-Carson transformation is required. We arrived at a differential equation given in Equation 7.8 that has no analyctical solution. If solved, a numerical problem in VECD turns into an analyctical problem. The outcome is saving computational time substantially and improving the accuracy.

$$E(t) = E_0 + \sum_{i=1}^{n} E_i e^{\frac{-t}{\rho_i}} \tag{7.6}$$

$$E^*(\omega) = E_{00} + \frac{E_0 - E_{00}}{1+\delta(j\omega\tau)^{-k}+(j\omega\tau)^{-h}+(j\omega\beta\tau)^{-1}} \tag{7.7}$$

$$\varepsilon(t) = \left(\frac{1}{E_0 - E_{00}} + \frac{t}{\rho}\right)\sigma(t) - \left(\frac{\varepsilon(t)}{E_0 - E_{00}} + \frac{\int_0^t \varepsilon(\xi)d\xi}{\rho}\right)E_0 - \frac{aE_0}{\tau^k}\int_0^t (t-\xi)^k \frac{d\varepsilon}{d\xi}d\xi - \frac{bE_0}{\tau^h}\int_0^t (t-\xi)^h \frac{d\varepsilon}{d\xi}d\xi \tag{7.8}$$

Where: j^2=-1; ω is angular frequency; τ is characteristic of time; σ(t) is stress at time t; δ, β, a and b are constants.

Still, unlike all other studies on VECD analysis that have deployed Sigmoid function to calibrate GM, in this study, 2S2P1D was used. So, the discrete model of GM was calibrated

by a continuous model (2S2P1D). The calibration of GM using 2S2P1D has been made by few researchers (Tiouajni et al., 2011; Di Benedetto et al., 2013). They first calibrated generalized Kelvin-Voigt and then applied it for calibrating GM. In this research, GM was directly calibrated using collocation method (Lv et al., 2021).

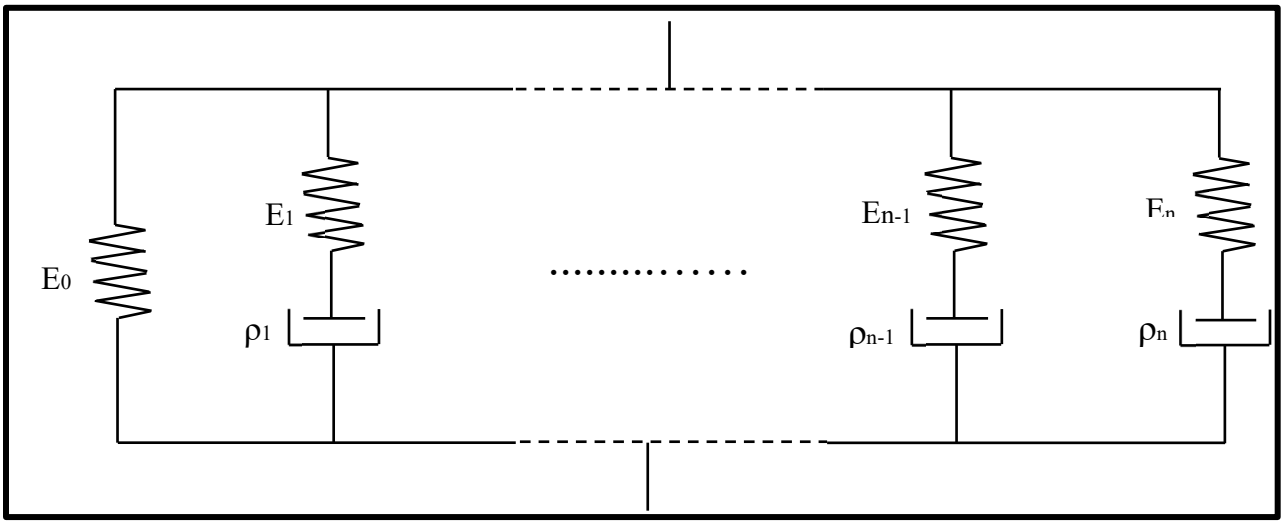

Figure 7.3 Schematic of generalized Maxwell (GM) model

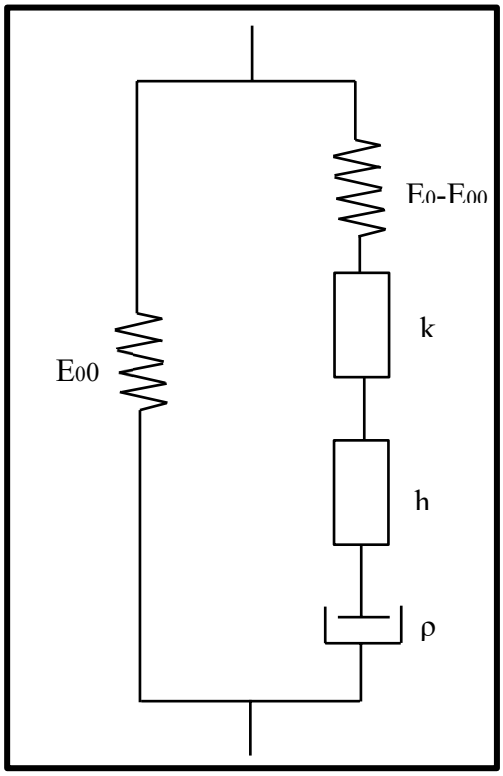

Figure 7.4 Schematic of 2S2P1D model

The calibrated GM within time domain is a relaxation modulus (E(t)) and it is used for the calculation of pseudo strain (ε^R). Equation 7.9 is the convolution integral that tracks the deformation of a visco-elastic material over time to determine ε^R. As a result, the irreversible strain is excluded and all is the reversible strain. So, it can be used for pure fatigue analysis, which deals with irreversible stiffness reduction. Equation 7.10 is the linear piecewise solution of Equation 7.9. Equation 7.11 is a solving technique that was used in this study to calculate the pseudo strain (Underwood, 2006).

$$\varepsilon^R = \frac{1}{E_R}\int_0^t E(t-\tau)\frac{d\varepsilon}{d\tau}d\tau \tag{7.9}$$

$$\varepsilon^R = \frac{1}{E_R}\left[\int_0^{t_1} E(t-\tau)\frac{d\varepsilon_1}{d\tau}d\tau + \int_0^{t_2} E(t-\tau)\frac{d\varepsilon_2}{d\tau}d\tau + \ldots + \int_0^{t_n} E(t-\tau)\frac{d\varepsilon_n}{d\tau}d\tau\right] \tag{7.10}$$

$$\varepsilon^{R(n+1)} = \frac{1}{E_R}[\eta_n^0 + \sum_{i=1}^{m} \eta_i^{n+1}] \quad (7.11)$$

Where: τ is time variable; E_R is the reference modulus that is taken as one; η_0 and η_i are internal state variables for elastic response of Maxwell element i at time interval n+1 that can be calculated using Equation 7.12 and 7.13, respectively.

$$\eta_n^0 = E_0(\varepsilon^{n+1} - \varepsilon^0) \quad (7.12)$$

$$\eta_i^{n+1} = e^{\frac{-\Delta t}{\rho_i}} \eta_i^n + E_i e^{\frac{-\Delta t}{\rho_i}} (\varepsilon^{n+1} - \varepsilon^n) \quad (7.13)$$

Since pseudo strain deals with the reversible portion of the strain, it reveals damage. Equation 7.14 presents the relationship between stress and pseudo strain in the frame of Hooke's law. From continuum damage perspective, reduction in pseudo stiffness (C) is as a result of damage (Hou, 2009). Pseudo stiffness takes specimen-to-specimen variability into account by using the complex dynamic modulus ratio (DMR) (Equation 7.15 and Equation 7.16).

$$\sigma = E_R \varepsilon^R \quad (7.14)$$

$$C = \frac{E_R}{DMR} \quad (7.15)$$

$$DMR = \frac{|E^*|_{tets}}{|E^*|_{LVE}} \quad (7.16)$$

$|E^*|_{test}$ is the complex dynamic modulus obtained from test and $|E^*|_{LVE}$ can be determined using Equation 7.17.

$$|E^*|_{LVE} = \sqrt{E'^2 + E''^2} \quad (7.17)$$

Where: E' and E" are the real and imaginary part of complex dynamic modulus, respectively, from generalized Maxwell modelling corresponding to the temperature and frequency that fatigue test is performed.

The damage (S) itself is a function of C and the aim of VECD modelling is to find the function and plot the curve, namely damage characteristic curve. According to work potential theory of Schapery (1982), the damage evolution is as given Equation 7.18.

$$\frac{dS}{dt} = (-\frac{W^R}{dS})^{\alpha} \tag{7.18}$$

Where: W^R is pseudo strain energy density; and α is damage evolution rate that can be taken as a function of the slope of complex dynamic modulus master curve (m) at a given temperature (Equation 7.19).

$$\alpha = 1 + \frac{1}{m} \tag{7.19}$$

Different methods has been adopted to solve Equation 7.16. In this study, as given in Equation 7.20, the one by Underwood (2006) was used.

$$S_{i+1} = S_i + (-0.5(\varepsilon^R)^2 \Delta C_i)^{(\frac{\alpha}{1+\alpha})} \Delta t^{(\frac{1}{1+\alpha})} \tag{7.20}$$

Where: Δ denotes the difference between two consecutive time step i and i+1.

The method explained above (rigorous method) becomes cumbersome as the number of cycles increases (Underwood et al., 2010). Therefore, only in as commanded, rigorous method was used only for the first pulse. After that, the simplified viscoelastic continuum damage (S-VECD) developed by Underwood et al. (2010) was employed. Equation 7.21, Equation 7.22 and Equation 7.23 shows the calculation of pseudo strain (ε^R), pseudo stiffness (C*) and damage (S) at each cycle, respectively, using S-VECD.

$$\varepsilon_{0,ta}^{R} = \frac{1}{E_R} \times \frac{\beta+1}{2}(\varepsilon_{pp}|E^*|_{LVE}) \tag{7.21}$$

$$C^* = \frac{\sigma_{0,ta}}{\varepsilon_{0,ta}^{R} \times DMR} \tag{7.22}$$

$$S_{i+1} = S_i + \Delta\xi^{\left(\frac{1}{1+\alpha}\right)} \times K_1^{\left(\frac{1}{1+\alpha}\right)}\left(-0.5\left(\varepsilon_{0,ta}^{R}\right)^2 \Delta C_i\right)^{\left(\frac{\alpha}{1+\alpha}\right)} \tag{7.23}$$

Where: within a cycle of loading, $\varepsilon_{0,ta}^{R}$ and ε_{pp} are the maximum tensile and peak-to-peak strain, respectively; E* is the complex dynamic modulus; $\sigma_{0,ta}$ is the maximum tensile stress; $\Delta\xi$ is the duration of tensile loading; β and K_1 are factors that can be computed using Equation 7.24 and Equation 7.25.

$$\beta = \frac{\sigma_{max}+\sigma_{min}}{\sigma_{max}-\sigma_{min}} \tag{7.24}$$

$$K_I = \frac{1}{\xi_f - \xi_i}\int_{\xi_i}^{\xi_f}(f(\xi))^{2\alpha}d\xi \tag{7.25}$$

Where: within a cycle, σ_{max} and σ_{min} are the maximum and minimum stress; ξ_i and ξ_f are the beginning and the end time of the tensile loading, respectively; and $f(\xi)$ is tensile loading function.

C vs S, namely damage characteristic curve, can be constructed using initially rigorous method ($\xi<\xi_p$) and then S-VECD ($\xi<\xi_p$). Once having the damage characteristic curve, a mathematical model can be used for fitting. Two models, as given in Equation 7.26 (Lee & Kim, 1988) and Equation 7.27 (Underwood, 2006), were developed for modelling damage characteristic curve.

$$C = 1 - aS^b \tag{7.26}$$

$$C = e^{aS^b} \tag{7.27}$$

Where: a and b are the coefficients of the models.

The model of the damage characteristic curve is used to predict fatigue life curve. If Equation (7.26) is used as in the case of this study, A and B of the Equation (7.5) for constructing fatigue curve can be calculated using Equation (7.28) and Equation (7.29).

$$A = 2\alpha \tag{7.28}$$

$$B = \frac{f(S_f)^k}{k(ab)^\alpha} \tag{7.29}$$

Where: f is frequency (10 Hz); S_f is the damage at failure which corresponds to the maximum phase angle; and k can be computed using Equation (7.30).

$$k = 1 + (1 - b)\alpha \tag{7.30}$$

Another fatigue performance criteria based on VECD is the rate of change of the averaged released pseudo strain energy throughout loading history (G^R) (Sabouri and Kim, 2014). The total released pseudo strain energy ($W_C{}^R$) for each cycle is the difference between the current maximum stored pseudo strain energy and the stored pseudo strain energy of the undamaged state (Equation 7.31).

$$(W_C^R)_i = \frac{1}{2}(\varepsilon_{0,ta}^R)_i^2(1 - F_i) \tag{7.31}$$

Where: F_i is the magnitude of pseudo stiffness at cycle i.

Once the G^R (Equation 7.32) starts to increase sharply, it indicates that the damage is accumulating faster and the material is failing faster. Thus, the number of cycles corresponding to that situation can be established as failure criterion.

$$G^R = \frac{\sum_{i=1}^{N_f}(W_C^R)_i}{{N_f}^2} \quad (7.32)$$

Where: N is the number of the cycle at which the G^R is calculated.

7.5 Results and discussion

7.5.1 Linear viscoelasticity (LVE) limit

Figure 7.5 shows complex dynamic modulus vs strain level up to LVE limit. FDG (57% RAP), CDG #2 (65% RAP), and CDG #1 (73% RAP) have the same LVE limit. 100% RAP is the softest mixture with the lowest complex dynamic modulus and LVE limit. It can be inferred that the impact of gradation is more than the bitumen stiffness on the stiffness of the asphalt mixtures.

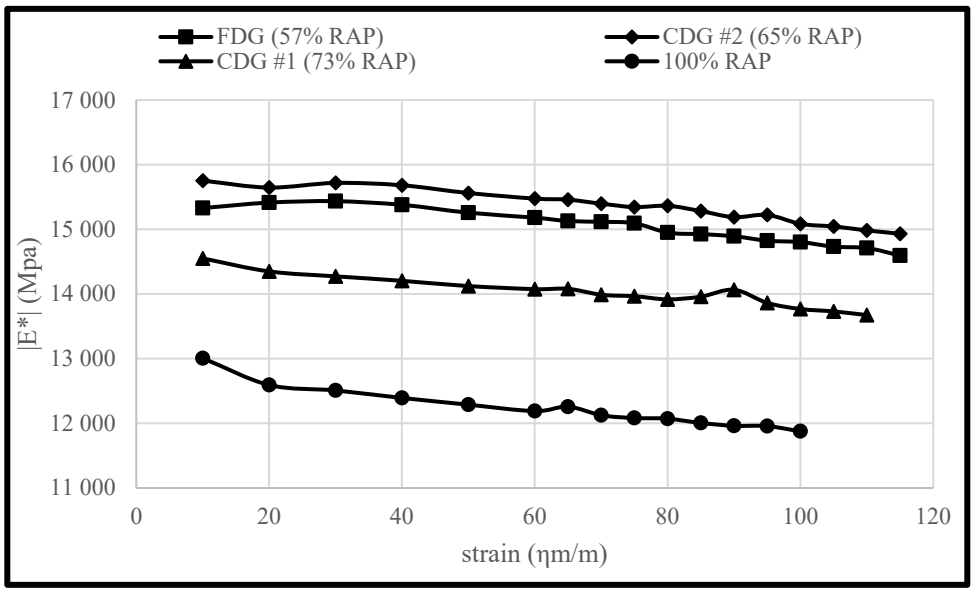

Figure 7.5 LVE test results

7.5.2 Fatigue life classical criteria

Having LVE limits of different mixture, the T/C fatigue test was performed within LVE domain. Figure 7.6 depicts the Wöhler curves at 10˚C and 10 Hz. Good correlation between fatigue life (N_f) and strain level can be established with respect to almost all classical criteria. However, maximum phase angle criterion does not yield a good correlation for 100% RAP. Notably, as 50% reduction in stiffness never occurred before rupture, the the avarage N_f of the other failure criteria were expressed as failure point of 50% reduction in stiffness. Also, in almost all cases, maximum phase angle fell at or very close to the rupture point.

All criteria give more or less the same pattern for the mixtures. It can be claimed that 100% RAP has higher fatigue life than CDG #1 (73% RAP). Similarly, FDG (57% RAP) has greater fatigue life than CDG #2 (65% RAP). But, comparing ftigue life of 100% RAP with FDG (57% RAP) and CDG #2 (65% RAP) or comparing CDG #1 (73% RAP) with FDG (57% RAP) and CDG #2 (65% RAP) depenends on the strain level. Since real pavement loads are different in magnitude, a pevment experiences different strain levels during its service life. Thus, it is not hard to determine the strain level that represents the traffic loading and, subsequently, decide which one of the mixtures under study has better fatigue cracking resistance. This is the shortcomings of the classical approach for fatigue life analysis that necessitates the utilization a strain-free fatigue analysis, i.e visco-elastic continuum damage (VECD).

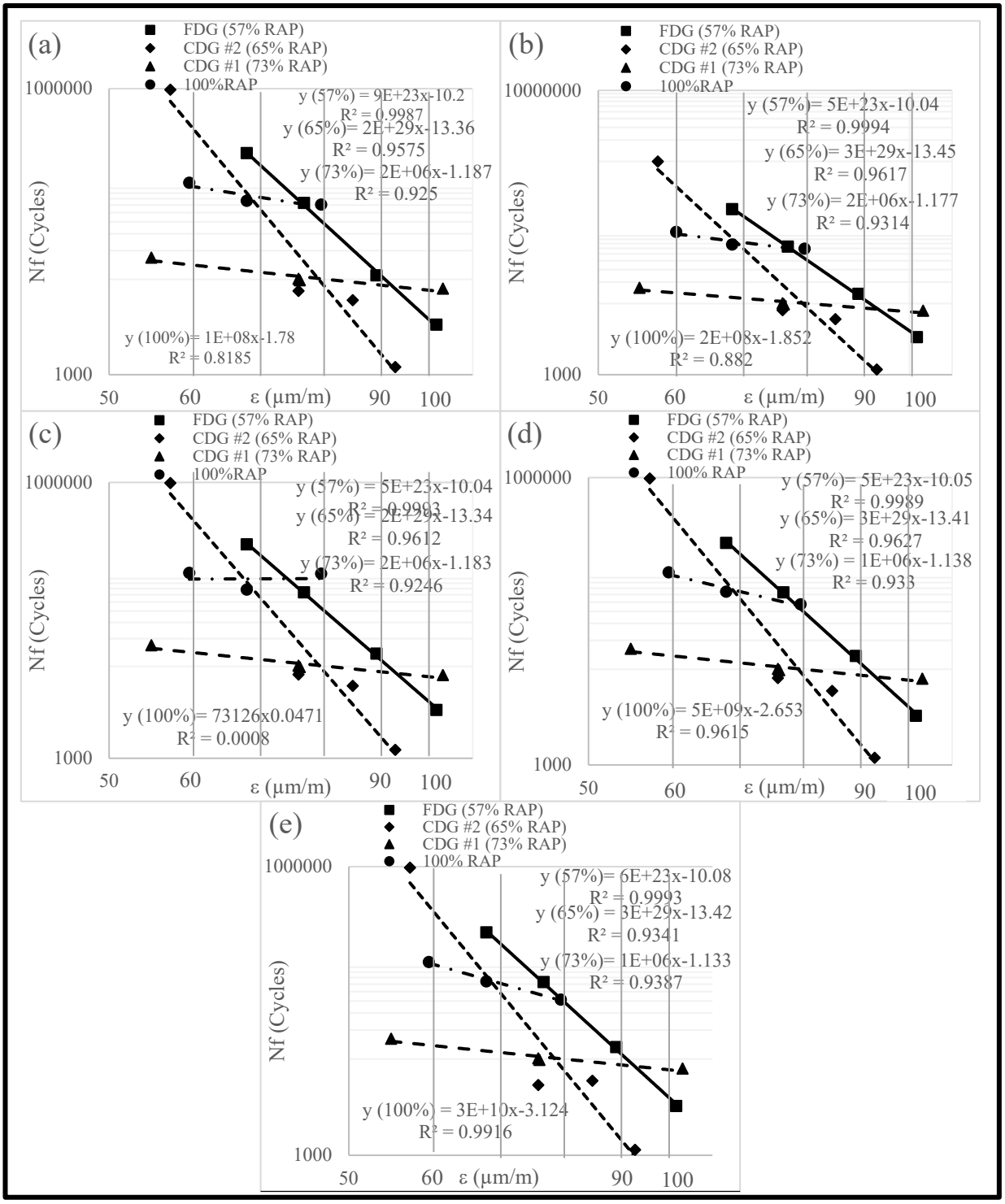

Figure 7.6 Wöhler curves based upon (a) 50% reduction in stiffness,
(b) inflection point of dissipated energy ratio (DER),
(c) maximum phase angle of Black curve,
(d) axial strain difference ($\Delta\varepsilon_{iax}$)>25%, and (e) phase angle difference ($\Delta\varphi_i$)> 5˚

7.5.3 4.3. Visco-elastic continuum damage (VECD)

Table 7.3 presents the damage evolution rates (α) of the mixtures. They are derived from the complex dynamic modulus master curves shown in Figure 7.7. The results of complex dynamic modulus master curve conforms with LVE test results; both indicate 100% RAP has the lowest stiffness in spite of having the stiffest bitumen. Thus, the damage evolution rate of 100% RAP is the highest.

Table 7.3 Damage evolution rate of different mixtures

	FDG (57% RAP)	CDG #2 (65% RAP)	CDG #1 (73% RAP)	100% RAP
Damage evolution rate(α)	7.490437	7.448089	7.443619	7.850258

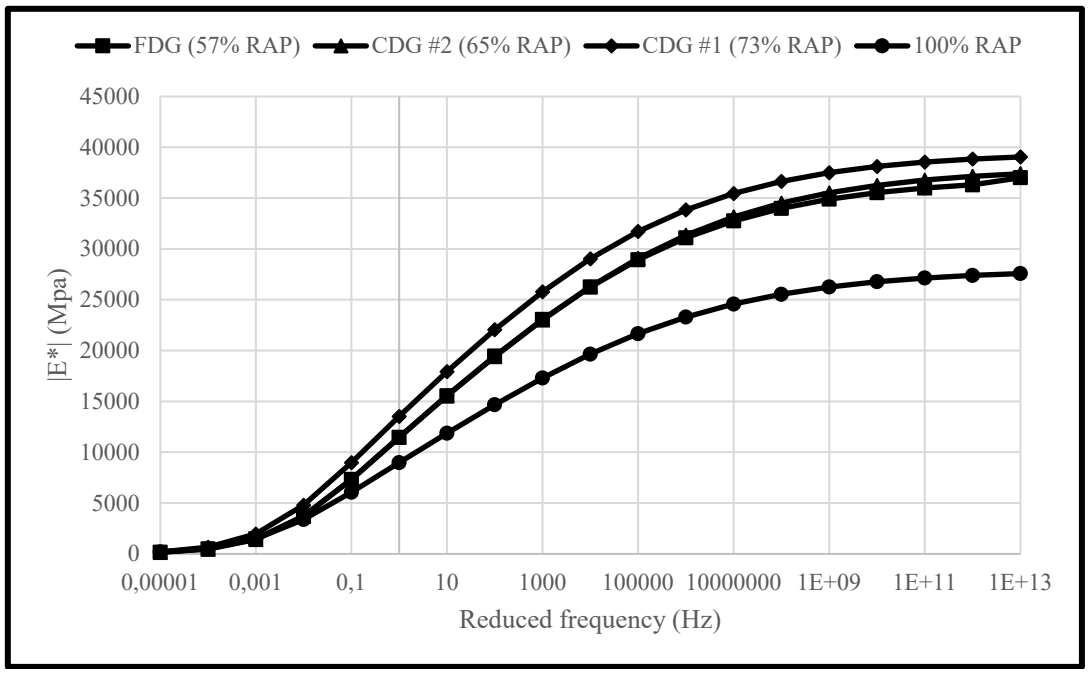

Figure 7.7 Complex dynamic modulus of different mixtures

Using collocation method, GM was calibrated based on the continuous model of 2S2P1D. As Cole-Cole curves in Figure 7.8 suggest, the calibration works well. For better assessment with

respect to high temperatures (Carret, 2018), the complex dynamic modulus in Black space are shown in Figure 7.9. Similar to Cole-Cole curves, the calibrated GM yields close complex dynamic modulus to 2S2P1D model. Bearing in mind that 2S2P1D is a continuous model that represents asphalt mixtures' behavior precisely, successful calibration of GM according to 2S2P1D means the validity of the calibrated GM for application in VECD analysis.

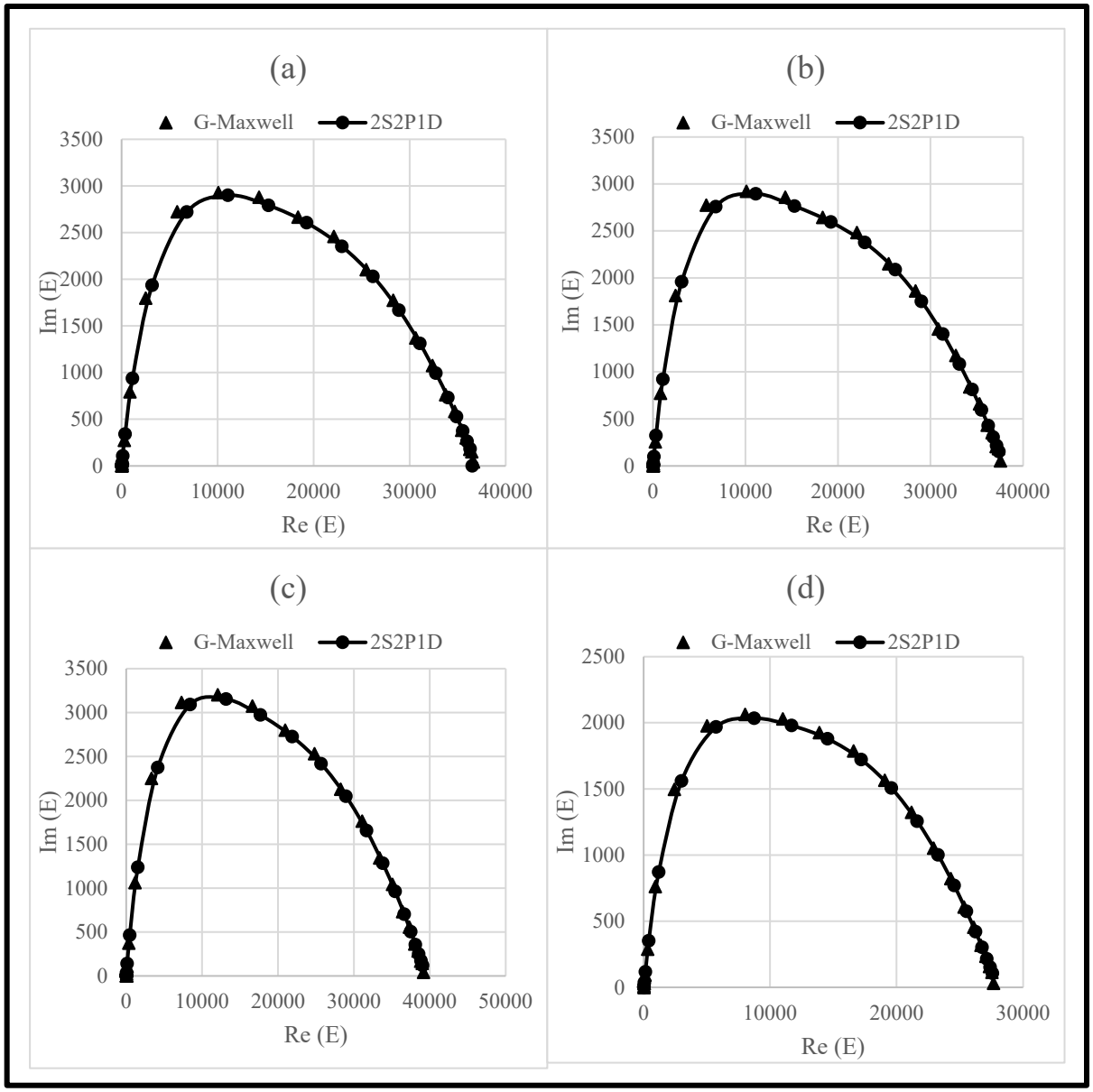

Figure 7.8 Cole-Cole curve of (a) FDG (57% RAP), (b) CDG #2 (65% RAP), (c) CDG #1 (73% RAP) and (d) 100% RAP by 2S2P1D and the calibrated GM model using 2S2P1D

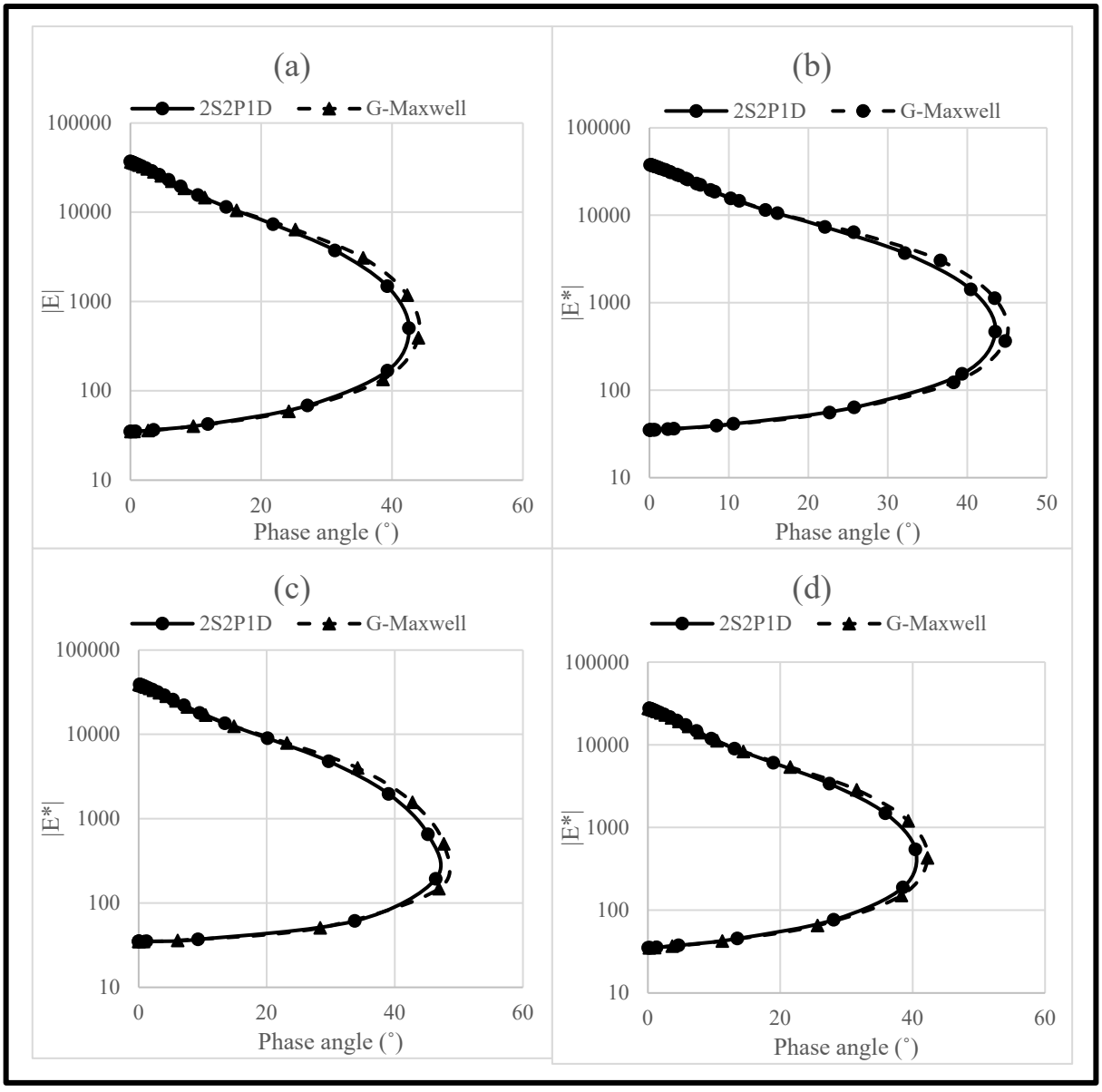

Figure 7.9 Complex dynamic modulus in Black space of (a) FDG (57% RAP)
(b) CDG #2 (65% RAP), (c) CDG #1 (73% RAP) and
(d) 100% RAP by 2S2P1D and the calibrated GM model using 2S2P1D

Figure 7.10 shows the damage characteristic curves of the mixtures. At failure point corresponding to sharp decline in phase angle (Reese, 1997), FDG (57% RAP) can contain significantly higher amount of damage than the other mixtures. The mixture is a FDG mixture by Bailey definitions. Hence, it is as expected because, unlike CDG, FDG mainly is devised for better cracking resistance. Also, the damage characteristic curves indicate that the mixtures

are quite brittle and rupture at a very high pseudo stiffness. This conforms the results of the fatigue test. Among them, 100% RAP has the lowest pseudo stiffness that confirms the fact that it is the softest mixture.

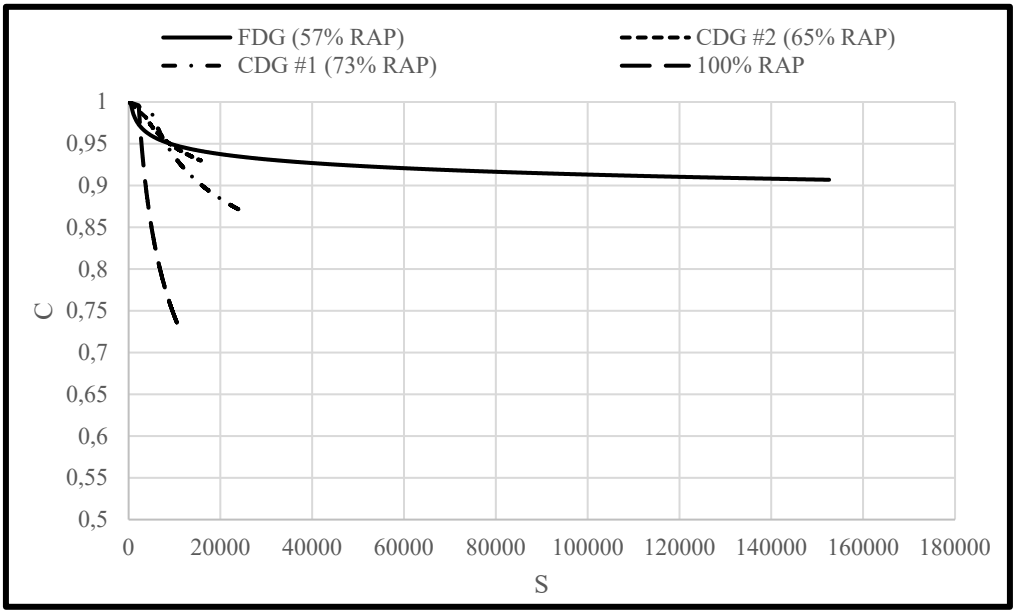

Figure 7.10 Damage characteristic curve of (a) FDG (57% RAP), (b) CDG #2 (65% RAP), (c) CDG #1 (73% RAP), and (d) 100% RAP

Figure 7.11 compares the Wöhler curves (fatigue curves) of the classical and VECD approach. The criterion of the classical approach is maximum phase angle in order to be the same VECD predictions. All the VECD-based Wöhler curves have steeper slope than classical approach. For 100% RAP and CDG #1 (73% RAP), the difference are big whereas it is small for FDG (57% RAP) and CDG #2 (65% RAP). These different changes in the slopes, as shown in Figure 7.12, result in the VECD-based Wöhler curves that makes the fatigue life comparison possible for different mixtures. Fatigue life increases with RAP content decrease.

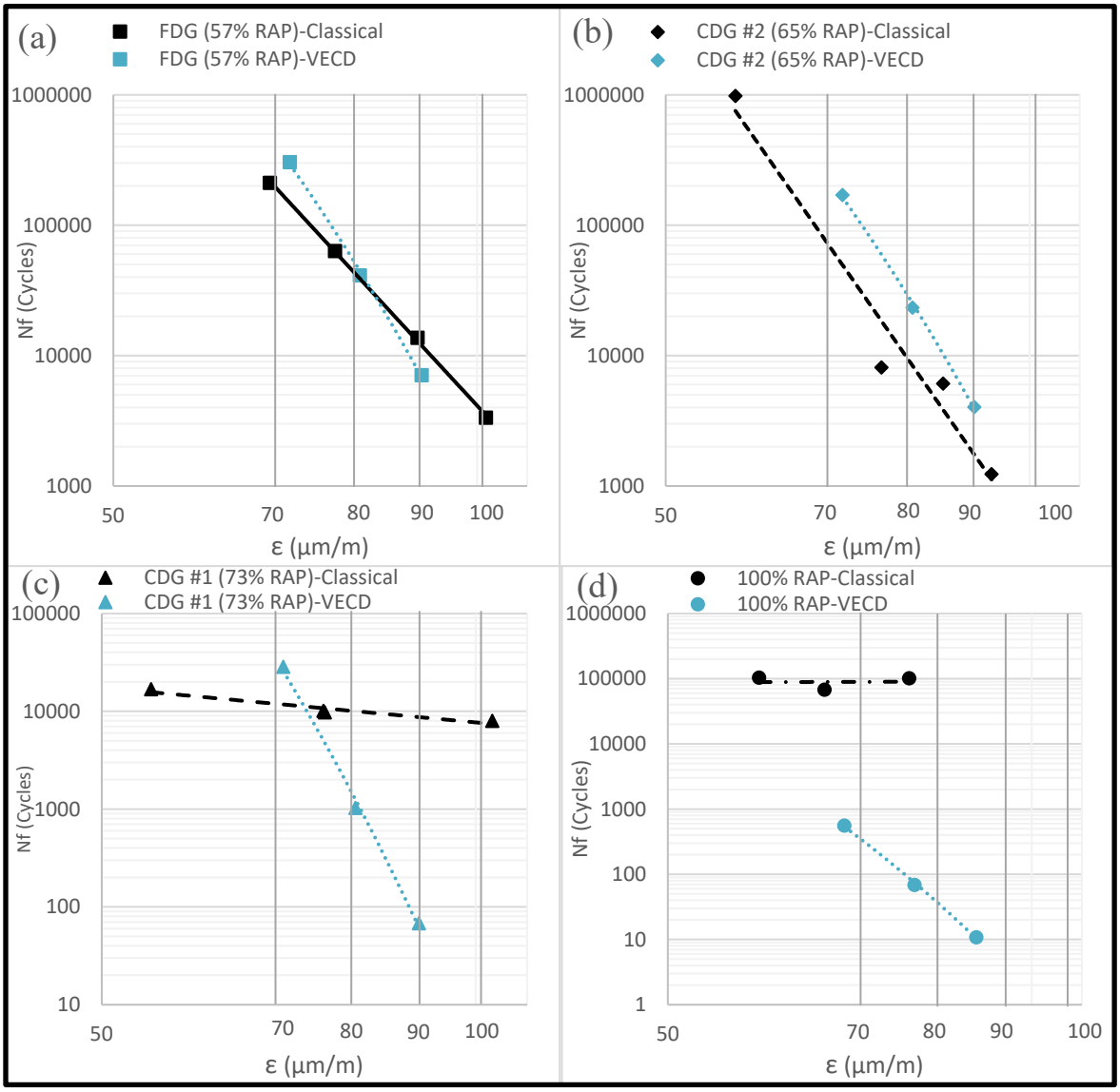

Figure 7.11 Classical- and VECD-based Wöhler curves of (a) FDG (57% RAP), (b) CDG #2 (65% RAP), (c) CDG #1 (73% RAP), and (d) 100% RAP

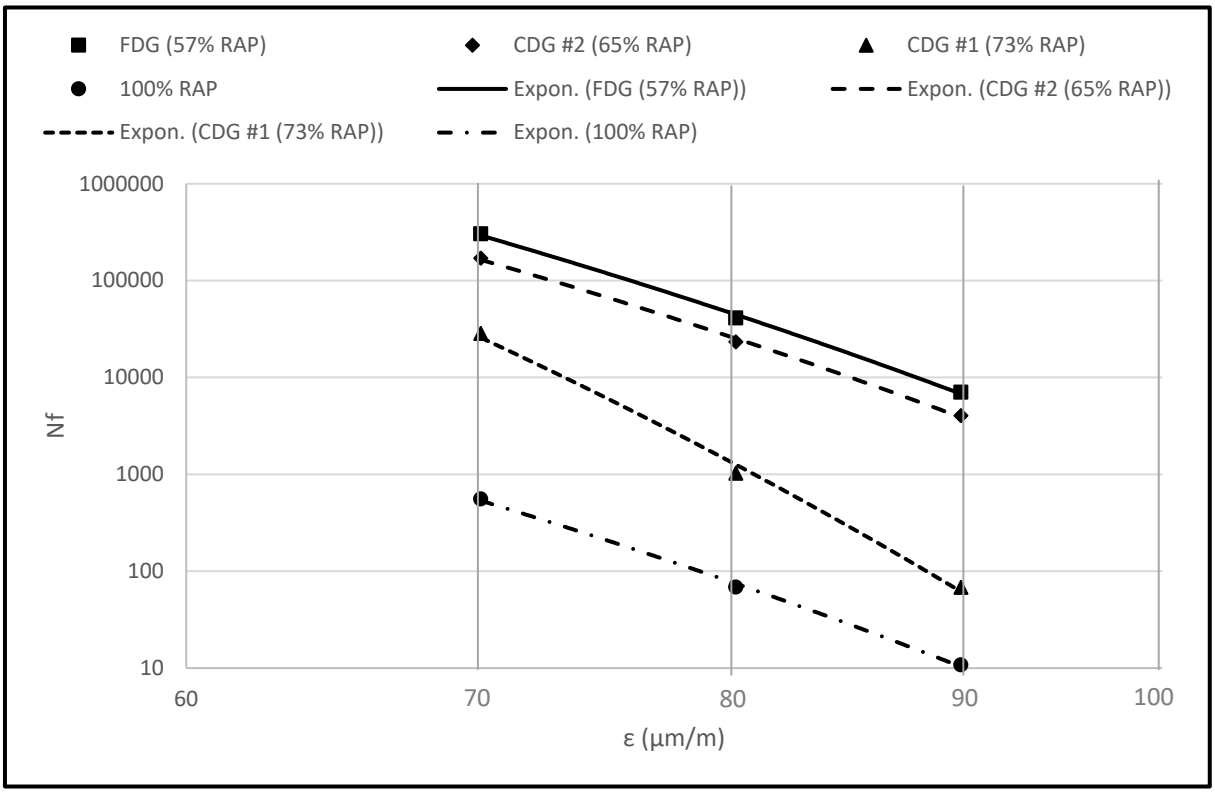

Figure 7.12 VECD-based Wöhler curves of the mixtures

Figure 7.13 shows the characteristic relationship of the mixtures with different RAP contents. It is evident that good power law relationship is established between G^R and N_f. These curves would collapse all within the same line regardless of the mixture type, if they had close damage characteristic (Sabouri and Kim, 2014). The advantage of the fatigue life characteristic curve is its independency from the mode of loading. There are controlled crosshead (CX), controlled stress (CS) and controlled on-specimen strain (COS) T/C fatigue testing and each leads to different fatigue performance. In reality, the traffic loading is a combination of the aforementioned loading modes (Sabouri and Kim, 2014). Having the G^R and N_f curves of two or more mixtures fallen along the same line reveals the similarity of their fatigue characteristic. Therefore, CDG #2 (65% RAP) and 100% RAP have similar fatigue characteristics and FDG (57% RAP) has close fatigue characteristics to them. On the other hand, CDG #1 (73% RAP) has a different fatigue characteristics from the others. These results are valid within LVE domain of the asphalt mixtures with very high RAP contents.

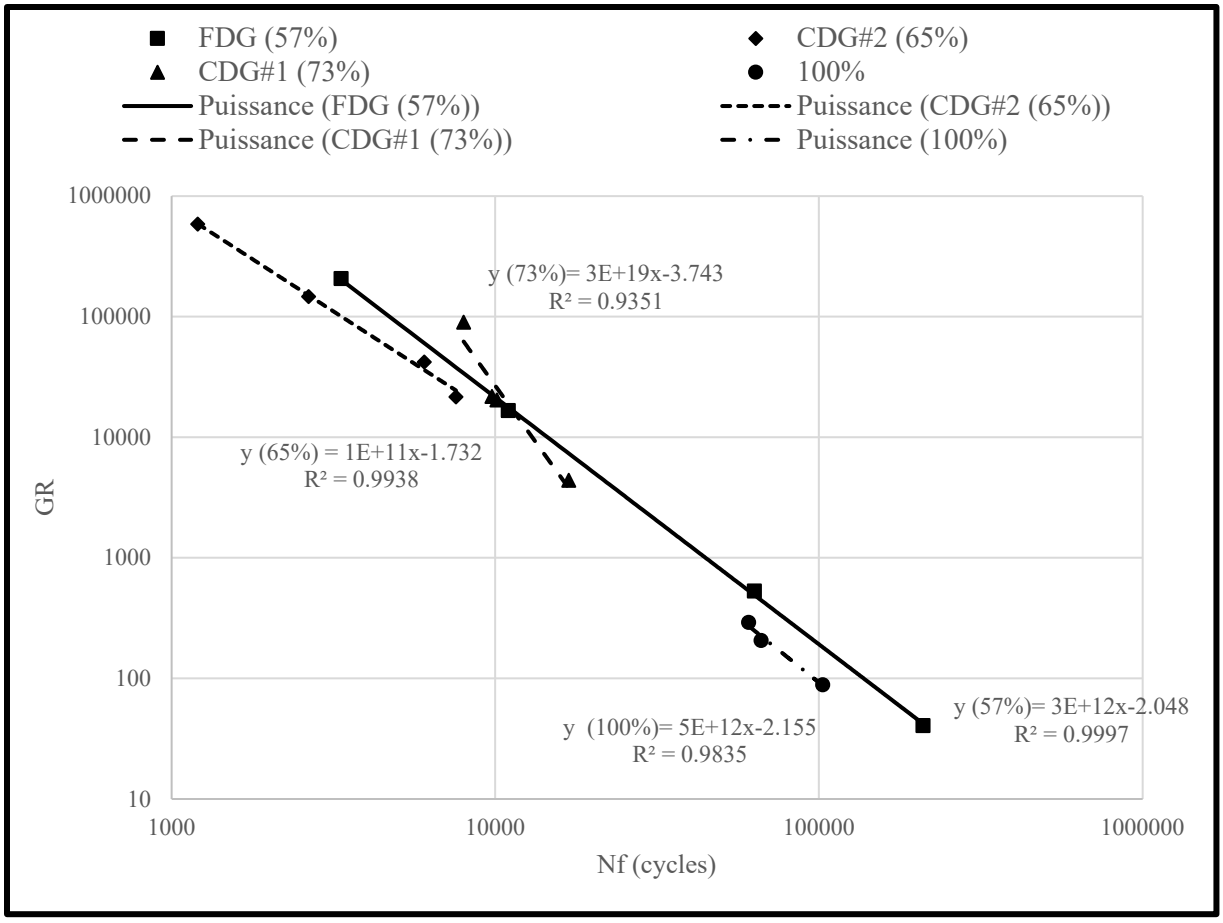

Figure 7.13 G^R vs N_f in COS loading mode for the mixtures

7.6 Conclusion

Performing fatigue analysis using classical and VECD approaches on asphalt mixtures containing very high RAP (>50%) reveals that:

- Both approaches can be successfully applied on asphalt mixtures with very high RAP contents. They gives fatigue life curves with strong relationship.

- The intrinsic fatigue properties of different asphalt mixtures containing very high RAP may vary. The difference can be observed in the G^R vs N_f curves.

- The strain level hinders fair fatigue life judgement of the asphalt mixtures with very high RAP contents once classical approach is used. VECD can remove the strain effect and predict Wöhler curves that make comparison possible.

- Using VECD-based Wöhler curves leads to a logical conclusion: more RAP, less fatigue life. This conclusion could not be withdrawn using classical-based Wöhler curves.

It is recommended to use VECD for fatigue life analysis of asphalt mixtures with very high RAP contents since it can remove the strain level effects off the performance evaluation. Also, since the 2S2P1D model is a physical model and can calibrate generalized Maxwell (GM) model precisely, it can be used within characterization phase of the VECD analysis. For future work, the transformation of 2S2P1D from frequency domain into time domain can make the current numerical method of VECD fatigue analysis into an analytical method. Differential Equation 7.8 needs to be solved.

Also it is good to note that even though VECD and G^R can remove the strain and loading mode, respectively, from fatigue life, the temperature and/or frequency impact is there. Those represent climatic and traffic conditions together. It means, to evaluate and compare fatigue performance of asphalt mixtures thoroughly, the fatigue testing should also be carried out at different temperatures and frequencies. Here, the fatigue testing was done at one frequency (10 Hz) and one temperature (10˚C). This is the limitation of this study that requires further investigation to solidify its findings.

CONCLUSION

This thesis aimed to develop guidelines to design asphalt mixtures with RAP contents greater than 50%. The first two chapters dealt with the development and the rest three chapters did the evaluation and investigation. Within the guideline development phase, the method for gradation improvement (Chapter 3) and mix design considerations (Chapter 4) were outlined. Within the evaluation phase, characterization (Chapter 5), rejuvenation (Chapter 6) and fatigue performance (Chapter 7) were studied. Characterization helps to understand the role of binder and aggregates on imparting properties to mixture. It gives the idea that the investment must be place on which element, based on the performance. The rejuvenation done in this study lied on the previous research but the evaluation of it was evaluated here. It is always important to have a realistic and effective method to assess the rejuvenation efficient. This study came up with an approach that provides easy and realistic assessment. Also, fatigue performance as the key weakness of the asphalt mixtures containing very high amount of RAP was evaluated. It is very important to evaluate fatigue deeply since fatigue is a complicated phenomenon. This thesis employed the simple classical Wöhler curve principle and the advanced linear visco-elastic continuum damage (VECD) to find which approach reveals more about the fatigue performance the asphalt mixtures with very high RAP contents.

In this thesis, the gradation of a reclaimed asphalt pavement (RAP) source was corrected by adding virgin aggregates in a way that several aggregate blends complying Bailey concepts were prepared. They contain 57%, 65%, 73% RAP by the weight of total aggregate blend and were designed based on Bailey method concepts. Then, guidelines of asphalt mixture specimens containing very high RAP (>50%) were proposed and used for mix design. A mix design based upon different aspects of performance including rutting, cracking, moisture damage and aging resistance were developed. An integrated performance index (PI) was defined to rank different asphalt mixtures with very high RAP contents accordingly. For deeper investigation into the performance and behavior of different asphalt mixtures, complex dynamic modulus and T/C fatigue were conducted. Additionally, rheological testing including PG, multiple stress creep recovery (MSCR), linear amplitude strain (LAS) tests were performed on extracted and recovered (E&R) and the blended asphalt binders prepared under

various blending conditions. This was done to understand the effectiveness of rejuvenation by the epoxidized soybean oil (ESO) and find the best blending condition representing the E&R asphalt binder. With accordance to the results obtained from the aforementioned testing program, following conclusions can be drawn:

- Except 100% RAP mixtures, volumetric mix design approach based upon 4% design air voids results insufficient coating for asphalt mixtures with very high RAP contents. It was found that 3% design air voids leads to better mixtures. In contrast, 100% RAP mixture designed according to 3% air voids had too much bitumen, hence, 4% is good for it. This can be attributed to homogeneity of mixtures.

- Using Bailey method concepts to rectify the gradation of 100% RAP mixture leads to significant improvement in rutting performance.

- The coarse dense-graded (CDG) aggregate blend which is design based on the average black and white curve gradation (65% RAP) had its fine part gradation modified. It has the best rutting resistance that shows the importance of building firm skeleton in fine part in addition to coarse part. The CDG that was designed based on black curve gradation (73%RAP) did not need to have its fine part gradation modified while the fine dense-graded (FDG) (57% RAP) had it modified. Consequently, the 57% RAP had higher rutting resistance than 73% RAP.

- The aging resistance must be included in the mix design of asphalt mixtures with very high RAP contents since this type of asphalt mixture must be rejuvenated and the long lasting of the rejuvenator effect is important. In this thesis, a simple and efficient method was introduced for that purpose incorporating SCB strength ratio after and before long term aging.

- The mix design framework proposed here is a balanced mix design that, unlike balanced mix design, provides comparison between mixtures quantitatively rather than

qualitatively and rationally. The PI used in this mix design method is an index that integrates all performance aspects of asphalt mixtures with high RAP contents relatively and based upon the importance of each performance aspect. In the proposed mix design, the optimal asphalt content (OAC) is determined according to volumetric properties and asphalt mixtures fabricated with different aggregate blends are compared performance-wise to find the best mixture. Since aggregate structure has a pivotal role in performance of asphalt mixtures, this method mainly focuses on it and uses the conventional methods for OAC.

- The study of the thermomechanical behavior of asphalt mixtures and binders was done to assess the correlation, if any, between them. This can help to predict the behavior of asphalt mixtures via simple and easy testing of asphalt binders. At higher temperatures and/or lower frequencies, the behaviors of asphalt mixture and binder are similar but, as the temperature lowers and/or frequency increases, they deviate. Therefore, at high temperatures, the prediction of the behavior of asphalt mixture with very high RAP content can be relied on asphalt binder behavior but, at lower temperatures, it can be derived from asphalt mixture testing. This indicates that, although asphalt binder is used in order to hold the aggregate structure in high temperatures and does not bear loads in large deal, its presence shapes the characteristics to asphalt mixtures.

- Once it comes to the efficiency of the rejuvenation, it is common to blend the RAP bitumen with the rejuvenating agent and the virgin bitumen under severe blending conditions. This might not be what takes place during production. Therefore, since rejuvenation is necessary in asphalt mixtures containing very high amount of RAP, it is important to come up with a blending conditions that represents the asphalt binder inside the asphalt mixture the most. Among the three blending conditions that were compared rheologically with the E&R asphalt binder, none could behave thoroughly like E&R asphalt binder. The properties corresponding to RTFO- and PAV-aged asphalt binder are approximately the same for E&R asphalt binder and the one prepared under low blending conditions (hand stirring at 150 ˚C for 1 min). On the other hand,

both intense and moderate blending conditions (2000 and 400 rpm for 60 and 12 min, respectively, at 150 ˚C) can be used for RTFO-aged properties. Thus, it can be deducted that low blending conditions provides molecular bonding as inside asphalt mixture while intense and moderate blending conditions give the same uniformity as expected in E&R asphalt binder.

- Fatigue is a very complicated phenomenon and it is the main concern of asphalt mixtures with very high amount of RAP. The simplicity of semi-circular bend (SCB) cannot fully cover the mechanism of fatigue failure. Also, Wöhler curves developed according to different criteria are useful but not comprehensive. Application of VECD coupled with the new criteria, namely the rate of change of the averaged released pseudo strain energy throughout loading history (G^R), can give insight into the fatigue life of asphalt mixtures with very high RAP contents. Based upon G^R, the 100% RAP mixture has the poorest fatigue performance, as expected, but the Wöhler curves shows it is not the least fatigue cracking resistant mixture, 73% RAP mixture is. Even, 100% RAP mixture can perform the best at high strain level. It cannot be true as the common sense dictates. The G^R vs fatigue life (N_f) curves prove the weakest fatigue performance of 100% RAP followed by 65% and 57% RAP. 73% RAP is generally a weak asphalt mixture but it can perform very well at low strain levels. It should be noted that this mixture type was designed based on black curve and did not have its fine part modified. Also, with RAP content increase, there is a transition from a visco-elastic behavior to a qausi-brittle behavior in fatigue performance.

- SCB used in the mix design found 73% RAP as the second most cracking resistance mixture and, due to the equal weight of different performance aspects, 73% and 65% RAP were determined as the optimum mixtures. This indicates that an asphalt mixture may have good cracking resistance at room temperature but not necessarily the best fatigue life. Also, it is recommended to give higher weight to cracking resistance in the PI, especially for the colder climate regions, because asphalt mixtures with very high RAP content generally have good rutting and moisture damage resistance.

Using asphalt mixtures that incorporates large amount of RAP is the future. This thesis recommends Bailey method concepts for constructing firm aggregate structure out of poor gradation of RAP and proposes a strong framework within mix design for ranking asphalt mixtures with different gradation complying Bailey method. The cracking resistance of this mixture type is a primary concern, therefore, it is recommended to deployed VECD to better assess the fatigue cracking resistance. Also, using the low blending condition is recommended to study low and intermediate properties of asphalt binder and understand the effectiveness of aging potential of the rejuvenated asphalt binder of RAP better. Investigating the thermomechanical behavior of asphalt mixtures is not a must. Instead, it is good to deploy the asphalt binder blended under intense or moderate conditions to see if the bitumen is stiff enough at high temperature to hold the aggregate skeleton sufficiently.

RECOMMENDATIONS

This thesis used black curve and the average of black and white curve as gradation for designing aggregate blends. There are more possibility between black and white curves as selected gradation that may results in better aggregate skeleton. Studying it is worthwhile and can lead to deeper insight into the real gradation of RAP.

The equal weights for all performance aspects is used only to show how the framework works. It is good idea to study and determine the weights according to climatic and traffic condition; run a campaign like asphalt pavement structural design (MEPDG) to find the best weights for different parts.

The study on similarity of asphalt binder blended under different blending conditions and the E&R one was based on rheology. It is recommended to conduct a study using chemical composition in order to develop better rejuvenating agent that can dilute and dissolve in the old asphalt binder of RAP.

This thesis successfully calibrated the general Maxwell (GM) model using 2S2P1D. Since 2S2P1D is a strong model for asphalt mixtures and binder and, unlike GM, it is a continuous model, if transformed into time domain, it can make a numerical problem into an analytical problem. As a result, the computation time and accuracy increase significantly. This study made an attempt to do so, but the differential equation does not seem to be solvable. It requires a good knowledge of mathematics. Also, VECD does not consider the thixotropy and self-heating effects of the binder during fatigue test. These effects can make significant impact on the fatigue results. Added to that is the nonlinearity of the binder even though the mixture is within the linear visco-elastic domain. It's been proved that binders can have strains up to 300 times greater that mixture once loaded (de Oliveira, da Silva, Júnior, Babadopulos & Soares, 2023). Therefore, thixotropy and self-heating and nonlinearity of binder is recommended to be taken into account for future studies based on VECD.

APPENDIX I

COMPLEX MODULUS TEST RESULTS AND 2S2P1D MODELING

Table A I. 1 Complex modulus test results and 2S2P1D model for 100% RAP asphalt mixture

frequency (experiment)	E* (real)	E*(imaginary)	|E*| test	|E*| 2S2P1D	Squared Error	Squared Mean
Temperature	-35					
10	26635.501	480.4626127	26639.83	26644.21	19.11305	1.9E+08
3	26160.1	479.1652808	26164.49	26372.43	43238.92	1.82E+08
1	25833.057	553.1124694	25838.98	26080.47	58316.89	1.74E+08
0.3	25586.074	692.2294022	25595.44	25705.13	12033.2	1.65E+08
0.1	25011.129	866.3788942	25026.13	25305.34	77958.93	1.55E+08
0.03	24597.589	911.9831676	24614.49	24796.51	33130.97	1.42E+08
Sum					224698	1.01E+09
Average			25646.56			
Temperature	-25					
10	24618.323	700.6163908	24628.29	25078.52	202703.2	1.49E+08
3	23826.82	834.3821671	23841.42	24532.54	477641.4	1.36E+08
1	23296.402	989.7461444	23317.42	23959.6	412398.9	1.23E+08
0.3	22679.943	1108.664255	22707.02	23242.89	287153.5	1.08E+08
0.1	21837.912	1149.94582	21868.17	22502.92	402913.1	92722304
0.03	20885.929	1381.000839	20931.54	21594.19	439105.9	76047233
Sum					2221916	6.84E+08
Average			22882.31			
Temperature	-15					
10	21620.673	1163.89479	21651.98	22160.46	258553.5	86244271
3	20521.232	1214.205324	20557.12	21211.38	428051.2	69517202
1	19649.166	1400.451434	19699.01	20255.73	309938.7	54494680
0.3	18605.653	1510.64314	18666.88	19113.86	199795.7	38939893
0.1	17586.767	1567.985204	17656.53	17991.92	112485.9	26196341
0.03	16475.044	1661.825392	16558.65	16684.94	15950.27	14525705
sum					1324775	2.9E+08
average			19131.69			
temperature	-5					
10	17803.816	1619.77869	17877.35	18183.05	93454.6	28189420
3	16545.947	1704.289583	16633.49	16887.57	64557.3	16111320
1	15390.558	1718.997014	15486.26	15644.03	24892.63	7674856
0.3	14122.853	1831.914483	14241.17	14227.35	191.0423	1832416

frequency (experiment)	E* (real)	E*(imaginary)	|E*| test	|E*| 2S2P1D	Squared Error	Squared Mean
0.1	12850.644	1835.066191	12981.01	12896.95	7066.255	541.2779
0.03	11464.644	1915.835275	11623.62	11408.58	46239.34	2146506
sum					236401.2	55955059
average			14807.15			
temperature	5					
10	13442.896	1896.321973	13575.99	13739.96	26887.67	750447.5
3	11952.25	1958.456937	12111.64	12268.8	24697.75	365884.9
1	10583.485	1942.187741	10760.22	10901.75	20032.94	3888494
0.3	9158.1195	1913.588407	9355.906	9384.028	790.8308	12177673
0.1	7835.2286	1864.946469	8054.119	7988.192	4346.354	23867991
0.03	6429.833	1844.86555	6689.266	6462.517	51415.25	41103012
sum					128170.8	82153503
average			10091.19			
temperature	15					
10	9168.8705	2069.8934	9399.609	9799.78	160133.8	9448885
3	7553.6123	2014.944143	7817.74	8272.066	206412.3	21174849
1	6196.0063	1901.309334	6481.163	6876.763	156499.5	35963012
0.3	4878.5352	1734.880363	5177.829	5376.445	39448.24	56208531
0.1	3753.9121	1534.415293	4055.402	4085.302	893.9815	77235593
0.03	2688.8645	1306.407334	2989.43	2837.73	23012.8	1.01E+08
sum					586400.6	3.01E+08
average			5986.862			
temperature	25					
10	5364.3567	1909.331379	5694.02	6314.657	385190.1	43020778
3	3993.3914	1687.326189	4335.233	4839.214	253996.9	64552643
1	2932.8104	1425.268741	3260.792	3597.797	113572.2	86041998
0.3	2016.4334	1125.414136	2309.234	2436.477	2031.79	1.09E+08
0.1	1373.1454	869.110753	1625.079	1612.422	160.1928	1.27E+08
0.03	866.36087	621.1310263	1066.014	973.9903	8468.282	1.42E+08
sum					763419.5	5.71E+08
average			3048.395			
temperature	35					
10	2657.4708	1411.189593	3008.921	3529.549	271053.5	87312778
3	1753.4464	1072.622366	2055.503	2381.54	106300	1.1E+08
1	1172.7641	797.4729667	1418.217	1571.388	23461.31	1.28E+08
0.3	732.36731	550.9703151	916.477	946.8746	660.2147	1.42E+08
0.1	465.44936	377.7720082	599.4621	577.8243	383.364	1.51E+08
0.03	285.68375	239.9914483	373.11	331.1919	1757.127	1.57E+08

frequency (experiment)	E* (real)	E*(imaginary)	|E*| test	|E*| 2S2P1D	Squared Error	Squared Mean
sum					403615.5	7.76E+08
average			1395.282			
Se: 379.0037			Sy: 8952.975			
Se/Sy: 0.042333			R^2: 0.998437			

Table A I. 2 Complex modulus test results and 2S2P1D model for 73% RAP asphalt mixture

frequency (experiment)	E* (real)	E*(imaginary)	|E*| test	|E*| 2S2P1D	Squared Error	Squared Mean
temperature	-35					
10	38694.22	387.8345	38696.16	38018.24	459580.5	3.66E+08
3	38183.62	568.9408	38187.86	37706.9	231328.4	3.54E+08
1	37752.03	560.9697	37756.2	37369.13	149823.9	3.41E+08
0.3	37331.76	576.4291	37336.21	36930.31	164749.3	3.25E+08
0.1	36786.45	927.0535	36798.13	36457.67	115916.4	3.08E+08
0.03	36858.65	765.9105	36866.6	35848.86	1035801	2.87E+08
sum					2157200	1.98E+09
average			37606.86			
temperature	-25					
10	36297.9	796.4339	36306.64	36231.98	5574.412	3.01E+08
3	35472.99	992.2918	35486.87	35582.68	9180.549	2.78E+08
1	34678.68	1184.922	34698.92	34891.98	37274.08	2.56E+08
0.3	33763.96	1184.819	33784.74	34015.21	53117.96	2.29E+08
0.1	32952.25	1484.321	32985.66	33095.8	12131.89	2.02E+08
0.03	31378.15	1531.194	31415.49	31947.82	283376.1	1.7E+08
sum					400655	1.44E+09
average			34113.05			
temperature	-15					
10	32298.62	1549.371	32335.76	32894.37	312043.2	1.96E+08
3	30932.24	1671.552	30977.37	31718.31	548986.9	1.64E+08
1	29710.57	1907.001	29771.71	30510.13	545260.9	1.35E+08
0.3	28142.86	2065.527	28218.55	29035.79	667873.6	1.03E+08
0.1	26752.42	2185.1	26841.51	27555.36	509586.1	75000660
0.03	24945.73	2111.603	25034.95	25792.09	573264.2	47568844
sum					3157015	7.21E+08
average			28863.31			
temperature	-5					
10	26573.85	2342.45	26676.89	26883.99	42891.73	63822848
3	24605.29	2430.864	24725.07	25066.26	116408.3	38083580

frequency (experiment)	E* (real)	E*(imaginary)	|E*| test	|E*| 2S2P1D	Squared Error	Squared Mean
1	22940.41	2570.065	23083.92	23294.49	44336.79	19354853
0.3	21086.38	2620.741	21248.62	21244.21	19.49428	5518434
0.1	19231.4	2902.139	19449.15	19287.84	26020	154266.7
0.03	16991.6	2785.575	17218.42	17063.18	24099.06	3355822
sum					253775.4	1.3E+08
average			22067.01			
temperature	5					
10	20132.95	2898.725	20340.56	20531	36269.23	2676272
3	17819.73	3030.92	18075.65	18353.61	77258.9	293181.7
1	15766.15	3030.031	16054.67	16296.88	58663.46	6750599
0.3	13527.41	3044.565	13865.8	13976.15	12178.95	24195734
0.1	11356.47	3018.267	11750.72	11810.62	3587.997	50189500
0.03	9143.479	2871.972	9583.915	9420.933	26562.99	89759276
sum					214521.5	1.74E+08
average			14945.22			
temperature	15					
10	13189.96	3242.759	13582.73	13976.15	154783.1	24195734
3	10671.32	3128.061	11120.33	11601.4	231426.6	53197654
1	8557.211	2998.374	9067.31	9420.933	125049.4	89759276
0.3	6419.725	2687.828	6959.69	7099.223	19469.47	1.39E+08
0.1	4661.857	2325.998	5209.912	5162.743	2224.927	1.89E+08
0.03	3161.132	1837.053	3656.162	3389.845	70924.62	2.4E+08
sum					603878.1	7.35E+08
average			8266.022			
	25					
10	7133.722	2961.755	7724.117	8192.23	219129.6	1.15E+08
3	5046.81	2530.371	5645.624	5961.138	99549.32	1.67E+08
1	3459.223	2068.958	4030.733	4183.504	23338.93	2.16E+08
0.3	2173.781	1526.133	2656.013	2644.138	2031.79	2.64E+08
0.1	1340.918	1071.727	1716.584	1642.716	5456.499	2.98E+08
0.03	775.5856	693.2836	1040.276	927.3824	12745.07	3.23E+08
sum					362251.3	1.38E+09
average			3802.225			
temperature	35					
10	3033.419	2013.469	3640.836	3773.733	17661.43	2.29E+08
3	1810.186	1427.338	2305.227	2345.662	1635.058	2.74E+08
1	1058.3	962.1514	1430.292	1439.066	76.98933	3.05E+08
0.3	579.0388	587.3186	824.76	803.9196	660.2147	3.27E+08

frequency (experiment)	E* (real)	E*(imaginary)	|E*| test	|E*| 2S2P1D	Squared Error	Squared Mean
0.1	336.0476	357.2295	490.4497	457.8408	383.364	3.4E+08
0.03	198.8494	210.5822	289.6307	241.4202	2324.252	3.48E+08
sum					22741.31	1.82E+09
average			1496.866			
Se: 418.2436			Sy: 13355.26			
Se/Sy: 0.031317			R^2: 0.999144			

Table A I. 3 Complex modulus test results and 2S2P1D model for 65% RAP asphalt mixture

frequency (experiment)	E* (real)	E*(imaginary)	|E*| test	|E*| 2S2P1D	Squared Error	Squared Mean
temperature	-35					
10	36060.28	534.3333	36064.24	35893.33	29210.86	3.58E+08
3	35489.97	537.4509	35494.04	35474.66	375.846	3.42E+08
1	34992.14	796.9568	35001.22	35026.23	625.6435	3.26E+08
0.3	34512.89	849.3979	34523.34	34451.78	5120.589	3.05E+08
0.1	33778.67	1071.845	33795.67	33842.39	2182.979	2.84E+08
0.03	32397.22	1614.126	32437.41	33070.49	400792.4	2.59E+08
sum					438308.3	1.87E+09
average			34552.65			
temperature	-25					
10	33668.86	935.8709	33681.86	34236.84	308001.9	2.98E+08
3	32865.03	1081.957	32882.84	33528.79	417257.7	2.74E+08
1	31947.86	1279.83	31973.49	32784.16	657186	2.5E+08
0.3	30829.41	1496.543	30865.71	31850.35	969505.3	2.21E+08
0.1	29692.19	1609.09	29735.76	30883.52	1317356	1.93E+08
0.03	28503.9	1793.817	28560.29	29692.43	1281756	1.62E+08
sum					4951063	1.4E+09
average			31283.32			
temperature	-15					
10	29585.79	1670.847	29632.94	30214.84	338612.8	1.75E+08
3	28299.09	1816.958	28357.36	28943.15	343156.4	1.43E+08
1	27071.23	1984.345	27143.86	27660.84	267270.1	1.14E+08
0.3	25660.28	2193.309	25753.85	26126.16	138613.5	83715533
0.1	23936.01	2386.009	24054.63	24615.44	314499.6	58352777
0.03	22150.31	2161.779	22255.55	22851.64	355315.8	34516776
sum					1757468	6.09E+08
average			26199.7			
temperature	-5					

frequency (experiment)	E* (real)	E*(imaginary)	|E*| test	|E*| 2S2P1D	Squared Error	Squared Mean
10	24063.9	2298.944	24173.47	24203.73	915.503	52232257
3	22276.16	2438.085	22409.18	22415.17	35.87713	29578752
1	20641.13	2515.21	20793.81	20701.7	8483.905	13876815
0.3	18673.08	2588.363	18851.62	18750.4	10245.71	3146573
0.1	16990.39	2668.402	17198.66	16914.34	80834.91	3868.108
0.03	14974.79	2750.712	15225.33	14849.58	141189.4	4523966
sum					241705.3	1.03E+08
average			19775.34			
temperature	5					
10	17696.08	2800.937	17916.38	17774.08	20247.92	636075.6
3	15532.68	2866.055	15794.89	15732.04	3950.036	1548780
1	13581.16	2912.321	13889.91	13822.74	4511.111	9946420
0.3	11435.46	2843.536	11783.69	11683.15	10109.32	28020006
0.1	9459.773	2731.207	9846.157	9698.38	21838.03	52971582
0.03	7525.508	2554.01	7947.09	7531.039	173098.4	89217445
sum					233754.9	1.82E+08
average			12863.02			
temperature	15					
10	11159.08	3015.722	11559.39	12010.05	203096.4	24665963
3	8871.069	2904.696	9334.513	9837.884	253382	50960383
1	6930.242	2694.866	7435.762	7855.439	176128.8	83194438
0.3	5109.87	2352.852	5625.539	5773.852	21996.82	1.26E+08
0.1	3591.744	1951.749	4087.78	4083.944	14.71984	1.66E+08
0.03	2374.424	1483.21	2799.607	2597.84	40709.93	2.07E+08
sum					695328.8	6.57E+08
average			6807.099			
temperature	25					
10	5881.109	2643.173	6447.775	6819.149	137918.6	1.03E+08
3	4057.664	2192.713	4612.226	4836.253	50188.19	1.47E+08
1	2764.83	1734.392	3263.802	3304.701	1672.721	1.87E+08
0.3	1722.493	1240.859	2122.902	2339.403	2031.79	2.14E+08
0.1	1091.16	857.8426	1387.993	1239.424	22072.74	2.48E+08
0.03	670.8672	552.437	869.0509	695.2651	30201.5	2.65E+08
sum					244085.5	1.16E+09
average			3117.291			
temperature	35					
10	2370.924	1683.232	2907.671	3175.65	71812.72	1.9E+08
3	1409.734	1148.828	1818.559	1941.287	15062.24	2.26E+08

frequency (experiment)	E* (real)	E*(imaginary)	|E*| test	|E*| 2S2P1D	Squared Error	Squared Mean
1	863.3153	764.6099	1153.231	1179.741	702.8002	2.5E+08
0.3	505.804	466.8671	688.3332	716.0704	660.2147	2.64E+08
0.1	322.5484	292.5683	435.4695	421.2717	383.364	2.74E+08
0.03	213.1821	181.5314	280.0005	212.8122	4514.256	2.81E+08
sum					93135.59	1.49E+09
average			1213.877			
Se: 459.4496			Sy: 12611.19			
Se/Sy: 0.036432			R^2: 0.998842			

Table A I. 4 Complex modulus test results and 2S2P1D model for 57% RAP asphalt mixture

frequency (experiment)	E* (real)	E*(imaginary)	|E*| test	|E*| 2S2P1D	Squared Error	Squared Mean
temperature	-35					
10	35393.24	491.0818	35396.65	34994.92	161381.6	327561958.5
3	34705.26	643.6894	34711.23	34582.15	16660.84	312791034.3
1	34380.76	755.7184	34389.07	34137.61	63233.22	297264341
0.3	33730.62	1030.883	33746.36	33565.09	32861.23	277850104.3
0.1	33270.62	1120.607	33289.48	32954.67	112097.5	257872928.3
0.03	32865.99	1159.892	32886.45	32177.79	502201.1	233525271.3
sum					888435.5	1706865638
average			34069.87			
temperature	-25					
10	33061.61	895.9156	33073.75	34137.61	1131802	297264341
3	32172.09	1052.009	32189.29	33565.09	1892822	277850104.3
1	31326.63	1241.625	31351.22	32954.67	2571055	257872928.3
0.3	30552.15	1344.027	30581.7	32177.79	2547490	233525271.3
0.1	29575.97	1421.29	29610.11	31360.69	3064563	209220094.3
0.03	28526.33	1384.109	28559.89	30337.04	3158273	180654895.5
sum					14366005	1456387635
average			30894.33			
temperature	-15					
10	29151.16	1553.053	29192.5	29463.32	73343.51	157931111.2
3	27866.45	1726.066	27919.85	28186.97	71351.37	127480286
1	26660.11	1839.375	26723.49	26894.67	29304.11	99968360.37
0.3	25374.5	1968.096	25450.71	25342.41	11728.61	71337654.58
0.1	23807.16	2153.436	23904.35	23809.54	8989.036	47793596.16
0.03	22309.42	2419.228	22440.21	22014.94	180851.7	26200957.25
sum					375568.4	530711965.5

frequency (experiment)	E* (real)	E*(imaginary)	|E*| test	|E*| 2S2P1D	Squared Error	Squared Mean
average			25938.52			
temperature			-5			
10	23861.19	2246.06	23966.67	23809.54	24689.45	47793596.16
3	22026.06	2344.246	22150.45	22014.94	18364.32	26200957.25
1	20380.48	2424.436	20524.18	20286.65	56419.56	11494809.22
0.3	18591.27	2585.426	18770.18	18309.71	212035.7	1997851.998
0.1	16806.08	2657.799	17014.94	16443.36	326708.5	205112.0869
0.03	14842.25	2776.48	15099.71	14341.61	574719.3	6526215.863
sum					1212937	94218542.57
average			19587.69			
temperature			5			
10	17917.52	2774.55	18131.07	18003.78	16204.1	1226607.593
3	15755.15	2871.098	16014.61	15946.13	4689.632	902725.4404
1	13793.42	2899.364	14094.85	14018.84	5777.275	8279492.22
0.3	11701.26	2899.114	12055.05	11863.11	36841.22	25332485.13
0.1	9651.548	2842.485	10061.42	9873.474	35322.35	49319405.65
0.03	7648.888	2647.672	8094.174	7714.053	144491.7	84312773.84
sum					243326.3	169373489.9
average			13075.2			
temperature			15			
10	11591.78	3065.138	11990.18	12053.19	3970.011	23455219.85
3	9256.45	2987.416	9726.588	9873.474	21575.53	49319405.65
1	7297.338	2812.105	7820.427	7900.129	6352.341	80930230.88
0.3	5344.83	2457.158	5882.587	5842.622	1597.195	122182736.6
0.1	3762.79	2035.709	4278.165	4174.636	10718.22	161839505.8
0.03	2418.858	1555.648	2875.92	2696.906	32046.19	201621429.4
sum					76259.49	639348528.1
average			7095.645			
temperature			25			
10	6183.586	2776.479	6778.316	7273.871	245574.7	92590216.27
3	4290.221	2317.49	4876.141	5273.335	157762.5	135092206.9
1	2886.418	1833.634	3419.594	3694.637	75648.87	174282629.4
0.3	1801.712	1306.019	2225.276	2339.403	13024.93	211901862.3
0.1	1108.89	893.1997	1423.883	1463.679	1583.696	238164307.6
0.03	656.6649	560.5943	863.4089	840.4506	527.0805	257788754.4
sum					494121.8	1109819977
average			3264.437			
temperature			35			

frequency (experiment)	E* (real)	E*(imaginary)	|E*| test	|E*| 2S2P1D	Squared Error	Squared Mean
10	2432.18	1779.686	3013.766	3273.734	67583.37	185572996.5
3	1433.932	1199.812	1869.682	2035.916	27633.78	220829588.2
1	871.6942	788.3286	1175.293	1257.912	6825.99	244557668
0.3	515.4341	475.9054	701.5399	716.0704	211.1344	261798273
0.1	323.1178	292.8453	436.0774	421.2717	219.206	271424970.9
0.03	206.0883	173.8557	269.626	236.1105	1123.288	277560311.1
sum					103596.8	1461743808
average			1244.331			
Se: 658.16171			Sy: 12349.9243			
Se/Sy: 0.05329277			R^2: 0.99752245			

Table A I. 5 Complex modulus test results and 2S2P1D model for 100% RAP asphalt binder

frequency	|G*| test	|G*| 2S2P1D	Squared Error	Squared Mean
temperature	-8			
10	287426.8	278294.2	83405320	6.23E+10
9	282914.3	272806.9	1.02E+08	5.96E+10
8	278106.8	266710.4	1.3E+08	5.66E+10
7	271928.3	259851.1	1.46E+08	5.34E+10
6	264735.1	252007.1	1.62E+08	4.99E+10
5	255719.9	242841.4	1.66E+08	4.58E+10
4	244966.2	231802.8	1.73E+08	4.12E+10
3	231070.8	217889.5	1.74E+08	3.58E+10
2	211692.2	198949	1.62E+08	2.9E+10
1.59	201626.4	188607.1	1.7E+08	2.56E+10
1	181565.4	168588.9	1.68E+08	1.96E+10
0.9	177486	164213	1.76E+08	1.84E+10
0.8	172385.5	159398.6	1.69E+08	1.71E+10
0.7	166865	154040.6	1.64E+08	1.57E+10
0.6	159824.1	147989.1	1.4E+08	1.42E+10
0.5	152039.8	141018.9	1.21E+08	1.26E+10
0.4	142944	132766.8	1.04E+08	1.08E+10
0.3	131186.2	122584.3	73993651	8.81E+09
0.2	116121.6	109109	49177316	6.46E+09
0.1	94153.64	88430.09	32758961	3.56E+09
sum			2.67E+09	5.86E+11
average	201237.9			

frequency	|G*| test	|G*| 2S2P1D	Squared Error	Squared Mean
temperature	-2			
10	194122	190707	11662487	2.62E+10
9	190004	186025.5	15827989	2.47E+10
8	184980	180864.6	16936472	2.31E+10
7	179942.2	175107.8	23371926	2.14E+10
6	173874.3	168588.9	27934737	1.96E+10
5	166616.6	161057.8	30899937	1.75E+10
4	157140.4	152109.7	25308756	1.52E+10
3	147119.6	141018.9	37218265	1.26E+10
2	131414.9	126253.7	26638137	9.51E+09
1.59	123465.8	118352.7	26143946	8.03E+09
1	109038.6	103383.1	31984350	5.57E+09
0.9	106085.9	100168	35021596	5.1E+09
0.8	102606.2	96654.71	35419779	4.61E+09
0.7	98758.5	92774.52	35807991	4.1E+09
0.6	94462.03	88430.09	36384269	3.56E+09
0.5	89580.17	83476.66	37252883	3E+09
0.4	83772.02	77683.46	37070525	2.4E+09
0.3	76669.02	70644.27	36297600	1.76E+09
0.2	67502.78	61521.82	35771808	1.08E+09
0.1	53970.64	47983.49	35845979	3.71E+08
sum			5.99E+08	2.1E+11
average	126556.3			
temperature	4			
10	119675.2	126253.7	43277087	9.51E+09
9	115844.3	122584.3	45427260	8.81E+09
8	112678.5	118564.2	34641246	8.07E+09
7	108915.2	114111.3	26999725	7.29E+09
6	104503.7	109109	21209037	6.46E+09
5	99622.36	103383.1	14143009	5.57E+09
4	93666.27	96654.71	8930787	4.61E+09
3	86273.71	88430.09	4649999	3.56E+09
2	76395.8	77683.46	1658061	2.4E+09
1.59	71201.4	72031.47	689015	1.88E+09
1	61918.72	61521.82	157527.8	1.08E+09
0.9	59833.64	59300.12	284639.5	9.35E+08
0.8	57656.98	56887.38	592273.7	7.93E+08
0.7	55260.11	54241.28	1038020	6.51E+08

frequency	|G*| test	|G*| 2S2P1D	Squared Error	Squared Mean
0.6	52591.81	51302.46	1662422	5.1E+08
0.5	49572.25	47983.49	2524146	3.71E+08
0.4	46015.14	44146.72	3490986	2.38E+08
0.3	41715.37	39553.49	4673719	1.17E+08
0.2	36200.76	33721.87	6144881	24983465
0.1	28213.81	25350.62	8197856	11376539
sum			2.3E+08	6.29E+10
average	73887.75			
temperature	10			
10	71826.19	77683.46	34307589	2.4E+09
9	69154.83	75049.8	34750730	2.15E+09
8	66767.14	72181.88	29319485	1.89E+09
7	64085.36	69026.82	24418000	1.62E+09
6	61054.41	65510.18	19853827	1.35E+09
5	57711.58	61521.82	14517992	1.08E+09
4	53715.48	56887.38	10060967	7.93E+08
3	48874.74	51302.46	5893812	5.1E+08
2	42491.87	44146.72	2738538	2.38E+08
1.59	39365.13	40452.48	1182311	1.38E+08
1	33484.32	33721.87	56434.27	24983465
0.9	32260.76	32323.78	3972.068	12961819
0.8	30953.3	30815.87	18888.55	4377877
0.7	29507.8	29174.94	110790.4	203774.9
0.6	27891.32	27368.82	273008.7	1835237
0.5	26075.98	25350.62	526148.2	11376539
0.4	23987.53	23047.5	883656.8	32217305
0.3	21499.88	20335.26	1356331	70362992
0.2	18351.41	16968.39	1912749	1.38E+08
0.1	13846.49	12304.28	2378388	2.7E+08
sum			1.85E+08	1.27E+10
average	41645.28			
temperature	16			
10	40982.57	44146.72	10011844	2.38E+08
9	39169.55	42419.13	10559798	1.88E+08
8	37542.68	40550.14	9044836	1.4E+08
7	35768.37	38509.25	7512388	95760293
6	33814.39	36253.91	5951251	56706635
5	31667.32	33721.87	4221180	24983465

frequency	|G*| test	|G*| 2S2P1D	Squared Error	Squared Mean
4	29158.58	30815.87	2746605	4377877
3	26187.05	27368.82	1396580	1835237
2	22378.5	23047.5	447558	32217305
1.59	20490.58	20862.08	138014.2	61802366
1	17030.27	16968.39	3830.094	1.38E+08
0.9	16336.84	16174.89	26226.76	1.57E+08
0.8	15583.74	15325.35	66767.77	1.8E+08
0.7	14759.96	14408.51	123514.2	2.05E+08
0.6	13852.69	13408.92	196929.8	2.35E+08
0.5	12842.65	12304.28	289834.9	2.7E+08
0.4	11687.98	11060.38	393885.7	3.12E+08
0.3	10330.1	9619.687	504685.6	3.65E+08
0.2	8642.437	7870.528	595843.9	4.35E+08
0.1	6286.405	5527.778	575515.4	5.38E+08
sum			54807087	3.68E+09
average	22225.63			
temperature	22			
10	22399.63	25350.62	8708326	11376539
9	21287.17	24240.76	8723705	20095190
8	20263.47	23047.5	7750816	32217305
7	19169.15	21753.6	6679393	48579849
6	17973.88	20335.26	5576114	70362992
5	16672.97	18757.97	4347206	99312451
4	15180.21	16968.39	3197564	1.38E+08
3	13429.52	14876.19	2092857	1.92E+08
2	11260.63	12304.28	1089205	2.7E+08
1.59	10178.66	11027.07	719803.6	3.13E+08
1	8257.395	8794.609	288598.7	3.97E+08
0.9	7879.957	8346.927	218061.4	4.15E+08
0.8	7471.656	7870.528	159098.7	4.35E+08
0.7	7027.646	7359.867	110370.9	4.56E+08
0.6	6541.694	6807.367	70581.98	4.8E+08
0.5	6005.651	6202.178	38622.99	5.07E+08
0.4	5399.319	5527.778	16501.63	5.38E+08
0.3	4694.941	4756.635	3806.109	5.74E+08
0.2	3839.369	3835.88	12.17137	6.19E+08
0.1	2690.619	2632.516	3375.906	6.81E+08
sum			49794019	6.3E+09

frequency	|G*| test	|G*| 2S2P1D	Squared Error	Squared Mean
average	11381.18			
temperature	28			
10	11878.24	12304.28	181509.9	2.7E+08
9	11222.63	11702.58	230350	2.9E+08
8	10615.21	11060.38	198178.9	3.12E+08
7	9970.22	10369.72	159599.3	3.37E+08
6	9273.226	9619.687	120035.1	3.65E+08
5	8519.513	8794.609	75677.71	3.97E+08
4	7669.517	7870.528	40405.33	4.35E+08
3	6684.59	6807.367	15074.11	4.8E+08
2	5484.278	5527.778	1892.221	5.38E+08
1.59	4897.196	4904.416	52.1285	5.67E+08
1	3872.104	3835.88	1312.16	6.19E+08
0.9	3672.062	3625.047	2210.4	6.3E+08
0.8	3459.325	3402.028	3282.954	6.41E+08
0.7	3229.2	3164.548	4179.84	6.53E+08
0.6	2980.164	2909.513	4991.513	6.66E+08
0.5	2706.857	2632.516	5526.516	6.81E+08
0.4	2402.831	2326.886	5767.691	6.97E+08
0.3	2056.421	1981.583	5600.678	7.15E+08
0.2	1644.61	1575.595	4763.105	7.37E+08
0.1	1108.029	1056.682	2636.544	7.65E+08
sum			1063046	1.08E+10
average	5667.311			
temperature	34			
10	6167.862	6202.178	1177.61	5.07E+08
9	5797.14	5874.995	6061.385	5.22E+08
8	5447.32	5527.778	6473.436	5.38E+08
7	5078.068	5156.721	6186.335	5.55E+08
6	4682.4	4756.635	5510.786	5.74E+08
5	4257.246	4320.106	3951.441	5.96E+08
4	3782.79	3835.88	2818.575	6.19E+08
3	3242.828	3285.266	1800.945	6.47E+08
2	2599.258	2632.516	1106.125	6.81E+08
1.59	2289.482	2318.796	859.3307	6.97E+08
1	1761.679	1788.211	703.9244	7.26E+08
0.9	1660.231	1684.674	597.4476	7.31E+08
0.8	1552.229	1575.595	545.958	7.37E+08

frequency	|G*| test	|G*| 2S2P1D	Squared Error	Squared Mean
0.7	1437.417	1459.96	508.2008	7.43E+08
0.6	1314.528	1336.396	478.1968	7.5E+08
0.5	1181.875	1202.95	444.1635	7.57E+08
0.4	1036.266	1056.682	416.8013	7.65E+08
0.3	872.89	892.7463	394.2719	7.75E+08
0.2	683.024	701.9785	359.2742	7.85E+08
0.1	444.347	461.8091	304.9239	7.99E+08
sum			40699.13	1.35E+10
average	2764.444			
temperature	40			
10	4610.771	4756.635	21276.21	5.74E+08
9	4432.153	4499.697	4562.205	5.87E+08
8	4197.168	4227.534	922.1171	6E+08
7	3945.48	3937.284	67.1731	6.14E+08
6	3655.246	3625.047	911.9731	6.3E+08
5	3333.751	3285.266	2350.839	6.47E+08
4	2961.89	2909.513	2743.313	6.66E+08
3	2546.483	2483.83	3925.451	6.89E+08
2	2013.499	1981.583	1018.611	7.15E+08
1.59	1752.834	1741.218	134.9287	7.28E+08
1	1341.366	1336.396	24.70377	7.5E+08
0.9	1263.538	1257.673	34.39736	7.54E+08
0.8	1179.749	1174.841	24.08445	7.59E+08
0.7	1088.801	1087.154	2.711305	7.64E+08
0.6	991.275	993.6005	5.408174	7.69E+08
0.5	891.221	892.7463	2.326485	7.75E+08
0.4	788.264	782.4327	34.00393	7.81E+08
0.3	666.307	659.1118	51.7707	7.88E+08
0.2	519.752	516.0873	13.42989	7.96E+08
0.1	339.074	336.9378	4.563446	8.06E+08
sum			38110.22	1.42E+10
average	2125.931			
temperature	46			
10	1056.716	1202.95	21384.44	7.57E+08
9	993.068	1131.66	19207.86	7.61E+08
8	925.9	1056.682	17103.86	7.65E+08
7	853.107	977.3455	15435.22	7.7E+08
6	776.191	892.7463	13585.13	7.75E+08

frequency	|G*| test	|G*| 2S2P1D	Squared Error	Squared Mean
5	693.615	801.601	11660.97	7.8E+08
4	604.125	701.9785	9575.313	7.85E+08
3	504.741	590.7077	7390.274	7.91E+08
2	389.75	461.8091	5192.51	7.99E+08
1.59	336.906	401.1344	4125.281	8.02E+08
1	249.831	300.6432	2581.877	8.08E+08
0.9	234.07	281.3772	2237.967	8.09E+08
0.8	217.114	261.2129	1944.711	8.1E+08
0.7	199.007	239.9933	1679.876	8.11E+08
0.6	179.879	217.5071	1415.875	8.13E+08
0.5	159.691	193.4576	1140.182	8.14E+08
0.4	137.857	167.4028	872.9553	8.15E+08
0.3	113.779	138.6273	617.4393	8.17E+08
0.2	86.576	105.8095	369.9269	8.19E+08
0.1	53.701	65.82572	147.0089	8.21E+08
sum			137668.7	1.59E+10
average	438.2812			
temperature	52			
10	495.455	461.8091	1132.049	7.99E+08
9	463.113	432.9431	910.2205	8E+08
8	429.481	402.6877	717.8805	8.02E+08
7	393.878	370.7966	532.7504	8.04E+08
6	356.303	336.9378	375.0118	8.06E+08
5	316.493	300.6432	251.2171	8.08E+08
4	273.242	261.2129	144.6998	8.1E+08
3	225.998	217.5071	72.09513	8.13E+08
2	172.504	167.4028	26.02207	8.15E+08
1.59	147.86	144.0544	14.48257	8.17E+08
1	107.888	105.8095	4.320231	8.19E+08
0.9	100.535	98.55066	3.937587	8.19E+08
0.8	92.814	90.98357	3.350479	8.2E+08
0.7	84.687	83.05693	2.657136	8.2E+08
0.6	76.125	74.70251	2.02348	8.21E+08
0.5	67.072	65.82572	1.553211	8.21E+08
0.4	57.361	56.28802	1.151296	8.22E+08
0.3	46.807	45.86991	0.878146	8.22E+08
0.2	35.005	34.17839	0.68328	8.23E+08
0.1	21.044	20.33151	0.507639	8.24E+08

frequency	|G*| test	|G*| 2S2P1D	Squared Error	Squared Mean
sum			4197.491	1.63E+10
average	198.1833			
temperature	58			
10	233.489	461.8091	52130.06	7.99E+08
9	217.391	432.9431	46462.72	8E+08
8	200.797	402.6877	40759.86	8.02E+08
7	183.346	370.7966	35137.73	8.04E+08
6	165.03	336.9378	29552.28	8.06E+08
5	145.692	300.6432	24009.87	8.08E+08
4	124.945	261.2129	18568.93	8.1E+08
3	102.373	217.5071	13255.86	8.13E+08
2	77.099	167.4028	8154.779	8.15E+08
1.59	65.564	144.0544	6160.743	8.17E+08
1	47.039	105.8095	3453.97	8.19E+08
0.9	43.595	98.55066	3020.125	8.19E+08
0.8	40.028	90.98357	2596.47	8.2E+08
0.7	36.315	83.05693	2184.808	8.2E+08
0.6	32.432	74.70251	1786.796	8.21E+08
0.5	28.352	65.82572	1404.28	8.21E+08
0.4	24.015	56.28802	1041.548	8.22E+08
0.3	19.352	45.86991	703.1993	8.22E+08
0.2	14.218	34.17839	398.4173	8.23E+08
0.1	8.291	20.33151	144.9739	8.24E+08
sum			290927.4	1.63E+10
average	90.46815			
temperature	64			
10	112.476	105.8095	44.44244	8.19E+08
9	104.303	98.55066	33.08936	8.19E+08
8	96.002	90.98357	25.18465	8.2E+08
7	87.317	83.05693	18.14822	8.2E+08
6	78.213	74.70251	12.32354	8.21E+08
5	68.639	65.82572	7.914537	8.21E+08
4	58.436	56.28802	4.613839	8.22E+08
3	47.395	45.86991	2.325913	8.22E+08
2	35.156	34.17839	0.955717	8.23E+08
1.59	29.639	28.84763	0.626268	8.23E+08
1	20.891	20.33151	0.313026	8.24E+08
0.9	19.284	18.75262	0.28236	8.24E+08

frequency	|G*| test	|G*| 2S2P1D	Squared Error	Squared Mean
0.8	17.625	17.122	0.253006	8.24E+08
0.7	15.907	15.4323	0.225341	8.24E+08
0.6	14.118	13.67401	0.197124	8.24E+08
0.5	12.251	11.83442	0.173536	8.24E+08
0.4	10.287	9.895664	0.153144	8.24E+08
0.3	8.194	7.830889	0.131849	8.25E+08
0.2	5.92	5.59531	0.105423	8.25E+08
0.1	3.355	3.098461	0.065812	8.25E+08
sum			151.5251	1.65E+10
average	42.2704			
temperature	70			
10	56.356	65.82572	89.67562	8.21E+08
9	52.141	61.15065	81.17371	8.22E+08
8	47.805	56.28802	71.96155	8.22E+08
7	43.299	51.2077	62.54761	8.22E+08
6	38.588	45.86991	53.02615	8.22E+08
5	33.664	40.2199	42.97982	8.23E+08
4	28.443	34.17839	32.89472	8.23E+08
3	22.848	27.62148	22.78615	8.23E+08
2	16.714	20.33151	13.0864	8.24E+08
1.59	13.977	17.03899	9.375781	8.24E+08
1	9.69	11.83442	4.598554	8.24E+08
0.9	8.912	10.87884	3.868464	8.24E+08
0.8	8.111	9.895664	3.185025	8.24E+08
0.7	7.285	8.881238	2.547976	8.25E+08
0.6	6.432	7.830889	1.956891	8.25E+08
0.5	5.545	6.738434	1.424285	8.25E+08
0.4	4.618	5.59531	0.955136	8.25E+08
0.3	3.641	4.388872	0.559312	8.25E+08
0.2	2.593	3.098461	0.255491	8.25E+08
0.1	1.433	1.683545	0.062773	8.25E+08
sum			498.9214	1.65E+10
average	20.60475			
temperature	76			
10	28.988	27.62148	1.867366	8.23E+08
9	26.71	25.52547	1.403107	8.24E+08
8	24.392	23.35638	1.072515	8.24E+08
7	21.995	21.10343	0.794898	8.24E+08

frequency	|G*| test	|G*| 2S2P1D	Squared Error	Squared Mean
6	19.507	18.75262	0.569083	8.24E+08
5	16.918	16.28507	0.400601	8.24E+08
4	14.192	13.67401	0.26831	8.24E+08
3	11.293	10.87884	0.171528	8.24E+08
2	8.15	7.830889	0.101832	8.25E+08
1.59	6.762	6.480378	0.079311	8.25E+08
1	4.615	4.388872	0.051134	8.25E+08
0.9	4.228	4.011841	0.046725	8.25E+08
0.8	3.832	3.626592	0.042193	8.25E+08
0.7	3.426	3.232171	0.03757	8.25E+08
0.6	3.009	2.827383	0.032985	8.25E+08
0.5	2.578	2.410674	0.027998	8.25E+08
0.4	2.131	1.979937	0.02282	8.25E+08
0.3	1.664	1.532138	0.017388	8.25E+08
0.2	1.169	1.062463	0.01135	8.25E+08
0.1	0.636	0.561823	0.005502	8.25E+08
sum			7.024213	1.65E+10
average	10.30975			
temperature	82			
10	15.335	17.122	3.193379	8.24E+08
9	14.089	15.77538	2.843893	8.24E+08
8	12.82	14.38628	2.453241	8.24E+08
7	11.515	12.94879	2.055756	8.24E+08
6	10.168	11.4553	1.657143	8.24E+08
5	8.769	9.895664	1.269372	8.24E+08
4	7.307	8.255694	0.90002	8.25E+08
3	5.764	6.514193	0.56279	8.25E+08
2	4.109	4.636047	0.277779	8.25E+08
1.59	3.386	3.812593	0.181981	8.25E+08
1	2.279	2.551017	0.073993	8.25E+08
0.9	2.082	2.325729	0.059404	8.25E+08
0.8	1.881	2.096321	0.046363	8.25E+08
0.7	1.675	1.862349	0.0351	8.25E+08
0.6	1.464	1.623257	0.025363	8.25E+08
0.5	1.248	1.378329	0.016986	8.25E+08
0.4	1.027	1.126605	0.009921	8.25E+08
0.3	0.793	0.86671	0.005433	8.25E+08
0.2	0.551	0.596491	0.002069	8.25E+08

frequency	|G*| test	|G*| 2S2P1D	Squared Error	Squared Mean
0.1	0.291	0.311935	0.000438	8.25E+08
sum			15.67042	1.65E+10
average	5.32765			
temperature	88			
10	8.36	9.895664	2.358264	8.24E+08
9	7.666	9.08683	2.018757	8.25E+08
8	6.954	8.255694	1.694406	8.25E+08
7	6.225	7.399373	1.379152	8.25E+08
6	5.473	6.514193	1.084084	8.25E+08
5	4.697	5.59531	0.806962	8.25E+08
4	3.89	4.636047	0.556587	8.25E+08
3	3.045	3.626592	0.338249	8.25E+08
2	2.147	2.551017	0.16323	8.25E+08
1.59	1.758	2.084735	0.106756	8.25E+08
1	1.169	1.378329	0.043819	8.25E+08
0.9	1.065	1.25339	0.035491	8.25E+08
0.8	0.959	1.126605	0.028091	8.25E+08
0.7	0.851	0.997788	0.021547	8.25E+08
0.6	0.741	0.86671	0.015803	8.25E+08
0.5	0.628	0.733075	0.011041	8.25E+08
0.4	0.513	0.596491	0.006971	8.25E+08
0.3	0.394	0.456399	0.003894	8.25E+08
0.2	0.271	0.311935	0.001676	8.25E+08
0.1	0.142	0.161502	0.00038	8.25E+08
sum			10.67516	1.65E+10
average	2.8474			
Se: 3372.171935		Sy: 55679.04993		
Se/Sy: 0.060564466		R^2: 0.996800208		

Table A I. 6 Complex modulus test results and 2S2P1D model for 73% RAP asphalt binder

frequency	|G*| test	|G*| 2S2P1D	Squared Error	Squared Mean
temperature	-8			
10	236314.3	242872.7	43013040	4.8E+10
9	231261.2	237689.1	41317963	4.57E+10
8	226846.7	231926.1	25799579	4.33E+10
7	220964.8	225437.6	20005945	4.06E+10

frequency	|G*| test	|G*| 2S2P1D	Squared Error	Squared Mean
6	214288.8	218013.6	13873749	3.77E+10
5	206084.8	209335.4	10566626	3.44E+10
4	196378.1	198883.2	6275553	3.06E+10
3	183647.9	185716.2	4278252	2.62E+10
2	167324.4	167825	250582.1	2.07E+10
1.59	157342.2	158083.1	548933.9	1.8E+10
1	139631	139309.6	103313.6	1.33E+10
0.9	136101.1	135224.3	768879.7	1.24E+10
0.8	131720.5	130738.9	963595.1	1.14E+10
0.7	126907.3	125759.5	1317272	1.04E+10
0.6	121496.9	120153	1806222	9.27E+09
0.5	115161.3	113720.4	2076218	8.07E+09
0.4	107556.9	106143.8	1996687	6.77E+09
0.3	98223.74	96861.78	1854947	5.33E+09
0.2	86512.27	84712.15	3240433	3.7E+09
0.1	68839.68	66441.42	5751612	1.81E+09
sum			1.86E+08	4.28E+11
average	158630.2			
temperature	-2			
10	148630.8	160059.2	1.31E+08	1.85E+10
9	144136.6	155655.3	1.33E+08	1.74E+10
8	140254.9	150807.2	1.11E+08	1.61E+10
7	135863.5	145408.9	91114510	1.48E+10
6	130746.2	139309.6	73331163	1.33E+10
5	124949.6	132283.6	53788112	1.18E+10
4	117898.9	123968.5	36840307	1E+10
3	108962.2	113720.4	22640318	8.07E+09
2	97393.74	100197.5	7861095	5.83E+09
1.59	90980.71	93028.77	4194544	4.78E+09
1	79336.15	79603.23	71331.81	3.11E+09
0.9	76805.82	76750.27	3085.54	2.8E+09
0.8	74083.57	73646.53	191000.4	2.48E+09
0.7	71031.41	70236.29	632213.9	2.15E+09
0.6	67635.53	66441.42	1425879	1.81E+09
0.5	63770.59	62146.9	2636372	1.47E+09
0.4	59348.07	57171.66	4736776	1.11E+09
0.3	54011.46	51202.02	7892960	7.47E+08
0.2	47001.44	43605.35	11533444	3.9E+08

frequency	|G*| test	|G*| 2S2P1D	Squared Error	Squared Mean
0.1	36787.77	32677.88	16891251	77616899
sum			7.1E+08	1.37E+11
average	93481.45			
temperature	4			
10	88269.3	100197.5	1.42E+08	5.83E+09
9	85391.54	96861.78	1.32E+08	5.33E+09
8	82675.72	93220.04	1.11E+08	4.81E+09
7	79559.65	89202.79	92990243	4.27E+09
6	75961.7	84712.15	76570420	3.7E+09
5	71988.06	79603.23	57990756	3.11E+09
4	67184.49	73646.53	41757961	2.48E+09
3	61313.33	66441.42	26297319	1.81E+09
2	53536.73	57171.66	13212741	1.11E+09
1.59	49691.79	52371.45	7180583	8.12E+08
1	42489.85	43605.35	1244339	3.9E+08
0.9	40917.11	41781.76	747623.9	3.21E+08
0.8	39296.43	39814.12	268004.4	2.54E+08
0.7	37511.99	37672.14	25647.21	1.91E+08
0.6	35510.93	35313.77	38872.51	1.31E+08
0.5	33245.41	32677.88	322090	77616899
0.4	30627.2	29669.64	916933.1	33660939
0.3	27504.42	26127.67	1895427	5106895
0.2	23538.18	21733.97	3255182	4553355
0.1	17862.99	15660.37	4851531	67362416
sum			7.15E+08	3.47E+10
average	52203.84			
temperature	10			
10	50335.12	57171.66	46738299	1.11E+09
9	48264.26	54927.99	44405302	9.65E+08
8	46365.6	52498.47	37612136	8.2E+08
7	44274.43	49843.03	31009240	6.75E+08
6	41936.6	46905.86	24693568	5.31E+08
5	39361.58	43605.35	18009554	3.9E+08
4	36330.17	39814.12	12137960	2.54E+08
3	32678.15	35313.77	6946471	1.31E+08
2	28036.11	29669.64	2668416	33660939
1.59	25729.95	26815.54	1178510	8688988
1	21469.73	21733.97	69822.64	4553355

frequency	|G*| test	|G*| 2S2P1D	Squared Error	Squared Mean
0.9	20602.35	20699.35	9408.833	10039302
0.8	19667.23	19592.14	5638.175	18281514
0.7	18646.18	18397.92	61633.96	29919947
0.6	17519.06	17096.84	178269.2	45846365
0.5	16262.69	15660.37	362785.8	67362416
0.4	14827.76	14044.84	612966.1	96491161
0.3	13133.65	12177.06	915070.6	1.37E+08
0.2	11025.6	9915.558	1232201	1.95E+08
0.1	8070.485	6901.72	1366011	2.88E+08
sum			2.3E+08	5.81E+09
average	27726.83			
temperature	16			
10	26996.06	29669.64	7147991	33660939
9	25692.28	28329.56	6955244	19907005
8	24499.22	26890.43	5717915	9136113
7	23208.85	25332.07	4508099	2144006
6	21798.24	23626.66	3343102	58165.71
5	20248.55	21733.97	2206481	4553355
4	18462.6	19592.14	1275877	18281514
3	16368.52	17096.84	530440.7	45846365
2	13755.05	14044.84	83979.12	96491161
1.59	12453.91	12536.77	6866.517	1.28E+08
1	10128.19	9915.558	45210.11	1.95E+08
0.9	9672.354	9392.536	78298.37	2.1E+08
0.8	9178.041	8837.05	116274.8	2.26E+08
0.7	8640.437	8242.944	158000.6	2.44E+08
0.6	8053.343	7601.824	203869.2	2.65E+08
0.5	7403.362	6901.72	251644.6	2.88E+08
0.4	6668.179	6124.477	295611.6	3.15E+08
0.3	5810.864	5240.011	325873.1	3.47E+08
0.2	4764.121	4190.953	328521.3	3.87E+08
0.1	3352.48	2834.51	268293.3	4.42E+08
sum			33847593	3.28E+09
average	13857.73			
temperature	22			
10	13801.05	14044.84	59433.81	96491161
9	13072.2	13333.69	68374.49	1.11E+08
8	12377.71	12576.03	39329.22	1.28E+08

frequency	|G*| test	|G*| 2S2P1D	Squared Error	Squared Mean
7	11637.63	11762.86	15683.05	1.47E+08
6	10834.04	10881.91	2290.685	1.69E+08
5	9960.9	9915.558	2055.869	1.95E+08
4	8974.222	8837.05	18816.13	2.26E+08
3	7827.228	7601.824	50806.87	2.65E+08
2	6428.481	6124.477	92418.31	3.15E+08
1.59	5743.28	5409.126	111658.6	3.41E+08
1	4546.17	4190.953	126179	3.87E+08
0.9	4313.034	3951.98	130359.7	3.97E+08
0.8	4063.575	3699.759	132362.2	4.07E+08
0.7	3795.189	3431.862	132006.1	4.18E+08
0.6	3504.257	3145.002	129064.5	4.29E+08
0.5	3184.276	2834.51	122336.5	4.42E+08
0.4	2827.598	2493.355	111718.5	4.57E+08
0.3	2420.814	2109.97	96624.21	4.73E+08
0.2	1936.961	1662.498	75329.73	4.93E+08
0.1	1305.732	1097.233	43471.82	5.19E+08
sum			1560319	6.41E+09
average	6627.718			
temperature	28			
10	6862.789	6901.72	1515.633	2.88E+08
9	6469.385	6524.237	3008.743	3.01E+08
8	6084.948	6124.477	1562.558	3.15E+08
7	5678.495	5698.285	391.6548	3.3E+08
6	5241.028	5240.011	1.034205	3.47E+08
5	4768.5	4741.618	722.6574	3.66E+08
4	4238.921	4190.953	2300.909	3.87E+08
3	3635.318	3567.951	4538.337	4.12E+08
2	2914.587	2834.51	6412.377	4.42E+08
1.59	2568.313	2484.347	7050.249	4.57E+08
1	1976.416	1896.352	6410.217	4.83E+08
0.9	1863.691	1782.332	6619.304	4.88E+08
0.8	1743.693	1662.498	6592.568	4.93E+08
0.7	1615.513	1535.811	6352.453	4.99E+08
0.6	1478.103	1400.862	5966.186	5.05E+08
0.5	1329.378	1255.664	5433.788	5.11E+08
0.4	1165.716	1097.233	4689.918	5.19E+08
0.3	981.82	920.6887	3737.035	5.27E+08

frequency	|G*| test	|G*| 2S2P1D	Squared Error	Squared Mean
0.2	767.864	716.8729	2600.09	5.36E+08
0.1	498.61	463.5235	1231.065	5.48E+08
sum			77136.78	8.75E+09
average	3094.154			
temperature	34			
10	3361.248	3218.72	20314.37	4.26E+08
9	3154.696	3031.648	15140.87	4.34E+08
8	2946.73	2834.51	12593.4	4.42E+08
7	2728.436	2625.477	10600.52	4.51E+08
6	2495.38	2402.074	8706.06	4.61E+08
5	2244.868	2160.792	7068.847	4.71E+08
4	1969.533	1896.352	5355.434	4.83E+08
3	1660.225	1600.089	3616.367	4.96E+08
2	1299.803	1255.664	1948.272	5.11E+08
1.59	1129.93	1093.066	1358.922	5.19E+08
1	847	823.0689	572.6961	5.31E+08
0.9	793.637	771.1997	503.4326	5.33E+08
0.8	737.274	716.8729	416.204	5.36E+08
0.7	677.757	659.6575	327.5919	5.39E+08
0.6	614.674	598.9727	246.5306	5.41E+08
0.5	547.174	534.0014	173.5185	5.44E+08
0.4	474.095	463.5235	111.7575	5.48E+08
0.3	393.356	385.556	60.84054	5.51E+08
0.2	301.47	296.412	25.58332	5.56E+08
0.1	189.234	187.2639	3.881121	5.61E+08
sum			89145.1	1.01E+10
average	1428.326			
temperature	40			
10	1280.973	1255.664	640.5573	5.11E+08
9	1201.521	1178.347	537.0487	5.15E+08
8	1120.913	1097.233	560.7414	5.19E+08
7	1033.283	1011.65	467.9965	5.22E+08
6	939.012	920.6887	335.743	5.27E+08
5	839.604	823.0689	273.4085	5.31E+08
4	730.671	716.8729	190.387	5.36E+08
3	610.127	598.9727	124.4182	5.41E+08
2	470.019	463.5235	42.19205	5.48E+08
1.59	406.014	400.2727	32.96236	5.51E+08

frequency	|G*| test	|G*| 2S2P1D	Squared Error	Squared Mean
1	300.702	296.412	18.40406	5.56E+08
0.9	282.138	276.6514	30.10241	5.57E+08
0.8	261.935	256.0302	34.86655	5.58E+08
0.7	240.18	234.402	33.38478	5.59E+08
0.6	216.949	211.5711	28.92167	5.6E+08
0.5	192.505	187.2639	27.46867	5.61E+08
0.4	166.079	161.0761	25.02865	5.62E+08
0.3	136.916	132.3585	20.77035	5.63E+08
0.2	103.951	99.92579	16.20232	5.65E+08
0.1	64.278	61.0243	10.58658	5.67E+08
sum			3451.191	1.09E+10
average	529.8885			
temperature	46			
10	604.454	716.8729	12638.01	5.36E+08
9	564.525	671.3569	11413.04	5.38E+08
8	523.524	623.7085	10036.94	5.4E+08
7	479.949	573.5553	8762.139	5.43E+08
6	433.841	520.3954	7491.666	5.45E+08
5	385.167	463.5235	6139.735	5.48E+08
4	332.259	401.8874	4848.112	5.51E+08
3	274.445	333.7794	3520.566	5.54E+08
2	208.836	256.0302	2227.293	5.58E+08
1.59	178.946	219.9439	1680.83	5.59E+08
1	130.29	161.0761	947.7861	5.62E+08
0.9	121.347	149.9419	817.6675	5.63E+08
0.8	112.003	138.3494	694.1343	5.63E+08
0.7	102.166	126.223	578.7391	5.64E+08
0.6	91.778	113.4617	470.1847	5.64E+08
0.5	80.798	99.92579	365.8723	5.65E+08
0.4	69.046	85.41006	267.7825	5.66E+08
0.3	56.252	69.58905	177.877	5.66E+08
0.2	41.953	51.87777	98.50102	5.67E+08
0.1	25.105	30.95242	34.19231	5.68E+08
sum			73211.08	1.11E+10
average	240.8342			
temperature	52			
10	280.248	256.0302	586.5014	5.58E+08
9	260.64	238.8167	476.2546	5.58E+08

frequency	|G*| test	|G*| 2S2P1D	Squared Error	Squared Mean
8	240.57	220.8631	388.3609	5.59E+08
7	219.487	202.0443	304.248	5.6E+08
6	197.366	182.193	230.2191	5.61E+08
5	174.036	161.0761	167.9581	5.62E+08
4	149.005	138.3494	113.5412	5.63E+08
3	121.842	113.4617	70.2287	5.64E+08
2	91.523	85.41006	37.36804	5.66E+08
1.59	77.724	72.55409	26.728	5.66E+08
1	55.632	51.87777	14.09426	5.67E+08
0.9	51.535	48.0181	12.3686	5.67E+08
0.8	47.296	44.02045	10.72922	5.68E+08
0.7	42.883	39.86373	9.115992	5.68E+08
0.6	38.269	35.52028	7.555479	5.68E+08
0.5	33.419	30.95242	6.08402	5.68E+08
0.4	28.263	26.10614	4.652036	5.68E+08
0.3	22.711	20.89813	3.286508	5.69E+08
0.2	16.629	15.18437	2.086955	5.69E+08
0.1	9.631	8.658195	0.94635	5.69E+08
sum			2472.327	1.13E+10
average	107.9355			
temperature	58			
10	130.985	132.3585	1.886639	5.63E+08
9	121.328	123.0969	3.12884	5.64E+08
8	111.543	113.4617	3.681576	5.64E+08
7	101.313	103.3921	4.322839	5.65E+08
6	90.632	92.80693	4.730334	5.65E+08
5	79.434	81.5939	4.665151	5.66E+08
4	67.525	69.58905	4.260318	5.66E+08
3	54.635	56.53325	3.603364	5.67E+08
2	40.394	41.96352	2.463387	5.68E+08
1.59	33.989	35.35331	1.861338	5.68E+08
1	23.855	24.84226	0.974686	5.68E+08
0.9	22.004	22.90074	0.804139	5.69E+08
0.8	20.088	20.89813	0.656306	5.69E+08
0.7	18.106	18.82573	0.518012	5.69E+08
0.6	16.048	16.67228	0.389728	5.69E+08
0.5	13.898	14.42266	0.275264	5.69E+08
0.4	11.641	12.05553	0.171837	5.69E+08

frequency	|G*| test	|G*| 2S2P1D	Squared Error	Squared Mean
0.3	9.238	9.538716	0.09043	5.69E+08
0.2	6.639	6.818086	0.032072	5.69E+08
0.1	3.726	3.782933	0.003241	5.69E+08
sum			38.5195	1.13E+10
average	48.85105			
temperature	64			
10	63.13	61.0243	4.433981	5.67E+08
9	58.351	56.53325	3.304205	5.67E+08
8	53.422	51.87777	2.384653	5.67E+08
7	48.305	47.03236	1.619623	5.67E+08
6	42.977	41.96352	1.027146	5.68E+08
5	37.421	36.62549	0.632836	5.68E+08
4	31.552	30.95242	0.359497	5.68E+08
3	25.256	24.84226	0.171179	5.68E+08
2	18.385	18.11757	0.071518	5.69E+08
1.59	15.331	15.10876	0.049392	5.69E+08
1	10.564	10.39697	0.027897	5.69E+08
0.9	9.703	9.538716	0.026989	5.69E+08
0.8	8.816	8.658195	0.024902	5.69E+08
0.7	7.905	7.75254	0.023244	5.69E+08
0.6	6.965	6.818086	0.021584	5.69E+08
0.5	5.989	5.849991	0.019324	5.69E+08
0.4	4.971	4.841564	0.016754	5.69E+08
0.3	3.901	3.782933	0.01394	5.69E+08
0.2	2.76	2.657985	0.010407	5.7E+08
0.1	1.509	1.435055	0.005468	5.7E+08
sum			14.24454	1.14E+10
average	22.86065			
temperature	70			
10	31.869	36.62549	22.6242	5.68E+08
9	29.343	33.83608	20.18778	5.68E+08
8	26.752	30.95242	17.64352	5.68E+08
7	24.081	27.96055	15.05088	5.68E+08
6	21.313	24.84226	12.45569	5.68E+08
5	18.439	21.57294	9.821609	5.69E+08
4	15.421	18.11757	7.271495	5.69E+08
3	12.218	14.42266	4.86051	5.69E+08
2	8.767	10.39697	2.656818	5.69E+08

frequency	|G*| test	|G*| 2S2P1D	Squared Error	Squared Mean
1.59	7.25	8.613536	1.85923	5.69E+08
1	4.913	5.849991	0.877952	5.69E+08
0.9	4.494	5.351338	0.735029	5.69E+08
0.8	4.066	4.841564	0.601499	5.69E+08
0.7	3.628	4.319327	0.477933	5.69E+08
0.6	3.179	3.782933	0.364735	5.69E+08
0.5	2.715	3.230163	0.265393	5.7E+08
0.4	2.236	2.657985	0.178071	5.7E+08
0.3	1.737	2.061981	0.105613	5.7E+08
0.2	1.212	1.435055	0.049753	5.7E+08
0.1	0.655	0.763538	0.01178	5.7E+08
sum			118.0995	1.14E+10
average	11.2144			
temperature	76			
10	16.428	18.11757	2.85465	5.69E+08
9	15.059	16.67228	2.60268	5.69E+08
8	13.676	15.18437	2.27518	5.69E+08
7	12.258	13.64797	1.93202	5.69E+08
6	10.797	12.05553	1.583905	5.69E+08
5	9.284	10.39697	1.238713	5.69E+08
4	7.711	8.658195	0.897178	5.69E+08
3	6.054	6.818086	0.583827	5.69E+08
2	4.287	4.841564	0.307541	5.69E+08
1.59	3.519	3.977792	0.21049	5.69E+08
1	2.35	2.657985	0.094855	5.7E+08
0.9	2.143	2.422758	0.078265	5.7E+08
0.8	1.932	2.183373	0.063188	5.7E+08
0.7	1.716	1.939371	0.049895	5.7E+08
0.6	1.496	1.690179	0.037705	5.7E+08
0.5	1.271	1.435055	0.026914	5.7E+08
0.4	1.04	1.172994	0.017688	5.7E+08
0.3	0.801	0.902557	0.010314	5.7E+08
0.2	0.552	0.621462	0.004825	5.7E+08
0.1	0.288	0.32541	0.0014	5.7E+08
sum			14.87123	1.14E+10
average	5.6331			
Se: 2530.832		Sy: 48811.38		
Se/Sy: 0.051849		R^2: 0.997655		

Table A I. 7 Complex modulus test results and 2S2P1D model for 65% RAP asphalt binder

frequency	|G*| test	|G*| 2S2P1D	Squared Error	Squared Mean
temperature	-8			
10	246804.7	266761.8	3.98E+08	5.88E+10
9	241173.2	261068.4	3.96E+08	5.6E+10
8	236276.7	254738.5	3.41E+08	5.31E+10
7	229817.5	247611.7	3.17E+08	4.98E+10
6	222529.3	239457.5	2.87E+08	4.63E+10
5	214736.2	229925.8	2.31E+08	4.23E+10
4	203758.7	218445.5	2.16E+08	3.77E+10
3	191618.4	203983.4	1.53E+08	3.23E+10
2	171122.5	184332.4	1.75E+08	2.56E+10
1.59	161173.6	173632.3	1.55E+08	2.23E+10
1	142315.2	153012.2	1.14E+08	1.66E+10
0.9	139524.4	148525	81011737	1.54E+10
0.8	134378.4	143598.5	85008801	1.42E+10
0.7	129232.5	138129.3	79152944	1.29E+10
0.6	123492.1	131971.3	71896614	1.16E+10
0.5	116961.1	124906	63120958	1.01E+10
0.4	109251.8	116584.2	53763476	8.51E+09
0.3	99754.06	106389.2	44024662	6.73E+09
0.2	87185.43	93044.5	34328708	4.72E+09
0.1	69163.02	72976.65	14543752	2.37E+09
sum			3.31E+09	5.27E+11
average	163513.4			
temperature	-2			
10	153633.8	175802.7	4.91E+08	2.29E+10
9	149678.7	170965.7	4.53E+08	2.15E+10
8	144749.5	165640.7	4.36E+08	2E+10
7	139982.4	159711.4	3.89E+08	1.83E+10
6	134480.2	153012.2	3.43E+08	1.66E+10
5	128324.5	145295.1	2.88E+08	1.46E+10
4	120808.7	136162.1	2.36E+08	1.25E+10
3	111367.6	124906	1.83E+08	1.01E+10
2	98759.76	110053	1.28E+08	7.35E+09
1.59	91975.71	102179.1	1.04E+08	6.06E+09
1	80018.45	87433.05	54976395	3.98E+09
0.9	77438.95	84299.48	47066903	3.6E+09

frequency	|G*| test	|G*| 2S2P1D	Squared Error	Squared Mean
0.8	74619.23	80890.45	39328289	3.2E+09
0.7	71476.14	77144.78	32133486	2.79E+09
0.6	68017.19	72976.65	24596186	2.37E+09
0.5	64084	68259.71	17436606	1.93E+09
0.4	59518.41	62795.1	10736739	1.48E+09
0.3	53930.77	56238.28	5324616	1.02E+09
0.2	46750.75	47894.4	1307924	5.55E+08
0.1	36383.97	35892.09	241938.4	1.33E+08
sum			3.29E+09	1.71E+11
average	95299.94			
temperature	4			
10	90754.82	102389.2	1.35E+08	6.09E+09
9	87605.51	98896.9	1.27E+08	5.56E+09
8	84631.48	95088.52	1.09E+08	5.01E+09
7	81279.2	90892.8	92421247	4.43E+09
6	77491.72	86209.49	75999469	3.83E+09
5	73276.12	80890.45	57978038	3.2E+09
4	68234.03	74701.51	41828189	2.54E+09
3	62074.56	67234.83	26628453	1.84E+09
2	54018.71	57662.25	13275378	1.11E+09
1.59	50049.52	52721.44	7139165	8.05E+08
1	42556.8	43730.27	1377022	3.76E+08
0.9	40959	41865.43	821623.6	3.07E+08
0.8	39286.77	39855.6	323574.7	2.41E+08
0.7	37438.25	37670.52	53951.52	1.78E+08
0.6	35379.41	35268.26	12354.48	1.19E+08
0.5	33066.85	32587.96	229336	68017353
0.4	30397.36	29535.39	742990.9	26984852
0.3	27219.78	25950.59	1610854	2591750
0.2	23216.99	21519.24	2882368	7960631
0.1	17522.12	15426.3	4392474	79466493
sum			7E+08	3.58E+10
average	52822.95			
temperature	10			
10	51250.15	62795.1	1.33E+08	1.48E+09
9	49070.77	60330.75	1.27E+08	1.3E+09
8	47049.79	57662.25	1.13E+08	1.11E+09
7	44844.76	54745.62	98026989	9.24E+08

frequency	|G*| test	|G*| 2S2P1D	Squared Error	Squared Mean
6	42391.17	51519.55	83327325	7.39E+08
5	39696.1	47894.4	67212043	5.55E+08
4	36543.59	43730.27	51648265	3.76E+08
3	32802.16	38787.25	35821293	2.09E+08
2	28000.16	32587.96	21047896	68017353
1.59	25629.02	29453.13	14623817	26137010
1	21277.79	23871.74	6728589	219921.4
0.9	20416.9	22735.35	5375203	2577152
0.8	19475.26	21519.24	4177843	7960631
0.7	18442.81	20207.55	3114302	17082911
0.6	17303.47	18778.49	2175698	30938120
0.5	16037.91	17200.73	1352162	50979072
0.4	14591.48	15426.3	696931.3	79466493
0.3	12892.51	13374.8	232607.7	1.2E+08
0.2	10779.57	10890.86	12386.16	1.81E+08
0.1	7823.699	7580.578	59107.9	2.81E+08
sum			7.68E+08	7.55E+09
average	27815.95			
temperature	16			
10	27193.77	28697.61	2261535	18982691
9	25839.85	27372.04	2347622	9189059
8	24588.68	25950.59	1854787	2591750
7	23249.45	24413.9	1355947	5358.551
6	21792.31	22735.35	889326.9	2577152
5	20200.2	20876.53	457429.6	12000438
4	18378.52	18778.49	159976.5	30938120
3	16238.66	16342.08	10695.35	63977921
2	13587.94	13374.8	45429.44	1.2E+08
1.59	12274.22	11914.29	129547.5	1.54E+08
1	9941.078	9385.805	308328.3	2.24E+08
0.9	9481.119	8882.952	357803.2	2.39E+08
0.8	8986.042	8349.545	405128.9	2.56E+08
0.7	8449.029	7779.827	447831.2	2.74E+08
0.6	7864.389	7165.965	487795.7	2.95E+08
0.5	7215.868	6496.798	517061.2	3.18E+08
0.4	6484.477	5755.422	531521.2	3.45E+08
0.3	5634.755	4913.867	519680	3.77E+08
0.2	4600.184	3918.897	464152.2	4.17E+08

frequency	|G*| test	|G*| 2S2P1D	Squared Error	Squared Mean
0.1	3215.006	2638.343	332539.9	4.71E+08
sum			13884139	3.63E+09
average	13760.78			
temperature	22			
10	13844.01	15426.3	2503645	79466493
9	13062.81	14645.2	2503944	94002696
8	12343.98	13813.01	2158056	1.11E+08
7	11583.48	12919.87	1785936	1.3E+08
6	10760.91	11952.26	1419306	1.53E+08
5	9873.622	10890.86	1034771	1.81E+08
4	8872.664	9706.268	694895.9	2.14E+08
3	7714.67	8349.545	403065.8	2.56E+08
2	6309.315	6726.885	174364.5	3.1E+08
1.59	5623.571	5941.172	100870.2	3.39E+08
1	4430.28	4603.178	29893.76	3.9E+08
0.9	4199.48	4340.7	19943.02	4E+08
0.8	3952.609	4063.669	12334.43	4.11E+08
0.7	3686.616	3769.423	6856.956	4.23E+08
0.6	3398.31	3454.346	3140.025	4.36E+08
0.5	3082.373	3113.314	957.34	4.51E+08
0.4	2730.811	2738.603	60.71193	4.67E+08
0.3	2332.028	2317.508	210.8404	4.85E+08
0.2	1859.403	1826.023	1114.238	5.07E+08
0.1	1246.356	1205.158	1697.31	5.35E+08
sum			12855063	6.37E+09
average	6545.365			
temperature	28			
10	6831.453	7580.578	561188	2.81E+08
9	6418.955	7165.965	558024.3	2.95E+08
8	6027.388	6726.885	489295.8	3.1E+08
7	5614.542	6258.772	415032.7	3.27E+08
6	5172.189	5755.422	340160.7	3.45E+08
5	4696.572	5208.006	261565.1	3.66E+08
4	4166.31	4603.178	190853.7	3.9E+08
3	3562.887	3918.897	126743	4.17E+08
2	2845.822	3113.314	71551.92	4.51E+08
1.59	2502.364	2728.709	51232.18	4.67E+08
1	1917.898	2082.879	27218.6	4.95E+08

frequency	|G*| test	|G*| 2S2P1D	Squared Error	Squared Mean
0.9	1806.983	1957.643	22698.5	5.01E+08
0.8	1688.868	1826.023	18811.44	5.07E+08
0.7	1563.013	1686.874	15341.57	5.13E+08
0.6	1428.263	1538.652	12185.64	5.2E+08
0.5	1282.588	1379.172	9328.407	5.27E+08
0.4	1122.892	1205.158	6767.626	5.35E+08
0.3	944.067	1011.248	4513.321	5.44E+08
0.2	736.32	787.385	2607.635	5.55E+08
0.1	476.054	509.1159	1093.091	5.68E+08
sum			3186213	8.91E+09
average	3040.271			
temperature	34			
10	3353.902	3535.315	32910.63	4.33E+08
9	3141.52	3329.843	35465.4	4.41E+08
8	2929.817	3113.314	33671.12	4.51E+08
7	2708.501	2883.721	30701.99	4.6E+08
6	2473.26	2638.343	27252.49	4.71E+08
5	2221.481	2373.328	23057.64	4.83E+08
4	1945.479	2082.879	18878.65	4.95E+08
3	1636.414	1757.475	14655.66	5.1E+08
2	1277.29	1379.172	10379.88	5.27E+08
1.59	1108.523	1200.581	8474.707	5.35E+08
1	828.456	904.0265	5710.905	5.49E+08
0.9	775.631	847.0554	5101.445	5.52E+08
0.8	720.005	787.385	4540.066	5.55E+08
0.7	661.282	724.5418	4001.808	5.58E+08
0.6	599.143	657.8881	3450.982	5.61E+08
0.5	532.757	586.5261	2891.114	5.64E+08
0.4	460.986	509.1159	2316.49	5.68E+08
0.3	381.89	423.4795	1729.687	5.72E+08
0.2	291.995	325.5673	1127.098	5.77E+08
0.1	182.725	205.6833	527.0857	5.82E+08
sum			266844.8	1.04E+10
average	1411.553			
temperature	40			
10	1211.747	1379.172	28031.02	5.27E+08
9	1136.833	1294.25	24780	5.31E+08
8	1058.4	1205.158	21537.79	5.35E+08

frequency	|G*| test	|G*| 2S2P1D	Squared Error	Squared Mean
7	973.515	1111.156	18945.13	5.4E+08
6	884.304	1011.248	16114.84	5.44E+08
5	788.925	904.0265	13248.36	5.49E+08
4	685.43	787.385	10394.82	5.55E+08
3	571.082	657.8881	7535.291	5.61E+08
2	439.095	509.1159	4902.931	5.68E+08
1.59	378.584	439.6438	3728.299	5.71E+08
1	279.284	325.5673	2142.142	5.77E+08
0.9	261.577	303.8631	1788.11	5.78E+08
0.8	242.466	281.2135	1501.369	5.79E+08
0.7	222.009	257.458	1256.63	5.8E+08
0.6	200.296	232.3814	1029.472	5.81E+08
0.5	177.524	205.6833	792.9489	5.82E+08
0.4	152.88	176.9197	577.9067	5.84E+08
0.3	125.773	145.3774	384.3334	5.85E+08
0.2	95.262	109.7546	210.0342	5.87E+08
0.1	58.706	67.02669	69.23385	5.89E+08
sum			158970.7	1.13E+10
average	497.1846			
temperature	46			
10	560.575	657.8881	9469.831	5.61E+08
9	523.316	615.7086	8536.39	5.63E+08
8	484.46	571.5818	7590.216	5.65E+08
7	443.43	525.1691	6681.285	5.67E+08
6	400.462	476.0149	5708.245	5.7E+08
5	354.869	423.4795	4707.401	5.72E+08
4	305.707	366.6101	3709.189	5.75E+08
3	251.949	303.8631	2695.069	5.78E+08
2	191.234	232.3814	1693.107	5.81E+08
1.59	163.686	199.2709	1266.283	5.83E+08
1	118.793	145.3774	706.7316	5.85E+08
0.9	110.439	135.2047	613.3419	5.86E+08
0.8	101.792	124.6219	521.205	5.86E+08
0.7	92.782	113.5619	431.8027	5.87E+08
0.6	83.262	101.9355	348.699	5.88E+08
0.5	73.196	89.61953	269.7322	5.88E+08
0.4	62.422	76.43388	196.3327	5.89E+08
0.3	50.719	62.0939	129.3884	5.89E+08

frequency	|G*| test	|G*| 2S2P1D	Squared Error	Squared Mean
0.2	37.633	46.09108	71.53907	5.9E+08
0.1	22.419	27.28576	23.68538	5.91E+08
sum			55369.47	1.16E+10
average	221.6573			
temperature	52			
10	259.619	257.458	4.669997	5.8E+08
9	241.256	240.0588	1.433173	5.81E+08
8	222.377	221.9175	0.211137	5.82E+08
7	202.636	202.909	0.074529	5.83E+08
6	181.95	182.8664	0.839797	5.84E+08
5	160.23	161.5572	1.761338	5.85E+08
4	137.011	138.6384	2.648347	5.86E+08
3	111.814	113.5619	3.055025	5.87E+08
2	83.654	85.33217	2.816252	5.88E+08
1.59	70.92	72.41075	2.222328	5.89E+08
1	50.538	51.65849	1.255496	5.9E+08
0.9	46.769	47.78973	1.041892	5.9E+08
0.8	42.88	43.78475	0.818577	5.9E+08
0.7	38.831	39.6229	0.627113	5.91E+08
0.6	34.598	35.27716	0.461256	5.91E+08
0.5	30.16	30.71076	0.30334	5.91E+08
0.4	25.452	25.87115	0.175684	5.91E+08
0.3	20.414	20.67744	0.069401	5.91E+08
0.2	14.887	14.99039	0.01069	5.92E+08
0.1	8.567	8.515085	0.002695	5.92E+08
sum			24.49807	1.18E+10
average	99.22815			
temperature	58			
10	122.21	128.1989	35.86651	5.86E+08
9	113.131	119.1565	36.30648	5.87E+08
8	103.852	109.7546	34.84017	5.87E+08
7	94.209	99.9347	32.7837	5.88E+08
6	84.167	89.61953	29.73003	5.88E+08
5	73.646	78.70213	25.56447	5.89E+08
4	62.46	67.02669	20.85464	5.89E+08
3	50.41	54.34762	15.50486	5.9E+08
2	37.134	40.228	9.572821	5.91E+08
1.59	31.177	33.83558	7.068042	5.91E+08

frequency	|G*| test	|G*| 2S2P1D	Squared Error	Squared Mean
1	21.789	23.69487	3.632355	5.91E+08
0.9	20.075	21.82584	3.065428	5.91E+08
0.8	18.307	19.89963	2.536461	5.92E+08
0.7	16.48	17.90823	2.039834	5.92E+08
0.6	14.581	15.84128	1.588302	5.92E+08
0.5	12.607	13.68491	1.161884	5.92E+08
0.4	10.54	11.41963	0.773745	5.92E+08
0.3	8.345	9.016131	0.450417	5.92E+08
0.2	5.976	6.4254	0.20196	5.92E+08
0.1	3.338	3.547884	0.044051	5.92E+08
sum			263.5862	1.18E+10
average	45.2217			
temperature	64			
10	59.315	67.02669	59.47013	5.89E+08
9	54.72	62.0939	54.37441	5.89E+08
8	50.005	56.9805	48.65759	5.9E+08
7	45.153	51.65849	42.32139	5.9E+08
6	40.116	46.09108	35.70155	5.9E+08
5	34.863	40.228	28.7832	5.91E+08
4	29.322	33.99692	21.85487	5.91E+08
3	23.416	27.28576	14.97507	5.91E+08
2	16.986	19.89963	8.489223	5.92E+08
1.59	14.135	16.59486	6.05093	5.92E+08
1	9.7	11.41963	2.95712	5.92E+08
0.9	8.899	10.47695	2.489927	5.92E+08
0.8	8.079	9.509821	2.047248	5.92E+08
0.7	7.234	8.515085	1.641179	5.92E+08
0.6	6.364	7.488717	1.264988	5.92E+08
0.5	5.464	6.4254	0.924289	5.92E+08
0.4	4.527	5.317783	0.625338	5.92E+08
0.3	3.546	4.155025	0.370911	5.92E+08
0.2	2.502	2.919426	0.174244	5.92E+08
0.1	1.362	1.576208	0.045885	5.92E+08
sum			333.2195	1.18E+10
average	21.2854			
temperature	70			
10	29.814	33.99692	17.49682	5.91E+08
9	27.407	31.37838	15.77186	5.91E+08

frequency	|G*| test	|G*| 2S2P1D	Squared Error	Squared Mean
8	24.945	28.67396	13.90514	5.91E+08
7	22.42	25.87115	11.91042	5.91E+08
6	19.813	22.95368	9.863874	5.91E+08
5	17.111	19.89963	7.776442	5.92E+08
4	14.282	16.67791	5.740407	5.92E+08
3	11.292	13.24132	3.799859	5.92E+08
2	8.079	9.509821	2.047248	5.92E+08
1.59	6.669	7.862154	1.423617	5.92E+08
1	4.504	5.317783	0.662243	5.92E+08
0.9	4.119	4.860077	0.549196	5.92E+08
0.8	3.725	4.392693	0.445813	5.92E+08
0.7	3.321	3.914489	0.352229	5.92E+08
0.6	2.908	3.424026	0.266282	5.92E+08
0.5	2.482	2.919426	0.191341	5.92E+08
0.4	2.042	2.398131	0.126829	5.92E+08
0.3	1.584	1.856426	0.074216	5.92E+08
0.2	1.103	1.288371	0.034362	5.92E+08
0.1	0.593	0.68259	0.008026	5.92E+08
sum			92.44621	1.18E+10
average	10.41065			
temperature	76			
10	15.323	15.84128	0.268612	5.92E+08
9	14.021	14.55927	0.289738	5.92E+08
8	12.71	13.24132	0.282304	5.92E+08
7	11.375	11.88261	0.257667	5.92E+08
6	10.005	10.47695	0.222737	5.92E+08
5	8.591	9.016131	0.180736	5.92E+08
4	7.122	7.488717	0.134481	5.92E+08
3	5.582	5.877699	0.087438	5.92E+08
2	3.943	4.155025	0.044954	5.92E+08
1.59	3.232	3.405372	0.030058	5.92E+08
1	2.154	2.264799	0.012276	5.92E+08
0.9	1.964	2.062266	0.009656	5.92E+08
0.8	1.77	1.856426	0.007469	5.92E+08
0.7	1.573	1.646927	0.005465	5.92E+08
0.6	1.371	1.433326	0.003885	5.92E+08
0.5	1.164	1.215051	0.002606	5.92E+08
0.4	0.954	0.991333	0.001394	5.92E+08

frequency	|G*| test	|G*| 2S2P1D	Squared Error	Squared Mean
0.3	0.734	0.76107	0.000733	5.92E+08
0.2	0.506	0.522525	0.000273	5.92E+08
0.1	0.265	0.272441	5.54E-05	5.92E+08
sum			1.84254	1.18E+10
average	5.21795			
Se: 5255.465		Sy: 53410.54		
Se/Sy: 0.098398		R^2: 0.991554		

Table A I. 8 Complex modulus test results and 2S2P1D model for 57% RAP asphalt binder

frequency	|G*| test	|G*| 2S2P1D	Squared Error	Squared Mean
temperature	-8			
10	206565	218848.3	1.51E+08	3.97E+10
9	201375.8	213744	1.53E+08	3.77E+10
8	196813.8	208083.7	1.27E+08	3.56E+10
7	191530.8	201729.4	1.04E+08	3.32E+10
6	185297.6	194483.1	84373561	3.06E+10
5	177428.8	186046.1	74256791	2.77E+10
4	167764.9	175932.8	66714342	2.45E+10
3	156516	163270.3	45620327	2.07E+10
2	140386.8	146208.5	33892048	1.61E+10
1.59	132655.9	136991.3	18795945	1.38E+10
1	116596.7	119384	7769127	9.97E+09
0.9	113167.6	115581	5824508	9.23E+09
0.8	109442.3	111417.9	3903055	8.45E+09
0.7	105301.8	106811.9	2280535	7.62E+09
0.6	100580.5	101646	1135180	6.75E+09
0.5	94985.81	95746.37	578452.8	5.81E+09
0.4	88467.09	88837.18	136972.4	4.81E+09
0.3	80703.5	80434.84	72177.82	3.71E+09
0.2	70528.94	69549.58	959147.7	2.5E+09
0.1	55249.02	53457.51	3209505	1.15E+09
sum			8.84E+08	3.4E+11
average	134567.9			
temperature	-2			
10	124805.5	138856.6	1.97E+08	1.42E+10
9	120716.5	134702.6	1.96E+08	1.33E+10
8	117455.3	130142.5	1.61E+08	1.22E+10
7	113533.5	125081.2	1.33E+08	1.11E+10

6	108940.3	119384	1.09E+08	9.97E+09
5	103815	112850.2	81634111	8.71E+09
4	97522.27	105159.3	58323645	7.34E+09
3	89699.31	95746.37	36566981	5.81E+09
2	79163.25	83446.24	18344037	4.09E+09
1.59	73728.51	76986.31	10613302	3.3E+09
1	63821.66	65014.1	1421930	2.07E+09
0.9	61637.14	62492.95	732407.3	1.85E+09
0.8	59336.79	59760.02	179124.4	1.62E+09
0.7	56797.11	56769.5	762.1727	1.39E+09
0.6	53974.96	53457.51	267755.8	1.15E+09
0.5	50763.25	49730.58	1066411	9.13E+08
0.4	46978.92	45442.77	2359769	6.72E+08
0.3	42419.93	40343.65	4310930	4.34E+08
0.2	36608.86	33934.53	7152017	2.08E+08
0.1	28235.82	24897.56	11143932	28999796
sum			1.03E+09	1E+11
average	76497.7			
temperature	4			
10	72383.54	88837.18	2.71E+08	4.81E+09
9	69666.57	85694	2.57E+08	4.38E+09
8	67227.85	82270.46	2.26E+08	3.94E+09
7	64489.61	78503.98	1.96E+08	3.48E+09
6	61378.46	74306.8	1.67E+08	3E+09
5	57932.52	69549.58	1.35E+08	2.5E+09
4	53801.7	64028.66	1.05E+08	1.98E+09
3	48810.68	57390.95	73621088	1.43E+09
2	42244.04	48923.91	44620608	8.65E+08
1.59	39040.32	44575.5	30638213	6.28E+08
1	32998.48	36707.45	13756455	2.96E+08
0.9	31728.99	35083.77	11254579	2.42E+08
0.8	30385.01	33337.36	8716344	1.91E+08
0.7	28906.04	31442.99	6436090	1.42E+08
0.6	27258.67	29365.85	4440222	97090181
0.5	25413.12	27055.59	2697696	56899402
0.4	23295.81	24434.54	1296722	24227302
0.3	20781.23	21371.55	348480.9	3456366
0.2	17619.45	17610.51	79.98149	3617260
0.1	13134.6	12493.24	411337.1	49268832
sum			1.56E+09	2.81E+10

average	41424.83			
temperature	10			
10	39992.91	45442.77	29701016	6.72E+08
9	38183.76	43520.22	28477803	5.76E+08
8	36554.98	41446.59	23927796	4.81E+08
7	34785.37	39190.27	19403091	3.87E+08
6	32823.99	36707.45	15081251	2.96E+08
5	30661.82	33934.53	10710673	2.08E+08
4	28140.29	30773.01	6931198	1.27E+08
3	25163.51	27055.59	3579961	56899402
2	21366.5	22453.49	1181553	8649900
1.59	19487.42	20154.48	444980.7	412249.3
1	16063.86	16113.87	2501.294	11550145
0.9	15384.91	15300.18	7179.226	17742980
0.8	14648.45	14433.03	46403.28	25800137
0.7	13843.98	13502.1	116882.1	36123906
0.6	12957.58	12493.24	215606.7	49268832
0.5	11972.65	11386.23	343888.5	66034905
0.4	10853.37	10150.28	494331.7	87649545
0.3	9541.551	8734.167	651868.6	1.16E+08
0.2	7922.688	7039.671	779718.3	1.56E+08
0.1	5686.432	4820.619	749632.4	2.16E+08
sum			1.43E+08	3.6E+09
average	21301.8			
temperature	16			
10	20737.52	22453.49	2944544	8649900
9	19657.43	21371.55	2938213	3456366
8	18679.17	20214.55	2357394	492991.1
7	17631.02	18967.66	1786599	296764.7
6	16487.67	17610.51	1260760	3617260
5	15243.61	16113.87	757345.4	11550145
4	13816.35	14433.03	380302.6	25800137
3	12151.34	12493.24	116896.5	49268832
2	10100.37	10150.28	2491.184	87649545
1.59	9084.848	9005.779	6251.98	1.1E+08
1	7296.25	7039.671	65832.57	1.56E+08
0.9	6945.965	6651.185	86895.11	1.65E+08
0.8	6569.36	6240.08	108425.4	1.76E+08
0.7	6161.094	5802.156	128836.6	1.88E+08
0.6	5716.46	5331.706	148035.6	2.01E+08

0.5	5227.407	4820.619	165476.6	2.16E+08
0.4	4676.426	4256.638	176221.8	2.33E+08
0.3	4039.501	3619.543	176364.5	2.53E+08
0.2	3275.233	2870.98	163420.3	2.77E+08
0.1	2257.415	1916.17	116447.9	3.1E+08
sum			13886754	2.48E+09
average	10287.72			
temperature	22			
10	10288.87	11386.23	1204199	66034905
9	9711.478	10786.92	1156571	76134357
8	9164.083	10150.28	972593.9	87649545
7	8581.486	9469.252	788127.8	1.01E+08
6	7953.149	8734.167	609989.5	1.16E+08
5	7275.674	7931.266	429801.3	1.34E+08
4	6511.611	7039.671	278847.8	1.56E+08
3	5629.597	6024.784	156172.5	1.82E+08
2	4566.459	4820.619	64597.22	2.16E+08
1.59	4050.945	4241.711	36391.72	2.33E+08
1	3161.143	3262.902	10354.89	2.64E+08
0.9	2989.432	3072.016	6820.069	2.7E+08
0.8	2806.103	2870.98	4209.057	2.77E+08
0.7	2609.431	2657.958	2354.867	2.84E+08
0.6	2397.111	2430.46	1112.187	2.92E+08
0.5	2165.908	2184.964	363.1483	3E+08
0.4	1911.136	1916.17	25.3453	3.1E+08
0.3	1622.524	1615.381	51.01645	3.2E+08
0.2	1282.859	1266.213	277.1049	3.33E+08
0.1	848.085	828.5691	380.8713	3.49E+08
sum			5723240	4.37E+09
average	4776.354			
temperature	28			
10	4972.956	4820.619	23206.61	2.16E+08
9	4675.671	4546.248	16750.36	2.24E+08
8	4382.521	4256.638	15846.48	2.33E+08
7	4073.139	3948.999	15410.83	2.42E+08
6	3741.804	3619.543	14947.68	2.53E+08
5	3385.233	3262.902	14964.87	2.64E+08
4	2990.131	2870.98	14196.9	2.77E+08
3	2541.447	2430.46	12318.01	2.92E+08
2	2012.98	1916.17	9372.096	3.1E+08

1.59	1761.682	1672.458	7960.851	3.18E+08
1	1337.287	1266.213	5051.58	3.33E+08
0.9	1257.018	1187.914	4775.353	3.36E+08
0.8	1172.675	1105.806	4471.444	3.39E+08
0.7	1081.899	1019.215	3929.334	3.42E+08
0.6	985.513	927.2298	3396.933	3.45E+08
0.5	881.805	828.5691	2834.064	3.49E+08
0.4	768.563	721.3128	2232.583	3.53E+08
0.3	642.388	602.3302	1604.629	3.58E+08
0.2	497.149	465.773	984.4558	3.63E+08
0.1	317.193	297.5248	386.8374	3.69E+08
sum			174641.9	6.11E+09
average	2173.953			
temperature	34			
10	2398.654	2430.46	1011.651	2.92E+08
9	2241.581	2285.609	1938.497	2.97E+08
8	2086.755	2133.284	2164.918	3.02E+08
7	1924.233	1972.14	2295.111	3.08E+08
6	1751.826	1800.363	2355.797	3.14E+08
5	1567.321	1615.381	2309.804	3.2E+08
4	1366.447	1413.339	2198.825	3.28E+08
3	1142.577	1187.914	2055.45	3.36E+08
2	884.598	927.2298	1817.469	3.45E+08
1.59	764.106	804.7494	1651.885	3.5E+08
1	566.035	602.3302	1317.34	3.58E+08
0.9	528.695	563.5984	1218.25	3.59E+08
0.8	489.58	523.0914	1123.015	3.61E+08
0.7	448.532	480.5006	1021.992	3.62E+08
0.6	405.158	435.4112	915.2583	3.64E+08
0.5	358.988	387.2408	798.2185	3.66E+08
0.4	309.256	335.1218	669.0389	3.68E+08
0.3	254.709	277.6491	526.2475	3.7E+08
0.2	193.209	212.2224	361.5112	3.72E+08
0.1	119.296	132.6654	178.742	3.76E+08
sum			27929.02	6.85E+09
average	990.0778			
temperature	40			
10	914.954	828.5691	7462.355	3.49E+08
9	858.738	776.1723	6817.099	3.51E+08
8	798.734	721.3128	5994.045	3.53E+08

7	734.094	663.5591	4975.168	3.55E+08
6	665.311	602.3302	3966.585	3.58E+08
5	592.086	536.8083	3055.627	3.6E+08
4	512.594	465.773	2192.21	3.63E+08
3	424.697	387.2408	1402.97	3.66E+08
2	324.348	297.5248	719.4831	3.69E+08
1.59	279.216	255.8506	545.94	3.71E+08
1	204.577	187.7999	281.4706	3.73E+08
0.9	190.669	174.9163	248.1468	3.74E+08
0.8	176.067	161.4971	212.281	3.74E+08
0.7	160.908	147.4531	181.0332	3.75E+08
0.6	144.903	132.6654	149.7578	3.76E+08
0.5	127.841	116.9688	118.2045	3.76E+08
0.4	109.579	100.1204	89.46447	3.77E+08
0.3	89.641	81.73378	62.5242	3.78E+08
0.2	67.275	61.11115	37.99308	3.78E+08
0.1	40.83	36.66275	17.36598	3.79E+08
sum			38529.72	7.36E+09
average	370.8531			
temperature	46			
10	418.746	465.773	2211.535	3.63E+08
9	390.631	435.4112	2005.269	3.64E+08
8	361.319	403.6857	1794.938	3.65E+08
7	330.304	370.3612	1604.577	3.66E+08
6	297.572	335.1218	1409.986	3.68E+08
5	262.991	297.5248	1192.585	3.69E+08
4	225.733	256.9125	972.162	3.71E+08
3	185.258	212.2224	727.0815	3.72E+08
2	139.859	161.4971	468.2088	3.74E+08
1.59	118.99	138.0838	364.5749	3.75E+08
1	85.638	100.1204	209.7409	3.77E+08
0.9	79.49	92.97952	181.9671	3.77E+08
0.8	73.043	85.56078	156.6949	3.77E+08
0.7	66.318	77.81958	132.2864	3.78E+08
0.6	59.295	69.69684	108.1982	3.78E+08
0.5	51.909	61.11115	84.67951	3.78E+08
0.4	44.045	51.9442	62.39736	3.79E+08
0.3	35.555	42.01025	41.67028	3.79E+08
0.2	26.211	30.98054	22.74853	3.8E+08
0.1	15.344	18.12898	7.756102	3.8E+08

sum			13759.06	7.47E+09
average	163.4126			
temperature	52			
10	192.292	187.7999	20.17883	3.73E+08
9	178.592	174.9163	13.51059	3.74E+08
8	164.458	161.4971	8.766728	3.74E+08
7	149.637	147.4531	4.76923	3.75E+08
6	134.113	132.6654	2.095418	3.76E+08
5	117.793	116.9688	0.679292	3.76E+08
4	100.379	100.1204	0.066856	3.77E+08
3	81.491	81.73378	0.05894	3.78E+08
2	60.547	61.11115	0.318262	3.78E+08
1.59	51.076	51.70618	0.397125	3.79E+08
1	36.063	36.66275	0.359699	3.79E+08
0.9	33.295	33.86872	0.329158	3.79E+08
0.8	30.44	30.98054	0.292185	3.8E+08
0.7	27.484	27.98426	0.250261	3.8E+08
0.6	24.411	24.8617	0.203132	3.8E+08
0.5	21.204	21.58827	0.147663	3.8E+08
0.4	17.809	18.12898	0.102386	3.8E+08
0.3	14.205	14.4304	0.050805	3.8E+08
0.2	10.274	10.4014	0.016232	3.8E+08
0.1	5.829	5.85164	0.000513	3.81E+08
sum			52.5933	7.56E+09
average	72.5696			
temperature	58			
10	89.711	100.1204	108.3563	3.77E+08
9	82.955	92.97952	100.491	3.77E+08
8	76.06	85.56078	90.26489	3.77E+08
7	68.867	77.81958	80.14876	3.78E+08
6	61.377	69.69684	69.21966	3.78E+08
5	53.534	61.11115	57.41316	3.78E+08
4	45.229	51.9442	45.09391	3.79E+08
3	36.313	42.01025	32.45868	3.79E+08
2	26.552	30.98054	19.61198	3.8E+08
1.59	22.193	26.00175	14.50656	3.8E+08
1	15.378	18.12898	7.56788	3.8E+08
0.9	14.136	16.68219	6.48308	3.8E+08
0.8	12.861	15.19282	5.437397	3.8E+08
0.7	11.543	13.65502	4.460632	3.8E+08

0.6	10.187	12.06124	3.512768	3.8E+08
0.5	8.777	10.4014	2.638691	3.8E+08
0.4	7.304	8.661433	1.842624	3.8E+08
0.3	5.75	6.820233	1.145399	3.8E+08
0.2	4.088	4.842754	0.569653	3.81E+08
0.1	2.252	2.658406	0.165166	3.81E+08
sum			651.3882	7.59E+09
average	32.75335			
temperature	64			
10	42.83	42.01025	0.671986	3.79E+08
9	39.483	38.83765	0.416475	3.79E+08
8	36.04	35.55568	0.234568	3.79E+08
7	32.488	32.14793	0.115649	3.79E+08
6	28.797	28.59296	0.041631	3.8E+08
5	24.955	24.8617	0.008705	3.8E+08
4	20.91	20.91265	7.03E-06	3.8E+08
3	16.616	16.68219	0.004381	3.8E+08
2	11.964	12.06124	0.009455	3.8E+08
1.59	9.914	10.00893	0.009012	3.8E+08
1	6.746	6.820233	0.005511	3.8E+08
0.9	6.175	6.243486	0.00469	3.8E+08
0.8	5.592	5.653345	0.003763	3.81E+08
0.7	4.995	5.048166	0.002827	3.81E+08
0.6	4.382	4.425865	0.001924	3.81E+08
0.5	3.749	3.78371	0.001205	3.81E+08
0.4	3.094	3.117952	0.000574	3.81E+08
0.3	2.41	2.423117	0.000172	3.81E+08
0.2	1.688	1.690371	5.62E-06	3.81E+08
0.1	0.902	0.902621	3.86E-07	3.81E+08
sum			1.532541	7.6E+09
average	15.1865			
temperature	70			
10	21.35	24.8617	12.33205	3.8E+08
9	19.626	22.91769	10.83521	3.8E+08
8	17.85	20.91265	9.37983	3.8E+08
7	16.018	18.8379	7.95185	3.8E+08
6	14.126	16.68219	6.534104	3.8E+08
5	12.166	14.4304	5.12751	3.8E+08
4	10.118	12.06124	3.776174	3.8E+08
3	7.961	9.542539	2.501264	3.8E+08

2	5.655	6.820233	1.357769	3.8E+08
1.59	4.65	5.623458	0.947621	3.81E+08
1	3.115	3.78371	0.447173	3.81E+08
0.9	2.842	3.454071	0.374631	3.81E+08
0.8	2.564	3.117952	0.306863	3.81E+08
0.7	2.281	2.774612	0.243653	3.81E+08
0.6	1.991	2.423117	0.186725	3.81E+08
0.5	1.694	2.062253	0.13561	3.81E+08
0.4	1.388	1.690371	0.091428	3.81E+08
0.3	1.071	1.305091	0.054799	3.81E+08
0.2	0.741	0.902621	0.026122	3.81E+08
0.1	0.389	0.475753	0.007526	3.81E+08
sum			62.61791	7.61E+09
average	7.3798			
temperature	76			
10	11.095	10.4014	0.481074	3.8E+08
9	10.155	9.542539	0.375109	3.8E+08
8	9.202	8.661433	0.292213	3.8E+08
7	8.225	7.755218	0.220695	3.8E+08
6	7.222	6.820233	0.161416	3.8E+08
5	6.185	5.85164	0.111129	3.81E+08
4	5.11	4.842754	0.071421	3.81E+08
3	3.986	3.78371	0.040921	3.81E+08
2	2.797	2.658406	0.019208	3.81E+08
1.59	2.284	2.171583	0.012638	3.81E+08
1	1.509	1.435199	0.005447	3.81E+08
0.9	1.373	1.305091	0.004612	3.81E+08
0.8	1.235	1.173096	0.003832	3.81E+08
0.7	1.094	1.039021	0.003023	3.81E+08
0.6	0.95	0.902621	0.002245	3.81E+08
0.5	0.804	0.763586	0.001633	3.81E+08
0.4	0.655	0.621496	0.001123	3.81E+08
0.3	0.501	0.475753	0.000637	3.81E+08
0.2	0.343	0.325421	0.000309	3.81E+08
0.1	0.178	0.168751	8.55E-05	3.81E+08
sum			1.808769	7.61E+09
average	3.74515			
Se: 3521.201		Sy: 42667.42		
Se/Sy: 0.082527		R^2: 0.994059		

APPENDIX II

FREQUENCY SWEEP TEST RESULTS FOR LINEAR AMPLITUDE STRAIN (LAS)

Table A II. 9 Frequency sweep test results of 65% RAP under various blending conditions

Frequency (Hz)	Intense blending condition (IB)		Moderate blending condition (MB)		Low blending condition (LB)	
	Complex Modulus (G*) (Pa)	Phase Angle (°)	Complex Modulus (G*) (Pa)	Phase Angle (°)	Complex Modulus (G*) (P)	Phase Angle (°)
2.00E-01	2.17E+07	3.38E+01	1.70E+07	3.57E+01	2.00E+07	3.44E+01
4.00E-01	2.80E+07	3.24E+01	2.24E+07	3.41E+01	2.59E+07	3.29E+01
6.00E-01	3.24E+07	3.16E+01	2.61E+07	3.31E+01	3.01E+07	3.19E+01
8.00E-01	3.58E+07	3.10E+01	2.90E+07	3.24E+01	3.33E+07	3.13E+01
1.00E+00	3.87E+07	3.05E+01	3.15E+07	3.19E+01	3.60E+07	3.08E+01
2.00E+00	4.86E+07	2.92E+01	4.00E+07	3.05E+01	4.54E+07	2.94E+01
4.00E+00	6.04E+07	2.80E+01	5.03E+07	2.92E+01	5.65E+07	2.80E+01
6.00E+00	6.83E+07	2.72E+01	5.72E+07	2.84E+01	6.39E+07	2.72E+01
8.00E+00	7.43E+07	2.67E+01	6.26E+07	2.78E+01	6.97E+07	2.67E+01
1.00E+01	7.93E+07	2.65E+01	6.70E+07	2.74E+01	7.43E+07	2.61E+01
2.00E+01	9.46E+07	2.42E+01	8.10E+07	2.53E+01	8.87E+07	2.43E+01
3.00E+01	1.05E+08	2.25E+01	9.06E+07	2.53E+01	9.81E+07	2.15E+01

APPENDIX III

GENERALIZED MAXWELL (GM) ELEMENTS CALIBRATED USING 2S2P1D

Table A III. 1 Parameters of GM elements calibrated by 2S2P1D

Element i	ρ_i	E_i			
		57% RAP	65% RAP	73% RAP	100% RAP
1	1E-13	252.4900858	315.0273679	240.0398053	172.8639841
2	1E-12	185.8226412	206.5732289	174.2483104	194.833733
3	1E-11	444.8632244	534.0122782	422.8652008	326.2189578
4	1E-10	459.2186639	512.4095897	435.0541009	410.798916
5	0.000000001	825.312474	951.786855	787.9015265	622.0019824
6	0.00000001	976.8764934	1069.154018	935.9296669	806.4834808
7	0.0000001	1507.159094	1667.977353	1455.702565	1133.798194
8	0.000001	1834.200767	1945.485066	1790.380407	1437.581653
9	0.00001	2516.572786	2667.629819	2487.108089	1861.449934
10	0.0001	2919.372761	2980.898725	2938.916463	2201.828547
11	0.001	3550.497078	3611.602689	3636.323057	2568.380474
12	0.01	3772.942221	3723.573936	3951.483123	2756.501871
13	0.1	4183.538119	4154.840337	4443.119729	2934.751988
14	1	4261.081277	4209.601434	4615.532153	2991.932194
15	10	4345.736039	4455.366602	4880.353896	3043.934703
16	100	2907.101027	2940.957703	3679.889154	2438.588167
17	1000	1162.828996	1119.448658	1595.692614	1165.291114
18	10000	361.137789	332.8538247	500.4810042	397.1301316
19	100000	104.0541513	92.86831639	133.3854683	119.8840887
20	1000000	29.24073453	25.411635	24.54476592	34.99014899
21	10000000	7.979407611	6.769236013	2.221926342	10.08243007
22	100000000	1.922889494	1.630070761	0.106633502	2.846394876
23	1000000000	0.287540026	0.263463425	0.004017119	0.747816965
24	10000000000	0.020535051	0.021365176	0.000144687	0.130699789
25	1E+11	0.000948594	0.001085595	5.55751E-06	0.011929025

LIST OF BIBLIOGRAPHICAL REFERENCES

AASHTO. (2001). *Standard specification for Superpave volumetric mix design.* AASHTO M 323. Washington, D.C., United States: American Association of State Highway and Transportation Officials.

AASHTO. (2014). *Estimating Damage Tolerance of Asphalt Binders Using the Linear Amplitude Sweep.* AASHTO TP 101. Washington, D.C., United States: American Association of State Highway and Transportation Officials.

AASHTO. (2017a). *Standard Specification for Superpave Volumetric Mix Design.* AASHTO M 323. Washington, D.C., United States: American Association of State Highway and Transportation Officials.

AASHTO. (2017b). *Standard Practice for Superpave Volumetric Design for Asphalt Mixtures.* AASHTO R 35. Washington, D.C., United States: American Association of State Highway and Transportation Officials.

AASHTO. (2019a). *Standard Method of Test for Determining the Flexural Creep Stiffness of Asphalt Binder Using the Bending Beam Rheometer (BBR).* AASHTO T 313. Washington, D.C., United States: American Association of State Highway and Transportation Officials.

AASHTO. (2019b). *Standard Method of Test for Multiple Stress Creep Recovery (MSCR) Test of Asphalt Binder Using a Dynamic Shear Rheometer (DSR).* AASHTO T 350. Washington, D.C., United States: American Association of State Highway and Transportation Officials.

AASHTO. (2020a). *Standard Method of Test for Determining the Fracture Potential of Asphalt Mixtures Using the Illinois Flexibility Index Test (I-FIT).* AASHTO TP 124. Washington, D.C., United States: American Association of State Highway and Transportation Officials.

AASHTO. (2020b). *Standard Method of Test for Determining the Fracture Energy of Asphalt Mixtures Using the Semicircular Bend Geometry (SCB).* AASHTO TP 105. Washington, D.C., United States: American Association of State Highway and Transportation Officials.

AASHTO. (2020c). Standard Method of Test for Determining the Rheological Properties of Asphalt Binder Using a Dynamic Shear Rheometer (DSR). AASHTO T 315. Washington, D.C., United States: American Association of State Highway and Transportation Officials.

Abdelaziz, A., Masad, E., Epps Martin, A., Mercado, E. A., & Bajaj, A. (2021). Multiscale characterization of aging and rejuvenation in asphalt binder blends with high RAP contents. *Journal of Materials in Civil Engineering, 33*(10), 04021287.

Airey, G. D., Rahimzadeh, B., & Collop, A. C. (2004). Linear rheological behavior of bituminous paving materials. *Journal of materials in civil engineering*, *16*(3), 212–220.

Ali, U. M. (2019). *Evaluating the cracking resistance of a superpave 5 mix and a conventional superpave mix using the Illinois Flexibility Index test.* Retrieved from https://il-asphalt.org/files/5015/4896/1293/Uthman_Mohamed_Ali_2018_UIUC.pdf

Al-Qadi, I. L., Aurangzeb, Q., Carpenter, S. H., Pine, W. J., & Trepanier, J. (2012*). Impact of high RAP contents on structural and performance properties of asphalt mixtures* (Report No. ICT-12-002). Retrieved from https://citeseerx.ist.psu.edu/viewdoc/download?doi=10.1.1.390.6903&rep=rep1&type=pdf

Al-Qadi, I. L., Ozer, H., Zhu, Z., Singhvi, P., Ali, M. U., Sawalha, M., Luque, A. E. F., Mainieri, J. J. G., & Zehr, T. G. (2019). Development of long-term aging protocol for implementation of the illinois flexibility index test (I-FIT) (Report No. FHWA-ICT-19-009). DOI: https://doi.org/10.36501/0197-9191/19-012

Anderson, M. (2005, November). *Using RAP in the Superpave Mix Design System*. Paper presented at Canadian Technical Asphalt Association, Victoria, BC, Canada. Retrieved from https://www.ctaa.ca/wp-content/uploads/2012/02/Anderson_CUPGA-2005-RAP.pdf

Apostolidis, P., Liu, X., Erkens, S., & Scarpas, A. (2019). Evaluation of epoxy modification in bitumen. *Construction and Building Materials*, *208*, 361-368.

Asphalt Pavement Alliance (APA). (2001). Recycling Asphalt Pavement Background. Retrieved from https://pavementinteractive.org/reference-desk/pavement-types-and-history/pavement-types/hma-recycling/

ASTM International. (2017a). *Standard Test Method for Indirect Tensile (IDT) Strength of Asphalt Mixtures.* ASTM Standard D6931. West Conshohocken, PA, United States: American Society for Testing and Materials.

ASTM International. (2017b). *Standard Practice for Recovery of Asphalt from Solution Using the Rotary Evaporator.* ASTM Standard D5404/D5404M. West Conshohocken, PA, United States: American Society for Testing and Materials.

ASTM International. (2018). *Standard Test Method for Evaluation of Asphalt Mixture Cracking Resistance using the Semi-Circular Bend Test (SCB) at Intermediate*

Temperatures. ASTM Standard D 8044. West Conshohocken, PA, United States: American Society for Testing and Materials.

ASTM International. (2019a). *Standard Test Method for Effect of Heat and Air on a Moving Film of Asphalt (Rolling Thin-Film Oven Test).* ASTM Standard D2872-19. West Conshohocken, PA, United States: American Society for Testing and Materials.

ASTM International. (2019b). *Standard Practice for Accelerated Aging of Asphalt Binder Using a Pressurized Aging Vessel (PAV).* ASTM Standard D6521-19. West Conshohocken, PA, United States: American Society for Testing and Materials.

ASTM International. (2019c). *Standard Test Method for Asphalt Content of Asphalt Mixture by Ignition Method.* ASTM Standard D6307-19. West Conshohocken, PA, United States: American Society for Testing and Materials.

ASTM International. (2019d). *Standard Test Method for Automated Extraction of Asphalt Binder from Asphalt Mixtures.* ASTM Standard D8159-19. West Conshohocken, PA, United States: American Society for Testing and Materials.

ASTM International. (2021). *Standard Practice for Recovery of Asphalt Binder from Solution Using the Rotary Evaporator.* ASTM Standard D5404/D5404M West Conshohocken, PA, United States: American Society for Testing and Materials.

Aurangzeb, Q., Al-Qadi, I. L., Abuawad, I. M., Pine, W. J., & Trepanier, J. S. (2012). Achieving desired volumetrics and performance for mixtures with high percentage of reclaimed asphalt pavement. *Transportation research record, 2294*(1), 34-42.

Bahia, H. U., Zhai, H., Onnetti, K., & Kose, S. (1999). Non-linear viscoelastic and fatigue properties of asphalt binders. *Journal of the Association of Asphalt Paving Technologists*, *68*, 1-34.

Barco Carrión, A. J. D., Lo Presti, D., & Airey, G. D. (2015). Binder design of high RAP content hot and warm asphalt mixture wearing courses. *Road materials and pavement design*, *16*(sup1), 460-474.

Basueny, A., Perraton, D., & Carter, A. (2014). Laboratory study of the effect of RAP conditioning on the mechanical properties of hot mix asphalt containing RAP. *Materials and structures*, *47*(9), 1425-1450.

Behnood, A. (2019). Application of rejuvenators to improve the rheological and mechanical properties of asphalt binders and mixtures: A review. *Journal of cleaner production*, *231*, 171-182.

Bodin, D., de La Roche, C., Piau, J. M., & Pijaudier-Cabot, G. (2002, August). *A damage approach for asphalt mixture fatigue tests*. Paper presented at Ninth International

Conference on Asphalt Pavements International Society for Asphalt Pavements, Copenhagen, Denmark.

Braham, A. F., Buttlar, W. G., Clyne, T. R., Marasteanu, M., & Turos, M. I. (2009, December). The effect of long-term laboratory aging on asphalt concrete fracture energy. *Journal of the Association of Asphalt Paving Technologists*, *78*, 417-445.

Bressi, S., Dumont, A. G., & Partl, M. N. (2016). A new laboratory methodology for optimization of mixture design of asphalt concrete containing reclaimed asphalt pavement material. *Materials and Structures*, *49*(12), 4975-4990.

Cai, X., Zhang, J., Xu, G., Gong, M., Chen, X., & Yang, J. (2019). Internal aging indexes to characterize the aging behavior of two bio-rejuvenated asphalts. *Journal of Cleaner Production*, *220*, 1231-1238.

Cantrell, L., Wen, H., & Wang, L. (2022). Development of a Model to Estimate Percentage of Reclaimed Asphalt Pavement (RAP) Binder Contribution Based on Design and Performance of Super High RAP Mixes. *Transportation Research Record*, 03611981221089574. DOI: 10.1177/03611981221089574

Carter, A., & Stroup-Gardiner, M. (2007). Indirect tension relaxation test to evaluate the effect of the addition of RAP to HMA mixes. *Journal of materials in civil engineering*, *19*(3), 219-226.

Carret, J. C. (2018). *Linear viscoelastic characterization of bituminous mixtures from dynamic tests back analysis* (Doctoral dissertation, Université de Lyon, Vaulx-en-Velin, France).

Chehab, G., Kim, R., Schapery, R., Witczak, M., & Bonaquist, R. (2003). Characterization of asphalt concrete in uniaxial tension using a viscoelastoplastic continuum damage model. *Journal of the Association of Asphalt Paving Technologists*, *72*, 315-355.

Chen, M., Leng, B., Wu, S., & Sang, Y. (2014). Physical, chemical and rheological properties of waste edible vegetable oil rejuvenated asphalt binders. *Construction and Building materials*, *66,* 286-298.

Chen, A., Liu, G., Zhao, Y., Li, J., Pan, Y., & Zhou, J. (2018). Research on the aging and rejuvenation mechanisms of asphalt using atomic force microscopy. *Construction and Building Materials*, *167*, 177-184.

Chesner, W. H., Collins, R. J., MacKay, M. H., & Emery, J. (2002). *User guidelines for waste and by-product materials in pavement construction* (No. FHWA-RD-97-148, Guideline Manual, Rept No. 480017). Durham, NH, United States: Recycled Materials Resource Center.

Chun, S., & Kim, K. (2016). Effectiveness of dominant aggregate size range–interstitial component criteria for consistently enhanced cracking performance of asphalt mixtures in the field. *Canadian Journal of Civil Engineering, 43*(6), 523-531.

Coenen, A. R., Kutay, M. E., Sefidmazgi, N. R., & Bahia, H. U. (2012). Aggregate structure characterisation of asphalt mixtures using two-dimensional image analysis. *Road Materials and Pavement Design*, *13*(3), 433-454.

Copeland, A. (2011). *Reclaimed asphalt pavement in asphalt mixtures: State of the practice* (No. FHWA-HRT-11-021). Washington, D.C., United States: Federal Highway Administration, Office of Research, Development, and Technology.

Clyne, T. R., Li, X., Marasteanu, M. O., & Skok, E. L. (2003). *Dynamic and resilient modulus of Mn/DOT asphalt mixtures* (No. MN/RC-2003-09,). Retrieved from https://www.lrrb.org/pdf/200309.pdf

Das, P. K., Baaj, H., Tighe, S., & Kringos, N. (2016). Atomic force microscopy to investigate asphalt binders: a state-of-the-art review. *Road Materials and Pavement Design*, *17*(3), 693-718.

de Oliveira, L. S., da Silva, L. S. V., Júnior, J. L. O. L., Babadopulos, L. F. D. A. L., & Soares, J. B. (2023). Linear viscoelasticity and fatigue life: Relationships between properties of asphalt binders and corresponding mixtures. *Construction and Building Materials, 372*, 130685.

Di Benedetto, H., Ashayer Soltani, A., & Chaverot, P. (1996). Fatigue damage for bituminous mixtures: a pertinent approach. *Journal of the Association of Asphalt Paving Technologists*, *65*, 142-158.

Di Benedetto, H., De La Roche, C., Baaj, H., Pronk, A., & Lundström, R. (2004). Fatigue of bituminous mixtures. *Materials and structures*, *37(3)*, 202-216.

Di Benedetto, H., & Corté, J. F. (2005). *Matériaux routiers bitumineux 2*. Paris: Hermès Lavoisier editions.

Di Benedetto, H., Gabet, T., Grenfell, J., Perraton, D., Sauzéat, C., & Bodin, D. (2013), Mechanical testing of bituminous mixtures. In Partl, M. N., Bahia, H. U., Canestrari, F., De la Roche, C., Di Benedetto, H., Piber, H., & Sybilski, D. (Eds.), *Advances in Interlaboratory Testing and Evaluation of Bituminous Materials: state-of-the-art report of the RILEM technical committee 206-ATB*. (pp. 143-256). Dordrecht: Springer.

Elkashef, M., & Williams, R. C. (2017a). Improving fatigue and low temperature performance of 100% RAP mixtures using a soybean-derived rejuvenator. *Construction and Building materials, 151,* 345-352.

Elkashef, M., Podolsky, J., Williams, R. C., & Cochran, E. (2017b). Preliminary examination of soybean oil derived material as a potential rejuvenator through Superpave criteria and asphalt bitumen rheology. *Construction and Building Materials, 149*, 826-836.

Elkashef, M., Williams, R. C., & Cochran, E. W. (2018a). Physical and chemical characterization of rejuvenated reclaimed asphalt pavement (RAP) binders using rheology testing and pyrolysis gas chromatography-mass spectrometry. *Materials and Structures*, *51*(1), 12.

Elkashef, M., Podolsky, J., Williams, R. C., & Cochran, E. W. (2018b). Introducing a soybean oil-derived material as a potential rejuvenator of asphalt through rheology, mix characterisation and Fourier Transform Infrared analysis. *Road Materials and Pavement Design*, *19*(8), 1750-1770.

Elseifi, M. A., Mohammad, L. N., Ying, H., & Cooper III, S. (2012). Modeling and evaluation of the cracking resistance of asphalt mixtures using the semi-circular bending test at intermediate temperatures. *Road Materials and Pavement Design*, *13*(sup1), 124-139.

Ghabchi, R., Singh, D., & Zaman, M. (2014). Evaluation of moisture susceptibility of asphalt mixes containing RAP and different types of aggregates and asphalt binders using the surface free energy method. *Construction and Building Materials*, *73*, 479-489.

Ghuzlan, K. A., Bara'W, A. M., & Al-Momani, A. S. (2020). Rutting performance of asphalt mixtures with gradations designed using Bailey and conventional Superpave methods. *Construction and building materials*, *261,* 119941.

Golalipour, A., Jamshidi, E., Niazi, Y., Afsharikia, Z., & Khadem, M. (2012). Effect of aggregate gradation on rutting of asphalt pavements. *Procedia-Social and Behavioral Sciences, 53,* 440-449.

Gong, H., Huang, B., & Shu, X. (2018). Field performance evaluation of asphalt mixtures containing high percentage of RAP using LTPP data. *Construction and Building Materials*, *176,* 118-128.

Guo, A., Cho, Y., & Petrović, Z. S. (2000). Structure and properties of halogenated and nonhalogenated soy-based polyols. *Journal of Polymer Science Part A: Polymer Chemistry*, *38*(21), 3900-3910.

Hajj, E. Y., Souliman, M. I., Alavi, M. Z., & Salazar, L. G. L. (2013). Influence of hydrogreen bioasphalt on viscoelastic properties of reclaimed asphalt mixtures. *Transportation research record*, *2371*(1), 13-22.

Hand, A.J.T., & Aschenbrener, T. (2021). *Tech Brief: Resource Responsible Use of Reclaimed Asphalt Pavement in Asphalt Mixtures* (Publication FHWA-HIF-22-003). Washington,

D.C., United States: Federal Highway Administration, Department of Transportation, Office of Preconstruction, Construction, and Pavements.

Hansen, K.R., & Copeland, A. (2013). *Asphalt Pavement Industry Survey on Recycled Materials and Warm-Mix Asphalt Usage: 2009-2012* (Information Series No. 138 (3e)). Lanham, MD, United States: National Asphalt Pavement Association (NAPA) in corporation with Federal Highway Administration.

Hashmi, S. M., & Firoozabadi, A. (2013). Self-assembly of resins and asphaltenes facilitates asphaltene dissolution by an organic acid. *Journal of colloid and interface science*, *394*, 115-123.

Harman, T., Youtcheff, J. & Bukowski, J. (2011). *THE MULTIPLE STRESS CREEP RECOVERY (MSCR) PROCEDURE*. *Publication* (FHWA HIF-11-038). Washington, D.C., United States: Federal Highway Administration, Department of Transportation, Office of Preconstruction, Construction, and Pavements.

Hernandez-Fernandez, N., Underwood, B. S., & Ossa-Lopez, A. (2020). Simulation of the asphalt concrete stiffness degradation using simplified viscoelastic continuum damage model. *International Journal of Fatigue*, *140*, 105850.

Hintz, C., Velasquez, R., Johnson, C., & Bahia, H. (2011). Modification and validation of linear amplitude sweep test for binder fatigue specification. *Transportation Research Record*, *2207*(1), 99-106.

Hill, B. (2011). *Performance evaluation of warm mix asphalt mixtures incorporating reclaimed asphalt pavement*. (MSc thesis, University of Illinois at Urbana-Champaign, Urbana-Champaign, IL, United States).

Hou, T. (2009). *Fatigue performance prediction of North Carolina mixtures using simplified viscoelastic continuum damage model.* (PhD Thesis, North Carolina State University, Raleigh, NC, United States).

Im, S., Karki, P., & Zhou, F. (2016). Development of new mix design method for asphalt mixtures containing RAP and rejuvenators. *Construction and Building Materials*, *115*, 727-734.

Imaninasab, R., Loria-Salazar, L., & Carter, A. (2022). Integrated performance evaluation of asphalt mixtures with very high reclaimed asphalt pavement (RAP) content. *Construction and Building Materials*, *347*, 128607.

Izaks, R., Haritonovs, V., Klasa, I., & Zaumanis, M. (2015). Hot mix asphalt with high RAP content. *Procedia Engineering*, *114*, 676-684.

Jiao, L., Elkashef, M., Harvey, J. T., Rahman, M. A., & Jones, D. (2022). Investigation of fatigue performance of asphalt mixtures and FAM mixes with high recycled asphalt material contents. Construction and Building Materials, 314, 125607.

Kandhal, P. S., & Mallick, R. B. (2001). Effect of mix gradation on rutting potential of dense-graded asphalt mixtures. *Transportation Research Record*, *1767(1),* 146-151.

Kaseer, F., Yin, F., Arámbula-Mercado, E., Martin, A. E., Daniel, J. S., & Salari, S. (2018). Development of an index to evaluate the cracking potential of asphalt mixtures using the semi-circular bending test. *Construction and Building Materials, 167*, 286-298.

Kim, Y. R., & Little, D. N. (1990). One-dimensional constitutive modeling of asphalt concrete. *Journal of engineering mechanics*, *116(4),* 751-772.

Kim, Y. R., Daniel, J. S., & Wen, H. (2002). *Fatigue performance evaluation of WesTrack asphalt mixtures using viscoelastic continuum damage approach* (No. FHWA/NC/2002-004). Washington, D.C., United States: Federal Highway Administration

Kim, M., Mohammad, L. N., & Elseifi, M. A. (2012). Characterization of fracture properties of asphalt mixtures as measured by semicircular bend test and indirect tension test. *Transportation Research Record, 2296*(1), 115-124.

Kim, Y. R., Castorena, C., Elwardany, M., Yousefi Rad, F., Underwood, S., Gundla, A., ... & Glaser, R. R. (2018). *Long-Term Aging of Asphalt Mixtures for Performance Testing and Prediction* (NCHRP Report 871). Washington, D.C., United States: Transportation Research Board of the National Academies.

Kuang, D., Jiao, Y., Ye, Z., Lu, Z., Chen, H., Yu, J., & Liu, N. (2018). Diffusibility enhancement of rejuvenator by epoxidized soybean oil and its influence on the performance of recycled hot mix asphalt mixtures. *Materials, 11(5),* 833.

Kurth, T. L., Nivens, S., Stevermer, C. P., & Tabatabaee, H. A. (2019a). *U.S. Patent No. 10,316,192.* Washington, DC: U.S. Patent and Trademark Office.

Kurth, T. L., Nivens, S., Stevermer, C. P., & Tabatabaee, H. A. (2019b). *U.S. Patent No.* 10,329,426. Washington, DC: U.S. Patent and Trademark Office.

LC Method. (2020a). *Tenue à l'eau (par trempage).* LC 26-00. Montreal, QC, Canada : Publications du Québec.

LC Method. (2020b). *Résistance à la déformation des enrobés à l'essai d'orniérage*. LC 26-410. Montreal, QC, Canada : Publications du Québec.

Lee, H.J., & Kim, Y.R. (1988). A Viscoelastic Continuum Damage Model of Asphalt Concrete with Healing. *Journal of Engineering Mechanics, 124*(11), 1224-1232.

Li, Y., Hao, P., Zhang, M., Sun, B., Liu, J., & Li, N. (2021). Synthesis and Characterization of Calcium Alginate Capsules Encapsulating Soybean Oil for In Situ Rejuvenation of Aged Asphalt. *Journal of Materials in Civil Engineering, 33*(11), 04021310.

Loria-Salazar, L. G. (2011). *Evaluation of New and Existing Test Methods to Assess Recycled Asphalt Pavement Properties for Mix Design*. (University of Nevada, Reno, NV, United States).

Lundstrom, R., & Isacsson, U. (2003). Asphalt fatigue modelling using viscoelastic continuum damage theory. *Road Materials and Pavement Design*, *4(1),* 51-75.

Lv, H., Liu, H., Tan, Y., Meng, A., Assogba, O. C., & Xiao, S. (2021). An extended search method for identifying optimal parameters of the generalized Maxwell model. *Construction and Building Materials*, *266*, 120796.

Ma, T., Huang, X., Zhao, Y., & Zhang, Y. (2015). Evaluation of the diffusion and distribution of the rejuvenator for hot asphalt recycling. *Construction and Building Materials*, *98*, 530-536.

Mangiafico, S., Di Benedetto, H., Sauzéat, C., Olard, F., Pouget, S., & Planque, L. (2013). Influence of reclaimed asphalt pavement content on complex modulus of asphalt binder blends and corresponding mixes: experimental results and modelling. *Road Materials and Pavement Design*, *14*(sup1), 132-148.

McDaniel, R. S., & Anderson, R. M. (2001). *Recommended use of reclaimed asphalt pavement in the Superpave mix design method: technician's manual* (NCHRP 452). Washington, D.C., United States: Transportation Research Board of the National Academies Press.

Monismith, C. L., & Deacon, J. A. (1969). Fatigue of asphalt paving mixtures. *Transportation Engineering Journal of ASCE*, *95*(2), 317-346.

Monismith, C. L., Epps, J. A., & Finn, F. N. (1985). Improved asphalt mix design (with discussion). *Association of Asphalt Paving Technologists Proc, 54,* 340-406.

Ministère des Transports du Québec (MTQ). (2006). *Hot Mix Asphalt: LC Method of Mix Design.* Montreal, QC, Canada: Publications du Québec.

Nazzal, M. D., Mogawer, W., Austerman, A., Qtaish, L. A., & Kaya, S. (2015). Multi-scale evaluation of the effect of rejuvenators on the performance of high RAP content mixtures. *Construction and Building Materials*, *101*, 50-56.

Newcomb, D. E., Brown, E. R., & Epps, J. A. (2007). *Designing HMA mixtures with high RAP content: A practical guide* (Quality Improvement Series 124). Lanham, MD, United States: National Asphalt Pavement Association (NAPA).

Norouzi, A., Sabouri, M., & Kim, Y. R. (2014). Evaluation of the fatigue performance of asphalt mixtures with high RAP content. In Kim, Y. R., *Asphalt Pavements* (pp. 1069-1077). London, United Kingdom: Journal of Tylor and Francis Group.

Olard, F., & Di Benedetto, H. (2003). General "2S2P1D" model and relation between the linear viscoelastic behaviours of bituminous binders and mixes. *Road materials and pavement design*, *4(2),* 185-224.

Olard, F., & Perraton, D. (2010). On the optimization of the aggregate packing characteristics for the design of high-performance asphalt concretes. *Road Materials and Pavement Design, 11(sup1)*, 145-169.

Orosa, P., Pérez, I., & Pasandín, A. R. (2022). Short-term resilient behaviour and its evolution with curing in cold in-place recycled asphalt mixtures. *Construction and Building Materials, 323*, 126559.

Osmari, P. H., Aragão, F. T. S., Leite, L. F. M., Simão, R. A., da Motta, L. M. G., & Kim, Y. R. (2017). Chemical, microstructural, and rheological characterizations of binders to evaluate aging and rejuvenation. *Transportation Research Record*, *2632(1),* 14-24.

Perraton, D., Baaj, H. & Carter, A. (2010). Comparison of some pavement design methods from a fatigue point of view: effect of fatigue properties of asphalt materials. *Road materials and pavement design, 11(4)*, 833-861.

Petrović, Z. S., & Cvetković, I. (2012). Vegetable oil-based hyperbranched polyols in flexible foams. *Contemporary Materials*, *3(1),* 63-71.

Podolsky, J. H., Saw, B., Elkashef, M., Williams, R. C., & Cochran, E. W. (2021). Rheology and mix performance of rejuvenated high RAP field produced hot mix asphalt with a soybean derived rejuvenator. *Road Materials and Pavement Design*, *22(8),* 1894-1907.

Portugal, A. C. X., Lucena, L. C. D. F. L., Lucena, A. E. D. F. L., Beserra Costa, D., & Patricio, J. D. (2018a). Evaluating the rheological effect of asphalt binder modification using soybean oil. *Petroleum Science and Technology*, *36*(17), 1351-1360.

Portugal, A. C. X., Lucena, L. C. D. F. L., Lucena, A. E. D. F. L., & Beserra da Costa, D. (2018b). Rheological performance of soybean in asphalt binder modification. *Road Materials and Pavement Design, 19*(4), 768-782.

Possebon, É. P., Specht, L. P., Di Benedetto, H., Schuster, S. L., & Pereira, D. D. S. (2022). Rheological properties, 2S2P1D modelling and SHStS transformation of 12 Brazilian bitumens and mixtures. *Road Materials and Pavement Design, 23*(sup1), 68-85.

Pradhan, S. K., and Sahoo, U. C. (2020). Influence of softer binder and rejuvenator on bituminous mixtures containing reclaimed asphalt pavement (RAP) material. *International Journal of Transportation Science and Technology, 11*(1), pp.46-59.

Rathore, M., & Zaumanis, M. (2020). Impact of laboratory mixing procedure on the properties of reclaimed asphalt pavement mixtures. *Construction and Building Materials*, *264*, 120709.

Reese, R. (1997). Properties of aged asphalt binder related to asphalt concrete fatigue life. *Journal of the Association of Asphalt Paving Technologists*, *66*, 604-632.

Rodezno, C., & Grant, J. (2018). *Asphalt Binder Extraction Protocol for Determining Amount & PG Characteristics of Binders Recovered from Asphalt Mixtures* (No. Project 0092-16-02). Wisconsin, United States: Wisconsin Department of Transportation (WisDOT).

Saliani, S. S., Carter, A., Baaj, H., & Tavassoti, P. (2019). Characterization of asphalt mixtures produced with coarse and fine recycled asphalt particles. *Infrastructures*, *4*(4), 67.

Sabouri, M., & Kim, Y.R. (2014). Development of a failure criterion for asphalt mixtures under different modes of fatigue loading. *Transportation Research Record, 2447*, 117-125.

Safaei , F., & Castetorena, C. (2016). Specification of Linear Amplitude Sweep Test Temperature and Modeling Temperature Effect on Asphalt Binder Fatigue. *Transportation Research Record, 2574*(1), pp. 92-100.

Schapery, R. A. (1982). Models for damage growth and fracture in nonlinear viscoelastic particulate composites. *U. S. National Congress of Applied Mechanics, 9,* 237-245.

Shirodkar, P., Mehta, Y., Nolan, A., Sonpal, K., Norton, A., Tomlinson, C., ... & Sauber, R. (2011). A study to determine the degree of partial blending of reclaimed asphalt pavement (RAP) binder for high RAP hot mix asphalt. *Construction and Building Materials*, *25*(1), 150-155.

Shirodkar, P., Mehta, Y., Nolan, A., Dubois, E., Reger, D., & McCarthy, L. (2013). Development of blending chart for different degrees of blending of RAP binder and virgin binder. *Resources, conservation and recycling*, *73*, 156-161.

Si, J., Li, Y., Wang, J., Niyigena, A. R., Yu, X., & Jiang, R. (2020). Improving the compatibility of cold-mixed epoxy asphalt based on the epoxidized soybean oil. *Construction and Building Materials*, *243*, 118235.

Sreedhar, S., & Coleri, E. (2018). Effects of binder content, density, gradation, and polymer modification on cracking and rutting resistance of asphalt mixtures used in Oregon. *Journal of Materials in Civil Engineering, 30*(11), 04018298.

Strategic Highway Research Program (SHRP). (1994). *SHRP 007: Short-And Long-Term Aging of Bituminous Mixes.* Washington, D.C., United States: SHRP Designation. Strategic Highway Research Program, National Research Council.

Subhy, A., Menegusso Pires, G., Jiménez del Barco Carrión, A., Lo Presti, D., & Airey, G. (2019). Binder and mixture fatigue performance of plant-produced road surface course asphalt mixtures with high contents of reclaimed asphalt. *Sustainability, 11*(13), 3752.

Sun, Z., Yi, J., Huang, Y., Feng, D., & Guo, C. (2016). Properties of asphalt binder modified by bio-oil derived from waste cooking oil. *Construction and Building Materials*, *102*, 496-504.

Tang, Q., Chen, Y., Gao, H., Li, Q., Xi, Z., Zhao, L., ... & Li, L. (2018). Bio-Based Epoxy Resin from Epoxidized Soybean Oil. In Kasi, M., *Soybean-Biomass, Yield and Productivity* (pp. 139-160). London, United Kingdom: IntechOpen.

Tapsoba, N., Sauzéat, C., Di Benedetto, H., Baaj, H., & Ech, M. (2014). Behaviour of asphalt mixtures containing reclaimed asphalt pavement and asphalt shingle. *Road Materials and Pavement Design*, *15*(2), 330-347.

Teymourpour, P., Bahia, H.U. (2014, September). *Linear Amplitude Sweep Test: Binder Grading Specification and Field Validation.* Paper presented at Binder Expert Task Group Meeting, Baton Rouge, LA, United States:

Tiouajni, S., Di Benedetto, H., Sauzéat, C., & Pouget, S. (2011). Approximation of linear viscoelastic model in the 3 dimensional case with mechanical analogues of finite size: Application to bituminous materials. *Road Materials and Pavement Design*, *12*(4), 897-930.

Tran, N. H., Taylor, A., & Willis, R. (2012). *Effect of rejuvenator on performance properties of HMA mixtures with high RAP and RAS contents* (NCAT Report, 12-05). Auburn, AL, United States: National Center for Asphalt Technology (NCAT).

Underwood, B. S. (2006). *Experimental Investigation and Constitutive Modeling of Asphalt Concrete Mixtures in Uniaxial Tension*. (MSc Thesis, North Carolina State University, Raleigh, NC, United States).

Underwood, B. S., Kim, Y. R., & Guddati, M. N. (2010). Improved calculation method of damage parameter in viscoelastic continuum damage model. *International Journal of Pavement Engineering*, *11*(6), 459-476.

Vavrik, W. R., Pine, W. J., & Carpenter, S. H. (2002). Aggregate blending for asphalt mix design: Bailey method. *Transportation Research Record, 1789*(1), 146-153.

Villegas-Villegas, R. E., & Loría-Salazar, L. G. (2012). Recycling of banana production waste bags in bitumens: A green alternative.

Wei, J. B., Shull, J. C., Lee, Y. J., & Hawley, M. C. (1996). Characterization of asphalt binders based on chemical and physical properties. *International Journal of Polymer Analysis and Characterization*, *3*(1), 33-58.

West, R. C., Willis, J. R., & Marasteanu, M. O. (2013). *Improved mix design, evaluation, and materials management practices for hot mix asphalt with high reclaimed asphalt pavement content* (NCHRP 752). Washington, D.C., United States: Transportation Research Board of the National Academies Press.

Williams, M. L., Landel, R. F., & Ferry J. D. (1955). The temperature dependence of relaxation mechanisms in amorphous polymers and other glass-forming liquids. *Journal of the American Chemical society*, *77(14)*, 3701–3707.

Williams, B. A., Willis, J. R., & Ross, T. C. (2019). *Asphalt Pavement Industry Survey on Recycled Materials and Warm-Mix Asphalt Usage: 2018* (Information Series No. 138 (9e)). Greenbelt, MD, USA: National Asphalt Pavement Association (NAPA) in corporation with Federal Highway Administration (FHWA).

Williams, B. A., Willis, J. R., & Shacat, J. (2020). *Asphalt Pavement Industry Survey on Recycled Materials and Warm-Mix Asphalt Usage: 2019* (Information Series No. 138 (10e)). Greenbelt, MD, USA: National Asphalt Pavement Association (NAPA) in corporation with Federal Highway Administration (FHWA).

Xiao, F., Amirkhanian, S., & Juang, C. H. (2007). Rutting resistance of rubberized asphalt concrete pavements containing reclaimed asphalt pavement mixtures. *Journal of Materials in Civil Engineering*, *19*(6), 475-483.

Yan, K., Lan, H., Duan, Z., Liu, W., You, L., Wu, S., & Miljković, M. (2021). Mechanical performance of asphalt rejuvenated with various vegetable oils. Construction and Building Materials, 293, 123485.

Yang, X., You, Z., & Mills-Beale, J. (2015). Asphalt binders blended with a high percentage of biobinders: Aging mechanism using FTIR and rheology. *Journal of Materials in Civil Engineering*, *27*(4), 04014157.

Yang, C., Wu, S., Cui, P., Amirkhanian, S., Zhao, Z., Wang, F., ... & Xie, J. (2022). Performance characterization and enhancement mechanism of recycled asphalt

mixtures involving high RAP content and steel slag. *Journal of Cleaner Production*, *336*, 130484.

Yin, J., Wang, S., & Lv, F. (2013). Improving the short-term aging resistance of asphalt by addition of crumb rubber radiated by microwave and impregnated in epoxidized soybean oil. *Construction and Building Materials, 49*, 712-719.

Yin, F., Arámbula-Mercado, E., Epps Martin, A., Newcomb, D., & Tran, N. (2017). Long-term ageing of asphalt mixtures. *Road Materials and Pavement Design*, *18*(sup1), 2-27.

Yu, X., Zaumanis, M., Dos Santos, S., & Poulikakos, L. D. (2014). Rheological, microscopic, and chemical characterization of the rejuvenating effect on asphalt binders. *Fuel, 135*, 162-171.

Yusoff, M., & Airey, G. D. (2010). The 2S2P1D: An excellent linear viscoelastic model. *Journal of Civil Engineering, Science and Technology, 1*(2), 1-7.

Zadshir, M., Oldham, D. J., Hosseinnezhad, S., & Fini, E. H. (2018). Investigating bio-rejuvenation mechanisms in asphalt binder via laboratory experiments and molecular dynamics simulation. *Construction and Building Materials, 190*, 392-402.

Zaumanis, M., Mallick, R. B., & Frank, R. (2013). Evaluation of rejuvenator's effectiveness with conventional mix testing for 100% reclaimed Asphalt pavement mixtures. *Transportation research record*, *2370*(1), 17-25.

Zaumanis, M., Mallick, R. B., Poulikakos, L., & Frank, R. (2014a). Influence of six rejuvenators on the performance properties of Reclaimed Asphalt Pavement (RAP) binder and 100% recycled asphalt mixtures. *Construction and Building Materials*, *71*, 538-550.

Zaumanis, M., Mallick, R. B., & Frank, R. (2014b). Determining optimum rejuvenator dose for asphalt recycling based on Superpave performance grade specifications. *Construction and Building Materials*, *69*, 159-166.

Zaumanis, M., Mallick, R. B., & Frank, R. (2014c). 100% recycled hot mix asphalt: A review and analysis. *Resources, Conservation and Recycling*, *92*, 230-245.

Zaumanis, M., Mallick, R. B., & Frank, R. (2015). Evaluation of different recycling agents for restoring aged asphalt binder and performance of 100% recycled asphalt. *Materials and Structures*, *48*(8), 2475-2488.

Zaumanis, M., Boesiger, L., Kunz, B., Cavalli, M. C., & Poulikakos, L. (2019). Determining optimum rejuvenator addition location in asphalt production plant. *Construction and Building Materials*, *198*, 368-378.

Zaumanis, M., Cavalli, M. C., & Poulikakos L. D. (2020). Effect of rejuvenator addition location in plant on mechanical and chemical properties of RAP binder. *International Journal of Pavement Engineering*, *21*(4), 507–515.

Zhang, J., Sabouri, M., Guddati, M. N., & Kim, Y. R. (2013). Development of a failure criterion for asphalt mixtures under fatigue loading. *Road Materials and Pavement Design*, *14*(sup2), 1-15.

Zhang, C., Ren, Q., Qian, Z., & Wang, X. (2019). Evaluating the effects of high RAP content and rejuvenating agents on fatigue performance of fine aggregate matrix through DMA flexural bending test. Materials, 12(9), 1508.

Zhang, W., Shen, S., Wu, S., Chen, X., Xue, J., & Mohammad, L. N. (2019). Effects of in-place volumetric properties on field rutting and cracking performance of asphalt pavement. *Journal of Materials in Civil Engineering, 31*(8), 04019150.

Zhao, S., Huang, B., Shu, X., & Woods M.E. (2015a). Quantitative characterization of binder blending: How much recycled binder is mobilized during mixing?. *Transportation Research Record*, *2506,* 72-80.

Zhao, S., Huang, B., & Shu X. (2015b). Investigation on binder homogeneity of RAP/RAS mixtures through staged extraction. *Construction and Building Materials*, *82,* 184-191.

Zhao, S., Huang, B., Shu, X., & Woods, M. E. (2016). Quantitative evaluation of blending and diffusion in high RAP and RAS mixtures. *Materials & Design*, *89*, 1161-1170.

Zhao, K., Wang, Y., Chen, L., & Li, F. (2018). Diluting or dissolving? The use of relaxation spectrum to assess rejuvenation effects in asphalt recycling. *Construction and Building Materials*, *188*, 143-152.

Zhou, F., Hu, S., Das, G., & Scullion, T. (2011). *High RAP mixes design methodology with balanced performance* (No. FHWA/TX-11/0-6092-2). Washington, D.C., United States: Federal Highway Administration (FHWA).

Ziari, H., Moniri, A., Imaninasab, R., & Nakhaei, M. (2019). Effect of copper slag on performance of warm mix asphalt. *International Journal of Pavement Engineering, 20*(7), 775-781.